Spring 2020

# Systematic Development of Photocatalysts

Mary Victoria Bobo

# SYSTEMATIC DEVELOPMENT OF PHOTOCATALYSTS

by

Mary Victoria Bobo

Bachelor of Science
Converse College, 2015

---

Submitted in Partial Fulfillment of the Requirements

For the Degree of Doctor of Philosophy in

Chemistry

College of Arts and Sciences

University of South Carolina

2020

Accepted by:

Aaron K. Vannucci, Major Professor

Susan D. Richardson, Committee Member

Dmitry V. Peryshkov, Committee Member

John R. Regalbuto, Committee Member

Cheryl L. Addy, Vice Provost and Dean of the Graduate School

# DEDICATION

I dedicate this work to my family, here and in Heaven, who have supported me every step of the way and held me steady in my faith through the best and worst days of my life. Also, to my friends who never ceased in their encouragement and who remind me every day that nothing is impossible.

# ACKNOWLEDGEMENTS

There are many people who deserve my thanks for their support during my graduate career. First and foremost is my advisor, Prof. Aaron K. Vannucci, whose guidance, insight, and support have afforded me success throughout my time in graduate school. I would also like to acknowledge the remaining members of my doctoral committee, Prof. Susan Richardson, Prof. Dmitry Peryshkov, and Prof. John Regalbuto, for their advice and insight.

I would like to acknowledge Prof. Natalia Shustova and her research group for allowing me to use their instrumentation, providing valuable contributions to my work. To the current and former members of my research group, Dr. Avishek Paul, Dr. Nivedita Das, Dr. Nicholas DeLucia, Dr. Mevan Dissanayake, Pooja Ayare, James Sitter, Jake Tillou, Maizie Helton, Jordan Reed, and Thi Ngo, for all their help and support. I must also acknowledge the invaluable contributions and help of Dr. Perry Pellechia, Dr. Mike Walla, Dr. Mark Smith, and Dr. William Cotham.

I must acknowledge my advisor at Converse College, Dr. Sheri Strickland, for inviting me to do independent chemical research in her lab and seeing my potential before I did. She and the remaining chemistry faculty at Converse College cultivated my interest in chemical research and inspired me to pursue a career in chemistry. I will always be thankful for the advice and support of these professors and the opportunities that I was afforded at Converse College. Finally, I would like to show my appreciation to

the University of South Carolina and all the professors and staff that make the Department of Chemistry and Biochemistry the incredible place that it is.

# ABSTRACT

Photocatalysis is a rapidly growing field and a powerful synthetic tool that has recently seen many advancements, showing immense promise to replace classic catalysis with a mild and elegant alternative methodology. Visible light driven catalysis relies on redox stable transition metal and organic based photoactive catalysts (photocatalysts) that absorb visible light efficiently and facilitate electron/energy transfer. The desire for greener and more renewable catalytic methods has caused research to shifted away from traditional transition metals (due to scarcity and environmental toxicity) and toward organic based photocatalysts. Due to similar photophysical and electrochemical characteristics of each of these classes of photocatalysts the organic based photocatalysts have not only shown the capability to replace transition metal catalysts but have been shown to outperform them. To accommodate the diverse demand of photocatalytic systems the systematic tailoring of photocatalyst structure is essential and has allowed the expanding scope of photocatalysis.

In order to meet the growing need for diverse and powerful photocatalysts, the systematic alteration of these compounds has been rapidly growing in literature. The ability to tailor a photocatalyst, organic or transition metal based, to desired electrochemical and photophysical properties by introduction of key functional groups to an established aromatic photocatalysts is key to meeting this demand. Synthesis based on structure and property relationships allows for the systematic tailoring of established

photocatalysts. To accomplish this tailoring, functional groups are chosen based on key characteristics such as electron density, halogen groups, and electron donating/withdrawing characteristics, that determine photophysical and electrochemical properties.

In order to effectively replace transition metal photocatalysts, organic photocatalysts need to mirror the photocatalytic capabilities of these complexes. Focusing on photophysical and electrochemical properties of the resulting photocatalysts has allowed the application of organic photocatalysts to a multitude of organic synthesis systems. Furthermore, the instillation of proper functional groups has also facilitated the incorporation of organic photocatalysts into photovoltaic devices and advancing the field of renewable energy.

# TABLE OF CONTENTS

# LIST OF TABLES

# LIST OF FIGURES

# CHAPTER 1

# INTRODUCTION: RECENT ADVANCEMENTS IN ORGANIC PHOTOCATALYSTS

## 1.1 Introduction

Photocatalysis has become a powerful tool for organic synthesis and seen vast advancements in the last decade. This methodology presents a mild and elegant replacement for classical catalysis, which often require exceedingly high temperatures and pressures. The photocatalysts used for light-driven systems must be redox stable, efficient light absorbers, and capable of electron/energy transfer. Due to their redox windows and substantial excited state lifetimes, Ru and Ir polypyridal dyes have been a gold standard in photoredox catalysis for almost 30 years, which may also be owed in part to their availability and well understood properties.[1-4] Since the renaissance of photocatalysis, historically used photocatalysts have found new roles in organic synthesis,[5-9] polymerization,[10] voltaic devices,[11-13] and solar fuel production.[14] A comprehensive database does not exist at the present for organic dyes, mostly due to the rapid growth of the field.

Photocatalysis proceeds through four basic steps, (1) initiation by photon absorption, (2) which allows access to the excited state, this results in a compound that is both a better reducer and oxidizer (3), and the catalytic cycle is closed by recovery of the catalyst original oxidation state. [15] Transition metal-based catalysts consist of highly conjugated π accepting ligands around an electron rich metal center. During photocatalysis transition metal photocatalysts complexes undergo a metal to ligand charge transfer (MLCT), accounting for the impressive excited state lifetimes averaging

1.1 to 1.9 μs.[16-18] The charge transfer occurs between the $t_{2g}$ orbital on the metal center to the π* orbital on the ligand.[6] The intersystem crossing of the excited electron yields the activated catalyst than can proceed through either a reduction or oxidation quenching pathway. A ligand to metal charge transfer (LMCT) is also possible.[19] The redox potentials of transition metal photocatalysts catalysts are easily tuned for given reactions, by exchanging the metal center or surrounding ligands. Focus on tailoring of transition metal photocatalysts has yielded an immense range of transition metal photocatalysts.

Though transition metal photoactive catalysts are ideal, the drawbacks of using them are substantial. Iridium and Ruthenium are some of the rarest elements in the earth's crust, making the resulting catalysts extremely expensive.[16] Polypyridal catalysts based around rare earth metals can often cost upwards of $1080/g.[20] The utilization of photocatalyzed systems introduces much greener methods, but the use of rare earth metals undermines this advantage. Not only are transition metals toxic to the environment, but often cause trace metal contamination in products.[21]

With a focus set on the creation of a green renewable catalytic methodology, research has begun to shift toward organic based photoactive catalysts. Photocatalytic systems offer an elegant and mild method for valuable reactivity.[22] In recent years a wide range of organic catalysts have been reported as alternative photoactive components.[21, 23-24] Organic based catalysts can replace their transition metal counterparts due to their similar photophysical and electrochemical characteristics, and have been shown to outperform them.[25-27] The catalysts are often much less expensive and environmentally benign.[28-29] Due to their highly conjugated and often planar nature organic photocatalysts are solvatochromic, owing to the immense importance of solvent choice in the given

catalytic system.[15] Unlike transition metal based photocatalysts, organic catalysts depend on a $\pi$ to $\pi^*$ transition during excitation. A charge transfer state (CT) exist for the organic catalyst, analogous to MLCT states.[15] The CT state occurs between the donor/acceptor moieties of the given compound. The systematic tailoring of organic photocatalysts is essential to expanding the scope of organic photocatalysis.

Similar to the editing of ligands around metal cores of transition metal photocatalysts, organic dyes or photocatalysts can be tailored to desired electrochemical and photophysical properties. Synthetic tailoring is done by introduction of key functional groups to an established aromatic photocatalysts. Electron density is one of the first characteristics to evaluate for the new moieties, with the increase of electron density an increase of the reductive strength of the given catalysts is seen, and vis versa. Halogens are a special case when it comes to electron density, due to their inductively electron withdrawing characteristic; however, the overwhelming electron density often offsets this, especially when more than one halogen group is present, meaning that halogens have very little effect on oxidation strength.[8] Electron donating/withdrawing characteristics of each group then comes into effect, especially considering that many organic photocatalyst are donor/acceptor molecules. Electron donating groups, such as the incorporation of carbazolyl onto cyanoarene, have been shown to increase the reduction potential of said photocatalyst, increases the change in reduction capability. Electron withdrawing groups maintain the opposite effect, the addition of these groups effectively decreases the reduction potential, while also increasing the oxidization potential of the compound. The decrease of the reduction potential occurs because electron withdrawing groups have little to no effect on the delocalization of electron hole

pairs of the donor/acceptor molecule, paramount for highly reducing photocatalysts. The above considerations cumulate to properly evaluate the "strength" of each component within the donor/acceptor molecule.

This review focuses on the tailoring of established organic photoactive catalysts to broaden the scope of organic photocatalysis. Organic photocatalysts are often based upon molecules that found their first use in the medical and pharmaceutical fields and were not originally used in catalytic methods. A surge in structure-property based synthesis of organic photocatalysts has allowed a vast advancement in the field of organocatalyzed synthesis and polymerization. Here within a selection of recent advancements are summarized.

**1.2 Cyanoarenes**

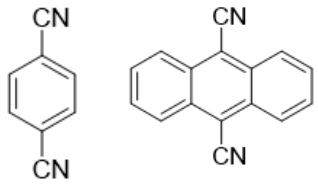


**Figure 1.1.** Photoactive cyanoarene catalysts.

Cyanoarenes have been thoroughly researched over the last thirty years as photoactive catalysts.[30-31] With a wide redox windows of reduction potentials ranging from -0.7 to -1.7 V and oxidation potentials of +2.0 V and greater, and fast catalytic turnovers yielding reactive radicals, the substrate and reaction scope of cyanoarene based photocatalysts is widely applicable and highly desirable.[32] Cyanoarenes are also a highly cited example of intermolecular electron transfer from singlet excited states.[32]

Cyanoarenes, among many other aromatic classes, have been investigated for the possibility of structural tailoring and the effects on the photophysical and electrochemical characteristics of the given molecule.[33] The first tailoring of cyanoarenes was the extension of the aromatic ring system, from benzene, to naphthalene and anthracene. With the establishment of cyanoarene based photocatalysts in a wide verity of syntheses, the classes of cyanoarenes was expanded by the Zeitzer group in 2018.


**Figure 1.2.** Structure of 1,2,3,5-tetrakis-(carbazole-9-yl)-4,6-dicyanobenzene (4CzIPN).

Among the class of cyanoarene class of photocatalysts, the most prevalent remains 1,2,3,5-tetrakis(carbazole-9-yl)-4,6-dicyanobenzene (4CzIPN) Figure 1.2. Due to the charge separation that occurs during photoexcitation, 4CzIPN exhibits a longer excited state lifetime than its predecessors, facilitated by the introduction of the carbazole groups around the cyanoarene core. The extension the aromatic core and/or the addition of aromatic groups creates a donor/acceptor molecule. Cyanoarene photocatalysts mimic the structure and electron transitions seen in transition metal photocatalysts, where photoexcitation leads to the transfer of an electron from the HOMO of the transition

metal atom, to the LUMO of the ligands surrounding the core. In organic molecules the processes caused by excitation is referred to as charge transfer (CT) Figure 1.3, also occurring during photoexcitation, the transfer of an electron from the HOMO on the donor moiety, to the LUMO on the acceptor core.[33] CT allows for organic photocatalysts to obtain comparative or better characteristics than transition metal photocatalysts.

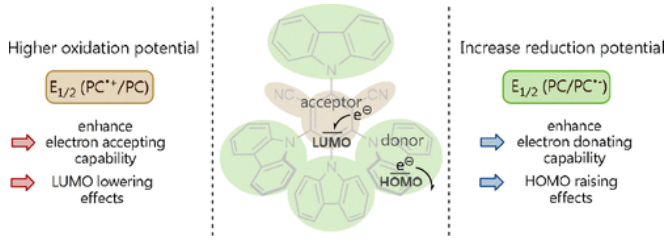


**Figure 1.3.** Donor/acceptor structure of organic cyanoarene photocatalysts[33] Reprinted with permission from Speckmeier, E.; Fischer, T. G.; Zeitler, K., A toolbox approach to construct broadly applicable metal-free catalysts for photoredox chemistry: deliberate tuning of redox potentials and importance of halogens in donor–acceptor cyanoarenes. *Journal of the American Chemical Society* **2018,** *140* (45), 15353-15365. Copyright 2020 American Chemical Society.

4CzIPN is commonly used catalyst for reductive, oxidative and redox neutral reactions due to well-balanced excited state redox potentials (-1.04 and +1.35 V vs SCE), and the ease of tunability through directed synthesis of the catalyst its self.[34] A fluorescence quantum yield of 0.946 alludes to a highly efficient organic photocatalyst, losing very little energy to nonradiative decay. 4CzIPN has an excited state lifetime of 5.1 microseconds, orders of magnitude longer than most organic photocatalyst and on par with transition metal counterparts. These properties make 4CzIPN one of the best organic

photocatalysts used commonly in literature, used successfully in both singular and dual photocatalytic systems.

Many catalytic reactions carried out using 4CzIPN are sought after by the polymers and pharmaceuticals industries, including synthesis of internal alkynes, alkylation of amines, radical coupling of C-C bonds, atom transfer radical polymerization, and synthesis of alkynyl sulfides.[35-42] Dual catalytic methods have also been achieved, such as hydroformylation and defluorinative alkylation.[34]

Because substituted cyanoarene photocatalysts adopt the donor/acceptor configuration in Figure 1.3, allowing for charge transfer states to occur during excitation, the strength of each component greatly affects the electrochemical character of the compound. The acceptor core of the photocatalyst, the cyanoarene moiety, is highly affected by the number of cyano groups on the core, Figure 1.4. The removal of which decreases the strength of the acceptor groups.[8] The addition of a halogen does increase the acceptor character of the photocatalyst (halogen effect). The donor moieties, mainly the carbazole and diphenylamine groups around the core, have a greater impact on the electrochemical properties, than the acceptor groups. The addition of the methoxy groups to carbazole and increasing the steric hinderance from the structure both serve to increase the strength of the donor moieties. The increased steric effect leads to further separation of the HOMO of the donor and LUMO of the acceptor moieties of the photocatalyst.

Comparing the redox properties of historically used cyanoarenes, such as 1-cyanonapthalene[30], to those newly synthesized to have higher aromaticity has given insight into the viability of tuning the properties of cyanoarene photocatalysts. The

tailoring of cyanoarene done by the Zeitler group has illustrated a comprehensive insight of the effects of aromatic, and halogen substitutions on the photocatalytically active core. In their 2018 paper, three newly synthesized, and 5 previously studied cyanoarene

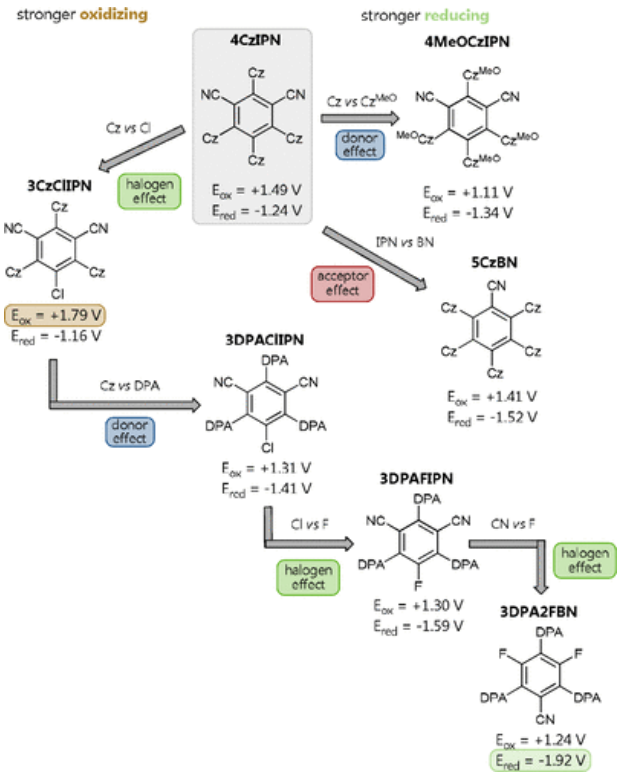


**Figure 1.4.** Catalyst structure of cyanoarene based, tailored photoactive catalysts. Cz (Carbazole), $Cz^{MeO}$ (3,6-dimethoxy-9H-carbazole), DPA (diphenylamine).[33] Reprinted with permission from Speckmeier, E.; Fischer, T. G.; Zeitler, K., A toolbox approach to construct broadly applicable metal-free catalysts for photoredox chemistry: deliberate tuning of redox potentials and importance of halogens in donor–acceptor cyanoarenes. *Journal of the American Chemical Society* **2018,** *140* (45), 15353-15365. Copyright 2020 American Chemical Society.

photocatalysts, were tailored in deliberate and specific manors to analyze the effects of aromatic, halogen, electron dense, and electron poor moieties on the electrochemical characteristics and performance of the previously reported 4CzIPN. The investigation of the halogen substitution was paramount due to their duality as inductive electron withdrawing and donating capabilities. Halogen substitution on the cyanoarene core showed little effect on the oxidation potential, though due to the increased electron density on the halogens, it led to stronger reducing photocatalysts. Branching off the previously substituted carbazole groups, methoxy-carbazole and diphenylamine groups were analyzed. The stronger the donating ability of a group, the better reductant the resulting catalyst became. The increased donor strength is due to the dependence of the reduction potential on the delocalization of the electron hole leading to charge separation. Following the trend of electron donation, the presence of electron withdrawing groups has minute effect on charge delocalization, therefore little effect on reduction potential, affecting oxidation potential more readily. The resulting new catalysts series was evaluated using challenging reductive, oxidative, and redox neutral reactions.

### 1.3 Acridinium

Acridinium dyes have been extensively synthetically edited for use in photoredox catalysis. This class of dyes are related through a central quinolinium structure and arylation of the core structure modifies the absorption of visible light, and limits side reactions and structural changes to the dye during reaction mechanisms. The extent of arylation has been shown to have a large effect on the chemical and physical properties of acridinium photoactive complexes. Acridinium was chosen as the core of new photocatalysts due to their robust nature, which are not susceptible to pH changes in

given systems, and they are soluble in a range of organic solvents, ideal for organic synthesis. Acridinium photocatalysts have found wide use in photoredox catalysis and namely *N*-Methyl Acridinium (Figure 1.4) has been used extensively in photoredox catalysis over the last two decades, due to their efficient use a photoinduced catalyst. The excited state reduction potential of ACR2 is 2.06 V vs SCE has allowed wide application of this catalyst across catalytic syntheses (Figure 1.5).[43] With the success of ACR2, more interest has been focused on extending this application by the tailoring of functional groups around the acridinium core. The facile tailoring of acridinium with the goal of more stable and more applicable photoactive catalysts, has allowed for a wide variety of acridinium photocatalysts, with redox potentials of $E_{red1/2}$=-0.84 V vs SCE (ACR7)[43] to $^{*}E_{red1/2}$=2.72 V vs SCE (ACR8)[22, 44]. Tailoring has extended the substrate scope and reaction window for the acridinium photocatalyst.

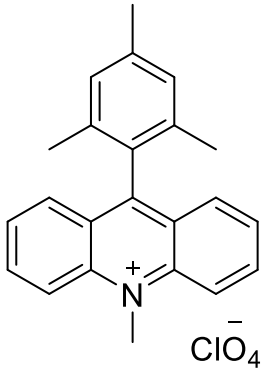


**Figure 1.5.** Structure of N-Methyl Acridinium (ACR2)

The DiRocco group showed a very important aspect of tailoring with their paper in 2016 reporting a total of six acridinium photocatalyst (ACR2-ACR7), focusing on the

systematic tailoring of *N*-Methyl Acridinium to evaluate the influence of functional groups on the photophysical and electrochemical properties and application to catalytic methods.[43] One of the important goals of this series is the synthesis of the catalysts on a commercial scale for applications in industrial scale synthesis. This study not only evaluated the addition of different functional groups for their electron-donating capabilities, but also their placement around the common acridinium core. Methoxy and tertbutyl groups were chosen and systematically altered around the central fused rings, and the phenyl group off the nitrogen group. ACR3 was synthesized with the addition of a phenyl group and tertbutyl functional groups, which increased the aromaticity and increased electron donating character of the catalyst. When compared to the properties of ACR2, the increase of in the excited state lifetime is seen, which may be due the creation of a donor/acceptor structure with the second aromatic ring. As stated earlier, the aromatic structure allows for the occurrence of charge transfer (CT), during excitation, between the core and outer rings (Figure 1.6). The addition of two methoxy groups to the acridinium backbone decreased the reduction potentials of the subsequent catalysts i.e. ACR4, however this is mitigated by the phenyl ring that is substituted to the nitrogen on the core. The decrease in the excited state reduction potential of this catalyst was caused by the decrease in $E_{00}$. Upon the addition of four methoxy groups on the core of the catalyst, as with ACR7, there was marked increase in the ground state reduction potential and a decrease in the $E_{00}$, resulting in a large decrease in the excited state reduction potentials.

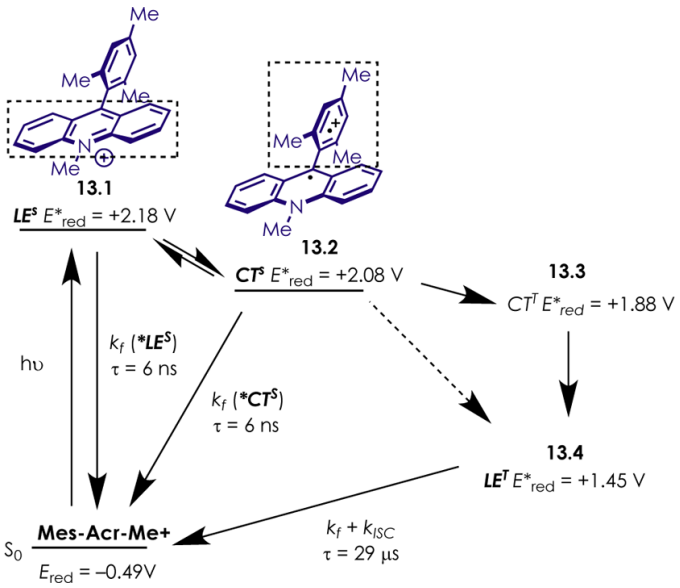


**Figure 1.6**. Jablonski diagram of $Acr^{+}$-Mes (ACR2), full representation of the excited state properties. [45-48] Reprinted with permission from Margrey, K. A.; Nicewicz, D. A., A general approach to catalytic alkene anti-Markovnikov hydrofunctionalization reactions via acridinium photoredox catalysis. *Accounts of chemical research* **2016,** *49* (9), 1997-2006. Copyright 2020 American Chemical Society.

Furthermore, the evaluation of the effect of functional group position (Figure 1.7) on the redox potentials of the resulting catalysts. The addition of methoxy groups at the 3 and 6 position around the acridinium core (ACR5), compared to the 2 and 7 positions on ACR4, caused an increase of over 100 mV vs SCE in reduction potentials; however, a decrease is seen in the excited state lifetimes. The addition of a dimethoxybenzene group (ACR6), instead of the *N*-phenyl group (ACR7) showed little to no influence on the redox potentials or excited state lifetimes of these two catalysts.[43] The tailoring of the catalysts in this study resulted in higher stability, and wider applicability in organic synthesis.

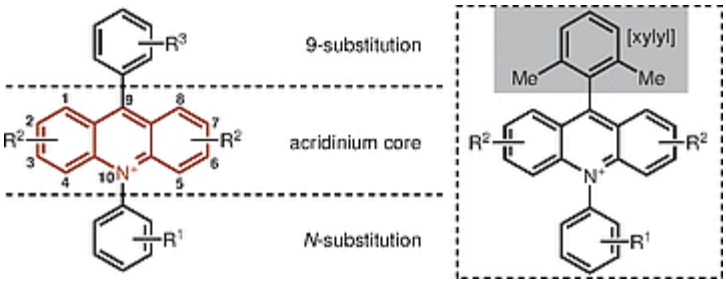


**Figure 1.7.** Structure and orientation of acridinium based photocatalysts.[49] Reprinted with permission from White, A. R.; Wang, L.; Nicewicz, D. A., Synthesis and Characterization of Acridinium Dyes for Photoredox Catalysis. *Synlett* **2019,** *30* (07), 827-832. Copyright 2020 Thieme.

**Table 1.1.** Effects of electron withdrawing functional groups. All potentials vs. SCE.

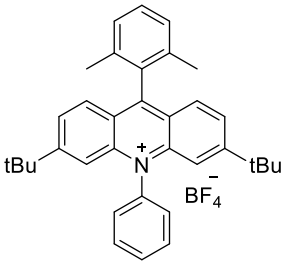

ACR12

$E_{red1/2}$=-0.56 V

*$E_{red1/2}$=+2.11 V

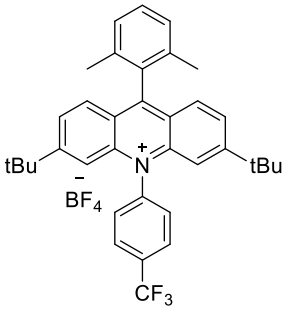

ACR19

$E_{red1/2}$=-0.51 V

*$E_{red1/2}$=+2.14 V

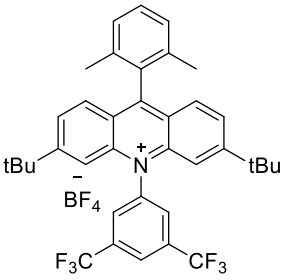

ACR20

$E_{red1/2}$=-0.45 V

*$E_{red1/2}$=+2.19 V

Building upon the initial study, the Nicewicz group at the University of North Carolina at Chapel Hill, reported a series of seventeen additional tailored acridinium catalysts in 2019. The work focused not only on extending understanding the effect of functional groups on the properties of the catalysts, but also on the extension of

aromaticity of the acridinium core.[49] Functional groups included not only tertbutyl and methoxy groups, but halogens, carboxyl, methyl, and trifluoromethyl groups. A wide selection of functional groups allowed the investigation of not only withdrawing/donating effects, but also the influence of electron density on properties of the respective catalysts. The functional groups were installed as R group substituents as in Figure 1.7.

Initially the mesityl group was replaced by 2,6-dimethylphenyl, in order to stabilize the catalyst during excitation and avoid the positive charge localized on the mesityl group. This substitution also results in a decrease in nonradiative decay pathways of the methyl group rotations, subsequently showed an immediate increase in the excited state lifetimes of the resulting catalyst ACR9.[49] Though the addition of aryl functional groups had important roles in the augmentation of excited state lifetime, the effects of the charge transfer state had much more of an influence. This is seen in the structure of ACR24, with the substitution of 2,6-dichlorophenyl, at the 9 position, increasing excited state lifetime to a high of 25.7 ns.

The addition of trifluoromethyl groups to the *N*-substituted phenyl group (Table 1.1) resulted in a decrease in the ground state reduction potential. Occurring due to the electron withdrawing properties of the group and increased when additional groups were added, evident from ACR19 to ACR20, a trend that is seen throughout the literature as well. It was also found that the placement of halogens on either phenyl group, *N*-substitution or 9-substitution, each have the same effect on electrochemical properties, and the resulting catalysts exhibit very similar properties. Introducing heterocyclic rings to the two substituted positions attenuated the electrochemical values as well. Specifically, a dual heterocyclic substitution for the mesityl group decreased the $E_{00}$ and

the ground state reduction potentials, resulting in an increase in the calculated excited state potentials. While the *N*-substituted pyridine group did not affect the singlet state energy it did decrease the ground state reduction potential by 60 mV, resulting in a stronger excited state reducer. ACR14 and ACR15 were synthesized with the intent of the effect of extended aryl cores. Substitution at the nitrogen on the pyridine had very little effect on the reduction values, though the singlet stat energy was reduced by 20mV, allowing a slight increase in the excited state reduction values. However, the significant change to the aryl core greatly decreased the excited state lifetimes, from the average of 10-20 ns, down to 0.3 and 1.1 ns respectively.

The systematic alteration of parent organic photocatalysts in the studies above, each result in new compounds with higher stability and resist degradation during catalytic activity.[43, 49] The new photocatalysts were applied to industrial important catalytic schemes, the initial series was tested against the decarboxylative conjugate addition of Cvz-Proline to dimethyl maleate, a known photocatalytic driven reaction. A very low conversion was seen with the parent catalyst ACR2, based on this result 5 additional catalyst were chosen to evaluate their performance. The yield was boosted from 5% to 66-88% yield and were further evaluated for industrial scale application via batch flow reactor methods. The success of these reactions further promoted the success of the new photoactive catalysts.[43]

Throughout literature, ACR2 has been used extensively for oxidative catalytic reactions, due to the modest oxidation powers of Ir and Ru photoactive catalysts. [50] The catalysis carried out by ACR2 include the oxidative synthesis of γ-lactams from alkenes and activated unsaturated amides, the oxidation of alkenes and electron-rich arenes, and

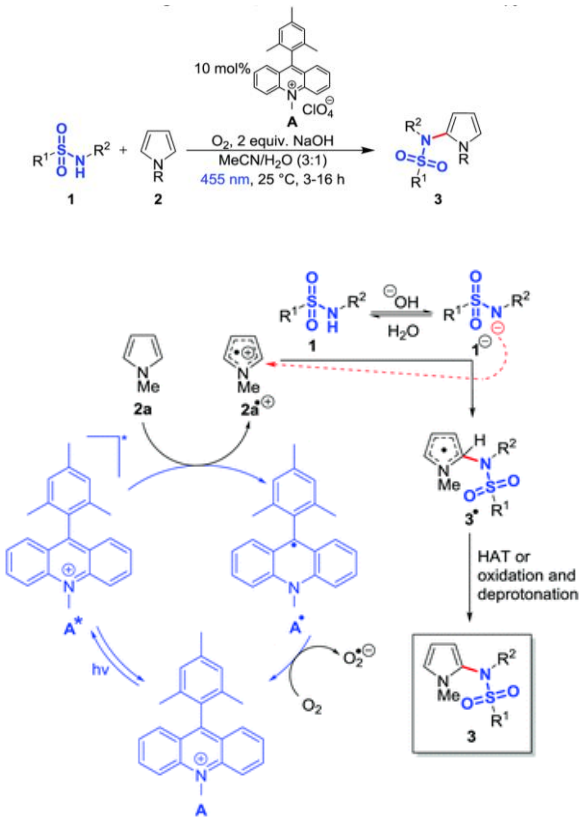


**Figure 1.8.** Visible light-mediated, metal-free C-H sulfonamidation of pyrroles.[58] Meyer, A. U.; Berger, A. L.; König, B., Metal-free C–H sulfonamidation of pyrroles by visible light photoredox catalysis. *Chemical Communications* **2016,** *52* (72), 10918-10921.- Published by The Royal Society of Chemistry.

the photocatalytic heteroarylation via C-C bond formation.[46-47, 50-56] This heteroarylation reaction utilizing ACR2 not only outperformed transition metal counterparts but presents a viably efficient and robust general process.[56] During the oxygenation of anthracenes and olefins with dioxygen via selective radical coupling, dioxygen via selective radical coupling, dioxygen is again seen to easily interact with the catalyst similar to that seen Figure 1.9, not only allowing the regeneration of the catalyst, but also partaking in the

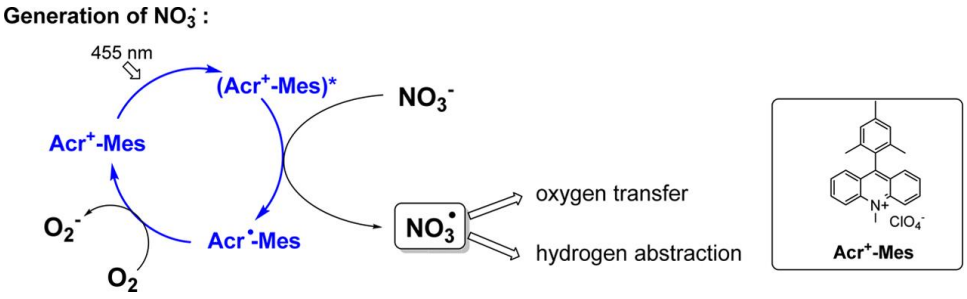


**Figure 1.9.** Anion oxidation to electrophilic species.[59] Reprinted with permission from Hering, T.; Meyer, A. U.; König, B., Photocatalytic anion oxidation and applications in organic synthesis. *The Journal of organic chemistry* **2016,** *81* (16), 6927-6936. Copyright 2020 American Chemical Society.

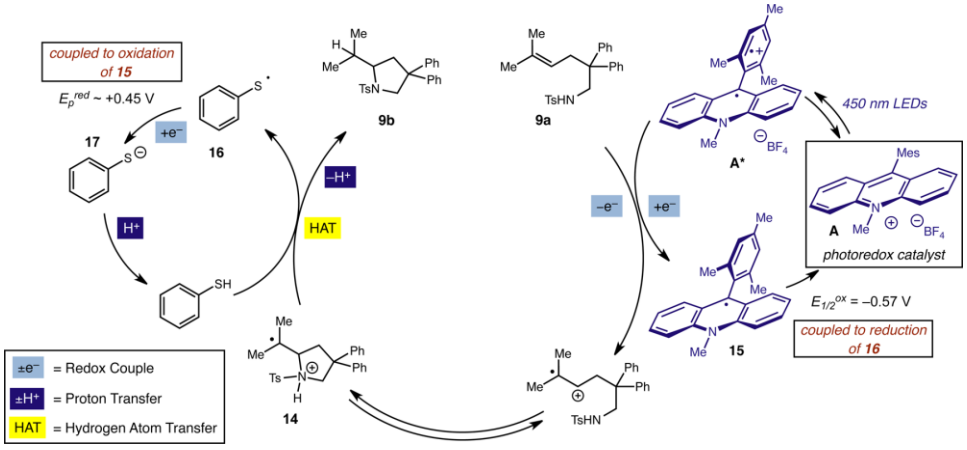


**Figure 1.10.** Anti-Markovnikov hydroamination of alkenes mechanism.[60] Reprinted with permission from Perkowski, A. J.; Nicewicz, D. A., Direct catalytic anti-Markovnikov addition of carboxylic acids to alkenes. *Journal of the American Chemical Society* **2013,** *135* (28), 10334-10337. Copyright 2020 American Chemical Society.

reaction. [57] A one-step *N*-(2-pyrrole)-sulfonamide synthesis from sulfonamides and pyrroles, utilizing oxygen as the terminal oxidant, resulting in C-N bond formation. [58] The reaction and mechanism in Figure 1.8, illustrates the high specificity brought to the reaction using ACR2, with limited oxidation power, and the required heterocycle

stability, along with the radical cation, cumulating in a successful multistep photocatalytic synthesis. The oxidation power of ACR2 was further used for anion oxidation, the conversion of chloride and nitrate anions into electrophilic chlorine species, carried out by the König group. As seen in Figure 1.9, this reaction unites ionic and radical chemistry in order to access heteroatom centered radicals.[59]

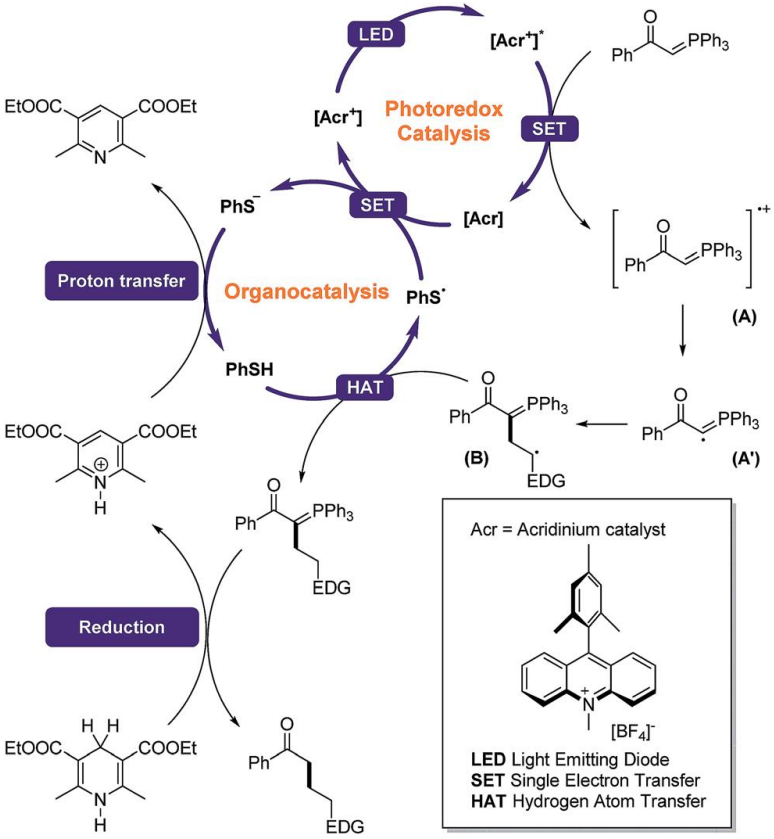


**Figure 1.11**. The hypothesized mechanism for the dual catalytic oxidative addition of phosphonium ylides to electron rich alkenes. [61] Das, M.; Vu, M. D.; Zhang, Q.; Liu, X.-W., Metal-free visible light photoredox enables generation of carbyne equivalents via phosphonium ylide C–H activation. *Chemical science* **2019,** *10* (6), 1687-1691.-Published by The Royal Society of Chemistry.

Due to the wide oxidative application of ACR2 ($Acr^+$-Mes) there has been a multitude of investigations done into anti-Markovnikov behavior of this photoactive catalyst. The anti-Markovnikov hydrofunctionalization of alkenes, was expanded to alkene hydroacetoxylation, hydrolactonization, hydroamination (Figure 1.10), and hydrotrifluoromethylation, all successfully carried out by ACR2. [45, 52, 60] The mechanism of anti-Markovnikov alkene hydrofunctionalization was carried out by Romero *et al.* supporting that the reaction proceeds through an alkene cation intermediate, and the alkenes are oxidized in the nanosecond timescale, matching the excited state lifetimes of the organic photocatalyst. [46] Dual catalytic systems take advantage of radical intermediates and was newly accessed by the acridinium photoactive catalyst. Dual catalytic photoredox/organocatalytic reactions were also employed for a benign method for phosphonium ylide addition to electron rich alkenes, and a mild regioselective catalytic synthesis (Figure 1.11). [61] Mechanistic and yield support is presented for the acridinium based photocatalysts can successfully replace their transition metal counterparts.

**1.4 Phenazine**

Naturally occurring and synthetically derived phenazine (Figure 1.12) based compounds represent a highly diverse class of compounds that is continuously growing. One of the first phenazine related compounds to be synthesized was Perkin's mauveine reported as early as 1860 and has since been patented.[62] Over the last century, research on phenazine based compounds has yielded an immense field of biologically active and medically important compounds.[63] Phenazine compounds have been reported and highly used as redox indicators, for titration reactions, and as oxidation agents.[64-65] Phenazines

are also often used as redox active antibiotics.[63, 66] The increased aromaticity of the phenazine core results in an absorption spectrum in the near visible range and the redox active nature of phenazine photocatalysts opens the door to a wide photocatalysis reaction scope. Inspired by the wide variety of phenazine based compounds already in use in the medical field, investigations have been conducted into the tuning/tailoring of said compounds for photochemistry.

Theriot *et al.* presented four photoactive redox catalysts based on *N*,*N*-diphenylphenazine with varying functional groups at the 4 position of each *N*-phenyl ring.[67] AZ1 through AZ4 in Table 1.2 were studied using density functional theory (DFT) to determine trends in the triplet excited-state reduction(Table 1.2). Basing the effects of substitution on AZ1, the trends in electrochemical properties are clear. The addition of electron withdrawing groups, seen in AZ3 and AZ4, resulted in a lower $^*E_{red1/2}$ making these catalysts less powerful reducers. Decreasing reduction potentials in the presence of electron withdrawing functional groups follows a trend that was maintained by AZ2, which was substituted with an electron donating group, methoxy, which showed an increasing in reducing power.[67] The resulting potentials of the electron withdrawing groups also shows the effects of electron density on redox potentials. With the trifluoromethyl group the decrease in potential is not as great of a change as the nitrile group, most likely due to the difference in electron density of the functional groups. Each of the four catalysts are significantly stronger reducers than most transition metal photocatalysts. It was proposed that the reducing power arises from the high triplet-state energies, combined with the stable radical cations that are formed upon oxidation.[67] The phenazine photocatalyst series was evaluated against an organocatalyzed ATRP reaction,

where each catalyst carried out the polymerization with low dispersity and high efficiency. Studies have also shown that phenazine photocatalysts operate under photoinduced electron transfer principals, in order to carry out further catalytic synthesis.[68]

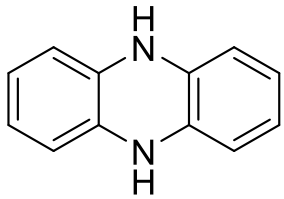

**Figure 1.12.** Phenazine molecular structure

Building off the information above, the attachment motif of naphthyl (Table 1.2 was also investigated. Again, the potentials for each were determined by DTF. Naphthyl was chosen to evaluate the spatial separation of the two singly occupied molecular orbitals (SOMOs) during excitation, and the delocalization of the excited electron over the diaryl groups. With a more spatial separation geometrically and stronger reduction potential 2-naphthyl (AZ5) also exhibits a longer excited state lifetime than its counterpart. 1-napthyl is still a strong reductant, though the geometry of AZ6 affords the new catalyst a lower $*E_{red1/2}$ and red shifts the absorption spectrum.

Further modification of phenazine-based photocatalysts was achieved through systematic modification of the phenazine core. Cole *et al.* examined the photocatalyst in Table 1.3 to determine how the photophysical and electrochemical properties altered catalyst activity. Organocatalyzed ATRP (O-ATRP) was chosen as the basis for a new series of photoactive catalysts. The addition of bromide moieties on the phenazine cores

(AZ7) led to a general structure the authors were able to build off of through Suzuki cross-coupling reactivity to yield the series of new photoactive catalysts shown in Table 1.3. The addition of the bromine groups, afforded higher electron density to the catalyst, increasing the oxidation potential and red shifting the absorption value, though the most drastic change is seen in the molar absorptivity, which increased two-fold, agreeing with literature values of compounds such as fluorescein versus Eosin Y, where halogenated dyes absorb light more efficiently. Following with the addition of new organic moieties at each of the aforementioned halogenated sites on AZ7, resulted in a highly tuned series of organic photoactive catalysts. By functionalization of the core the possibility of side reactions is bypassed, decreasing the number of possibly activated carbon-halogen sites on the catalysts.[69]

The experimentally determined excited state reduction potential value for AZ2 is -1.74 V vs SCE, using this as a reference point, the effect of each new moiety is evident. The addition of halogenated moieties decreases the $^*E_{red1/2}$ as seen in AZ8 vs AZ2, the electron withdrawing character of the $CF_3$ group decreases the reducing power of the resulting catalyst. The biphenyl and naphthyl groups on AZ9 and AZ10 respectively, serve to increase the aromaticity of the complex and increase the value of the $E_{00}$ for each. Subsequently the $^*E_{red1/2}$ is increased by at least 100 mV. A similar increase was seen for AZ11, a methoxyphenyl functionalization, though this was solely due to an increase in the value of the $E_{00}$ and no increase in the ground state oxidation potential, unlike the catalysts above. The final catalyst was synthesized with four dimethylaniline groups, AZ12, maintains the lowest oxidation potential of the series and resulted in

minimal change in the $E_{00}$ value, compared to the parent catalyst (AZ2). Due to these factors AZ12 results in the strongest reducer with $^*E_{red1/2}$ = -1.88 V vs SCE.[69]

**Table 1.2.** Structures of the diphenyl dihydrophenazine photocatalysts.[67] (All potentials reported versus SCE)

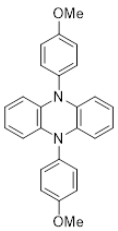


AZ2

$^*E_{red1/2}$ = -2.36 V

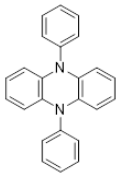


AZ1

$^*E_{red1/2}$ = -2.34 V

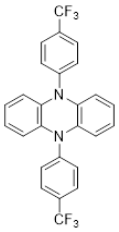


AZ3

$^*E_{red1/2}$ = -2.24 V

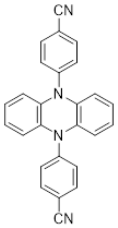


AZ4

$^*E_{red1/2}$ = -2.06 V

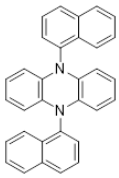


AZ6

$^*E_{red1/2}$ = -2.12 V

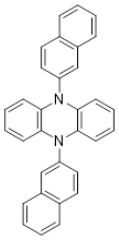


AZ5

$^*E_{red1/2}$ = -2.20 V

**Table 1.3.** Tetrasubstituted 5,10-di(4-trifluoromethyl-phenyl)-5,10-dihydrophenazine[69]

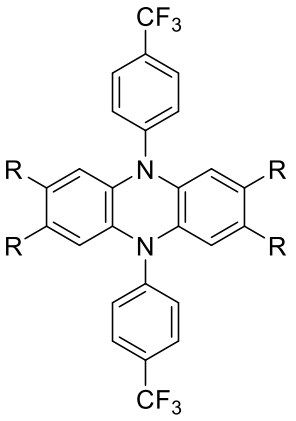


AZ2 R= H

AZ7 R= Br

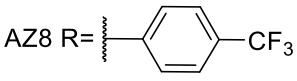


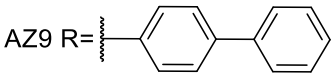


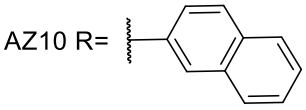


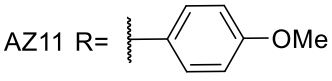


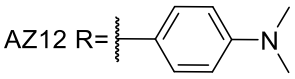

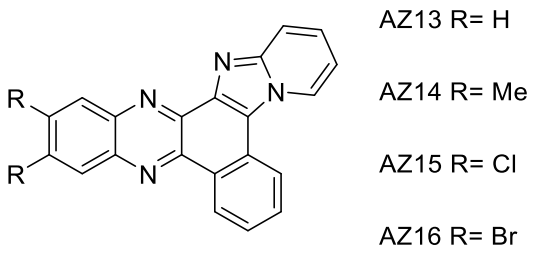


**Figure 1.13**. Diazobenzo[a]fluorene derivative photosensitizers[70]

The synthetic approach used by Cole *et al.* resulted in five complexes with $\lambda_{max,abs}$ that are red shifted by 20 nm or more due to the increased organic nature and aromaticity of the new series. Absorption well into the visible rang is important for photoredox catalysts, to avoid degradation of reactants during catalysis. More importantly the molar absorptivity of the new series is increased more than twice the value of the parent catalyst AZ2, from 10,800 to 22,200 $M^{-}cm^{-}$ for AZ7 and AZ9 respectively. The new series of phenazine based catalyst are not just more powerful reduction agents, but more efficient at light absorption.[69]

In their study published in 2012, Podemska *et al.* presented highly characterized series of photosensitizers based on diazobenzo[a]fluorene (AZ13 in Figure 1.13), for polymerization. The AZ13 parent complex, itself has an advantage over other reported phenazine based catalysts, with $\lambda_{max,abs}$ well into the visible region, essential to photocatalysis applications.[70] All the reported catalyst also maintain high molar absorptivity values, ranging from 8,300 to 11,100 $M^{-}cm^{-}$ for AZ16 and AZ14 respectively.

Full electrochemical characterization of the photocatalysts in Figure 1.13 was reported and gives more support to the trends seen previously in this review.[70] Tailoring was carried out at the R sites indicated in Figure 1.13, with both methyl groups and two different halogens. A comparison between AZ13 and the remaining catalysts in the series, shows a drastic decrease in the $E_{00}$, and weaker excited state reductants and oxidants; however, the ground state potentials did show some changes determined by their new functional groups. When comparing AZ13 with its methylated counterpart (AZ14) the ground state potentials change by only 10-20 mV, though the excited state values decrease by about 500 mV each. The deleterious effect is also seen for the excited state lifetimes. Aliphatic addition to the catalyst's backbone negatively affects all characteristics of the original catalyst.

Subsequent tailoring focused on the effects of varying halogen groups on the catalyst characteristics. The comparison of the two different halogen groups is important due to the multiple factors that affect halogen performance, such as electron withdrawing and donating effects, electron density, and the size of the given halogen moiety. In the case of both AZ15 and AZ16, the $E_{00}$ value was lowered by 500 to 650 mV, which subsequently affects the excited state redox potentials, adversely.[70] In fact, $E_{ox1/2}$ increased for both halogenated catalysts. A greater change was seen for the brominated catalyst, due to the larger halogen group. Though one area where the chlorinated catalyst out performs its counterpart is in the excited state lifetime (AZ15=4.5ns).[70]

The most common application for phenazine based photoactive catalysts is for radical based polymerization and this class of photocatalysts are an ideal replacement for

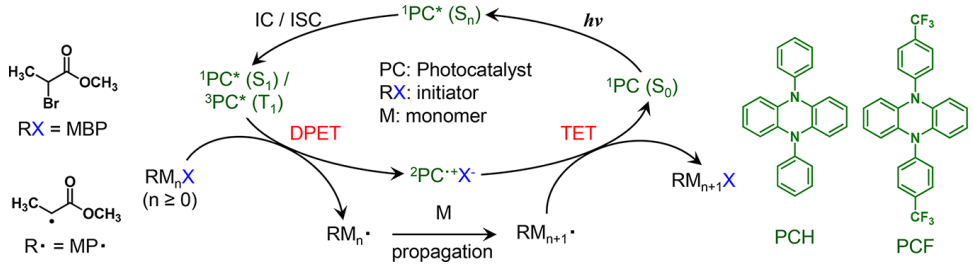


**Figure 1.14.** Organic Photoredox Catalysis of Atom-Transfer Radical Polymerization (The photocatalytic cycle for O-ATRP with N,N′-diaryl-dihydrophenazines (PC) and alkyl bromide initiators, with electron transfer either from the $S_1$ or $T_1$ state of the photocatalyst. DPET = Dissociative photoinduced electron transfer. TET = Thermal electron transfer. The chemical structures of the PCs used in this study are shown on the right.).[68] Reprinted with permission from Koyama, D.; Dale, H. J.; Orr-Ewing, A. J., Ultrafast observation of a photoredox reaction mechanism: photoinitiation in organocatalyzed atom-transfer radical polymerization. *Journal of the American Chemical Society* **2018,** *140* (4), 1285-1293. Copyright 2020 American Chemical Society.

transition-metal based photoactive catalyst. Theriot *et al.* applied their catalyst series to ATRP, one of the most common and widely spread methods for polymerization, AZ1-AZ4 were used for organic photoinduced electron transfer (PET).[67] The success of these catalyst is owed to their strong reduction potentials and is supported by their impressive control over the polymerization, including conversion and dispersity. DFT and computational design were utilized to determine to explore catalytic activity of the series. Koyama *et al.* investigated the reaction mechanism of AZ1 and AZ2. It was that the first triplet excited state is responsible for the PET, that initiates organocatalyzed ATRP (O-ATRP) seen in Figure 1.14.[68] The O-ATRP mechanism shows that polymerization proceeds from photoexcitation of the catalyst followed by either internal conversion (IC) or intersystem crossing (ISC) to the $T_1$ excited state, from which PET occurs and initiation of the polymerization begins. The catalytic cycle is then closed by terminal electron transfer (TET), which not only regenerates the catalyst, but also terminates

polymerization. The importance of the of not only strong excited state reduction potentials, but sufficient oxidation potentials is shown, as the later controls the polymerization. Data supports that electron transfer and bromide dissociation are very fast, too fast to be determine.[68] The comparison of the two catalyst, shows that a shorter excited state lifetime, slower PET, lower reduction potentials, and low ISC quantum yields allow more control over polymerization. This study also determined that the free energies of excited states are the best factor to use to determine PET rates.[68]

Typical organic catalyst loading in O-ATRP is 1000 ppm due to shorter excited state lifetimes, though in the study done by Cole *et al.* which resulted in the series in Table 1.3, the resulting catalysts were productive at as low as 5 ppm. With a high initiation efficiency a system rivaling transition metal based photocatalysts was reported, which often require a catalyst loading of 50 ppm.[69] Similar to past studies, the catalysts maintain strong control over polymerization along with high degree of conversion.

The diazobenzo[a]fluorene based photoactive catalyst series in Figure 1.13, was utilized as photosensitizers by Podemska *et al.* and applied to the visible light driven dual component photoinitiated multiacrylate free radical polymerization. Photosensitizers that were more easily reduced were more productive during polymerization. Furthermore, the halogenated complexes AZ15 and AZ16 are more successful at accessing their excited state due to the presence of heavy atoms and are active in the above polymerizing systems. Better performance by the photocatalysts during electron transfer events.[70] A year later the same group published a second paper focused on the photochemical performance of the same series of photoactive complexes. Investigation into the cationic polymerization which is highly dependent upon PET was carried out.[71] The investigation

into photochemical behavior, such as fluorescence and photobleaching properties, yielded results that support earlier findings, namely that those catalysts that are easier to oxidize, have more control over polymerization and higher yields.

### 1.5 Thiazine

Thiazine based compounds have been used extensively in photoredox catalysis, the most notable example of which is methylene blue. Methylene blue (Figure 1.15) was first reported in 1876 and used widely in the medical field, but would not see use in photochemistry for almost a century. [72-73] Weil *et al.* were one of the first to report utilization of methylene blue as a photooxidant in 1965, taking advantage of the moderately good excited state oxidation potential.[74] With a well-established history, thiazine based catalyst are still widely applicable in photochemistry. Thiazine has been extensively tailored to expand the electrochemical range and application.

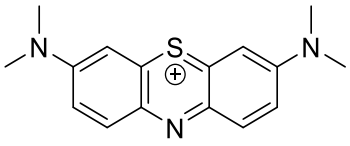


**Figure 1.15.** Methylene Blue

The removal of methyl groups decreased $E_{red1/2}$ by 130 mV, but the increase of the $E_{00}$ energy resulted in a stronger excited state oxidant (Thionin), while addition of methyl groups to the thiazine core had no effect on ground state energies as with 1,9-dimethyl Methylene Blue. Overall the extension of electron density resulted in four additional photoactive catalyst, all with stronger excited state oxidation potentials.[1] The series maintains high absorptivity in the visible light range, and gains a substantial range

of electrochemical values, $*E_{ox1/2}$=0.97 and 1.35 V vs SCE for Methylene Blue and Thionin respectively. [1, 72, 75-78] Thiazine photocatalysts are widely applied for boronic acid oxidation, photooxidation for ring opening, radical trifluoromethylation, acyl radical cyclization, thiophosphate synthesis, and reductive dehalogenations.[1, 25, 79-83]

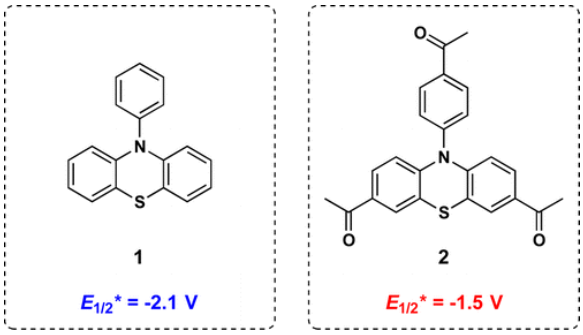


**Figure 1.16.** Structure and reduction potential of 10H-phenothiazine and tris-acetyl-PTH.[84] Reprinted with permission from Poelma, S. O.; Burnett, G. L.; Discekici, E. H.; Mattson, K. M.; Treat, N. J.; Luo, Y.; Hudson, Z. M.; Shankel, S. L.; Clark, P. G.; Kramer, J. W., Chemoselective radical dehalogenation and C–C bond formation on aryl halide substrates using organic photoredox catalysts. *The Journal of organic chemistry* **2016,** *81* (16), 7155-7160. Copyright 2020 American Chemical Society.

Functionalizing thiazine with a *N*-phenyl group has produced the very successful photocatalysts, 10H-pheothiazine (PTH). Due to its moderate $*E_{1/2}$, PTH has found a wide application as a photocatalyst in reductive synthesis, primarily in the field of polymer chemistry (Figure 1.16). Owing to the structure of PTH, it adopts a charge transfer configuration, similar to acridinium salts, between the thiazine core and *N*-phenyl functional group.[85] PTH has undergone extensive tailoring for purposes outside of catalysis and found applications a biological agent, like the compound in Figure 1.17.

Data further supports the non-toxic nature of thiazine based catalysts, highlighting their advantages over transition metal based counterparts.[86]

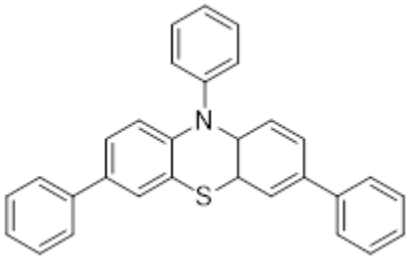


**Figure 1.17.** Structure of phenyl substituted PTH.

PTH has been thoroughly investigated as a photocatalyst for atom transfer radical polymerization (ATRP). Polymerization is in need of metal free systems capable of controlled polymer synthesis, to avoid contamination while maintaining ideal yields and desired products. PTH fills this need and is tolerant of a wide variety of functional materials, and shows high versatility in product formations.[87-88] Pan *et al.* further functionalized PTH with *N*-methoxyphenyl and *N*-naphthyl groups.[89] The resulting photoactive catalysts performed similarly in the polymerization of acrylonitrile, supporting that the electrochemical properties are dependent on the structure of the thiazine moiety, as opposed to the *N*-functional group. More research continues to utilize the control that PTH offers over polymerization and the advantages of a metal free catalyst in controlled radical polymerization (CRP) and surface-initiated atom transfer radical polymerization (SI-ATRP) with catalyst loadings a low as 0.02 mol %.[90-91]

Outside of polymerization, PTH has replaced transition metal photocatalysts in radical driven catalytic schemes. Boyington *et al.* utilized PTH for the regioselective

synthesis of arylethylamine (Figure 1.18). A powerful catalytic reductant is required for arylethylamine synthesis, to activate the aryl halide (PTH), and a catalytic hydrogen atom source such as cyclohexanethiol (CySH) work together as illustrated. PTH is used to activate the aryl halide to a radical anion, which transitions into a neutral radical. Allowing for regioselective addition followed by a hydrogen atom transfer (HAT) reaction resulting in the desired product.[92] All catalytic species are regenerated through the production of $CO_2$ and NaI. This work illustrated the reductive power of PTH and established a mild dual catalytic method for the synthesis of regiospecific arylethylamine, with a range of functional group tolerance, which extends to electron poor aryl chlorides.

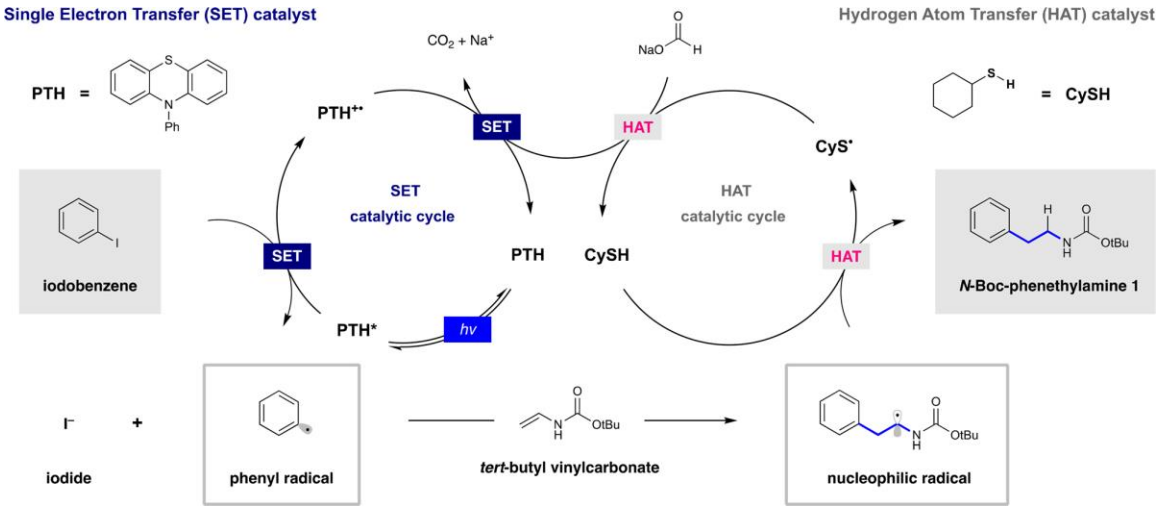


**Figure 1.18.** Proposed mechanism for the regioselective synthesis of arylethylamine.[92] Reprinted with permission from Boyington, A. J.; Seath, C. P.; Zearfoss, A. M.; Xu, Z.; Jui, N. T., Catalytic Strategy for Regioselective Arylethylamine Synthesis. *Journal of the American Chemical Society* **2019,** *141* (9), 4147-4153. Copyright 2020 American Chemical Society.

Poelma *et al.* illustrated the advantage of tailoring a photocatalyst for specific synthetic behavior (Figure 1.16).[84] The method in Figure 1.19 utilizes aryl substrates with two different halogen groups. As PTH (catalyst 1) is successful at activating both

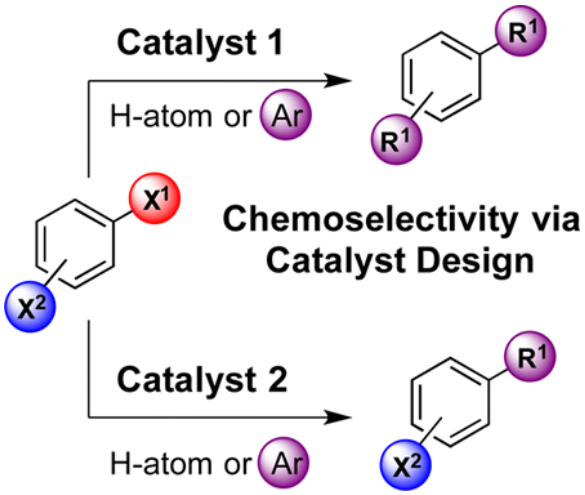


**Figure 1.19.** Representation of the synthetic scheme of chemoselective dehalogenation and chemoselective C-C bond formation on a poly halogenated substrate using an organic photoredox catalyst (X=halides, Ar=aryl group, R=H atom or aryl group).[84] Reprinted with permission from Poelma, S. O.; Burnett, G. L.; Discekici, E. H.; Mattson, K. M.; Treat, N. J.; Luo, Y.; Hudson, Z. M.; Shankel, S. L.; Clark, P. G.; Kramer, J. W., Chemoselective radical dehalogenation and C–C bond formation on aryl halide substrates using organic photoredox catalysts. *The Journal of organic chemistry* **2016,** *81* (16), 7155-7160. Copyright 2020 American Chemical Society.

halogen sites, resulting in a disubstituted product, tailoring (catalyst 2) allowed for a single site activation. By the substitution of three acetyl groups on PTH (tris-acetyl-PTH in Figure 1.16) the $*E_{1/2}$ drops from -2.1 to -1.5 V vs SCE. Decrease in potential allows for the tris-acetyl-PTH photoactive catalyst to selectively activate only one position on the substrate, followed by C-C bond formation or hydrogen atom addition. This work established a new organic photocatalytic method, under mild conditions, for chemoselective dehalogenation and bond formation with the aim of synthesizing

lamellarins.[84] The work described above are just a few of the many studies that utilize the highly active PTH catalyst, including radical dehalogenation, selective halogenation of amides, and numerous cross coupling catalytic methods.[93-94]

### 1.6 Oxazine

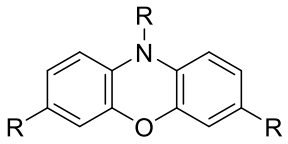


**Figure 1.20.** Phenoxazine based photoactive catalyst, tailoring occurring at the indicated R-groups.

The oxazine class of compounds consist of aromatic units linked by saturated nitrogen and oxygen atoms as shown in Figure 1.20. Oxazine based dyes have historically consisted of Nile Blue, Nile Red, and Brilliant Cresyl Blue. The use of the former was first reported in 1907, as a histochemical indicator for tissue lipid detection.[95] Nile Blue and Nile Red are commonly used for biological staining, and the former has been used extensively in the medical field, especially in the field of oncology.[95-99] Nile Red has been reported as a highly successful catalyst for the dehalogenation of α-bromoacetophenone, cementing the use of phenoxazines as redox active catalysts.[29] In a study published by Pitre *et al.* common dyes were compared for their application to light driven reductive dehalogenation. Showing that not only does Brilliant Cresyl Blue produce higher yields than other oxazine dyes, but also compares to them in C-C bond formation reactions.[1] Inspired by these results, the field of organic photocatalysts has

reported multiple studies focused on the tailoring of the oxazine backbone to yield new catalysts capable of a wide array of synthesis.

In the following studies a total of sixteen new phenoxazine based photoactive catalysts are reported. McCarthy *et al.* published a study in 2018 focusing on the comparison of systematic tailoring of phenoxazine based catalyst and electrochemical/photophysical properties. Organic catalysts with electron poor or highly conjugated substituents that can access charge transfer (CT) excited states, which leads to longer excited state lifetimes and increased redox potentials, when compared to those that do not form CT states. The hypothesis was presented that tailoring the properties of phenoxazine based catalysts could easily be accomplished by modifying the *N*-aryl and core functional groups, and consist of the first report that focuses on phenoxazine derivatives for photoredox catalysis.[15] The effects of increasing the aryl character of a catalyst can be seen when comparing OX7 to OX1 (Figure 1.21), where the later results from the addition of a biphenyl group to the core of OX7. Biphenyl addition stabilizes the LUMO orbital ($\pi^*$) of the catalyst, which in turn causes the red shift in the $\lambda_{max,abs}$ by 25 nm and more than doubles the molar absorptivity. Each of the modifications done in this study, alters the energies of the $\pi^*$, respectively altering the excited state redox potentials of the new catalysts.[15] All core modifications synthesized were designed to increase the aryl character, aimed at red shifting absorption into the visible range, to avoid needing UV light to activate the catalyst. UV light is a small part of the solar spectrum and can cause undesired side reactions.

The excited state reduction potentials ($^*E_{red1/2}$) of phenoxazine derivatives also were shown to be highly tunable depending on the synthetic modifications performed.

The modification of the phenoxazine core with 4-methoxyphenyl substituents resulted in the largest magnitude reduction potential in the photocatalyst series at -1.91 V vs SCE (OX8), which is comparable to the most highly reducing transition metal photocatalysts. The resulting series of photocatalyst showed that complexes with electron donating substituents on the core maintained the strongest excited state reduction potentials. Which occurs due to both the increased energy of the LUMO π* orbital and due to the electron density that is transferred to the core of the phenoxazine molecule resulting in a more stable charged radical species that is subsequently formed upon excited state electron transfer. The core of phenoxazine photocatalyst is so stable that the species are sometimes easier to oxidize than the neutral cores of unsubstituted catalysts.[15] The same trend is seen with electron withdrawing substituents and oxidation power of the given catalyst. The electron donating/withdrawing trend holds true with catalysts like OX10 and OX9, the later with two benzonitrile groups substituted onto the core, resulting in the least reducing catalyst due to the electron withdrawing effect of the nitrile groups. Electron withdrawing functional groups actively lower the triplet state energy, subsequently lowering the excited state potentials.[15] The series of phenoxazine photocatalysts is strongly reducing (*$E_{red1/2}$ = -1.42 to -1.91 V vs SCE).

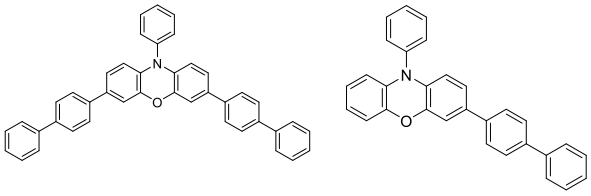

OX1 OX2

**Figure 1.21.** Structures of phenoxazine catalysts OX1 and OX2.

In addition to substitutions at the aryl position, variations to the substituents on the nitrogen atoms such as naphthyl, phenyl, and trifluoromethylphenyl groups can also have an impact on the photocatalyst properties. Altering the substituent attached to the nitrogen atom, however, resulted in a smaller magnitude of catalytic property variation compared to aryl substitutions.[15] The increased aryl substitution, at the aryl or nitrogen positions also serve to increase the reduction power of the respective catalysts. Substitution at the aryl position was required for those complexes with no core modifications, in order for these catalysts to access a charge transfer state. A highly conjugated functional group at this position allowed for the electron transfer to occur within the catalyst during excitation.

**Table 1.4.** Illustrated effect of phenyl and naphthyl connectivity on $E_{00}$ values.[100]

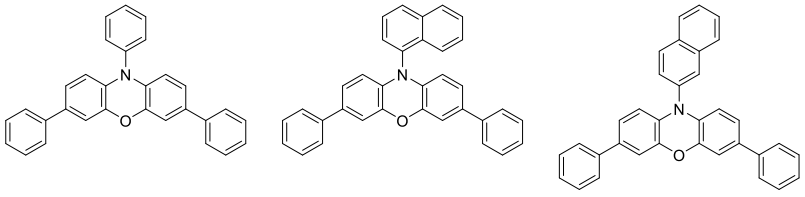

| OX4 | OX5 | OX6 |
|---|---|---|
| $E_{00}$ = 3.027 V | $E_{00}$ = 2.790 V | $E_{00}$ = 2.857 V |

Sartor *et al.* published a study focused on the connectivity of naphthyl groups at the *N*-aryl position of the phenoxazine backbone seen in Table 1.4. Two distinct catalyst, OX5 and OX6, with differing attachment of the naphthyl groups were synthesized for the evaluation of the effect on charge transfer states. As evident in Table 1.4, the substitution of phenyl with a naphthyl group serves to decrease the $E_{00}$ values by a minimum of 170

mV. When comparing the 1-naphthyl and 2-naphthyl group, this geometry causes a decrease in $E_{00}$ energy for the more restricted and compact OX5 complex. Decrease in singlet state energy occurs due to the alteration of the distance between donor and acceptor moieties (Figure 1.22), the resulting increased distance helps to stabilize the orbitals in question and increases the singlet state energy.[100] The distance between the donor and acceptor moiety not only affects the charge transfer state but has a deleterious effect of the inter system crossing quantum yield. Charge transfer states can also greatly improve the intersystem crossing quantum yield, with little impact on photophysical properties, resulting in highly active photoactive catalysts OX1 and OX2.[101]

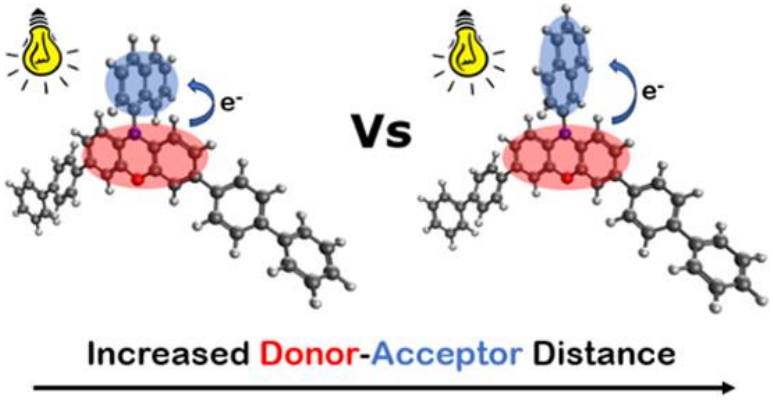


**Figure 1.22.** Donor/Acceptor structure of phenoxazine based photoactive catalysts.[100] Reprinted with permission from Sartor, S. M.; Lattke, Y. M.; McCarthy, B. G.; Miyake, G. M.; Damrauer, N. H., Effects of Naphthyl Connectivity on the Photophysics of Compact Organic Charge-Transfer Photoredox Catalysts. *The Journal of Physical Chemistry A* **2019,** *123* (22), 4727-4736. Copyright 2020 American Chemical Society.

Du *et al.* produced a highly reducing phenoxazine based catalyst (OX2) that resulted in a photocatalyst that compared to or outperformed most transition metal photocatalyst in redox properties and visible light absorption. OX2 is capable of

accessing intramolecular charge transfer excited states allowing it to access triplet excited states and achieve an excited-state lifetime in the microsecond range.[16] This excited-state lifetime is much larger than many of the previously reported phenoxazine photocatalysts which have lifetimes in the nanosecond time frame. The reported lifetime for OX2 also exceeds that of many transition metal photocatalysts. All resulting in a phenoxazine based photocatalyst with broad catalytic applicability and a good candidate to replace transition metal catalysts.

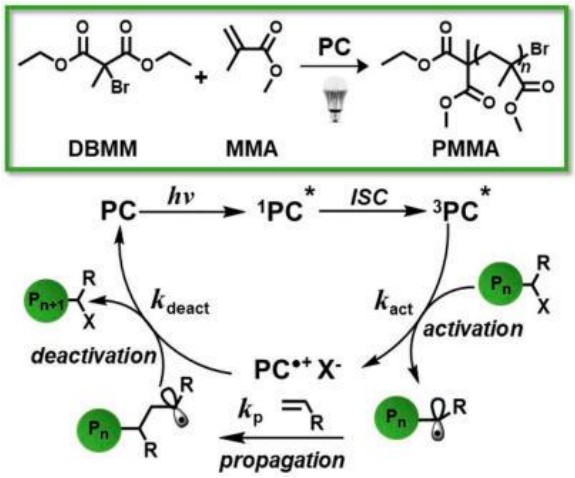


**Figure 1.23.** The reaction scheme for O-ATRP of MMA (top) and the proposed mechanism (bottom).[15] Reprinted with permission from McCarthy, B. G.; Pearson, R. M.; Lim, C.-H.; Sartor, S. M.; Damrauer, N. H.; Miyake, G. M., Structure–property relationships for tailoring phenoxazines as reducing photoredox catalysts. *Journal of the American Chemical Society* **2018,** *140* (15), 5088-5101. Copyright 2020 American Chemical Society.

Phenoxazine catalysts have been widely applied to organocatalyzed atom transfer radical polymerization, along with other catalytic cross coupling reactions. Organic based catalyst are more desirable due to the contamination probability of metal based

catalysis.[15] The series of catalysts developed by McCarthy *et al.* were applied toward O-ATRP, where OX3, OX14, and OX11 all maintained control over dispersity and molecular weight during the polymerization, owed to their strong visible light absorption and powerful excited state reduction potentials.[15] In Figure 1.23, the proposed mechanism polymerization is initiated by the excited state photocatalyst (PC*), which creates a carbon centered radical causing propagation. This reaction also yields a PC-halogen pair, thought to be responsible for deactivation of polymerization, closing the catalytic cycle. Catalyst OX2 performs highly controlled O-ATRP, in a continuous flow setup for an efficient and strong method applicable to a wide scope of methacrylate monomers, with catalyst loading as low as 0.005 mol % (Figure 1.24).[102] The continuous flow set up allows the lower catalyst loading also corresponded to a higher conversion and uniform irradiation.

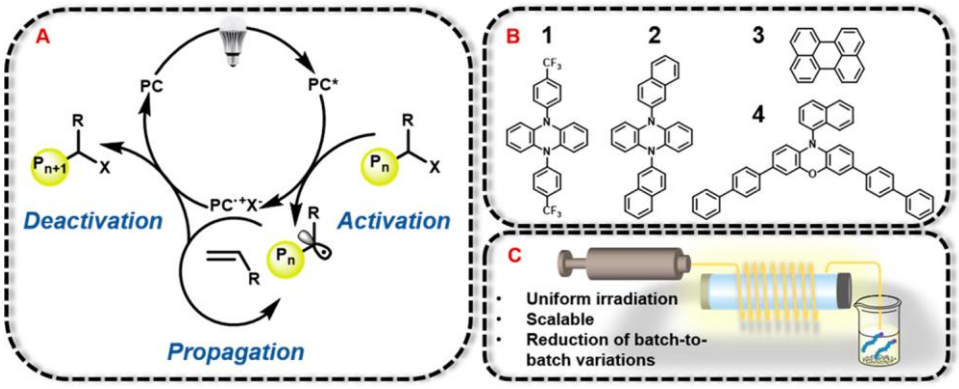


**Figure 1.24.** (A) The proposed oxidative quenching mechanism for O-ATRP. (B) A selection of photoactive catalyst investigated in this study. (C) Continuous flow reactor set up.[102] Reprinted with permission from Ramsey, B. L.; Pearson, R. M.; Beck, L. R.; Miyake, G. M., Photoinduced organocatalyzed atom transfer radical polymerization using continuous flow. *Macromolecules* **2017,** *50* (7), 2668-2674. Copyright 2020 American Chemical Society.

Due to the deleterious effect of oxygen to many photoactive catalysts, a study was done specifically for O-ATRP under air. This study focused on OX2, OX8, OX9, OX10, OX11, and OX14, with OX2 outperforming its counterparts. The series of phenoxazine catalysts performed comparatively under air, to an inert atmosphere; however, reactions run under nitrogen maintained the best control over parameters of the polymerization cycle.[103]

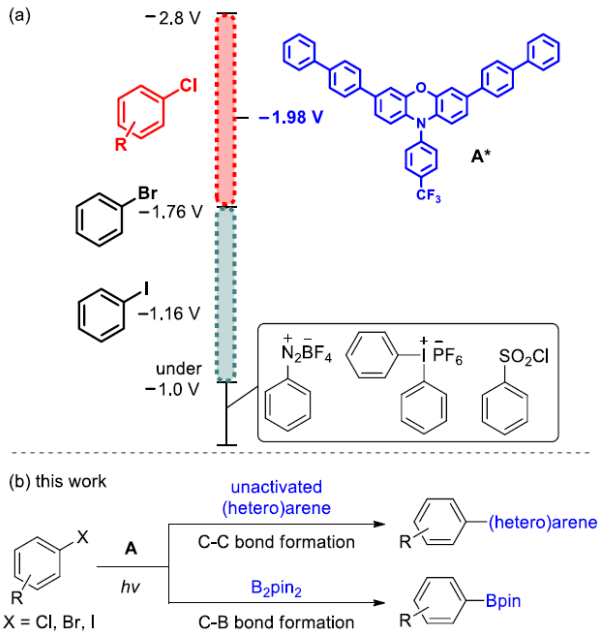


**Figure 1.25.** (a) Excited state reduction potential of OX16 (A*) versus aryl-halogen bond potentials. (b) C-C and C-B bond formation reactions from arene functionalization.[104] Reprinted with permission from Lee, D. S.; Kim, C. S.; Iqbal, N.; Park, G. S.; Son, K.-s.; Cho, E. J., Organophotocatalytic Arene Functionalization: C–C and C–B Bond Formation. *Organic Letters* **2019**. Copyright 2020 American Chemical Society.

Application for phenoxazine photocatalysts extends past polymerization into cross coupling reactions. OX2 was applied to atom transfer radical addition/substitutions with

$CF_3I$ to alkenes and heterocycles and dual photoredox catalyzed C-N and C-S cross coupling reactions, with exceedingly high yields in each case.[16] Arene functionalization was successfully carried out with OX16 for C-C and C-B formation, this methodology is capable of reducing aryl halides including aryl chlorides due to the high excited state

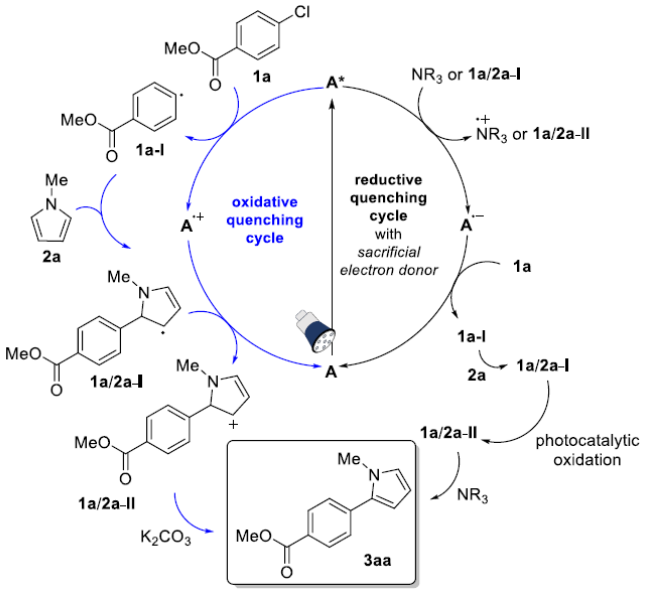


**Figure 1.26.** Proposed mechanism for aryl-chloride functionalization.[104] Reprinted with permission from Lee, D. S.; Kim, C. S.; Iqbal, N.; Park, G. S.; Son, K.-s.; Cho, E. J., Organophotocatalytic Arene Functionalization: C–C and C–B Bond Formation. *Organic Letters* **2019**. Copyright 2020 American Chemical Society.

reduction potential of OX16 catalyst (Figure 1.25).[104] Due to the photoactive nature and strong excited state reduction potential of this catalyst, the reaction proceeds through a photocatalyst oxidative quenching cycle without a sacrificial electron donor (SED), as shown in Figure 1.26. In the presence of an amine SED the catalytic mechanism proceeds first through a photocatalyst reductive quenching step, followed by electron transfer to the substituent. The reaction is tolerable to a wide substrate scope and

proceeds through a mild and chemoselective mechanism.[104] Allylation and benzylation of aldehydes and ketones was carried out with OX2.[101] Comparable yields to transition metal based photocatalysts and maintained a large substrate scope are reported. The proposed mechanism in Figure 1.27 eliminates the need for metal reductants, and is enabled by a dual electron photoinduced process.[101]

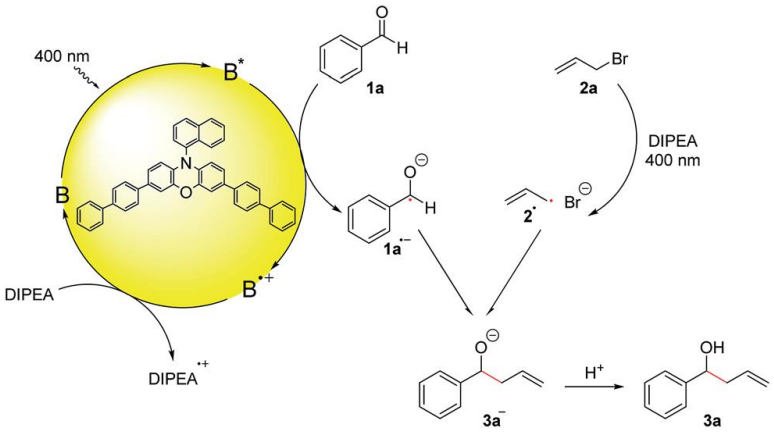


**Figure 1.27.** The proposed reaction mechanism of Barbier reactions utilizing OX2, through oxidative quenching.[101] Berger, A. L.; Donabauer, K.; König, B., Photocatalytic Barbier reaction–visible-light induced allylation and benzylation of aldehydes and ketones. *Chemical science* **2018,** *9* (36), 7230-7235.-Published by The Royal Society of Chemistry

## 1.7 Xanthene

Xanthene based compounds consist of three fused six membered rings, the middle of which contains an oxygen. Xanthene based photocatalysts including fluorescein, rose bengal, rhodamine 6G, rhodamine B and Eosin Y are redox active, and widely applied as catalysts.[1, 89, 105-106] Rose bengal has been successful in systems such as aza-Henry reactions and α-cyanation of tertiary aromatic amines, fluorescein has been utilized for the radical iodoperfluoroalkylation of alkenes and alkynes, along with the synthesis of

1,2-diketones.[89, 106-107] Rhodamine catalysts have been utilized as fluorophores, and open to tailoring for a wider application scope, with Rhodamine 6G capable of chromoselective photocatalysis for substitution reactions and C-H arylation reactions.[29, 108-110] Eosin Y specifically has been utilized as both a molecular homogenous photoactive catalysts, along with a surface mounted catalyst for heterogeneous applications which allows for the aerobic oxidation of benzyl halides.[111] The synthesis of trisubstituted pyridines and aryl ketones, dehalogenation, deoxygenation, C-H bond alkylation, and many more have been successfully carried out by Eosin Y.[24, 29, 112-113] With the high success rate of xanthene based catalysts, the opportunity arrives to utilize and build upon their superior qualities..

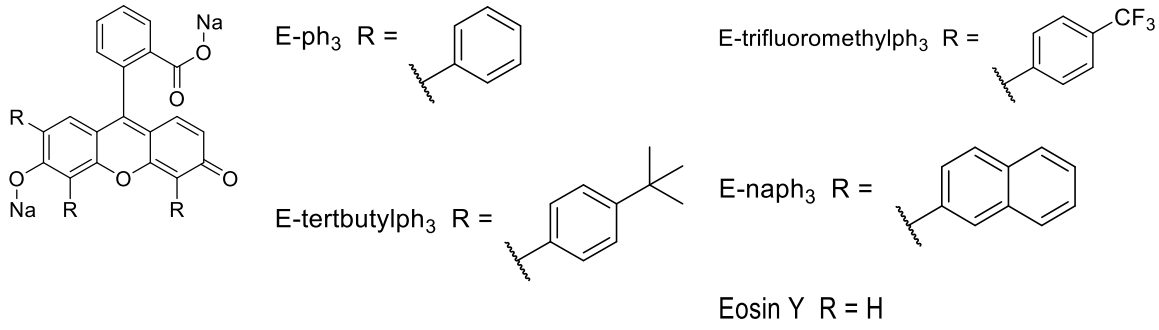


**Figure 1.28.** Photoactive catalytic series based on Eosin Y.

In a study carried out by our group, the systematic synthesis of a new series of Eosin Y based photoactive catalysts was reported (Figure 1.28). Four new photoactive xanthene catalysts were synthesized by taking advantage of the $sp^2$-C-Br groups around the core of Eosin Y, using Suzuki cross coupling to substitute new aromatic functional groups at three of the four sites, with hydrogenation occurring at the fourth site. The electrochemical and photophysical characterization was carried out in acetonitrile,

essential due to the solvatochromic nature of organic dyes. Using the comparison of new photocatalysts to the parent, Eosin Y, there clear trends that arise.

The functionalization of the xanthene core with aromatic substituents resulted in four complexes with $\lambda_{max,abs}$ red shifted by a more than 20 nm in the green region of visible light, the most abundant region of the solar spectrum. A red shift in $\lambda$ is also seen in the emission spectrums of each new catalysts. The new xanthene based photocatalysts also exceed a majority of other organic and metal based photoactive catalyst with molar absorptivity ranging from ten to fifty thousand, making them very efficient at absorbing and translating the energy in visible light. Efficiency is supported by the values for fluorescence quantum yield, all of which are at least triple the value for their transition metal-based catalysts, which is maintained at 0.10.

Comprehensive electrochemical characterization was performed, including redox potentials, singlet state energies, and excited state lifetimes. For those compounds with electron withdrawing characteristics, E-trifluoromethylph$_3$, which draw the electron density from the core and decrease the reduction potential of the compound. The three remaining derivatives with increased electron donating character and increased electron density, E-ph$_3$, E-naph$_3$, and E-tertbutylph$_3$, show increased reduction potential, following the trend seen in previous studies, that electron donating yields more powerful reductants. The phenyl derivative saw a 110 mV increase in the reduction potential. The $E_{00}$ values for each of the new catalysts is decreased from the parent Eosin Y value, due to the increased aromatic content of the new series which stabilizes the molecular orbitals and decreases the energy of the singlet state.

The catalytic activity of the xanthene based photocatalysts is not only dependent upon the redox potentials of the given catalyst, but also the excited state lifetime. Similar to many organic based catalysts, the lifetimes of these catalysts lie in the nanosecond range and are maintained similar to that of Eosin Y. In fact, the presence of the bulkier and aliphatic containing tertbutyl-phenyl moieties, the excited state lifetime is increased to 4.4 ns.

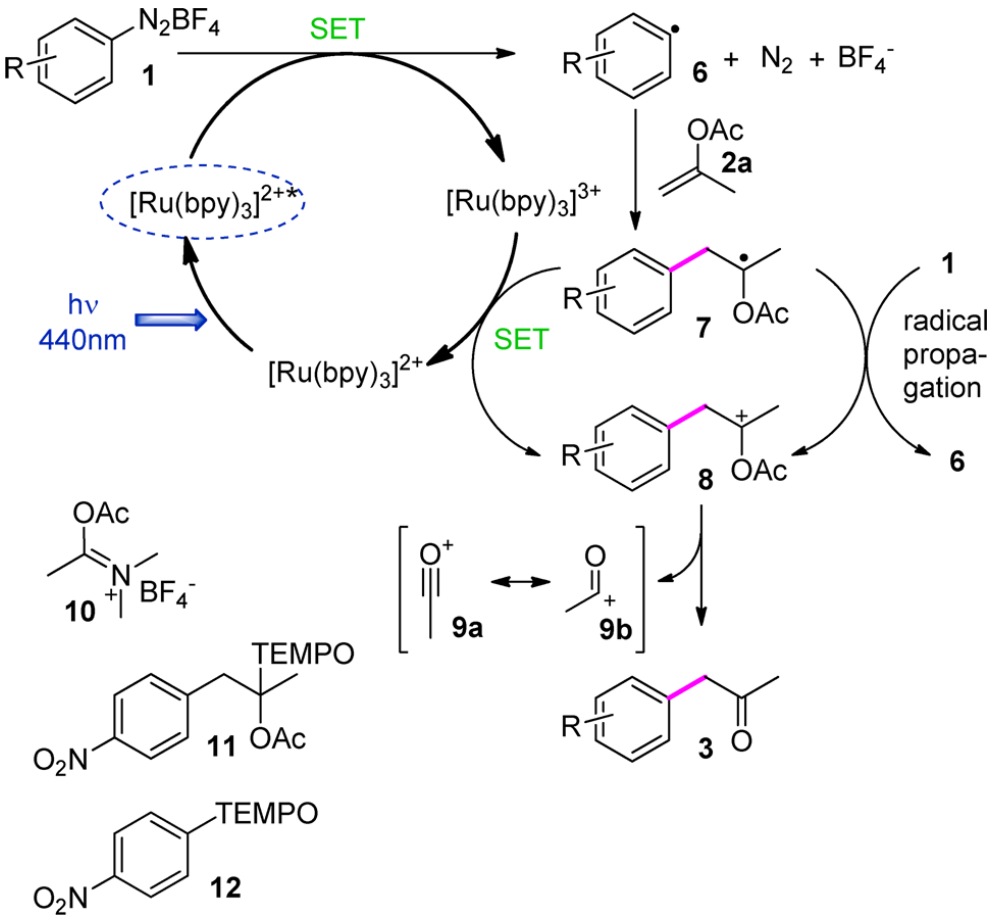


**Figure 1.29.** Mechanism of photo-driven enol arylation catalyzed by transition metal based catalysts, which were replaced by organic photocatalysts in the present study.[114] Reprinted with permission from Hering, T.; Hari, D. P.; König, B., Visible-light-mediated α-arylation of enol acetates using aryl diazonium salts. *The Journal of organic chemistry* **2012,** *77* (22), 10347-10352. Copyright 2020 American Chemical Society.

We applied the new photocatalysts to a catalytic system that had been shown previously successful for Eosin Y. Eosin Y catalyzed enol arylation was reported by the

**Table 1.5.** Photocatalytic enol arylation yields.

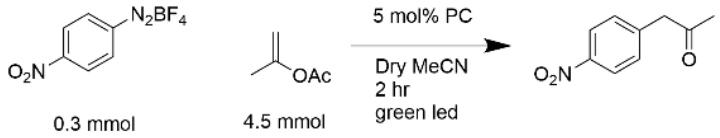


| Photocatalyst | % Yield | Turnover Number |
|---|---|---|
| E-ph$_3$ | 51 | 10 |
| E-trifluoromethylph$_3$ | 25 | 5 |
| E-tertbutylph$_3$ | 36 | 7 |
| E-naph$_3$ | 19 | 4 |
| Eosin Y Dianion | 31 | 6 |
| No PC | 3 | NA |

König research group and is extremely important in the pharmaceutical and bioactive field.[114-116] Chosen due to the initial reduction conducted by the photoactive catalyst (mechanism shown in Figure 1.29), and for the purpose of testing the reductive power of the new photocatalysts. From the results shown in Table 1.5, all the resulting catalysts successfully catalyze enol arylation. The catalyst with the strongest reduction potential, E-ph$_3$, resulted in the highest yield, as to be expected. The final yields reported in Table 1.5 follow the general trend that as the reduction potential increases, the yield of the reaction increases, in agreeance with the first step in the mechanism (Figure 1.29) involving the reduction of the diazonium salt.

## 1.8 Conclusion

This review presents a selection of recent advancements in the tailoring of organic photoactive catalysts. Organic based photocatalysts offer many advantages over classical catalysis, including mild and elegant methods that allow for targeted activation resulting in a decrease in undesired side reactions. The result of the tailoring above is a range of catalysts with enhanced photophysical and electrochemical properties These advancements represent the vast scope of organic photocatalysis. Though the last decade has seen a boom in this field, there remains room for advancement in not only catalyst scope, but chemo-, regio-, and enantioselectivity. These organic catalysts and the studies that produced them have increased our knowledge of not only their application but the effects of tailoring on their important properties.

**Table 1.6.** Comprehensive table of organic photocatalysts.

| Photocatalyst (solvent) | $\lambda_{max,abs}$ ($\varepsilon$ ($10^4$ $M^{-1}cm^{-1}$)) | $\tau_0$ | $^*E_{red1/2}$ (V vs SCE) | $^*E_{ox1/2}$ (V vs SCE) | $E_{red1/2}$ (V vs SCE) | $^*E_{ox1/2}$ (V vs SCE) | $E_{00}$ | Structure |
|---|---|---|---|---|---|---|---|---|
| **Cyanoarenes** | | | | | | | | |
| DCB[117-119] | 290 | 9.7 ns | 2.55 | | -1.46 | | 4.01 | 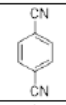 |
| DCA[31, 120, 121] | 422 | 14.9 ns | 1.99 | | -0.91 | | 2.90 | 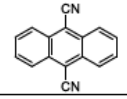 |
| 4CzIPN[34-42, 122] (MeCN) | | 12.7 ns | 1.43 | -1.18 | -1.24 | 1.49 | 2.67 | 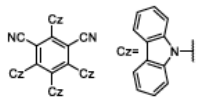 |
| 3CzClIPN[33] (MeCN) | | 6.9 ns | 1.56 | -0.93 | -1.16 | 1.79 | 2.72 | 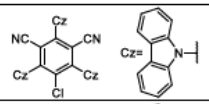 |
| 5CzBN[33] (MeCN) | | 16.3 ns | 1.31 | -1.42 | -1.52 | 1.41 | 2.83 | 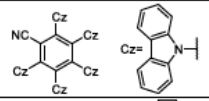 |
| 3DPAClIPN[33] (MeCN) | | 11.5 ns | 1.24 | -1.34 | -1.41 | 1.31 | 2.65 | 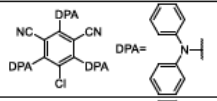 |
| 3DPAFIPN[33] (MeCN) | | 4.2 ns | 1.09 | -1.38 | -1.59 | 1.30 | 2.68 | 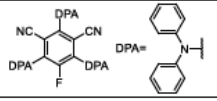 |
| 3DPA2FBN[33] (DCM) | | 4.2 ns | 0.92 | -1.60 | -1.92 | 1.24 | 2.84 | 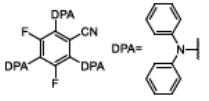 |

| Photocatalyst (solvent) | $\lambda_{max,abs}$ ($\varepsilon$ ($10^4$ $M^{-}cm^{-}$)) | $\tau_0$ | $^*E_{red1/2}$ (V vs SCE) | $^*E_{ox1/2}$ (V vs SCE) | $E_{red1/2}$ (V vs SCE) | $^*E_{ox1/2}$ (V vs SCE) | $E_{00}$ | Structure |
|---|---|---|---|---|---|---|---|---|
| 4MeOCzIPN[3] [3] (MeCN/DCM 5:1) | | | 1.27 | -1.50 | -1.34 | 1.11 | 2.61 | 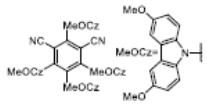 |
| 5MeOCzBN[33] (MeCN) | | | 1.15 | -1.79 | -1.66 | 1.02 | 2.81 | 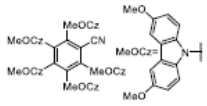 |
| **Acridinium** | | | | | | | | |
| ACR1[32, 123] | | | | | | | | 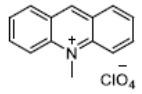 |
| ACR2[43] $Acr^+$-Mes | 430 | 6.4 ns | 2.06 | | -0.57 | | 2.63 | 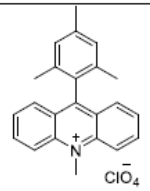 |
| ACR3[43] | 420 | 14.4 ns | 2.08 | | -0.59 | | 2.67 | 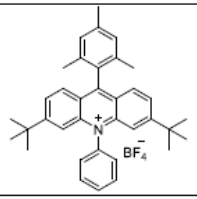 |

| Photocatalyst (solvent) | $\lambda_{max,abs}$ ($\varepsilon$ ($10^4$ $M^{-}cm^{-}$)) | $\tau_0$ | $^*E_{red1/2}$ (V vs SCE) | $^*E_{ox1/2}$ (V vs SCE) | $E_{red1/2}$ (V vs SCE) | $^*E_{ox1/2}$ (V vs SCE) | $E_{00}$ | Structure |
|---|---|---|---|---|---|---|---|---|
| ACR4[43] | 466 | 18.7 ns | 1.90 | | -0.57 | | 2.47 | 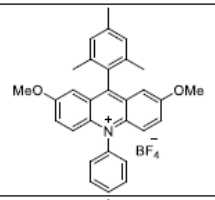 |
| ACR5[43] | 407 | 3.0 ns | 2.01 | | -0.71 | | 2.72 | 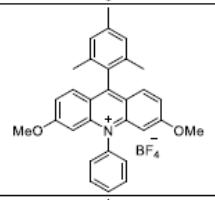 |
| ACR6[43] | 414 | 1.3 ns | 1.65 | | -0.82 | | 2.47 | 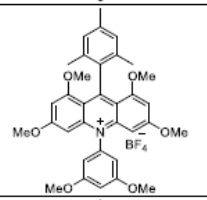 |
| ACR7[43] | 412 | 1.3 ns | 1.62 | | -0.84 | | 2.46 | 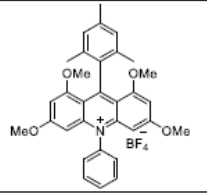 |
| ACR8[22, 44] 3-cyano-1-methylquinolinium perchlorate | | | 2.72 | | | | | 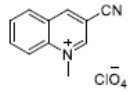 |

| Photocatalyst (solvent) | $\lambda_{max,abs}$ ($\varepsilon$ ($10^4$ $M^{-}cm^{-}$)) | $\tau_0$ | $^*E_{red1/2}$ (V vs SCE) | $^*E_{ox1/2}$ (V vs SCE) | $E_{red1/2}$ (V vs SCE) | $^*E_{ox1/2}$ (V vs SCE) | $E_{00}$ | Structure |
|---|---|---|---|---|---|---|---|---|
| ACR9[49] | 419 | 16.4 ns | 2.11 | | -0.56 | | 2.67 | 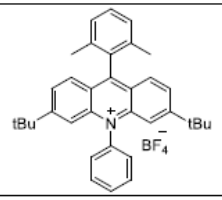 |
| ACR10[49] | 421 | 16.8 ns | 2.13 | | -0.54 | | 2.67 | 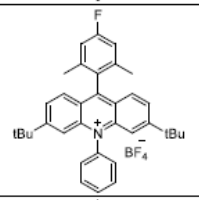 |
| ACR11[49] | 427 | 16.1 ns | 2.16 | | -0.47 | | 2.63 | 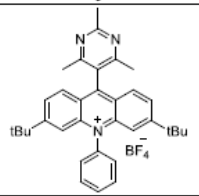 |
| ACR12[49] | 425 | 17.1 ns | 2.21 | | -0.43 | | 2.64 | 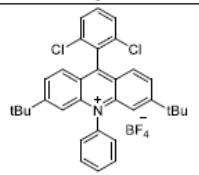 |
| ACR13[49] | 431 | 19.0 ns | 2.09 | | -0.53 | | 2.62 | 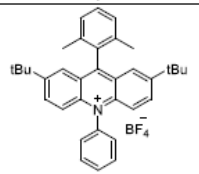 |

| Photocatalyst (solvent) | $\lambda_{max,abs}$ ($\varepsilon$ ($10^4$ $M^{-}cm^{-}$)) | $\tau_0$ | $^*E_{red1/2}$ (V vs SCE) | $^*E_{ox1/2}$ (V vs SCE) | $E_{red1/2}$ (V vs SCE) | $^*E_{ox1/2}$ (V vs SCE) | $E_{00}$ | Structure |
|---|---|---|---|---|---|---|---|---|
| ACR14[49] | 460 | 0.3 ns | 2.07 | | -0.53 | | 2.60 | 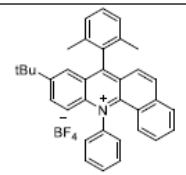 |
| ACR15[49] | 462 | 0.3 ns | 2.06 | | -0.54 | | 2.60 | 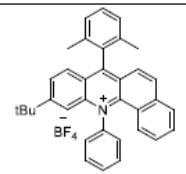 |
| ACR16[49] | 422 | 1.1 ns | 2.05 | | -0.58 | | 2.63 | 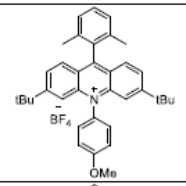 |
| ACR17[49] | 419 | 17.6 ns | 2.11 | | -0.55 | | 2.66 | 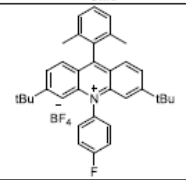 |
| ACR18[49] | 421 | 18.4 ns | 2.12 | | -0.54 | | 2.66 | 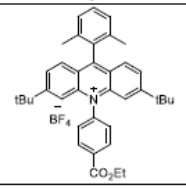 |

| Photocatalyst (solvent) | $\lambda_{max,abs}$ ($\varepsilon$ ($10^4$ $M^{-1}cm^{-1}$)) | $\tau_0$ | $^*E_{red1/2}$ (V vs SCE) | $^*E_{ox1/2}$ (V vs SCE) | $E_{red1/2}$ (V vs SCE) | $^*E_{ox1/2}$ (V vs SCE) | $E_{00}$ | Structure |
|---|---|---|---|---|---|---|---|---|
| ACR19[49] | 421 | 20.7 ns | 2.14 | | -0.51 | | 2.65 | 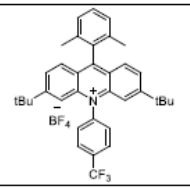 |
| ACR20[49] | 425 | 20.8 ns | 2.19 | | -0.45 | | 2.64 | 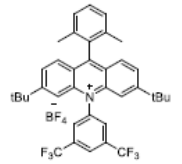 |
| ACR21[49] | 419 | 2.7 ns | 2.17 | | -0.50 | | 2.67 | 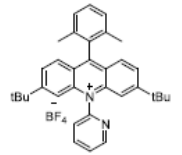 |
| ACR22[49] | 421 | 22.8 ns | 2.14 | | -0.53 | | 2.67 | 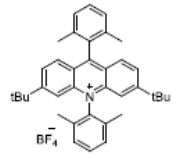 |
| ACR23[49] | 422 | 23.7 ns | 2.13 | | -0.54 | | 2.67 | 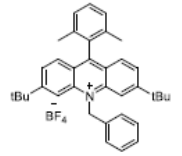 |

| **Photocatalyst (solvent)** | **$\lambda_{max,abs}$ ($\varepsilon$ ($10^4$ $M^{-}cm^{-}$))** | **$\tau_0$** | ***$E_{red1/2}$ (V vs SCE)** | ***$E_{ox1/2}$ (V vs SCE)** | **$E_{red1/2}$ (V vs SCE)** | ***$E_{ox1/2}$ (V vs SCE)** | **$E_{00}$** | **Structure** |
|---|---|---|---|---|---|---|---|---|
| ACR24[49] | | 25.7 ns | 2.20 | | -0.39 | | 2.59 | 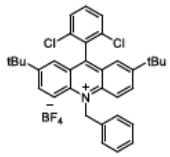 |
| **Phenazines** | | | | | | | | |
| AZ1 N,N'-diphenyl-5,10-dihydrophenazine[67, 68] (DMA) | 369 (0.61) | 3 ns | -2.34 (determined by DFT) | | | | | 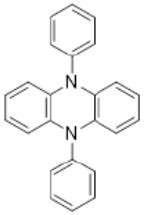 |
| AZ2 5,10-di(4-trifluoromethylphenyl)-5,10-dihydrophenazine[68, 69] (DMAc) | 367 (0.52) | 1-3 ns | -2.24 (calculate in different solvent) -1.74 in DMAc | | | 0.28 | 2.02 | 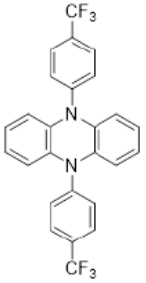 |

| **Photocatalyst (solvent)** | **$\lambda_{max,abs}$ ($\varepsilon$ ($10^4$ $M^{-}cm^{-}$))** | **$\tau_0$** | ***$E_{red1/2}$ (V vs SCE)** | ***$E_{ox1/2}$ (V vs SCE)** | **$E_{red1/2}$ (V vs SCE)** | ***$E_{ox1/2}$ (V vs SCE)** | **$E_{00}$** | **Structure** |
|---|---|---|---|---|---|---|---|---|
| AZ3<br>5,10-dihydro-5,10-bis(4-methoxyphenyl)-phenazine[67] | | | -2.36 (determined by DFT) | | | | | 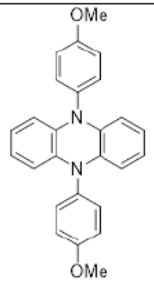 |
| AZ4<br>4,4'-(5,10-phenazinediyl)bis-benzonitrile[67] | | | -2.06 (determined by DFT) | | | | | 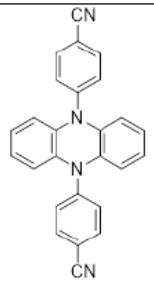 |
| AZ5<br>5,10-dihydro-5,10-di-2-naphthalenyl-phenazine[16, 124]<br>(DMA) | 343 (0.60) | 4.3 µs | -2.20 (determined by DFT) | | | 0.21 | 1.90 | 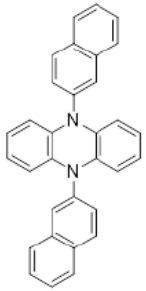 |

| **Photocatalyst (solvent)** | **$\lambda_{max,abs}$ ($\varepsilon$ ($10^4$ $M^{-1}cm^{-1}$))** | **$\tau_0$** | **$^*E_{red1/2}$ (V vs SCE)** | **$^*E_{ox1/2}$ (V vs SCE)** | **$E_{red1/2}$ (V vs SCE)** | **$^*E_{ox1/2}$ (V vs SCE)** | **$E_{00}$** | **Structure** |
|---|---|---|---|---|---|---|---|---|
| AZ6<br>5,10-dihydro-5,10-di-1-naphthalenyl-phenazine[124]<br>(DMA) | 362<br>(0.50) | | -2.12<br>(determined by DFT) | | | | | 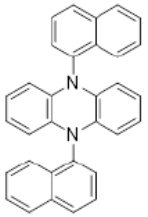 |
| AZ7<br>2,3,7,8-tetrabromo-5,10-di(4-trifluoromethylphenyl)-5,10-dihydrophenazine[69]<br>(DMAc) | 385<br>(1.08) | | | | | 0.60 | | 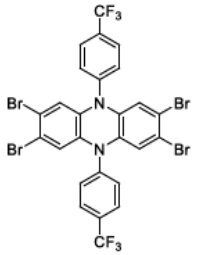 |
| AZ8<br>2,3,5,7,8,10-hexakis(4-(trifluoromethyl)phenyl)-5,10-dihydrophena | 385<br>(1.44) | | -1.68 | | | 0.45 | 2.13 | 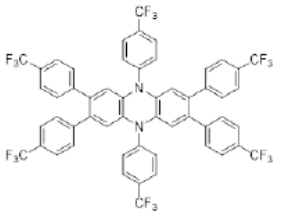 |

| **Photocatalyst (solvent)** | **$\lambda_{max,abs}$ ($\varepsilon$ ($10^4$ $M^{-}cm^{-}$))** | **$\tau_0$** | ***$E_{red1/2}$ (V vs SCE)** | ***$E_{ox1/2}$ (V vs SCE)** | **$E_{red1/2}$ (V vs SCE)** | ***$E_{ox1/2}$ (V vs SCE)** | **$E_{00}$** | **Structure** |
|---|---|---|---|---|---|---|---|---|
| zine[69]<br>(DMAc) | | | | | | | | |
| AZ9<br>2,3,7,8-tetra([1,1'-biphenyl]-4-yl)-5,10-bis(4-(trifluoromethyl)phenyl)-5,10-dihydrophenazine[69]<br>(DMAc) | 389<br>(2.22) | | -1.86 | | | 0.34 | 2.20 | 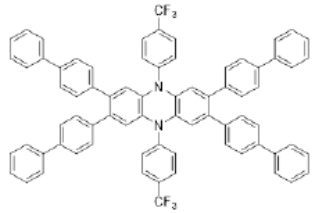 |
| AZ10<br>2,3,7,8-tetra(naphthalen-2-yl)-5,10-bis(4-(trifluoromethyl)phenyl)-5,10-dihydrophena | 388<br>(2.00) | | -1.84 | | | 0.38 | 2.22 | 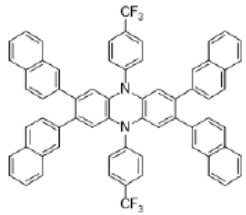 |

| **Photocatalyst (solvent)** | **$\lambda_{max,abs}$ ($\varepsilon$ ($10^4$ $M^{-}cm^{-}$))** | **$\tau_0$** | ***$E_{red1/2}$ (V vs SCE)** | ***$E_{ox1/2}$ (V vs SCE)** | **$E_{red1/2}$ (V vs SCE)** | ***$E_{ox1/2}$ (V vs SCE)** | **$E_{00}$** | **Structure** |
|---|---|---|---|---|---|---|---|---|
| zine[69]<br>(DMAc) | | | | | | | | |
| AZ11<br>2,3,7,8-tetrakis(4-methoxyphenyl)-5,10-bis(4-(trifluoromethyl)phenyl)-5,10-dihydrophenazine[69]<br>(DMAc) | 388<br>(1.14) | | -1.81 | | | 0.27 | 2.08 | 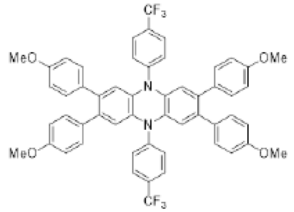 |
| AZ12<br>4,4',4'',4'''-tetrakis(N,N-dimethylaniline)-(5,10-bis(4-(trifluoromethyl)phenyl)-5,10- | 392<br>(1.46) | | -1.88 | | | 0.15 | 2.03 | 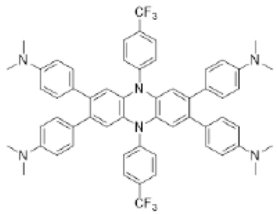 |

| **Photocatalyst (solvent)** | **$\lambda_{max,abs}$ ($\varepsilon$ ($10^4$ $M^{-}cm^{-}$))** | **$\tau_0$** | ***$E_{red1/2}$ (V vs SCE)** | ***$E_{ox1/2}$ (V vs SCE)** | **$E_{red1/2}$ (V vs SCE)** | ***$E_{ox1/2}$ (V vs SCE)** | **$E_{00}$** | **Structure** |
|---|---|---|---|---|---|---|---|---|
| dihydrophenazine[69] (DMAc) | | | | | | | | |
| AZ13 Benzo[*a*]pyrido[2',1':2,3]imidazo[4,5-*c*]phenazine[70, 71] ($CHCl_3$) | 443 (0.98) | 3.8 ns | -2.17 | 1.70 | -1.45 | 0.98 | 3.15 | 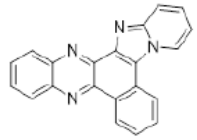 |
| AZ14 2,3-dimethyl-benzo[*a*]pyrido[2',1':2,3]imidazo[4,5-*c*]phenazine[70, 71] ($CHCl_3$) | 443 (1.11) | 3.0 ns | -1.63 | 1.15 | -1.47 | 0.99 | 2.62 | 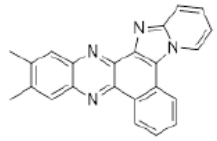 |

| Photocatalyst (solvent) | $\lambda_{max,abs}$ ($\varepsilon$ ($10^4$ $M^{-}cm^{-}$)) | $\tau_0$ | $^*E_{red1/2}$ (V vs SCE) | $^*E_{ox1/2}$ (V vs SCE) | $E_{red1/2}$ (V vs SCE) | $^*E_{ox1/2}$ (V vs SCE) | $E_{00}$ | Structure |
|---|---|---|---|---|---|---|---|---|
| AZ15 2,3-dichloro-benzo[*a*] pyrido[2',1':2, 3]imidazo[4, 5-*c*] phenazine[70, 71] ($CHCl_3$) | 460 (1.07) | 4.5 ns | -1.61 | 1.29 | -1.37 | 1.05 | 2.66 | 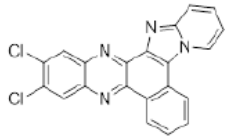 |
| AZ16 2,3-dibromo-benzo[*a*] pyrido[2',1':2, 3]imidazo[4, 5-*c*] phenazine[70, 71] ($CHCl_3$) | 462 (0.83) | 1.2 ns | 1.15 | -1.40 | -1.35 | 1.10 | 2.50 | 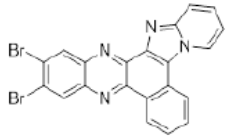 |
| **Thiazines** | | | | | | | | |
| Methylene Blue[1, 72, 75, 76] | 664 (9.00) | 32us | 0.97 | | -0.47 | | 1.50 | 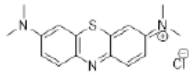 |
| Thionin[1, 75, 77, 78] | 598 (5.80) | 20us | 1.35 | | -0.34 | | 1.69 | 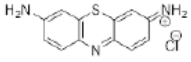 |

| **Photocatalyst (solvent)** | **$\lambda_{max,abs}$ ($\varepsilon$ ($10^4$ $M^{-}cm^{-}$))** | **$\tau_0$** | **$^*E_{red1/2}$ (V vs SCE)** | **$^*E_{ox1/2}$ (V vs SCE)** | **$E_{red1/2}$ (V vs SCE)** | **$^*E_{ox1/2}$ (V vs SCE)** | **$E_{00}$** | **Structure** |
|---|---|---|---|---|---|---|---|---|
| New Methylene Blue N[1] | 622 (1.80) | 11us | 1.34 | | -0.39 | | 1.73 | 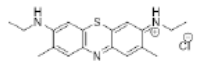 |
| 1,9-dimethyl Methylene Blue[1] | 652 (8.50) | 12us | 1.03 | | -0.47 | | 1.50 | 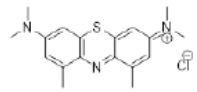 |
| Methylene Green[1] | 654 (6.00) | 14us | 1.28 | | -0.22 | | 1.50 | 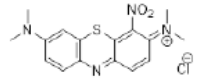 |
| Tris-acetyl-PTH[84] | Visible light | | -1.5 | | | | | 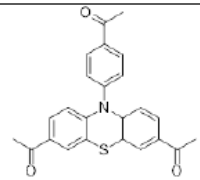 |
| PTH (10H-Phenothiazine)[93] | | | -2.1 | | | 0.68 | | 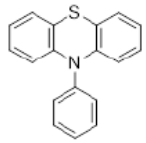 |
| **Oxazines** | | | | | | | | |

| Photocatalyst (solvent) | $\lambda_{max,abs}$ ($\varepsilon$ ($10^4$ $M^{-}cm^{-}$)) | $\tau_0$ | $^*E_{red1/2}$ (V vs SCE) | $^*E_{ox1/2}$ (V vs SCE) | $E_{red1/2}$ (V vs SCE) | $^*E_{ox1/2}$ (V vs SCE) | $E_{00}$ | Structure |
|---|---|---|---|---|---|---|---|---|
| Nile Blue[1, 95-98] (MeCN) | 630 (5.60) In MeCN:$H_2O$ | 1.76 ns | 0.87 | | -1.05 | | 1.92 | 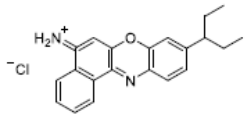 |
| Nile Red[29, 99, 125] (MeCN)[126] | 543 | 4.56 ns | | | -1.02 | | | 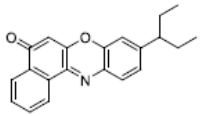 |
| Brilliant Cresyl Blue ALD[1] (MeCN) | 616 (4.50) | 0.51 ns | 1.67 | | -0.31 | | 1.98 | 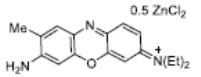 |
| OX1[15] | 389 (2.40) | | -1.72 | | | 0.42 | 2.14 | 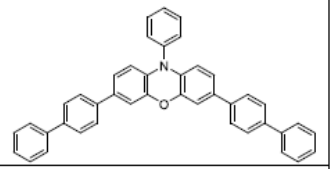 |
| OX2[16] | 388 (2.66) | 480± 50 µs | -1.80 | | | 0.65 | 2.45 | 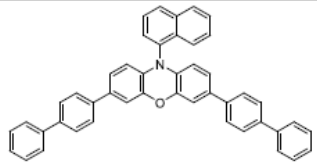 |

| Photocatalyst (solvent) | $\lambda_{max,abs}$ ($\varepsilon$ ($10^4$ $M^{-1}cm^{-1}$)) | $\tau_0$ | $^*E_{red1/2}$ (V vs SCE) | $^*E_{ox1/2}$ (V vs SCE) | $E_{red1/2}$ (V vs SCE) | $^*E_{ox1/2}$ (V vs SCE) | $E_{00}$ | Structure |
|---|---|---|---|---|---|---|---|---|
| OX3[15] | 384 (2.59) | | -1.70 | | | 0.43 | 2.13 | 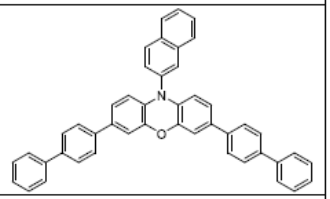 |
| OX4[100] | | 3.24 ns | | | -2.7 | 0.637 | 3.027 | 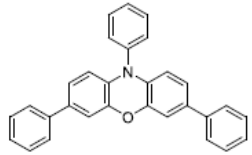 |
| OX5[100] | 371 (1.50) | 6.32 ns | | | -2.350 | 0.663 | 2.790 | 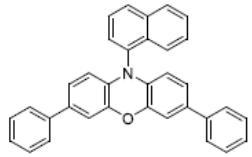 |
| OX6[100] | 367 (1.83) | 8.03 ns | | | -2.396 | 0.642 | 2.857 | 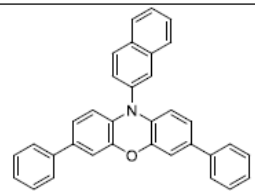 |
| OX7[15] | 362 (1.03) | | -1.71 | | | 0.53 | 2.24 | 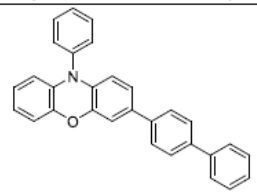 |

| Photocatalyst (solvent) | $\lambda_{max,abs}$ ($\varepsilon$ ($10^4$ $M^{-}cm^{-}$)) | $\tau_0$ | $^*E_{red1/2}$ (V vs SCE) | $^*E_{ox1/2}$ (V vs SCE) | $E_{red1/2}$ (V vs SCE) | $^*E_{ox1/2}$ (V vs SCE) | $E_{00}$ | Structure |
|---|---|---|---|---|---|---|---|---|
| OX8[15] | 363 (2.20) | | -1.91 | | | 0.37 | 2.28 | 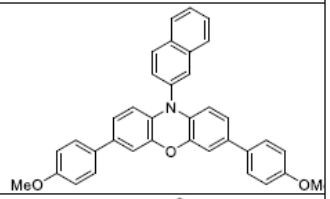 |
| OX9[15] | 411 (2.23) | | -1.42 | | | 0.62 | 2.04 | 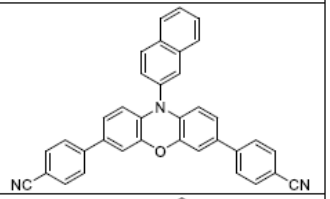 |
| OX10[15] | 388 (2.11) | | -1.58 | | | 0.58 | 2.16 | 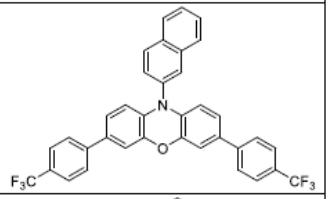 |
| OX11[15] | 384 (2.53) | | -1.69 | | | 0.40 | 2.09 | 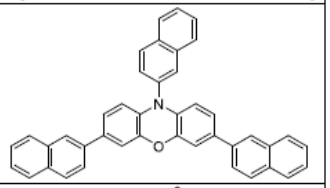 |
| OX12[15] | 355 (1.911) | | -1.72 | | | 0.46 | 2.18 | 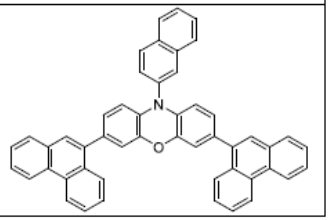 |

| Photocatalyst (solvent) | $\lambda_{max,abs}$ ($\varepsilon$ ($10^4$ $M^{-1}cm^{-1}$)) | $\tau_0$ | $^*E_{red1/2}$ (V vs SCE) | $^*E_{ox1/2}$ (V vs SCE) | $E_{red1/2}$ (V vs SCE) | $^*E_{ox1/2}$ (V vs SCE) | $E_{00}$ | Structure |
|---|---|---|---|---|---|---|---|---|
| OX13[15] | 379 (2.06) | | -1.85 | | | 0.45 | 2.30 | 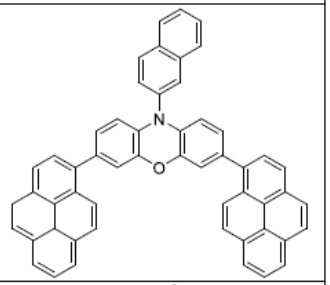 |
| OX14[15] | 382 (3.77) | | -1.88 | | | 0.30 | 2.18 | 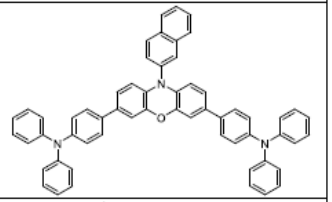 |
| OX15[15] | 369 (1.081) | | -1.60 | | | 0.54 | 2.14 | 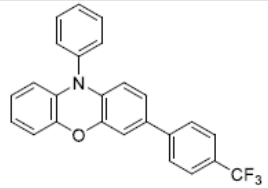 |
| OX16[104] (MeCN) | 383 (2.70) | | | -1.98 | | 0.72 | 2.86 | 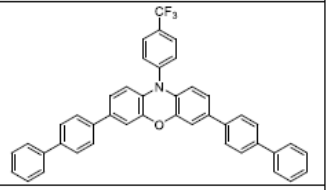 |
| **Xanthene** | | | | | | | | |

| **Photocatalyst (solvent)** | **$\lambda_{max,abs}$ ($\varepsilon$ ($10^4$ $M^{-1}cm^{-1}$))** | **$\tau_0$** | ***$E_{red1/2}$ (V vs SCE)** | ***$E_{ox1/2}$ (V vs SCE)** | **$E_{red1/2}$ (V vs SCE)** | ***$E_{ox1/2}$ (V vs SCE)** | **$E_{00}$** | **Structure** |
|---|---|---|---|---|---|---|---|---|
| Fluorescein[127-129] (MeOH) | 491 ($H_2O$) | 4.73 ns | | | -1.22 | 0.83 | | 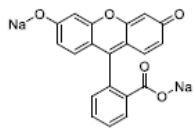 |
| Rose Bengal[127, 130] (MeOH) | 549 | 0.50 ns | 1.18 | -1.33 | -0.99 | 0.84 | 2.17 | 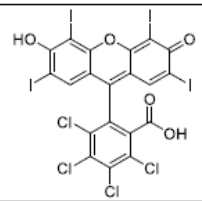 |
| Eosin Y (MeCN) | 528 (7.78) | 4.1 ns | 1.30 | -1.53 | -1.00 | 0.77 | 2.30 | 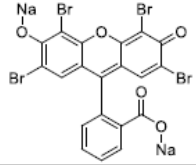 |
| E-$ph_3$ (MeCN) | 550 (4.16 | 3.4 ns | 1.10 | -1.82 | -1.11 | 0.39 | 2.21 | 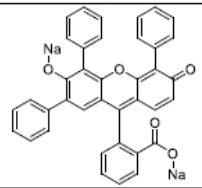 |
| E-trifluoromethylph$_3$ (MeCN) | 553 (4.98) | 4.1 ns | 1.20 | -1.65 | -0.99 | 0.54 | 2.19 | 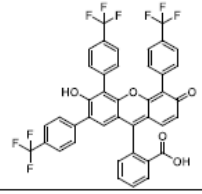 |

| **Photocatalyst (solvent)** | **$\lambda_{max,abs}$ ($\varepsilon$ ($10^4$ $M^{-}cm^{-}$))** | **$\tau_0$** | ***$E_{red1/2}$ (V vs SCE)** | ***$E_{ox1/2}$ (V vs SCE)** | **$E_{red1/2}$ (V vs SCE)** | ***$E_{ox1/2}$ (V vs SCE)** | **$E_{00}$** | **Structure** |
|---|---|---|---|---|---|---|---|---|
| E-tertbutylph$_3$ (MeCN) | 559 (6.01) | 2.7 ns | 1.14 | -1.89 | -1.06 | 0.31 | 2.20 | 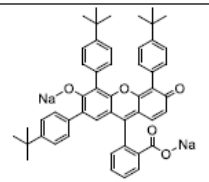 |
| E-naph$_3$ (MeCN) | 564 4.88) | 3.2 ns | 1.12 | -1.72 | -1.08 | 0.48 | 2.20 | 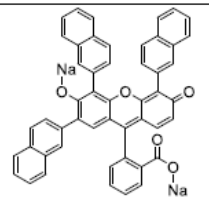 |

## 1.9 Reference


1. Pitre, S. P.; McTiernan, C. D.; Scaiano, J. C., Library of cationic organic dyes for visible-light-driven photoredox transformations. *ACS omega* **2016,** *1* (1), 66-76.

2. Juris, A.; Balzani, V.; Barigelletti, F.; Campagna, S.; Belser, P. l.; von Zelewsky, A. v., Ru (II) polypyridine complexes: photophysics, photochemistry, eletrochemistry, and chemiluminescence. *Coord. Chem. Rev.* **1988,** *84*, 85-277.

3. Flamigni, L.; Barbieri, A.; Sabatini, C.; Ventura, B.; Barigelletti, F., Photochemistry and photophysics of coordination compounds: iridium. In *Photochemistry and Photophysics of Coordination Compounds II*, Springer: 2007; pp 143-203.

4. Ballardini, R.; Varani, G.; Indelli, M. T.; Scandola, F.; Balzani, V., Free energy correlation of rate constants for electron transfer quenching of excited transition metal complexes. *J. Am. Chem. Soc.* **1978,** *100* (23), 7219-7223.

5. Jun Xuan, W.-J. X., Visible Light Photoredox Catalysis. *Angew. Chem.* **2012,** *51*, 6828-6838.

6. Prier, C. K., Rankic, D. A., MacMillan, D. W. C., Visible Light Photoredox Catalysis with Transition Metal Complexes: Applications in Organic Synthesis. *Chem. Rev.* **2013,** *113*, 5322-5363.

7. Yoon, T. P., Ischay, M. A., Du, J., Visible light photocatalysis as a greener approach to photochemical synthesis. *Nature Chem.* **2010,** *2*, 527-532.

8. Zeitler, K., Photoredox catalysis with visible light. *Angew. Chem. Int. Edit.* **2009,** *48* (52), 9785-9789.

9. Tucker, J. W.; Stephenson, C. R., Shining light on photoredox catalysis: theory and synthetic applications. *J. Org. Chem.* **2012,** *77* (4), 1617-1622.

10. Dumur, F., Recent Advances on Visible Light Metal-Based Photocatalysts for Polymerization under Low Light Intensity. *Catalysts* **2019,** *9* (9), 736-776.

11. Nazeeruddin, M. K.; Baranoff, E.; Grätzel, M., Dye-sensitized solar cells: a brief overview. *Sol. Energy* **2011,** *85* (6), 1172-1178.

12. Grätzel, M., Dye-sensitized solar cells. *J. Photoch. Photobio. C* **2003,** *4* (2), 145-153.

13. Hagfeldt, A.; Boschloo, G.; Sun, L.; Kloo, L.; Pettersson, H., Dye-sensitized solar cells. *Chem. Rev. (Washington, DC, U. S.)* **2010,** *110* (11), 6595-6663.

14. Dasgupta, S.; Brunschwig, B. S.; Winkler, J. R.; Gray, H. B., Solar fuels editorial. *Chem. Soc. Rev.* **2013,** *42* (6), 2213-2214.

15. McCarthy, B. G.; Pearson, R. M.; Lim, C.-H.; Sartor, S. M.; Damrauer, N. H.; Miyake, G. M., Structure–property relationships for tailoring phenoxazines as reducing photoredox catalysts. *J. Am. Chem. Soc.* **2018,** *140* (15), 5088-5101.

16. Du, Y.; Pearson, R. M.; Lim, C. H.; Sartor, S. M.; Ryan, M. D.; Yang, H.; Damrauer, N. H.; Miyake, G. M., Strongly reducing, visible-light organic photoredox catalysts as sustainable alternatives to precious metals. *Chem-Eur. J.* **2017,** *23* (46), 10962-10968.

17. McCusker, J. K., Femtosecond absorption spectroscopy of transition metal charge-transfer complexes. *Acc. Chem. Res.* **2003,** *36* (12), 876-887.

18. Yeh, A. T.; Shank, C. V.; McCusker, J. K., Ultrafast electron localization dynamics following photo-induced charge transfer. *Science* **2000,** *289* (5481), 935-938.

19. Zhang, Y.; Petersen, J. L.; Milsmann, C., A luminescent zirconium (IV) complex as a molecular photosensitizer for visible light photoredox catalysis. *J. Am. Chem. Soc.* **2016,** *138* (40), 13115-13118.

20. Azzaroni, O., Polymer Brushes Here, There, and Everywhere: Recent Advances in their Practical Applications and Emerging Opportunities in Multiple Research Fields. *J. Polym. Sci. A Polym. Chem.* **2012,** *50* (16), 3225-3258.

21. Hari, D. P., Konig, B., Synthetic applications of eosin Y in photoredox catalysis. *Chem. Commun.* **2014,** *50*, 6688-6699.

22. Nicewicz, D. A., Nguyen, T. M., Recent Applications of Organic Dyes as Photoredox Catalyst in Organic Synthesis. *ACS Catal.* **2013,** *4* (1), 355-360.

23. Majek, M., Filace, F., von Wangelin, A. J., On the mechanism of photocatalytic reactions with eosin Y. *Beilstein J. Org. Chem.* **2014,** *10*, 981-989.

24. Srivastava, V.; Singh, P. P., Eosin Y catalysed photoredox synthesis: a review. *RSC Adv.* **2017,** *7* (50), 31377-31392.

25. Pitre, S. P.; McTiernan, C. D.; Ismaili, H.; Scaiano, J. C., Mechanistic insights and kinetic analysis for the oxidative hydroxylation of arylboronic acids by visible light photoredox catalysis: A metal-free alternative. *J. Am. Chem. Soc.* **2013,** *135* (36), 13286-13289.

26. Guo, S.; Zhang, H.; Huang, L.; Guo, Z.; Xiong, G.; Zhao, J., Porous material-immobilized iodo-Bodipy as an efficient photocatalyst for photoredox catalytic organic reaction to prepare pyrrolo [2, 1-a] isoquinoline. *Chem. Commun. (Cambridge, U. K.)* **2013,** *49* (77), 8689-8691.

27. Huang, L.; Zhao, J.; Guo, S.; Zhang, C.; Ma, J., Bodipy derivatives as organic triplet photosensitizers for aerobic photoorganocatalytic oxidative coupling of amines and photooxidation of dihydroxylnaphthalenes. *J. Org. Chem.* **2013,** *78* (11), 5627-5637.

28. Heitz, D. R.; Rizwan, K.; Molander, G. A., Visible-Light-Mediated Alkenylation, Allylation, and Cyanation of Potassium Alkyltrifluoroborates with Organic Photoredox Catalysts. *J. Org. Chem.* **2016,** *81* (16), 7308-7313.

29. Neumann, M.; Füldner, S.; König, B.; Zeitler, K., Metal-free, cooperative asymmetric organophotoredox catalysis with visible light. *Angew. Chem. Int. Edit.* **2011,** *50* (4), 951-954.

30. Gassman, P. G.; Bottorff, K. J., Photoinduced lactonization. A useful but mechanistically complex single electron transfer process. *J. Am. Chem. Soc.* **1987,** *109* (24), 7547-7548.

31. Lewis, F. D.; Dykstra, R. E.; Gould, I. R.; Farid, S., Cage escape yields and direct observation of intermediates in photoinduced electron-transfer reactions of cis-and trans-stilbene. *J. Phys. Chem.* **1988,** *92* (25), 7042-7043.

32. Romero, N. A., Nicewicz, D. A., Organic Photoredox Catalysis. *Chem. Rev. (Washington, DC, U. S.)* **2016,** *116* (17), 10075-10166.

33. Speckmeier, E.; Fischer, T. G.; Zeitler, K., A toolbox approach to construct broadly applicable metal-free catalysts for photoredox chemistry: deliberate tuning of redox potentials and importance of halogens in donor–acceptor cyanoarenes. *J. Am. Chem. Soc.* **2018,** *140* (45), 15353-15365.

34. Shang, T.-Y.; Lu, L.-H.; Cao, Z.; Liu, Y.; He, W.-M.; Yu, B., Recent advances of 1, 2, 3, 5-tetrakis (carbazol-9-yl)-4, 6-dicyanobenzene (4CzIPN) in photocatalytic transformations. *Chem. Commun. (Cambridge, U. K.)* **2019,** *55* (38), 5408-5419.

35. Song, Z.-Y.; Zhang, C.-L.; Ye, S., Visible light promoted coupling of alkynyl bromides and Hantzsch esters for the synthesis of internal alkynes. *Org. Biomol. Chem.* **2019,** *17* (1), 181-185.

36. Sherwood, T. C.; Xiao, H.-Y.; Bhaskar, R. G.; Simmons, E. M.; Zaretsky, S.; Rauch, M. P.; Knowles, R. R.; Dhar, T. M., Decarboxylative intramolecular arene alkylation using N-(acyloxy) phthalimides, an organic photocatalyst, and visible light. *J. Org. Chem.* **2019,** *84* (13), 8360-8379.

37. Patel, N. R.; Kelly, C. B.; Siegenfeld, A. P.; Molander, G. A., Mild, redox-neutral alkylation of imines enabled by an organic photocatalyst. *ACS Catal.* **2017,** *7* (3), 1766-1770.

38. Lima, F.; Grunenberg, L.; Rahman, H. B.; Labes, R.; Sedelmeier, J.; Ley, S. V., Organic photocatalysis for the radical couplings of boronic acid derivatives in batch and flow. *Chem. Commun. (Cambridge, U. K.)* **2018,** *54* (44), 5606-5609.

39. Jiang, H.; Studer, A., Transition-Metal-Free Three-Component Radical 1, 2-Amidoalkynylation of Unactivated Alkenes. *Chem-Eur. J.* **2019,** *25* (2), 516-520.

40. Huang, Z.; Gu, Y.; Liu, X.; Zhang, L.; Cheng, Z.; Zhu, X., Metal-Free Atom Transfer Radical Polymerization of Methyl Methacrylate with ppm Level of Organic Photocatalyst. *Macromol. Rapid Commun.* **2017,** *38* (10), 1600461.

41. Ju, T.; Fu, Q.; Ye, J. H.; Zhang, Z.; Liao, L. L.; Yan, S. S.; Tian, X. Y.; Luo, S. P.; Li, J.; Yu, D. G., Selective and Catalytic Hydrocarboxylation of Enamides and Imines

with CO2 to Generate α, α-Disubstituted α-Amino Acids. *Angew. Chem. Int. Edit.* **2018,** *57* (42), 13897-13901.

42. Santandrea, J.; Minozzi, C.; Cruché, C.; Collins, S. K., Photochemical Dual-Catalytic Synthesis of Alkynyl Sulfides. *Angew. Chem. Int. Edit.* **2017,** *56* (40), 12255-12259.

43. Joshi-Pangu, A., Levesque, F., Roth, H. G., Oliver, S. F., Campeau, L., Nicewicz, D., DiRocco, D. A., Acridinium-Based Photocatalysts: A Sustainable Option in Photoredox Catalyst. *J. Org. Chem.* **2016,** *81*, 7244-7249.

44. Ohkubo, K.; Kobayashi, T.; Fukuzumi, S., Direct oxygenation of benzene to phenol using quinolinium ions as homogeneous photocatalysts. *Angew. Chem. Int. Edit.* **2011,** *50* (37), 8652-8655.

45. Margrey, K. A.; Nicewicz, D. A., A general approach to catalytic alkene anti-Markovnikov hydrofunctionalization reactions via acridinium photoredox catalysis. *Acc. Chem. Res.* **2016,** *49* (9), 1997-2006.

46. Romero, N. A.; Nicewicz, D. A., Mechanistic insight into the photoredox catalysis of anti-markovnikov alkene hydrofunctionalization reactions. *J. Am. Chem. Soc.* **2014,** *136* (49), 17024-17035.

47. Benniston, A. C.; Harriman, A.; Li, P.; Rostron, J. P.; van Ramesdonk, H. J.; Groeneveld, M. M.; Zhang, H.; Verhoeven, J. W., Charge shift and triplet state formation in the 9-mesityl-10-methylacridinium cation. *J. Am. Chem. Soc.* **2005,** *127* (46), 16054-16064.

48. Fukuzumi, S.; Kotani, H.; Ohkubo, K.; Ogo, S.; Tkachenko, N. V.; Lemmetyinen, H., Electron-transfer state of 9-mesityl-10-methylacridinium ion with a much longer

lifetime and higher energy than that of the natural photosynthetic reaction center. *J. Am. Chem. Soc.* **2004,** *126* (6), 1600-1601.

49. White, A. R.; Wang, L.; Nicewicz, D. A., Synthesis and Characterization of Acridinium Dyes for Photoredox Catalysis. *Synlett* **2019,** *30* (07), 827-832.

50. Fagnoni, M.; Dondi, D.; Ravelli, D.; Albini, A., Photocatalysis for the Formation of the C− C Bond. *Chem. Rev. (Washington, DC, U. S.)* **2007,** *107* (6), 2725-2756.

51. Gesmundo, N. J.; Grandjean, J.-M. M.; Nicewicz, D. A., Amide and amine nucleophiles in polar radical crossover cycloadditions: synthesis of γ-lactams and pyrrolidines. *Org. Lett.* **2015,** *17* (5), 1316-1319.

52. Nguyen, T. M.; Nicewicz, D. A., Anti-Markovnikov hydroamination of alkenes catalyzed by an organic photoredox system. *J. Am. Chem. Soc.* **2013,** *135* (26), 9588-9591.

53. Fukuzumi, S.; Ohkubo, K.; Suenobu, T., Long-lived charge separation and applications in artificial photosynthesis. *Acc. Chem. Res.* **2014,** *47* (5), 1455-1464.

54. Hering, T.; Slanina, T.; Hancock, A.; Wille, U.; König, B., Visible light photooxidation of nitrate: the dawn of a nocturnal radical. *Chem. Commun. (Cambridge, U. K.)* **2015,** *51* (30), 6568-6571.

55. Romero, N. A.; Margrey, K. A.; Tay, N. E.; Nicewicz, D. A., Site-selective arene CH amination via photoredox catalysis. *Science* **2015,** *349* (6254), 1326-1330.

56. Matsui, J. K.; Molander, G. A., Organocatalyzed, Photoredox Heteroarylation of 2-Trifluoroboratochromanones via C–H Functionalization. *Org. Lett.* **2017,** *19* (4), 950-953.

57. Kotani, H.; Ohkubo, K.; Fukuzumi, S., Photocatalytic oxygenation of anthracenes and olefins with dioxygen via selective radical coupling using 9-mesityl-10-methylacridinium ion as an effective electron-transfer photocatalyst. *J. Am. Chem. Soc.* **2004,** *126* (49), 15999-16006.

58. Meyer, A. U.; Berger, A. L.; König, B., Metal-free C–H sulfonamidation of pyrroles by visible light photoredox catalysis. *Chem. Commun. (Cambridge, U. K.)* **2016,** *52* (72), 10918-10921.

59. Hering, T.; Meyer, A. U.; König, B., Photocatalytic anion oxidation and applications in organic synthesis. *J. Org. Chem.* **2016,** *81* (16), 6927-6936.

60. Perkowski, A. J.; Nicewicz, D. A., Direct catalytic anti-Markovnikov addition of carboxylic acids to alkenes. *J. Am. Chem. Soc.* **2013,** *135* (28), 10334-10337.

61. Das, M.; Vu, M. D.; Zhang, Q.; Liu, X.-W., Metal-free visible light photoredox enables generation of carbyne equivalents via phosphonium ylide C–H activation. *Chemical science* **2019,** *10* (6), 1687-1691.

62. Perkin, W. H., LXXIV.—On mauveine and allied colouring matters. *J. Chem. Soc.* **1879,** *35*, 717-732.

63. Laursen, J. B.; Nielsen, J., Phenazine natural products: biosynthesis, synthetic analogues, and biological activity. *Chem. Rev. (Washington, DC, U. S.)* **2004,** *104* (3), 1663-1686.

64. Venkataraman, K., *The chemistry of synthetic dyes*. Elsevier: 2012; Vol. 4.

65. Kirk, R. E.; Othmer, D. F.; Mann, C. A., Encyclopedia of Chemical Technology. Vol. II. *J. Phys. Chem.* **1949,** *53* (4), 591-591.

66. Dietrich, L. E.; Teal, T. K.; Price-Whelan, A.; Newman, D. K., Redox-active antibiotics control gene expression and community behavior in divergent bacteria. *Science* **2008,** *321* (5893), 1203-1206.

67. Theriot, J. C.; Lim, C.-H.; Yang, H.; Ryan, M. D.; Musgrave, C. B.; Miyake, G. M., Organocatalyzed atom transfer radical polymerization driven by visible light. *Science* **2016,** *352* (6289), 1082-1086.

68. Koyama, D.; Dale, H. J.; Orr-Ewing, A. J., Ultrafast observation of a photoredox reaction mechanism: photoinitiation in organocatalyzed atom-transfer radical polymerization. *J. Am. Chem. Soc.* **2018,** *140* (4), 1285-1293.

69. Cole, J. P.; Federico, C. R.; Lim, C.-H.; Miyake, G. M., Photoinduced organocatalyzed atom transfer radical polymerization using low ppm catalyst loading. *Macromolecules* **2019,** *52* (2), 747-754.

70. Podemska, K.; Podsiadły, R.; Szymczak, A. M.; Sokołowska, J., Diazobenzo [a] fluorene derivatives as visible photosensitizers for free radical polymerization. *Dyes Pigm.* **2012,** *94* (1), 113-119.

71. Podemska, K.; Podsiadly, R.; Orzel, A.; Sokołowska, J., The photochemical behavior of benzo [a] pyrido [2′, 1′: 2, 3] imidazo [4, 5-c] phenazine dyes. *Dyes Pigm.* **2013,** *99* (3), 666-672.

72. Kayser, R.; Young, R., The photoreduction of methylene blue by amines—I. A flash photolysis study of the reaction between triplet methylene blue and amines. *Photochem. Photobiol.* **1976,** *24* (5), 395-401.

73. Ohlow, M. J.; Moosmann, B., Phenothiazine: the seven lives of pharmacology's first lead structure. *Drug Discov. Today* **2011,** *16* (3-4), 119-131.

74. Weil, L.; Seibles, T. S.; Herskovits, T. T., Photooxidation of bovine insulin sensitized by methylene blue. *Arch. Biochem. Biophys.* **1965,** *111* (2), 308-320.

75. Timpe, H.-J.; Neuenfeld, S., Photoreduction of some dyes by styrene. *J. Chem. Soc., Faraday Trans.* **1992,** *88* (16), 2329-2336.

76. Ohno, T.; Lichtin, N. N., Electron transfer in the quenching of triplet methylene blue by complexes of iron (II). *J. Am. Chem. Soc.* **1980,** *102* (14), 4636-4643.

77. Steiner, U.; Winter, G.; Kramer, H. E., Investigation of physical triplet quenching by electron donors. *J. Phys. Chem.* **1977,** *81* (11), 1104-1110.

78. Fischer, H.; Kramer, H. E.; Maute, A., Blitzlichtuntersuchungen über die ausbleichreaktion von thionin mit allylthioharnstoff, II. *Z. Phys. Chem. (Muenchen, Ger.)* **1970,** *69* (3_4), 113-131.

79. Cocquet, G.; Ferroud, C.; Guy, A., A mild and efficient procedure for ring-opening reactions of piperidine and pyrrolidine derivatives by single electron transfer photooxidation. *Tetrahedron* **2000,** *56* (19), 2975-2984.

80. Pitre, S. P.; McTiernan, C. D.; Ismaili, H.; Scaiano, J. C., Metal-free photocatalytic radical trifluoromethylation utilizing methylene blue and visible light irradiation. *ACS Catal.* **2014,** *4* (8), 2530-2535.

81. Jiang, H.; Mao, G.; Wu, H.; An, Q.; Zuo, M.; Guo, W.; Xu, C.; Sun, Z.; Chu, W., Synthesis of dibenzocycloketones by acyl radical cyclization from aromatic carboxylic acids using methylene blue as a photocatalyst. *Green Chem.* **2019,** *21* (19), 5368-5373.

82. Zhang, H.; Zhan, Z.; Lin, Y.; Shi, Y.; Li, G.; Wang, Q.; Deng, Y.; Hai, L.; Wu, Y., Visible light photoredox catalyzed thiophosphate synthesis using methylene blue as a promoter. *Org. Chem. Front.* **2018,** *5* (9), 1416-1422.

83. Alonso, F.; Beletskaya, I. P.; Yus, M., Metal-Mediated Reductive Hydrodehalogenation of Organic Halides. *Chem. Rev. (Washington, DC, U. S.)* **2002,** *102* (11), 4009-4092.

84. Poelma, S. O.; Burnett, G. L.; Discekici, E. H.; Mattson, K. M.; Treat, N. J.; Luo, Y.; Hudson, Z. M.; Shankel, S. L.; Clark, P. G.; Kramer, J. W., Chemoselective radical dehalogenation and C–C bond formation on aryl halide substrates using organic photoredox catalysts. *J. Org. Chem.* **2016,** *81* (16), 7155-7160.

85. Stockmann, A.; Kurzawa, J.; Fritz, N.; Acar, N.; Schneider, S.; Daub, J.; Engl, R.; Clark, T., Conformational control of photoinduced charge separation within phenothiazine− pyrene dyads. *J. Phys. Chem. A* **2002,** *106* (34), 7958-7970.

86. Manav, N.; Verma, V.; Pandey, V.; Rather, H.; Vasita, R.; Gupta, I., Synthesis and studies of phenothiazine based AIE fluorogens. *Indian J. Chem. Sec. B* **2019,** *58B*, 238-246.

87. Treat, N. J.; Sprafke, H.; Kramer, J. W.; Clark, P. G.; Barton, B. E.; Read de Alaniz, J.; Fors, B. P.; Hawker, C. J., Metal-free atom transfer radical polymerization. *J. Am. Chem. Soc.* **2014,** *136* (45), 16096-16101.

88. Discekici, E. H.; Pester, C. W.; Treat, N. J.; Lawrence, J.; Mattson, K. M.; Narupai, B.; Toumayan, E. P.; Luo, Y.; McGrath, A. J.; Clark, P. G., Simple benchtop approach to polymer brush nanostructures using visible-light-mediated metal-free atom transfer radical polymerization. *ACS Macro Lett.* **2016,** *5* (2), 258-262.

89. Pan, X.; Lamson, M.; Yan, J.; Matyjaszewski, K., Photoinduced metal-free atom transfer radical polymerization of acrylonitrile. *ACS Macro Lett.* **2015,** *4* (2), 192-196.

90. Chen, M.; MacLeod, M. J.; Johnson, J. A., Visible-light-controlled living radical polymerization from a trithiocarbonate iniferter mediated by an organic photoredox catalyst. *ACS Macro Lett.* **2015,** *4* (5), 566-569.

91. Yan, J.; Pan, X.; Schmitt, M.; Wang, Z.; Bockstaller, M. R.; Matyjaszewski, K., Enhancing initiation efficiency in metal-free surface-initiated atom transfer radical polymerization (SI-ATRP). *ACS Macro Lett.* **2016,** *5* (6), 661-665.

92. Boyington, A. J.; Seath, C. P.; Zearfoss, A. M.; Xu, Z.; Jui, N. T., Catalytic Strategy for Regioselective Arylethylamine Synthesis. *J. Am. Chem. Soc.* **2019,** *141* (9), 4147-4153.

93. Discekici, E. H.; Treat, N. J.; Poelma, S. O.; Mattson, K. M.; Hudson, Z. M.; Luo, Y.; Hawker, C. J.; de Alaniz, J. R., A highly reducing metal-free photoredox catalyst: design and application in radical dehalogenations. *Chem. Commun. (Cambridge, U. K.)* **2015,** *51* (58), 11705-11708.

94. Ma, B.; Lu, F.; Yang, H.; Gu, X.; Li, Z.; Li, R.; Pei, H.; Luo, D.; Zhang, H.; Lei, A., Visible Light Mediated External Oxidant Free Selective C5 Bromination of 8-Aminoquinoline Amides under Ambient Conditions. *Asian J. Org. Chem.* **2019,** *8* (7), 1136-1140.

95. Smith, J. L., On the simultaneous staining of neutral fat and fatty acid by oxazine dyes. *J Pathol Bacteriol* **1908,** *12* (1), 1-4.

96. Lin, C.-W.; Shulok, J. R.; Kirley, S. D.; Cincotta, L.; Foley, J. W., Lysosomal localization and mechanism of uptake of Nile blue photosensitizers in tumor cells. *Cancer Res.* **1991,** *51* (10), 2710-2719.

97. Daehne, S.; Resch-Genger, U.; Wolfbeis, O. S., *Near-infrared dyes for high technology applications*. Springer Science & Business Media: 2012; Vol. 52.

98. Jose, J.; Burgess, K., Benzophenoxazine-based fluorescent dyes for labeling biomolecules. *Tetrahedron* **2006,** *62* (48), 11021-11037.

99. Greenspan, P.; Mayer, E. P.; Fowler, S. D., Nile red: a selective fluorescent stain for intracellular lipid droplets. *J. Cell Biol.* **1985,** *100* (3), 965-973.

100. Sartor, S. M.; Lattke, Y. M.; McCarthy, B. G.; Miyake, G. M.; Damrauer, N. H., Effects of Naphthyl Connectivity on the Photophysics of Compact Organic Charge-Transfer Photoredox Catalysts. *J. Phys. Chem. A* **2019,** *123* (22), 4727-4736.

101. Berger, A. L.; Donabauer, K.; König, B., Photocatalytic Barbier reaction–visible-light induced allylation and benzylation of aldehydes and ketones. *Chemical science* **2018,** *9* (36), 7230-7235.

102. Ramsey, B. L.; Pearson, R. M.; Beck, L. R.; Miyake, G. M., Photoinduced organocatalyzed atom transfer radical polymerization using continuous flow. *Macromolecules* **2017,** *50* (7), 2668-2674.

103. McCarthy, B.; Miyake, G. M., Organocatalyzed atom transfer radical polymerization catalyzed by core modified N-aryl phenoxazines performed under air. *ACS Macro Lett.* **2018,** *7* (8), 1016-1021.

104. Lee, D. S.; Kim, C. S.; Iqbal, N.; Park, G. S.; Son, K.-s.; Cho, E. J., Organophotocatalytic Arene Functionalization: C–C and C–B Bond Formation. *Org. Lett.* **2019,** *21*, 9950-9953.

105. Shi, L.; Xia, W., Photoredox functionalization of C–H bonds adjacent to a nitrogen atom. *Chem. Soc. Rev.* **2012,** *41* (23), 7687-7697.

106. Pan, Y.; Kee, C. W.; Chen, L.; Tan, C.-H., Dehydrogenative coupling reactions catalysed by Rose Bengal using visible light irradiation. *Green Chem.* **2011,** *13* (10), 2682-2685.

107. Yajima, T.; Ikegami, M., Metal-Free Visible-Light Radical Iodoperfluoroalkylation of Terminal Alkenes and Alkynes. *Eur. J. Org. Chem.* **2017,** *2017* (15), 2126-2129.

108. Choi, A.; Miller, S. C., Silicon Substitution in Oxazine Dyes Yields Near-Infrared Azasiline Fluorophores That Absorb and Emit beyond 700 nm. *Org. Lett.* **2018,** *20* (15), 4482-4485.

109. Ghosh, I.; Ghosh, T.; Bardagi, J. I.; König, B., Reduction of aryl halides by consecutive visible light-induced electron transfer processes. *Science* **2014,** *346* (6210), 725-728.

110. Ghosh, I.; Marzo, L.; Das, A.; Shaikh, R.; König, B., Visible light mediated photoredox catalytic arylation reactions. *Acc. Chem. Res.* **2016,** *49* (8), 1566-1577.

111. Li, Z.; Zhang, W.; Zhao, Q.; Gu, H.; Li, Y.; Zhang, G.; Zhang, F.; Fan, X., Eosin Y covalently anchored on reduced graphene oxide as an efficient and recyclable photocatalyst for the aerobic oxidation of α-aryl halogen derivatives. *ACS Sustain. Chem. Eng.* **2015,** *3* (3), 468-474.

112. Rohokale, R. S.; Koenig, B.; Dhavale, D. D., Synthesis of 2, 4, 6-trisubstituted pyridines by oxidative Eosin Y photoredox catalysis. *J. Org. Chem.* **2016,** *81* (16), 7121-7126.

113. Yan, D. M.; Chen, J. R.; Xiao, W. J., New Roles for Photoexcited Eosin Y in Photochemical Reactions. *Angew. Chem. Int. Edit.* **2019,** *58* (2), 378-380.

114. Hering, T.; Hari, D. P.; König, B., Visible-light-mediated α-arylation of enol acetates using aryl diazonium salts. *J. Org. Chem.* **2012,** *77* (22), 10347-10352.

115. Edmondson, S.; Danishefsky, S. J.; Sepp-Lorenzino, L.; Rosen, N., Total synthesis of spirotryprostatin A, leading to the discovery of some biologically promising analogues. *J. Am. Chem. Soc.* **1999,** *121* (10), 2147-2155.

116. Goehring, R. R.; Sachdeva, Y. P.; Pisipati, J. S.; Sleevi, M. C.; Wolfe, J. F., Photoinduced cyclizations of mono-and dianions of N-acyl-o-chloroanilines and N-acyl-o-chlorobenzylamines as general methods for the synthesis of oxindoles and 1, 4-dihydro-3 (2H)-isoquinolinones. *J. Am. Chem. Soc.* **1985,** *107* (2), 435-443.

# CHAPTER 2

# SYNTHESIS AND CHARACTERIZATION OF NEW EOSIN Y BASED ORGANIC PHOTOCATALYSTS

## 2.1 Abstract

Organic photocatalysts have shown great potential in recent years. In order to effectively replace transition metal photocatalysts, this study focused on mirroring the tuning of these complexes and applied it to organic photocatalysts. In order to design a series of organic photoredox compounds with a broad range of reactivity, the photocatalyst Eosin Y, a xanthene derivative, was chosen as a precursor to synthesize a new series of organic photocatalysts. The synthesis, characterization, and catalytic evaluation of these tunable organic light absorbing complexes was undertaken. Substitutions of the bromine atoms of Eosin Y led to four previously unreported photocatalysts with tunable properties. Reduction potentials of this series of photocatalysts varied by 110 mV, which shows these catalysts can be tuned for specific reactions. The excited state lifetimes (ns) of the new photocatalysts are comparable to those of the parent complex, but the $\lambda_{max}$ for absorbance was strongly red-shifted into the green light section of the solar spectrum. The measured fluorescence quantum yields ranging from 0.39 to 0.65 and outperformed most transition metal photocatalysts. To demonstrate the application and performance of this series, the new organic photocatalysts were used for the catalytic enol arylation. The high tunability of these dyes lead to rational design of organic photocatalysts for specific subsets of reactions.

## 2.2 Introduction

Photocatalysis is one of the fastest growing fields in the past decade, due to the unique reactivity and ability to meet a growing need for sustainable processes. Photocatalytic systems have been used as powerful and valuable strategies for the activation of organic molecules while maintaining mild reaction conditions. This catalytic approach has shown great promise for the synthesis of natural products, highly valued in the pharmaceutical industry.[5-7, 22, 32, 113, 117] Photoredox catalysis offers a unique ability to selectively activate the photocatalyst, due to the inability of most organic molecules to absorb visible light. The development of photoactive catalysts capable of initiating electron/energy transfer reactions from reactive photoexcited states, applicable toward a range of processes including carbon dioxide transformation, proton reduction, water oxidation, numerous organic coupling syntheses, polymerization, and access radical pathways. [10, 15, 117-118] Single electron transfer is initiated by visible light absorption, produces the unique reactivity required for photoactive systems. Photocatalysis can proceed through two different quenching cycles, reductive and oxidative as seen in Figure 2.1. After visible light excitation of the photocatalyst (PC), the reductive path proceeds with a single electron transfer from a substrate or sacrificial electron donor (B) to the PC, followed by the reduction of a substrate (A). The oxidative pathway proceeds through initial reduction of A followed by B reducing the PC to its original state.

Utilization of visible light, the most abundant part of the solar spectrum, allows for a greener approach to many established systems and opens a multitude of new elegant synthetic pathways previously thought impossible. At the forefront of photocatalysis are transition metal based photocatalysts particularly those with ruthenium(II) and

iridium(III) centers.[16-18, 29] Ruthenium(II) and iridium(III) polypyridyl photocatalysts have been extensively utilized due to having desirable properties including a range of redox potentials, excited state lifetimes in the millisecond range, and chemical stability. Even with these advantages, transition metal complexes are not sustainable or cost effective due to the expense and toxicity of rare earth transition metals. Additionally transition metals can cause significant issues for the polymer and pharmaceutical industries, where a minute contamination of products can cause massive problems and profit loss.[15, 21, 43] In recent years organic based photocatalysts have been investigated, in an attempt to combat the inherent issues from transition metal catalysts, leading to a wide range of organic photocatalyst driven reactions.

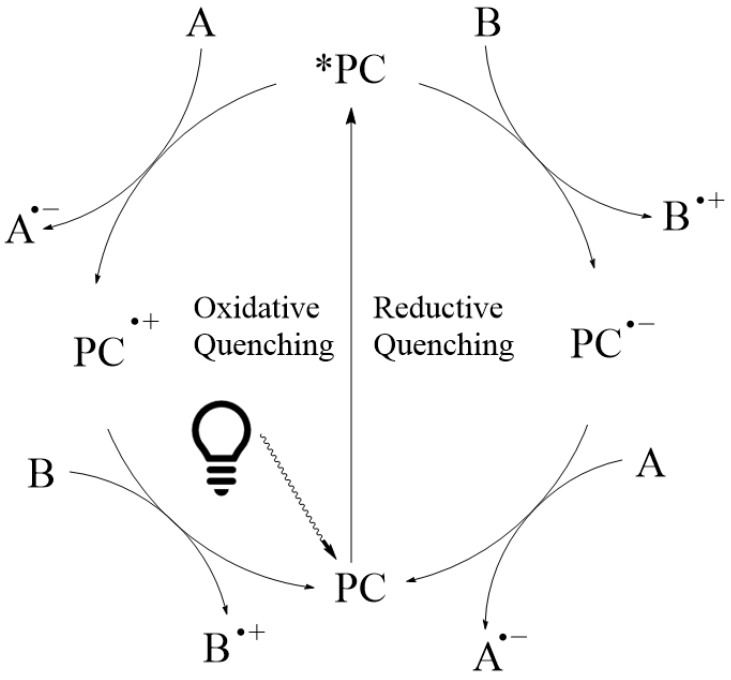


**Figure 2.1.** General reductive/oxidative scheme of photocatalysis.

Leading research has focused on the development and use of sustainable, inexpensive, and environmentally safe organic photocatalysts (PC), to replace the transition metal complexes. Organic PCs have been reported with a wide range of properties and some have been shown to out preform transition metal PCs.[15, 22, 28-29, 50, 93, 109, 119-123] Organic PCs have many advantages over metal based catalysts, including synthetic versatility, lower cost, and the ability to fine tune the spectral and electrochemical properties through known organic synthetic modifications.[124] Additionally, many of the reported organic PCs are environmentally benign.

The most desired organic photocatalysts are those that strongly and efficiently absorb visible light. While transition metal counterparts are dependent on MLCT (metal to ligand charge transfer), organic PCs rely on the analogous intramolecular charge transfer (CT).[15-16] Absorption of visible light initiates the catalytic cycle resulting in an outer sphere electron transfer as shown in Figure 2.1. The single electron transfer event is governed by the redox potentials of each substrate in the system, and the redox stability of the PC. Ideal organic PCs maintain redox reversibility, strong absorption in the visible spectrum, and high fluorescence quantum yields to avoid non-productive, non-radiative decay of the excited states. Though much work has been done in this area, there remains room for advancements, including the low solubility of many organic dyes in organic solvents and narrow redox windows compared to transition metal PCs.

Eosin Y, a xanthene derivative, has previously been investigated as a photoredox catalyst capable of partaking in both oxidative and reductive catalytic cycles. Examples of Eosin Y catalyzed reactions include direct C-H bond arylation, carbon-carbon and carbon-phosphorous bond formation, intermolecular C-H arylation, synthesis of triaryl

pyridines, and aromatic dehalogenation.[23-24, 112, 125-130] Xanthene derivatives show promise as photocatalysts due to the significant sustainability, commercial availability, low cost, and environmentally benign nature.[29] Eosin Y has also been shown to successfully replace transition metal PCs and to be more reactive than other related organic complexes, which encouraged us to look into the other possibilities of this organic dye.[28-29] However, there are drawbacks to using Eosin Y as a photocatalyst, including low solubility in organic solvents, four reactive $sp^2$ carbon–halogen bonds, and a shorter excited-state lifetime than transition metal PCs. In order to combat some of these issues, we set out to investigate the possibility of synthetically modifying the carbon-bromine bonds on the Eosin Y dianion (the parent complex) to create a new series of photocatalysts, as shown in Figure 2.2. Functionalizing the xanthene core of Eosin Y by eliminating the halogens served to increase the chemical stability of the PCs and increase the solubility of the new PCs in organic solvents.

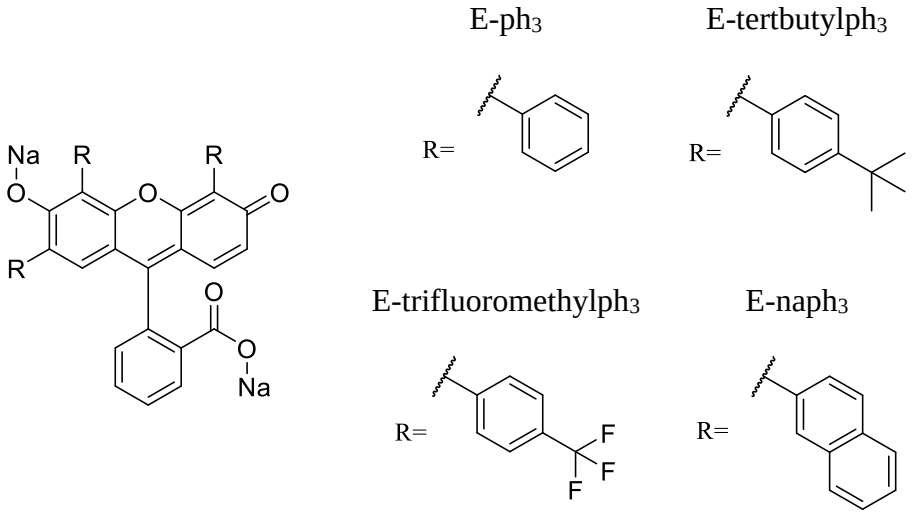


**Figure 2.2**. Eosin Y based photocatalysts series.

In this paper we report four new organic photocatalysts as part of a series of tunable catalysts based on Eosin Y. Among these are a phenyl (E-ph$_3$), a trifluoromethylphenyl (E-trifluoromethylph$_3$), a tertbutyl phenyl (E-tertbutylph$_3$), and a naphyl (E-naph$_3$) derivative. Electrochemical and photophysical characterization, including redox potentials, absorption and emission spectroscopy, fluorescence quantum yield, and excited state lifetimes are reported alongside the data for the reported Eosin Y parent complex. These PCs were also evaluated for catalytic performance through an α-arylation of enol acetates with aryl diazonium salts.[114]

### 2.3 Results and Discussion

**Table 2.1.** Photophysical data of new compounds. All data obtained in anhydrous acetonitrile. [a] Molar extinction coefficient (x $10^4$ $M^{-1}$ $cm^{-1}$). [b] $\lambda_{ex}$=490 nm

| Photocatalyst | $\lambda_{max,abs}$ ($\varepsilon$)[a] | $\lambda_{max,em}$[b] | $\Phi_{N2}$ | $\Phi_{air}$ | $\tau_{N2}$ | $\tau_{air}$ |
|---|---|---|---|---|---|---|
| E-ph$_3$ | 550 (4.16) | 575 | 0.51 | 0.47 | 3.4 ns | 3.2 ns |
| E-trifluoromethylph$_3$ | 553 (4.98) | 572 | 0.65 | 0.59 | 4.1 ns | 3.9 ns |
| E-tertbutylph$_3$ | 559 (6.01) | 579 | 0.39 | 0.39 | 2.7 ns | 2.7 ns |
| E-naph$_3$ | 564 (4.88) | 589 | 0.47 | 0.39 | 3.2 ns | 2.8 ns |
| Eosin Y | 528 (7.78) | 549 | 0.69 | 0.63 | 4.1 ns | 4.0 ns |

There is currently a compendium of knowledge about how photophysical properties affect the performance of PCs. Photophysical properties allow researchers to evaluate and rationally design a PC to specific reaction set ups, where the performance

lies heavily on the absorption of visible light and sufficient redox properties in order for the intended reaction to proceed. The photophysical properties of the four newly synthesized photocatalysts, summarized in Table 2.1, were thoroughly examined and compared against Eosin Y.

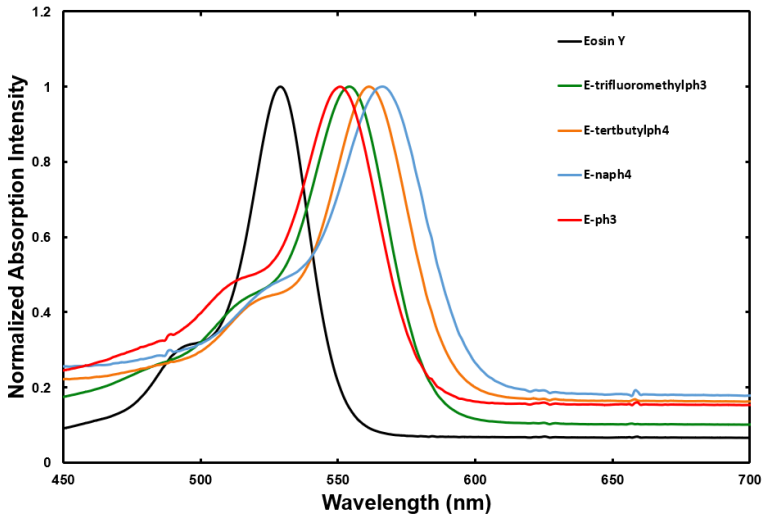


**Figure 2.3.** Overlay of absorption spectra in anhydrous acetonitrile.

In photocatalytic systems the visible light excitation is often the first step in the mechanism, for this purpose a thorough understanding of these photophysical properties is paramount. During excitation, photon absorption causes the electron excitation from the ground state, a π orbital (LUMO), to the π* orbital (HOMO).[129] The absorption spectra showing the $\lambda_{max,abs}$ for each of the new PCs is shown in Figure 2.3. The $\lambda_{max,abs}$ are red-shifted into the green section of the visible spectrum for each of the new PCs compared to the parent Eosin Y compound. The red shift of the absorption seen in the new PCs occurs due to the substitution of aryl groups onto the xanthene core of Eosin Y. This substitution stabilizes the π* orbital, which in turn allows the PC to absorb light of a

lower energy.[15] This trend is clearly seen in the steady increase of shift from Eosin Y's $\lambda_{max,abs}$, increasing steadily from the phenyl to the naphthyl functional groups (Figure 2.3). The shoulder peak in each of the spectra occurs due to the π-stacking between molecules and increases in magnitude proportional to concentration of the photocatalyst.[129]

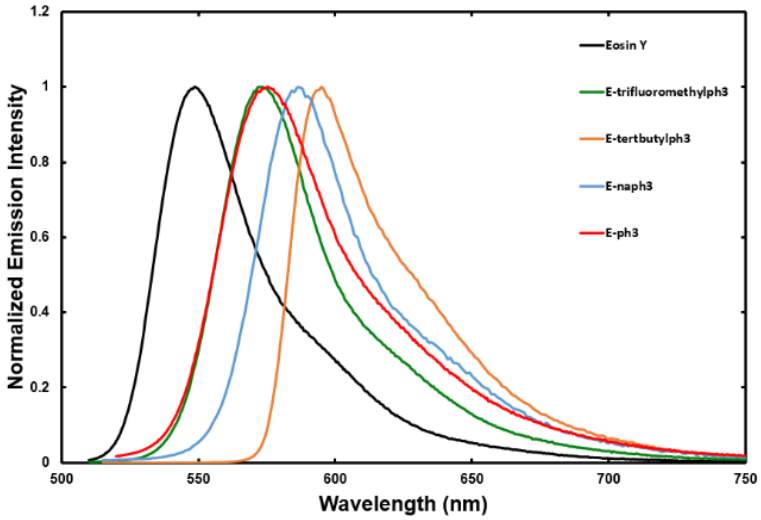


**Figure 2.4.** Overlay of emission spectra in anhydrous acetonitrile.

The $\lambda_{max,em}$ of each new PC was determined in MeCN and is shown in Figure 2.4 to avoid solvatochromic effects. The parent complex, Eosin Y, is a solvatochromic compound, meaning that its photophysical properties are highly susceptible to the polarity of the solvent in which it is dissolved. Analogous to the $\lambda_{max,abs}$ values reported above, the emission of the new organic PCs are shifted to longer wavelengths versus the parent Eosin Y. The smallest shift occurs with E-trifluoromethylph$_3$ which is likely due to the nine halogen groups that comprise the substituted functional groups.[15] Red shift of $\lambda_{max,em}$ is also due to the extension of the aryl core modifications with the emission of E-

$ph_3$ at 575 nm and E-$naph_3$ at 589 nm, shifting 26 and 40 nm respectively and correlating with the increasing aromaticity of each functional group. The red shifts observed are indicative of the alteration occurring with the π* orbital due to functionalization of the xanthene core.

Large magnitude molar extinction coefficients are essential to photoactive catalysts. Typical transition metal PCs, such as polypyridal iridium(III) and ruthenium(II) complexes, absorb in the UV and blue region, and have molar extinction coefficient values at about 13,100 $M^{-1}$ $cm^{-1}$.[16] Organic photocatalysts absorb far more light in the visible range, for instance the molar extinction coefficient for Eosin Y is 77,800 $M^{-1}$ $cm^{-1}$. The molar extinction coefficient values for this series of new PCs are reported in Table 2.1, with values on par with the parent PC, such as E-$naph_3$ with a value of 48,800 $M^{-1}$ $cm^{-1}$ and exceeding the transition metal PCs. E-trifluoromethyl$ph_3$ with a value of 49,800 $M^{-1}$ $cm^{-1}$. These molar extinction coefficient values support that not only does the new series of organic PCs absorb better than transition metal PCs, but they absorb further into the visible range taking advantage of the most abundant region of the visible light spectrum.

Fluorescence quantum yield (Φ) for each photocatalyst was determined through utilization of the emission data observed. These values are inversely proportional to the amount of energy lost to nonradiative decay. Quantum yield needs to be high because photocatalytic systems depend on the energy absorbed by the PC and translated into electronic energy. The parent PC, Eosin Y, is found to have a Φ of 0.69. Each of the functionalized PCs reported in this study maintain moderate to high Φs and are efficient absorbers of visible light, losing little energy to nonradiative decay.

Excited state lifetimes (τ) of PCs are essential to photocatalysis and must be sufficient for the intermolecular electron transfers to occur. Lifetimes were obtained for all new PCs, including the parent complex, and summarized in Table 2.1. The lifetimes were determined by from steady-state and time-resolved emission decay data. The overlap of the normalized absorption and emission spectra of each PC shows the stokes shift of each new organic PC averages out at 25nm (Figures A.2-A.6). This stokes shift is indicative of the π-π* transition, typical of aromatic organic compounds. Lifetime data was obtained under inert atmosphere ($N_2$) and air and showed minute changes which supports a singlet excited-state transition, because the presence of oxygen would cause a deleterious effect with any triplet excited state. Lifetime values for this study were obtained in acetonitrile and when compared to literature values commonly reported for Eosin Y, our value is much shorter. This is due to the literature typically reported excited-state lifetimes of Eosin Y in aqueous or aqueous-mixed solvents despite the fact that most photoredox studies that utilize Eosin Y are performed in dry, organic solvents.[24] Eosin Y is a solvatochromic compound, affecting photophysical data such as the excited state lifetime, enhancing the possibility of a triplet excited state, especially in highly polar protic solvents.[24] However, due to the importance of acetonitrile in organic synthesis methods, performing characterization in this solvent is essential. Though the lifetimes reported above are shorter than transition metal PCs, by utilizing the newly synthesized series of organic PCs in an established photocatalytic reaction, we support their use and applicability.

Cyclic voltammetry (CV) was carried out to evaluate the redox potentials of each compound, and the results are reported in Table 2.2. Redox potentials are an important

characterization because they correspond to the energy of the electron that will undergo single electron transfer during the catalytic cycle. Electrochemical characterization of each compound was carried out in anhydrous acetonitrile using tetrabutylammonium hexafluorophosphate (TBAH) supporting electrolyte. The voltammograms of each compound reported here are shown in the supporting information. For the PCs synthesized in this work the potential corresponds to the gain or loss of a single electron from or to the π cloud on the xanthene core. Comparing the redox potentials of each new PC against the parent PC, Eosin Y, allows us to shed light on the tunability of this series. The reduction potentials of the new PCs varied by 120 mV or more, supporting the tunability of the parent PC. As shown in Table 2.2, reduction potentials of the four new PCs range between -0.99 V and -1.11 V vs SCE. Reduction and oxidation power of the organic PCs are determined by the energy of the highest occupied molecular orbital (HOMO) and lowest unoccupied molecular orbital (LUMO). By raising the HOMO orbital, the ground state reduction potential is increased to a more negative potential for the given compound, augmenting the ability to reduce a broader range of substrates. This effect can be accomplished by varying the electron donating ability/electron density of the functional groups around the xanthene core. The stronger electron donation of the new moiety, the larger the change in the reduction potential. The shift in potential is due to the shift in the HOMO energy. The effects of core functionalization are seen in the ground state redox potentials reported in Table 2.2.

When comparing the new PCs against the parent complex, Eosin Y, the four new functional groups illustrate the influence of electron donating/withdrawing and aromaticity on the redox potentials of the new PCs. Due to the electron donating ability

of the phenyl groups that replace the electron withdrawing bromines on the parent the reduction potential is increased. The more powerful potential is caused by an increase in the HOMO, as theorized above. In the case of E-trifluoromehtylph$_3$, the most electron withdrawing functional group, the addition of the trifluoromethyl group on the phenyl ring negates all the electron donating power of the phenyl group, yielding an orbital with a slightly lower energy than that of Eosin Y. E-naph$_3$ ($E_{red\ ½}$ = -1.08 V vs SCE) and E-ph$_3$ ($E_{red\ ½}$ = -1.11 V vs SCE) show that larger aromatic functional groups afford a less powerful reductant. This may be due to naphthyl being a poorer electron donor than phenyl. Lastly E-tertbutylph$_3$ ($E_{red\ ½}$ =-1.06 V vs SCE) establishes the effect of aliphatic groups on reduction potentials. Also, of note are the oxidation potentials that ranged from +0.31 V to +0.54 V vs SCE, decreased from Eosin Y (+0.77 V vs SCE), illustrating the tunability and versatility of this method.

**Table 2.2.** Electrochemical data of new Eosin Y based photocatalytic series. All data obtained in anhydrous acetonitrile.

| Photocatalyst | $E_{red\ ½}$ | $E_{00}$ | $E_{ox\ ½}$ |
|---|---|---|---|
| E-ph$_3$ | -1.11 | 2.21 | +0.39 |
| E-trifluoromethylph$_3$ | -0.99 | 2.19 | +0.54 |
| E-tertbutylph$_3$ | -1.06 | 2.20 | +0.31 |
| E-naph$_3$ | -1.08 | 2.20 | +0.48 |
| Eosin Y | -1.00 | 2.30 | +0.77 |

The oxidation potential of the E-ph3 and E-trifluoromethylph3, follow the trend that the more electron donating (phenyl) affords a lower oxidation potential and the

trifluoromethylphenyl moiety has a higher oxidation potential than the latter. The phenyl group has the best electron donating character resulting in the lowest oxidation potential (+0.32 V vs SCE) shifted 650 mV from the parent complex. The electron donating characteristics of phenyl groups, with respect to bromine atoms of Eosin Y, increases the electron density in the π cloud, making it more difficult for electrons to be accepted, hence the higher reduction potential of E-ph$_3$. The donor group expected to result in the highest oxidation potential of the new series (trifluoromethylphenyl) due to the electron withdrawing character of the fluorine.

$$*E_{red} = E_{red½} + E_{00} \qquad \text{(Eqn 2.1)}$$

Excited state reduction potentials are determined by the difference between the ground state oxidation potential and singlet state energy (Eqn 2.1). Transition metal photocatalysts singlet state energies average to between 2.0 V and 2.5 V, to which the values for our organic PC are comparable.[6] Though CVs showed no reversibility (Figure A.7-A.11) this could be due to the breaking of the xanthene core planarity that occurs when an electron in injected into the π*-orbitals during reduction. Though reversibility is seen for Eosin Y in a combination of acetonitrile and deionized water, as seen in previously reported work[24] and reproduced in our lab (Figure A.12). This difference in CV response to solvent once again illustrates that solvent plays a crucial role in chemical characteristics of xanthene-based photocatalysts.

The catalytic viability of this newly synthesized series of PCs was confirmed through a previously established photocatalytic reaction. Each of the PCs reported here were evaluated on their ability to carry out the photocatalytic arylation of enol acetate,[114] as shown in Figure 2.5. The arylation proceeds through an initial reduction of the

diazonium salt (1), which allowed for evaluation of the reductive capability of this series of PCs. As shown in Table 2.3, all the PCs reported here produced catalytic yields showing that these PCs are catalytically active for reductive photocatalysis cycles. Eosin Y produced 31% yield in two hours, which is lower than previously reported for this reaction, which is likely due to the change in solvent from DMSO to acetonitrile.[114] Eosin Y is only sparingly soluble in acetonitrile, whereas the new PCs reported here are soluble in acetonitrile and a range of organic solvents. This illustrates another advantage of these reported PCs for photocatalytic organic synthesis.

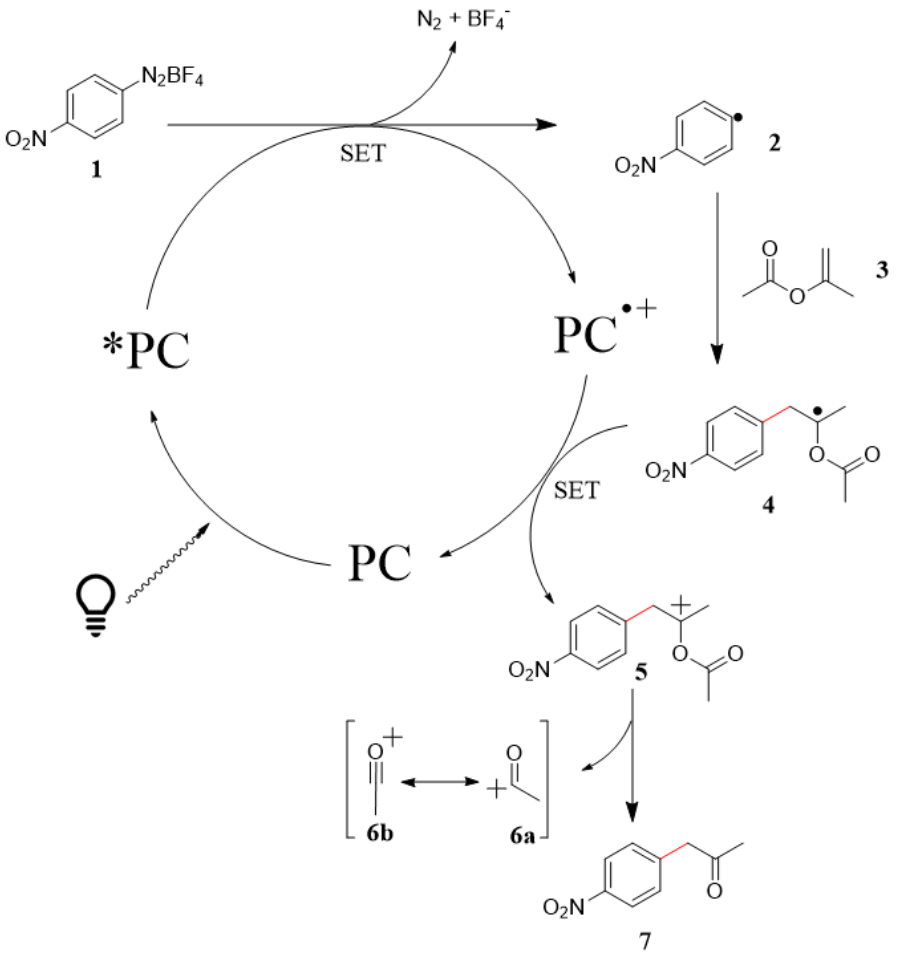


**Figure 2.5.** Catalytic cycle for arylation of isopropenyl acetate.

## 2.4 Conclusions

In conclusion this work presents four new Eosin Y based organic PCs. The results of this study support that systematic structural alteration of an organic PC allows for the tuning of photophysical and electrochemical properties. Functionalization of the xanthene core produced a series of PCs with redshifted $\lambda_{abs}$ and $\lambda_{em}$ values. Structural alterations maintained the high molar extinction coefficients of the parent, Eosin Y, and significant fluorescent quantum yields common to organic PCs. Elimination of the carbon-bromine bonds stabilized these compounds to bond activation and increased their solubility in organic solvents. The tunability of this structure was further highlighted by the reduction potentials ranging from -0.99 V to -1.11 V vs SCE. Catalytic activity was tested through application to photocatalytic arylation of isopropenyl acetate, for which E-$ph_3$ and E-tertbutyl$ph_3$ exceeded the yields of Eosin Y.

**Table 2.3.** Photocatalytic arylation of enol acetate.

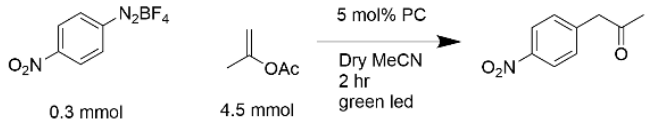


| Photocatalyst | % Yield (2hr) | Turnover Number |
|---|---|---|
| E-$ph_3$ | 51 | 10 |
| E-trifluoromethyl$ph_3$ | 25 | 5 |
| E-tertbutyl$ph_3$ | 36 | 7 |
| E-$naph_3$ | 19 | 4 |
| Eosin Y Dianion | 31 | 6 |
| No PC | 3 | NA |

## 2.5 Experimental

*Materials***.** Anhydrous acetonitrile (MeCN) (99.8%, water ≤50 ppm) was used for all characterization and photocatalytic reactions, unless indicated otherwise. All reactants and synthetic reagents used without further purification. All synthetic reactants and solvents used without further purification. Photocatalytic enol arylation carried out according to literature, except for the use of acetonitrile.[114]

*Synthesis***.** *General synthesis of organic photocatalysts.* Eosin Y disodium (200 mg, 0.289 mmol), eight equivalents of the respective boronic acid (2.31 mmol), and potassium carbonate (639.45 mg, 4.63 mmol) were added to a two-neck round bottom flask charged with a stir bar, 1:1 deionized $H_2O$ / ethanol, and flushed continuously with nitrogen. Tetrakis(triphenylphosphine)palladium(0) (33.4 mg, 0.0289 mmol) was quickly added to the reaction mixture, the round bottom was sealed and allowed to reflux at 120 °C for 24 hours. Reaction mixture was cooled under nitrogen, and the ethanol was removed under reduced pressure. Excess 1M HCl was added to solution and a red solid precipitated immediately, solid collected via vacuum filtration and allowed to dry under vacuum for 1 hour. The solid was then dissolved in ethyl ether and filtered, filtrate retained and dried under reduced pressure. The subsequent solid was dissolved in acetonitrile and filtered, filtrate retained and dried under reduced pressure again. Resulting crude product was purified by preparatory TLC (E-$ph_3$ in 100% ether, and the remaining used 30% ethyl acetate in toluene). Product deprotonated with 1.1 equivalents of sodium hydroxide in acetonitrile to obtain the dianion product.

*E-ph3*. ($C_{38}H_{22}O_5Na_2$) 1H NMR (400 MHz, $(CD_3)_2CO$) $\delta_H$ 8.00 (1H, *J* = 7.6 Hz), 7.82 (1H, t, *J* = 3.2 Hz), 7.70 (1H, t, *J* = 3.2 Hz), 7.65 (2H, m), 7.58 (2H, t, *J* = 5.1 Hz), 7.49 (2H, d, *J* = 3.9 Hz), 7.41 (5H, m), 7.36-7.28 (3H, m), 7.27-7.23 (3H, m), 6.78 (2H, d, *J* = 1.6 Hz), 6.76 (1H, s). $^{13}C$ ($(CD_3)_2CO$, 100.66 MHz): $\delta_C$ 169.25, 156.92, 152.39, 149.57, 138.25, 138.07, 135.95, 133.16, 132.00, 130.75, 130.22, 130.06, 129.76, 129.52, 129.18, 129.13, 129.09, 128.94, 128.90, 128.85, 128.58, 128.58, 128.39, 127.85, 127.56, 127.53, 126.81, 125.46,124.94, 120.00, 118.41, 115.92, 112.64, 112.02, 103.89. Calculated Mass [M]+ = 561.1692; Found Mass = 561.1676.

*E-trifluoromethylph3*. ($C41H19O_5F_9Na_2$) $^1H$ NMR ($(CD_3)_2CO$, 400 MHz) $\delta_H$ 8.01 (1H, d, *J* = 7.6 Hz), 7.93 (3H, q, *J* = 7.3 Hz), 7.83 (1H, t, *J* = 3.2 Hz), 7.72 (1H, t, *J* = 7.3 Hz), 7.68 (2H, s), 7.66 (6H, t, *J* = 4.9 Hz), 7.61 (1H, m), 7.50 (1H, d, *J* = 7.6 Hz), 6.90 (2H, m), 6.82 (1H, s). $^{13}C$ ($(CD_3)_2CO$, 100.66 MHz): $\delta_C$ 169.29, 157.21, 152.86, 150.05, 142.36, 142.22, 137.78, 136.17, 133.14, 132.59, 131.03, 130.96, 130.93, 130.59, 130.41, 130.11, 129.94, 129.69, 129.37, 129.34, 129.02, 127.93, 126.84, 126.72, 126.67, 126.11, 126.07, 125.95, 125.91, 125.87, 125.72, 125.68, 125.65, 125.61, 125.58, 125.04, 124.14, 124.02, 117.70, 113.37, 112.52, 104.26. Calculated Mass [M]+ = 765.1318; Found Mass = 765.1321.

*E-tertbutylph3*. ($C_{50}H_{46}O_5Na_2$) $^1H$ NMR (400 MHz, $(CD_3)_2CO$) $\delta_H$ 7.96 (1H, t, *J* = 9.2 Hz), 7.77 (1H, t, *J* = 7.2 Hz), 7.67 (1H,t, *J* = 7.4 Hz), 7.64-7.54 (4H, m), 7.48 (1H, d, *J* = 8.5 Hz), 7.42-7.28 (8H, m), 6.82-6.67 (3H, m), 1.42 (6H, s), 1.34 (6H, s), 1.28 (15H, s). $^{13}C$ ($(CD_3)_2CO$, 100.66 MHz): $\delta_C$ 169.43, 157.11, 153.71, 153.51, 152.39, 151.27, 150.67, 150.61, 150.40, 149.63, 138.73, 136.08, 135.55, 135.36, 131.87, 131.69, 130.89, 130.27, 129.82, 129.60, 129.41, 129.11, 128.93, 128.82, 127.82, 127.98, 127.17, 126.99,

126.86, 126.78, 126.52, 126.34, 126.13, 125.97, 125.80, 125.72, 125.53, 124.99, 118.28, 115.55, 112.64, 112.00, 103.99, 84.16, 35.22, 34.96, 34.80, 31.93, 31.77, 31.69, 31.66, 31.59, 31.50, 31.43. Calculated Mass [M]+ = 729.3575; Found Mass = 729.3574.

*E-naph*$_3$. ($C_{50}H_{28}O_5Na_2$) $^1$H NMR ($(CD_3)_2CO$, 400 MHz) $\delta_H$ 8.23 (1H, s), 8.10 (1H, d, *J* = 8.5 Hz), 8.05-7.97 (4H, m), 7.94 (1H, s), 7.89-7.79 (7H, m), 7.76 (1H, t, *J* = 7.5 Hz), 7.68-7.55 (5H, m), 7.50 (1H, d, *J* = 7.7 Hz), 7.48-7.41 (4H, m), 7.04 (2H, d, *J* = 13.1 Hz), 6.87 (1H, s). $^{13}$C ($(CD_3)_2CO$, 100.66 MHz): $\delta_C$ 169.63, 157.57, 152.84, 150.16, 136.07, 136.02, 135.83, 134.56, 134.56, 134.24, 134.18, 133.94, 133.39, 133.26, 131.40, 130.92, 130.71, 130.18, 129.73, 129.46, 129.13, 129.06, 128.96, 128.83, 128.81, 128.78, 128.60, 128.55, 128.44, 128.33, 128.27, 128.22, 127.99, 127.57, 127.21, 127.13, 126.99, 126.98, 126.86, 126.72, 125.79, 125.79, 125.17, 118.51, 113.11, 112.48, 104.27. Calculated Mass [M]+ = 711.2166; Found Mass = 711.2167.

*Instrumental*. 1 H NMR and 13C NMR spectroscopy were performed using a 400 MHz instrument, reference $(CD_3)_2CO$ peak for 1 H NMR defined as 2.05 ppm and as 29.84 and 206.26 ppm for 13C NMR. The mass spectrometry was performed with an electron ionization of 70 eV, and the spectrometer was scanned from 450 to 50 m/z at low resolution.

*Absorption* data were recorded on an Agilent 8453 UV−visible photo diode array spectrophotometer using a 1x1 cm quartz cuvette.

*Electrochemical measurements.* Cyclic voltammetry (CV) performed on a CH Instruments 601D potentiostat with a 3 mm diameter glassy carbon working electrode, a Pt wire (99.99%) counter electrode, and a saturated calomel electrode (SCE) as the

reference electrode. All values reported versus SCE. The glassy carbon electrode was manually prepared by polishing the surface with 0.05 μm Alumina suspension. Solutions for electrochemical characterization contained 100 mM tetrabutylammonium hexafluorophosphate ($TBAPF_6$) which was further purified by recrystallization in ethanol, dried under vacuum at 80°C over 24 hours. Anhydrous acetonitrile was purged with $N_2$ for 5 min before any measurements were taken. A green light emitting diode (led) was used for all photocatalytic reactions. Differential pulse voltammetry (DPV) experiments were run on a Pine wavedriver 20 biopotentiostat system using the same electrode selection and method as CV.

*Steady-State and Time-Resolved Emission* data were collected at room temperature using an Edinburgh FLS980 spectrometer. Nitrogen samples were first bubble degassed for 30 minutes before spectra were obtained. Samples were excited using light output from a housed 450 W Xe lamp passed through a single grating (1800 l/mm, 250 nm blaze) Czerny-Turner monochromator. Emission from the sample was first passed through a 495 nm long-pass color filter, then a single grating (1800 l/mm, 500 nm blaze) Czerny-Turner monochromator and finally detected by a peltier-cooled Hamamatsu R928 photomultiplier tube.

The dynamics of emission decay were monitored by using the FLS980's time-correlated single-photon counting capability (1024 channels; 100 ns window) with data collection for 10,000 counts. Excitation for TCSPC was provided by an Edinburgh EPL-445 ps pulsed light emitting diode (445 ± 10 nm, pulse width 892 ps) operated at 10 MHz. Emission was passed through a 495 nm long-pass filter and then a single grating (1800 l/mm, 500 nm blaze) Czerny−Turner monochromator and finally detected by a

Peltier-cooled Hamamatsu R928 photomultiplier tube. Time-resolved emission data were fit by using a reconvolution fit using an IRF with MeCN.

*Quantum Yield* data were collected at room temperature using a Hamamatsu Quantaurus-QY Spectrometer. Samples were excited using a 505 nm output from a 150 W Xenon arc lamp and detected by a back-illuminated cooled 1024 channel CCD detector.

*Enol arylation* was carried out under a nitrogen atmosphere in a seven mL vial charged with a stir bar. All substrates used without further purification. To the vial was added *p*-nitrobenzenediazonium tetrafluoroborate (0.45 M), isopropenyl acetate (15 equivalents), and the respective photocatalyst (5 mol%). Once transferred to glovebox dry acetonitrile was added, and the vial was sealed before 2hr irradiation with a green led. All yields were determined by quantitative NMR with an internal standard of dimethyl terephthalate.

**2.6 References**

1. Yan, D. M.; Chen, J. R.; Xiao, W. J., New Roles for Photoexcited Eosin Y in Photochemical Reactions. *Angew. Chem. Int. Edit.* **2019,** *58* (2), 378-380.

2. Nicewicz, D. A., Nguyen, T. M., Recent Applications of Organic Dyes as Photoredox Catalyst in Organic Synthesis. *ACS Catal.* **2013,** *4* (1), 355-360.

3. Shaw, M. H., Twilton, J., MacMillan, D. W. C., Photoredox Catalysis in Organic Chemistry. *J. Org. Chem.* **2016,** *81*, 6898-6926.

4. Prier, C. K., Rankic, D. A., MacMillan, D. W. C., Visible Light Photoredox

Catalysis with Transition Metal Complexes: Applications in Organic Synthesis. *Chem. Rev.* **2013,** *113*, 5322-5363.

5. Romero, N. A., Nicewicz, D. A., Organic Photoredox Catalysis. *Chem. Rev. (Washington, DC, U. S.)* **2016,** *116* (17), 10075-10166.

6. Yoon, T. P., Ischay, M. A., Du, J., Visible light photocatalysis as a greener approach to photochemical synthesis. *Nature Chem*. **2010,** *2*, 527-532.

7. Jun Xuan, W.-J. X., Visible Light Photoredox Catalysis. *Angew. Chem.* **2012,** *51*, 6828-6838.

8. Narayanam, J. M.; Stephenson, C. R., Visible light photoredox catalysis: applications in organic synthesis. *Chem. Soc. Rev*. **2011,** *40* (1), 102-113.

9. McCarthy, B. G.; Pearson, R. M.; Lim, C.-H.; Sartor, S. M.; Damrauer, N. H.; Miyake, G. M., Structure–property relationships for tailoring phenoxazines as reducing photoredox catalysts. *J. Am. Chem. Soc.* **2018,** *140* (15), 5088-5101.

10. Dumur, F., Recent Advances on Visible Light Metal-Based Photocatalysts for Polymerization under Low Light Intensity. *Catalysts* **2019,** *9* (9), 736-776.

11. Du, Y.; Pearson, R. M.; Lim, C. H.; Sartor, S. M.; Ryan, M. D.; Yang, H.; Damrauer, N. H.; Miyake, G. M., Strongly reducing, visible-light organic photoredox catalysts as sustainable alternatives to precious metals. *Chem-Eur. J.* **2017,** *23* (46), 10962-10968.

12. McCusker, J. K., Femtosecond absorption spectroscopy of transition metal charge-transfer complexes. *Acc. Chem. Res.* **2003,** *36* (12), 876-887.

13. Yeh, A. T.; Shank, C. V.; McCusker, J. K., Ultrafast electron localization dynamics following photo-induced charge transfer. *Science* **2000,** *289* (5481), 935-938.

14. Neumann, M.; Füldner, S.; König, B.; Zeitler, K., Metal-free, cooperative asymmetric organophotoredox catalysis with visible light. *Angew. Chem. Int. Edit.* **2011,** *50* (4), 951-954.

15. Joshi-Pangu, A., Levesque, F., Roth, H. G., Oliver, S. F., Campeau, L., Nicewicz, D., DiRocco, D. A., Acridinium-Based Photocatalysts: A Sustainable Option in Photoredox Catalyst. *J. Org. Chem.* **2016,** *81*, 7244-7249.

16. Hari, D. P., Konig, B., Synthetic applications of eosin Y in photoredox catalysis. *Chem. Commun.* **2014,** *50*, 6688-6699.

17. Ghosh, I.; Ghosh, T.; Bardagi, J. I.; König, B., Reduction of aryl halides by consecutive visible light-induced electron transfer processes. *Science* **2014,** *346* (6210), 725-728.

18. Meyer, A. U.; Slanina, T. s.; Yao, C.-J.; König, B., Metal-free perfluoroarylation by visible light photoredox catalysis. *ACS Catal.* **2015,** *6* (1), 369-375.

19. Discekici, E. H.; Treat, N. J.; Poelma, S. O.; Mattson, K. M.; Hudson, Z. M.; Luo, Y.; Hawker, C. J.; de Alaniz, J. R., A highly reducing metal-free photoredox catalyst: design and application in radical dehalogenations. *Chem. Commun. (Cambridge, U. K.)* **2015,** *51* (58), 11705-11708.

20. Ravelli, D.; Fagnoni, M., Dyes as visible light photoredox organocatalysts. *ChemCatChem* **2012,** *4* (2), 169-171.

21. Fagnoni, M.; Dondi, D.; Ravelli, D.; Albini, A., Photocatalysis for the Formation of the C− C Bond. *Chem. Rev. (Washington, DC, U. S.)* **2007,** *107* (6), 2725-2756.

22. Marin, M. L.; Santos-Juanes, L.; Arques, A.; Amat, A. M.; Miranda, M. A., Organic photocatalysts for the oxidation of pollutants and model compounds. *Chem. Rev. (Washington, DC, U. S.)* **2011,** *112* (3), 1710-1750.

23. Fukuzumi, S.; Ohkubo, K., Selective photocatalytic reactions with organic photocatalysts. *Chemical Science* **2013,** *4* (2), 561-574.

24. Jiang, Z.; Sun, H.; Wang, T.; Wang, B.; Wei, W.; Li, H.; Yuan, S.; An, T.; Zhao, H.; Yu, J., Nature-based catalyst for visible-light-driven photocatalytic CO 2 reduction. *Energy Environ. Sci.* **2018,** *11* (9), 2382-2389.

25. Heitz, D. R.; Rizwan, K.; Molander, G. A., Visible-Light-Mediated Alkenylation, Allylation, and Cyanation of Potassium Alkyltrifluoroborates with Organic Photoredox Catalysts. *J. Org. Chem.* **2016,** *81* (16), 7308-7313.

26. Fukuzumi, S.; Ohkubo, K., Organic synthetic transformations using organic dyes as photoredox catalysts. *Org. Biomol. Chem.* **2014,** *12* (32), 6059-6071.

27. Meyer, A. U.; Strakova, K.; Slanina, T.; Koenig, B., Eosin Y (EY) photoredox-catalyzed sulfonylation of alkenes: scope and mechanism. *Chem-Eur. J.* **2016,** *22* (25), 8694-8699.

28. Rohokale, R. S.; Koenig, B.; Dhavale, D. D., Synthesis of 2, 4, 6-trisubstituted pyridines by oxidative Eosin Y photoredox catalysis. *J. Org. Chem.* **2016,** *81* (16), 7121-7126.

29. Majek, M., Filace, F., von Wangelin, A. J., On the mechanism of photocatalytic reactions with eosin Y. Beilstein *J. Org. Chem.* **2014,** *10*, 981-989.

30. Srivastava, V.; Singh, P. P., Eosin Y catalysed photoredox synthesis: a review. *RSC Adv.* **2017,** *7* (50), 31377-31392.

31. Yu, X.; Yang, Z.; Qiu, B.; Guo, S.; Yang, P.; Yu, B.; Zhang, H.; Zhao, Y.; Yang, X.; Han, B., Eosin Y-Functionalized Conjugated Organic Polymers for Visible-Light-Driven CO2 Reduction with H2O to CO with High Efficiency. *Angew. Chem. Int. Edit.* **2019,** *58* (2), 632-636.

32. Abe, R.; Hara, K.; Sayama, K.; Domen, K.; Arakawa, H., Steady Hydrogen Evolution from Water on Eosin Y-Fixed TiO2 Photocatalyst using a Silane-Coupling Reagent under Visible Light Irradiation. *J. Photochem. Photobiol., A* **2000,** *137* (1), 63-69.

33. Manivannan, G.; Mailhot, G.; Bolte, M.; Lessard, R., Xanthene dye sensitized dichromated poly (vinyl alcohol) recording materials: holographic characterization and ESR spectroscopic study. *Pure Appl. Opt.* **1994,** *3* (5), 845-857.

34. Hazebroucq, S.; Labat, F.; Lincot, D.; Adamo, C., Theoretical insights on the electronic properties of eosin Y, an organic dye for photovoltaic applications. *J. Phys. Chem. A* **2008,** *112* (31), 7264-7270.

35. Hopkinson, M. N., Sahoo, B., Jun-Long Li, Glorius, F., Dual Catalysis Sees the Light: Combining Photoredox with Organo-, Acid, and Transition-Metal Catalysis. *Chem. Eur. J.* **2014,** *20*, 3874-3886.

36. Hering, T.; Hari, D. P.; König, B., Visible-light-mediated α-arylation of enol acetates using aryl diazonium salts. *J. Org. Chem.* **2012,** *77* (22), 10347-10352.

# CHAPTER 3

# BIS-CYCLOMETALATED IRIDIUM COMPLEXES CONTAINING 4,4'-BIS(PHOSPHONOMETHYL)-2,2'-BIPYRIDINE LIGANDS: PHOTOPHYSICS, ELECTROCHEMISTRY, AND HIGH VOLTAGE DYE-SENSITIZED SOLAR CELL DEVICES

*Bobo, M. V.; Paul, A.; Robb, A. J.; Arcidiacono, A. M.; Smith, M. D.; Hanson, K.; Vannucci, A. K., Bis-Cyclometalated Iridium Complexes Containing 4,4′-Bis(phosphonomethyl)-2,2′-bipyridine Ligands: Photophysics, Electrochemistry, and High-Voltage Dye-Sensitized Solar Cells. *Inorg. Chem.* **2020**.

## 3.1 Abstract

In this report, the synthesis and characterization of two bis-cyclometalated iridium(III) complexes are presented. Single crystal X-ray diffraction shows that $[Ir(ppy)_2(4,4'$-bis(diethylphosphonomethyl)-2,2′-bipyridine)]$PF_6$ adopts a pseudo octahedral geometry. The complexes have an absorption feature in the near-visible UV region and emit green light with excited state lifetimes in the hundreds of nanoseconds. The redox properties of these complexes show reversible behavior for both oxidative and reductive events. $[Ir(ppy)_2(4,4'$-bis(phosphonomethyl)-2,2′-bipyridine)]$PF_6$ readily binds to metal oxide supports, like nanostructured Sn(IV)-doped $In_2O_3$ and $TiO_2$, while still retaining reversible redox chemistry. When incorporated as the photoanode in dye-sensitized solar cells, the devices exhibit open circuit voltages >1 V which is a testament to their strength of these Ir complexes as photochemical oxidants.

## 3.2 Introduction

Octahedral polypyridyl complexes of ruthenium(II) and iridium(III) have attracted a great deal of interest due to their photophysical and redox properties with applications including organic light emitting devices (OLEDs),[131] dye-sensitized solar cells (DSSCs),[132-134] homogeneous photocatalysis,[135-136] luminescent probes,[137] and dye-sensitized photoelectric synthesis cells (DSPECs).[138] Of specific importance to this report, cyclometalated Ir(III) complexes have been particularly useful due to ease of synthesis, high stability, and unique photophysical/electrochemical properties.[139]

Cyclometalating ligands, such as 2-phenylpyridine (ppy), are formally anionic and both *bis*- and *tris*-cyclometalated complexes have been reported as efficient photocatalysts.[140-141] The primary advantage of using a third-row transition metal for optoelectronic devices is the large d-orbital splitting compared to second row transition metals. This splitting makes the dissociative $e_g$ orbitals less accessible and increases the stability of the photosensitizer. Furthermore, a heavy atom effect enhances spin-orbit coupling and increases radiative relaxation pathways.[142-143]

General requirements of an Ir(III) photosensitizer for any of the above-mentioned applications includes chemical stability, high molar absorptivity in the visible and near-UV spectrum, long-lived excited-state lifetimes, and well-defined redox properties. Iridium complexes of the general formula $[Ir(C\hat{}N)_2(N\hat{}N)]^+$, where C^N is a cyclometalating ligand and N^N is a bidentate polypyridyl ligand, are good targets for tunable photosensitizers. It has been shown that electron withdrawing moieties on the C^N ligands tend to stabilize the metal-based HOMOs of these complexes, while electron donating moieties on the N^N ligands tend to destabilize the LUMOs.[144-145] This tuning of molecular orbital energies can have a large impact on the stability, photophysical,[146] and redox properties[147-148] of the complex.

Beyond the general properties needed for efficient Ir(III) photosensitizers listed above, tuning of specific properties can be achieved for targeted applications. Previous research has demonstrated that emission wavelengths can be tuned by over 300 nm, and quantum yields can vary greatly depending on the modifications made to the cyclometalating ligands on the Ir complexes.[131, 149-151] For DSSC and DSPEC applications, Ir(III) photosensitizers require high molar absorptivity and reversible redox

properties, as well as a means of chemically binding to metal oxide electrodes.[132, 152] This molecular attachment can be achieved using carboxylate, phosphonate, or hydroxymate moieties binding to the surface of the oxide supports.[138, 153] Of these, phosphonates binds particularly well even in aqueous conditions[154] and are a common choice for DSSCs and DSPECs.[133, 155] However, reports of cyclometalated Ir(III) complexes containing phosphonate binding groups suitable for DSSCs are limited.

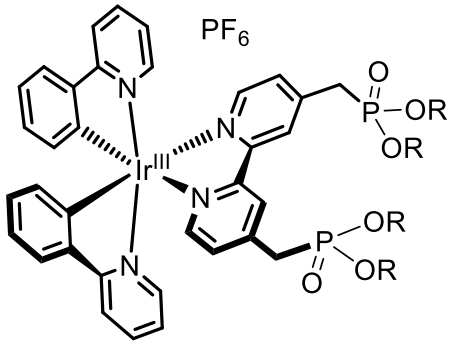


**Figure 3.1**. Molecular structures of **1** and **2**.

Herein we characterize the physical properties of two Ir(III) complexes shown in Figure 3.1, $[Ir(ppy)_2(4,4'\text{-bis(diethylphosphonomethyl)-}2,2'\text{-bipyridine})]PF_6$ (**1**), and $[Ir(ppy)_2(4,4'\text{-bis(phosphonomethyl)-}2,2'\text{-bipyridine})]PF_6$ (**2**). Photophysical characteristics, including absorption, emission, excited-state lifetime, and quantum yield, are reported and compared to DFT computations, as well as previously reported cyclometalated compounds. Electrochemical studies were also performed in order to determine the redox properties of these complexes. Lastly, it has been shown that **2** is capable of binding to metal oxide electrodes for use in DSSCs.

### 3.3 Results and discussion

#### 3.3.1 Structure

Complex **1** crystallizes in the monoclinic system and the structure is shown in Figure 3.2. The pattern of systematic absences in the intensity data was consistent with the space groups *C*2/*c* and *Cc*, the former of which was confirmed by structure solution. The asymmetric unit in *C*2/*c* consists of one [Ir($C_{11}H_8N$)$_2$($C_{20}H_{30}N_2O_6P_2$)] cation and half

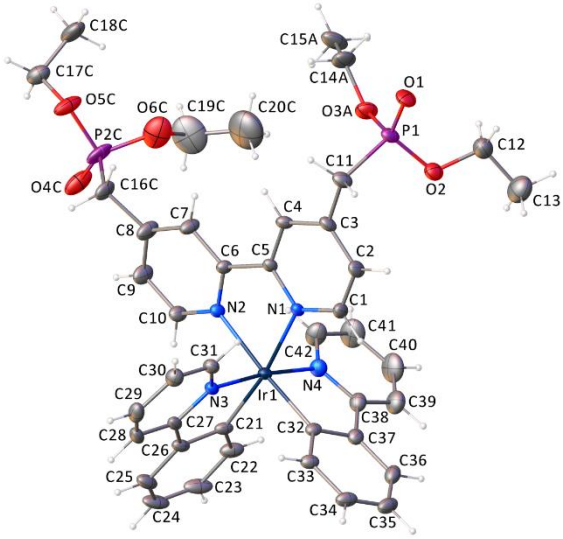


**Figure 3.2**. Crystal structure of **1** with $PF_6$ anions not shown. Displacement ellipsoids drawn at the 40% probability level. One conformation of the disordered diethylphosphonomethyl groups shown for clarity.

each of two independent hexafluorophosphate anions. One $PF_6^-$ anion (P3) is located on a crystallographic two-fold axis of rotation and the other (P4) is located on a crystallographic inversion center (see SI for more details). Average Ir-N bond lengths between the Ir center and the 4,4′-bis(diethylphosphonomethyl)-2,2′-bipyridine ligand

(2.136 Å) are roughly 0.09 Å longer than Ir-N bond lengths between the Ir center and the ppy ligands (2.047 Å). The distances between the Ir and the nitrogen atoms of the 4,4′-bis(diethylphosphonomethyl)-2,2′-bipyridine however are not statistically different compared to related Ir(III) complexes that lack phosphonomethyl moieties.[140] Multiple attempts to crystallize complex **2** did not result in crystals suitable for X-ray diffraction studies.

### 3.3.2 Photophysical measurements

The photophysical properties of **1** and **2** were measured in deaerated acetonitrile and DMF, respectively, and the results are summarized in Table 3.1. The absorption and emission profile of **1** measured in $N_2$ deaerated acetonitrile are shown in Figure 3.3. The absorption spectrum is similar to related Ir(III) photosensitizers previously reported in the literature[147] with absorption bands in the UV region (< 300 nm) are attributed to ligand based π-π* transitions, and less intense absorption bands in the near-UV and visible regions are attributed to the metal-to-ligand charge transfer. Upon excitation at 355 nm at room temperature, **1** exhibits an emission with a $\lambda_{max}$ at 565 nm. Previous reports have proposed that emissions from these *bis*-cyclometalated complexes of the general formula $[Ir(C\hat{}N)_2(N\hat{}N)]^+$ arise from strong mixing between both the ligand-based and metal-to-ligand-base charge transfers.[142, 156] Emission from **1** is considerably red-shifted compared to many neutral, *tris*-cyclometalated Ir(III) complexes,[148] due to the absence of the third cyclometalated ligand. The excited state decay (Figure B.1) of **1** in $N_2$ deaerated acetonitrile under 405 nm excitation could be fit with a single exponential giving a lifetime of 570 ns. This lifetime is nearly identical to the closely related $[Ir(ppy)_2(dtb\text{-}bpy)]^+$ complex, where dtb-bpy is 4,4′-bis(*tert*-butyl)-2,2′-bipyridine.[139] The emission

quantum yield ($\Phi_{em}$) of **1** was determined to be 0.39 in $N_2$ deaerated acetonitrile. This $\Phi_{em}$ value is comparable to many cyclometalated Ir(III) complexes that have been investigated for use in OLEDs,[148] but nearly double that of the closely related $[Ir(ppy)_2(dtb\text{-}bpy)]^+$ complex.[139]

**Table 3.1**. Comparison of physical properties of cyclometalated Ir(III) complexes.

| Complex | [a]Abs | ε | [a]Ems | Φ | [b]$\tau_{air}$ | [b]$\tau_{N2}$ | [c]$E_{ox}$ | $E_{red,1}$ | $E_{red,2}$ | $E_{red,3}$ |
|---|---|---|---|---|---|---|---|---|---|---|
| **1** | 355 | 7781 | 565 | 0.39 | 98 | 570 | 1.29 | -1.32 | -2.16 | -2.41 |
| **2** | 380 | 6209 | 535 | 0.15 | 410 | 890 | 1.40 | -1.78 | -2.20 | -2.51 |
| [d]$[Ir(ppy)_2(dtb\text{-}bpy)]^+$ | 376 | 8500 | [e]581 | 0.24 | 65 | 557 | 1.33 | -1.38 | - | - |

[a]Units of nm. [b]Lifetime (τ) units of ns. [c]All potentials are reported as V vs SCE. [d]dtb-bpy is 4,4′-bis(*tert*-butyl)-2,2′-bipyridine. [e]Data taken from ref [142]. Data collected for **2** were recorded in DMF, data collected for **1** and reported for $[Ir(ppy)_2(dtb\text{-}bpy)]^+$ were recorded in acetonitrile.

Complex **2** is only soluble in highly polar, organic solvents, thus absorption and emission data were collected in DMF. As shown in Figure B.2, complex **2** exhibited strong absorption bands at wavelengths shorter than 350 nm. Also analogous to complex **1**, weaker intensity bands at wavelengths greater than 350 nm were observed and attributed to metal-to-ligand charge transfer (MLCT) transitions. TD-DFT calculations were performed to further support a $d\pi - \pi^*$ transition. Figure 3.3 compares the calculated and experimental absorption spectra for **2** in DMF. The blue vertical bars illustrate the computed transitions for the lowest energy transitions and the heights reflect the relative computed oscillator strengths. Figure 3.3 also shows the computed HOMO and LUMO orbitals, which illustrate the MLCT nature of the transition.

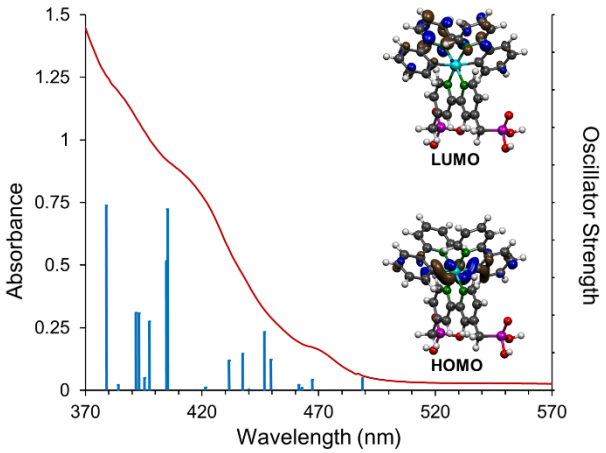


**Figure 3.3**. UV-visible absorption spectrum of **2** in DMF (red line) and calculated TD-DFT transitions (blue lines), along with the computed HOMO and LUMO molecular orbitals.

The emission spectrum of **2** was blue-shifted compared to **1**, with a $\lambda_{max}$ of 535 nm. It has been previously shown that the methylene bridge electronically decouples the $PO_3R_2$ groups from the photoactive core of transition metal coordination complexes.[157] Therefore, the spectral shift is most likely not due to the deesterification, but instead the difference in solvent, MeCN for **1** and DMF for **2** with the former being more stabilized in the excited state than the later. Unfortunately, due to differences in solubilities, the two complexes could not be compared in the same solvent. In $N_2$ deaerated DMF, complex **2** exhibited a luminescence quantum yield of 0.15 and lifetime of 890 ns which is comparable to previously reported *bis*-cyclometalated Ir(III) complexes in DMF.[146] Again the difference in quantum yield and lifetime between **1** and **2** is likely due to the differences in solvent. Unfortunately, due to the drastic differences in solubility, we were unable to find shared solvent to further verify this hypothesis. For both **1** and **2,** there was a greater than two-fold decrease in excited state lifetime under ambient atmosphere

relative to $N_2$ deaerated samples (Table B.1). In accord with previous assignments,[148] excited state quenching by $O_2$ lends further support that the emission occurs primarily from a long-lived, triplet state. The above photophysical data for complex **1** and **2** demonstrate that structural modification of *bis*-cyclometalated iridium complexes, with metal ion binding groups for example, can be achieved while still maintaining favorable long-lived excited states and high emission quantum yields.

### 3.3.3 Electrochemical measurements

Electrochemical measurements were used to examine the redox potentials and stability of these new complexes and the results are summarized in Table 3.1. The cyclic voltammograms of **1** in acetonitrile are shown in Figure 3.4. The red scan in Figure 3.4 shows the first cathodic wave of **1** occurs at $E_{red,1}$ = -1.32 V versus the saturated calomel electrode (SCE) and is reversible with a $\Delta E_p \approx 70$ mV and an anodic to cathodic current ratio of unity. This one-electron reduction is attributed to the reduction of the neutral bpy-$PO_3Et_2$ ligand. Tunable redox properties are important for properly matching photoredox catalysts with desired substrate and product scopes.[158]

Performing a full cyclic voltammetry scan (black trace in Figure 3.4), led to the appearance of two more cathodic waves, and one anodic wave. The two additional one-electron cathodic waves at $E_{red,2}$ = -2.16 V and $E_{red,3}$ = -2.41 V vs SCE are attributed to the reduction of the ppy ligands and are quasi-reversible ($\Delta E_p \approx 80$ mV, anodic/cathodic current less than unity). The reduction of the ppy ligands also leads to the observation of an additional, irreversible anodic event near -0.5 V vs SCE. This additional anodic event is clearly not observed in the red cyclic voltammogram; thus, it arises from reduction of

the ppy ligands. This irreversible anodic wave is attributed to a small amount of decomposition of complex **1** that can occur under highly negative applied potentials. Lastly, a quasi-reversible anodic wave is observed with an $E_{ox}$ = 1.29 V vs SCE. This wave is attributed to the Ir(IV/III) redox couple and is within 40 mV of the value reported for $[Ir(ppy)_2(4,4'\text{-bis}(\textit{tert}\text{-butyl})\text{-}2,2'\text{-bipyridine})]PF_6$.[142]

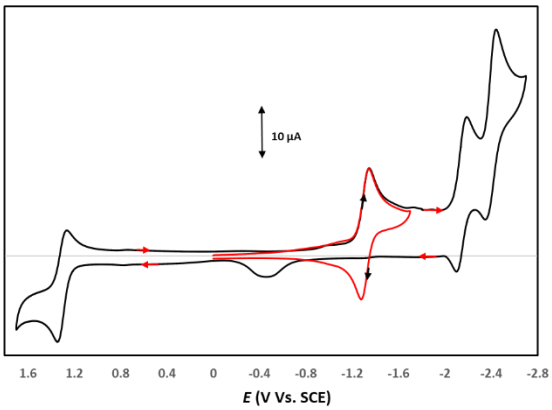


**Figure 3.4**. Cyclic voltammograms of 1.0 mM **1** in acetonitrile with 0.1 M $NBu_4PF_6$ supporting electrolyte (Glassy carbon working electrode; Pt counter electrode; scan rate = 100 $mVs^{-1}$). Both red and black voltammograms started at 0.0 V vs SCE and initially scanned towards negative potentials.

The phosphonate groups of complex **2** are known to bind strongly to metal oxide supports[159] which is a key step in the preparation of DSSCs and DSPECs.[138] To examine the possible binding of **2** to a metal oxide support we first soaked a nanostructured Sn(IV)-doped $In_2O_3$ (nanoITO) electrode in a DMF solution containing 0.1 mM **2** overnight. The high surface area, conductive nanoITO electrodes were prepared according to literature procedure.[160] The oxidative cyclic voltammogram of a nanoITO

electrode derivatized with **2** is shown in the supporting information Figure B.3. A redox couple was observed at $E_{ox}$ = 1.45 V vs SCE and is attributed to the Ir(IV/III) oxidation, which gives evidence that complex **2** does bind to metal oxide supports. Using the equation $Q = nFA\Gamma$, where Q is the integrated charge of the cyclic voltammogram wave, n is the number of electrons transferred and equal to 1, $F$ is the Faraday constant, and A is the area of the electrode, the surface coverage ($\Gamma$) of **2** on the nanoITO electrode was determined to be $9.96\times10^{-7}$ mol/cm$^2$.[159] Closest packed, monolayer surface coverage and oxidative stability are desirable traits for photosensitizers in DSSCs and DSPECs.[161]

Due to ITO electrodes being unstable under negative applied potentials, the electrochemical reduction of **2** was performed in a homogeneous solution. Furthermore, due to poor solubility of **2**, differential pulse voltammetry (DPV) was used to study **2**, as DPV is a more sensitive technique compared to cyclic voltammetry. Figure B.4 shows that complex **2** undergoes three one-electron reductions, analogous to complex **1**. The second and third reductions of **2** occurred at $E_{red,2}$ = -2.20 V and $E_{red,3}$ = -2.51 V vs SCE are assigned to the reductions of the ppy ligands and are only slightly more negative than the ppy reduction potentials found for complex **1**. The first reduction of **2**, however, occurs at -1.78 V vs SCE which is roughly 500 mV more negative compared to the first reduction of **1**. This shift in reduction potential is consistent with the blue shift in the emission data when comparing the two complexes.

### 3.3.4 Devices

For a proof-of-concept demonstration of the oxidative strength of these iridium chromophores we generate a dye-sensitized solar cell (DSSC). The DSSC components,

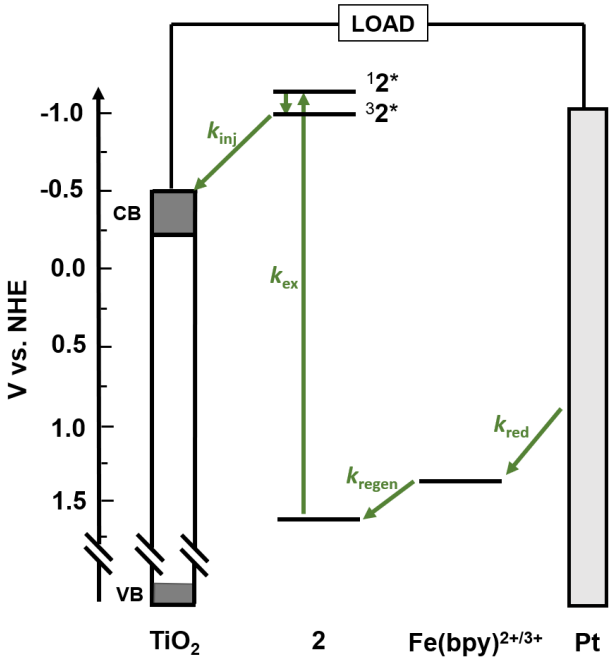


**Figure 3.5**. Dynamic events, energetics (vs NHE) of $TiO_2$, **2**, and $Fe(bpy)_3$ with productive processes shown in green. ($k_{ex}$ = excitation, $k_{inj}$ = electron injection, $k_{regen}$ = regeneration, $k_{red}$ = mediator reduction).

energetics, and dynamic events are depicted in Figure 3.5. The DSSCs were composed of $TiO_2$ or $TiO_2$-**2** photoanodes, a platinum cathode, and an electrolyte containing 0.1 M $Fe^{II}(bpy)_3(BF_4)_2$, 0.01 M $Fe^{III}(bpy)_3(PF_6)_3$, and 0.1 M 4-*tert*-butylpyridine in a MeCN solution. The $TiO_2$-**2** anode was prepared by first doctor blading and sintering a $TiO_2$ sol-gel paste on FTO coated glass and then soaking the $TiO_2$ in a 0.50 mM solution of **2** in DMSO. In contrast to the $TiO_2$ only film, a new low energy absorption feature from 360-500 nm can be observed for $TiO_2$-**2** that is consistent with the absorption onset of **2** in solution (Figure B.5). $Fe^{II}(bpy)_3^{3+/2+}$ was selected as the redox mediator because its redox couple ($E_{1/2ox}$ = 1.37 V vs NHE) is >500 mV more positive than the traditional cobalt

polypyridyl ($E_{1/2ox}$ = 0.4-0.85 V vs NHE) and $I^-/I_3^-$ (0.35 V vs NHE) mediators,[162-163] and has recently been implemented by Delcamp and coworkers in high voltage DSSCs.[164-165]

The triplet excited state oxidation potential for **2** was calculated by using $E_{1/2}^* = E_{1/2ox} - \Delta G_{ES}$,[166] where $E_{1/2ox}$ is the ground state oxidation potential ($E_{1/2}^{ox}$ = 1.64 V vs NHE; SCE is 0.24 V vs NHE)[167] and $\Delta G_{ES}$ is the thermally equilibrated lowest energy excited state ($\Delta G_{ES}$ = 2.65 eV) determined from the tangent to the inflection point on the high energy emission side of **2**. The excited state potential of **2** ($E_{1/2}^*$ = -1.0 eV) is sufficient for excited state electron transfer ($k_{inj}$) into the conduction band of $TiO_2$ ($E_{CB}$ = -0.5 eV).[13] Additionally, following electron injection there >250 meV driving force for regeneration ($k_{regen}$) of the oxidized dye by $Fe^{II}(bpy)_3^{2+}$.

J-V curves for the devices containing either $TiO_2$ or $TiO_2$-**2** photoanodes were acquired and the results are shown in Figure 3.6 with the relevant metrics reported in Table 3.2. Under one sun irradiation (AM1.5), the short circuit current ($J_{SC}$), fill factor (FF), and power conversion efficiency (η) were relatively low. This is not surprising given that the $J_{SC}$ is directly dependent on the light harvesting efficiency of the dye. The low spectral overlap between **2** and the solar spectrum, combined with the less than 0.1 O.D. (80% transmittance), are inherent limitations to the current device performance. However, despite the low overall performance the device exhibited an 870 mV open circuit voltage ($V_{OC}$). This high voltage is remarkable for two reasons. First, it is on par with current record DSSCs.[168] Second, in a DSSC the maximum $V_{oc}$ is dictated by the energy difference between the quasi Fermi level of the electrons within the semiconductor and potential of the redox mediator.[11] While the mediator potential here is fixed, the Fermi level, and resulting $V_{oc}$, is dictated by the ratio between the rate of

electrons entering and exiting the metal oxide.[169] Thus, despite the extremely low light harvesting efficiency and limited number of electron entering the conduction band, the $V_{OC}$ of $TiO_2$-**2** is still >800 mV. To maximize the potential of this device, we decided to increase the photon flux and the number of injected electrons by irradiating the sample with a 4 mW/cm$^2$, 395 nm LED. This LED is the equivalent of 6.7 times AM1.5 sun intensity integrating from 390-400 nm. Under high intensity excitation, we see a dramatic increase in both $J_{SC}$ and $V_{OC}$ giving 0.140 mA/cm$^2$ and 1060 mV, respectively. It is worth noting that with no device optimization (i.e. co-surfactant, $TiCl_4$ treatment, optimized thickness, back reflector, etc.) at least one device achieved a $V_{OC}$ as high as 1.12 V.

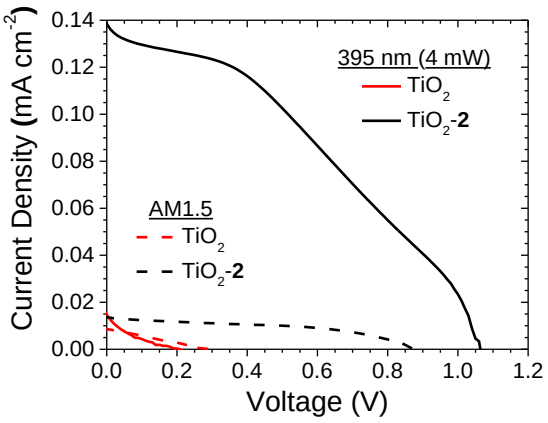


**Figure 3.6**. Photocurrent density – voltage (J-V) curves for DSSCs with photoanodes composed of $TiO_2$ (red) and $TiO_2$-**2** (black) with $Fe(bpy)^{2+/3+}$ redox mediator under 1 sun (dashed) and 4 mW of 395 nm LED excitation (solid).

Given the strong spectral overlap between $TiO_2$ and **2**, a $TiO_2$ only device was used as a control to determine its contribution to the overall performance. As can be seen in Figure 3.6 and Table 3.2, the $TiO_2$ only devices exhibited notable lower performance

than $TiO_2$-**2**. In fact, from the incident photon-to-current efficiency (IPCE) measurement (Figure B.3), the dramatic decrease in IPCE below ~350 nm can be attributed to light absorption but minimal photocurrent generation by the $TiO_2$ directly. Thus, the observed device performance can be attributed directly to the dye sensitization process.

**Table 3.2**. Performance characteristics of DSSCs containing $TiO_2$ and $TiO_2$-**2** photoanodes with $Fe(bpy)^{2+/3+}$ redox mediator under 1 sun and 395 nm ($4W/cm^2$) excitation.[a]

| Sample | Excitation | $J_{sc}$($mA \cdot cm^{-2}$) | $V_{oc}$(mV) | FF | η (%) |
|---|---|---|---|---|---|
| $TiO_2$ | AM 1.5 | 0.009 | 275 | 0.27 | 0.06 |
| | 395 nm | 0.015 | 200 | 0.22 | 0.01 |
| $TiO_2$-**2** | AM 1.5 | 0.014 | 870 | 0.48 | 0.60 |
| | 395 nm | 0.140 | 1060 | 0.36 | 0.80 |

[a]All data were reproducible across three independent samples with <10% deviation from the numbers reported here.

### 3.4 Conclusions

Two bis-cyclometalated Ir(III) complexes containing phosphonomethyl substituted bipyridine ligands have been synthesized and characterized. Even with surface binding groups, the phosphonated bis-cyclometalated Ir(III) complexes retain their photophysical and electrochemical properties including long-lived excited-state lifetimes, high emission quantum yields, and reversible redox chemistry. Furthermore, complex **2** was shown to be suitable for attachment to metal oxide surfaces and use in DSSCs. Despite the low light harvesting efficiency, the devices exhibited remarkable high open circuit voltages (>1 V). These results indicate that molecule **2** can serve as a strong oxidant in a high voltage photochemical device. The spectral limitations reduce its utility in solar energy conversion but this surface bound dye could serve as a strong light driven oxidizing agent for synthetically challenging photoredox reactions.[170]

### 3.5 Experimental

All chemicals were purchased from Sigma-Aldrich, VWR or Alfa Aesar and used without further purification. Deaerated acetonitrile (MeCN) 99.8%, water ≤ 50 ppm) and deaerated dimethylformamide (DMF) were used for all work. No unexpected or new hazards are associated with this work. As is the case with all chemical research safety precautions such as personal protective equipment (gloves, lab coat, safety glasses) were used and all work was performed in well ventilated chemical hoods and laboratories.

The 4,4′-bis(diethylphosphonoethyl)-2,2′-bipyridine (bpy-$CH_2PO_3Et_2$) ligand was synthesized according to a previously reported procedure.[147] Complex **1** was synthesized with a procedure analogous to a previously reported procedure.[147] To a 3:1 ethanol:water mixture, 200 mg (0.18 mmol) of $[Ir(ppy)_2(\square\text{-}Cl)]_2$ and 179 mg (0.39 mmol) of bpy-$CH_2PO_3Et_2$ were added. The reaction solution was heated at reflux temperature for 8 hours. The reaction mixture was then allowed to cool to room temperature and the ethanol was removed under vacuum. The product was precipitated from the reaction mixture with the addition of $KPF_6$ to the aqueous solution. The solid product was then filtered, rinsed with water, and dried under vacuum for a final yield of 82% (141 mg, 0.147 mmols). $^1$H NMR (400 MHz, $CD_3CN$) δ ppm 8.44 (s, 2H), 8.10 (d, 2H), 7.90 (d, 2H), 7.86-7.81 (m, 3H), 7.64 (d, 2H), 7.45-7.43 (m, 2H), 7.09-7.02 (m, 4H), 6.94 (t, 2H), 6.30 (d, 2H), 4.07-3.39 (m, 8H), 3.44 (s, 2H), 3.37(s, 2H), 1.21-1.13 (m, 13H). $^{13}$C NMR (100 MHz, $CD_3CN$) δ ppm 167.45, 155.52, 150.25, 149.06, 146.57, 144.02, 138.57, 131.58, 130.37, 129.44, 125.66, 124.92, 123.47, 122.55, 119.91, 62.51, 33.46, 32.13, 15.65. $^{31}$P NMR (121.5 MHz, $CD_3CN$) δ ppm 22.63. Elemental Analysis: Calc. for $IrC_{42}H_{46}O_6N_4P_3F_6$: C, 45.78; H, 4.20; N, 5.08. Found: C, 45.55; H, 4.80; N, 4.85.

Complex **2** was synthesized by dissolving 100 mg (0.09 mmol) of **1** and 167 mg (1.09 mmol) of $(CH_3)_3SiBr$ in 20 ml of a dry 1:1 acetonitrile:dichloromethane solution under a $N_2$ atmosphere. The reaction mixture was sealed in a Teflon screw cap glass container and heated at 70 °C while stirring for 12 hours. The solvent was then removed by rotary evaporation. The yellow solid product was washed thoroughly with both diethyl ether and water, then dried for a final yield of 82% (63 mg, 0.074 mmols). $^1$H NMR (400 MHz, $d_6$-DMSO) δ ppm 8.71 (s, 2H), 8.16 (d, 2H), 7.83-7.81 (m, 4H), 6.59 (d, 2H), 7.50 (d, 2H), 7.40 (d, 2H), 7.09 (d, 2H), 6.93 (t, 2H), 6.81 (t, 2H), 6.11 (d, 2H), 3.09 (s, 2H), 3.04 (s, 2H). $^{13}$C NMR (100 MHz, $d_6$-DMSO) δ ppm 167.35, 155.16, 151.25, 150.20, 149.26, 149.02, 144.27, 139.12, 131.47, 130.67, 129.94, 126.26, 125.50, 124.48, 122.61, 120.50, 37.49, 36.26. $^{31}$P NMR (121.5 MHz, $d_6$-DMSO) δ ppm 14.79. Elemental Analysis: Calc. for $IrC_{34}H_{30}O_6N_4P_3F_6$: C, 44.04; H, 3.26; N, 6.04. Found: C, 43.61; H, 3.88; N, 6.00.

$Fe^{II}(bpy)_3(BF_4)_2$ was synthesized following previous literature procedure,[171] with the following modification. Once all reactants were dissolved, a saturated aqueous solution of $NaBF_4$ was added dropwise to the reaction solution, until no more red precipitate was formed. $Fe^{III}(bpy)_3(PF_6)_3$ was synthesized from literature procedure as follows, except the use of $NH_3PF_6$ instead of $KPF_6$.[172]

*Electrochemical measurements* contained 0.1 M tetrabutylammonium hexafluorophosphate ($TBAPF_6$) which was further purified by recrystallization from ethanol and dried under vacuum for 24 hours at 80 $^o$C. Differential pulse voltammetry (DPV) experiments were conducted on a Pine wavedriver 20 biopotentiostat system. Cyclic voltammetry (CV) was carried out using a CH Instruments 601D potentiostat. The

working electrode was a 3-mm diameter glassy-carbon electrode (CH Instruments), prepared by manually polishing with 0.05 μm Alumina suspension (DE agglomerated, Allied High Tech Product, iNC). A Pt wire (99.99%) was used as the counter electrode. The reference electrode was a saturated calomel electrode (SCE) (CH Instruments).

Electrochemical measurements using nanoITO as the working electrode also used Pt wire as the counter electrode and SCE as the reference electrode. The three-dimensional, conductive nanoITO electrodes were prepared according to literature procedure.[160] Derivatization of the nanoITO electrodes was achieved by soaking the electrodes in a 0.1 mM solution of **2** in methanol overnight.

*Absorption* data were recorded on an Agilent 8453 UV−visible photo diode array spectrophotometer using a 1 × 1 cm quartz cuvette.

*Steady-State and Time-Resolved Emission* data were collected at room temperature using an Edinburgh FLS980 spectrometer. Detreated samples were first bubbled with $N_2$ for one hour before spectra were obtained. Samples were excited using light output from a housed 450 W Xe lamp passed through a single grating (1800 l/mm, 250 nm blaze) Czerny-Turner monochromator. Emission from the sample was passed through a single grating (1800 l/mm, 500 nm blaze) Czerny-Turner monochromator and finally detected by a peltier-cooled Hamamatsu R928 photomultiplier tube.

The dynamics of emission decay were monitored by using the FLS980's time-correlated single-photon counting capability (1024 channels; 10 μs window for samples in $O_2$ and 20 μs window for $N_2$ samples) with data collection for 5,000 counts. Excitation for TCSPC was provided by an Edinburgh EPL-405 ps pulsed light emitting diode (405 ±

10 nm, pulse width 58 ps) operated at 10 MHz. Emission was passed through a single grating (1800 l/mm, 500 nm blaze) Czerny−Turner monochromator and finally detected by a Peltier-cooled Hamamatsu R928 photomultiplier tube. Time-resolved emission data were fit using a mono-exponential function (equation 3.1) using Edinburgh software package.

$$y = A_1 e^{-k1x} + y_0 \qquad (\mathbf{3.1})$$

*Quantum Yield* data were collected at room temperature using a Hamamatsu Quantaurus-QY Spectrometer. Samples and the solvent-only reference were place in a 13 cm × 1 cm round bottom quartz tube containing ~1 mL of solvent. Samples were excited using a 405 nm output from a 150 W Xenon arc lamp and detected by a back-illuminated cooled 1024 channel CCD detector. Quantum yields were calculated using the Quantaurus software package.

*NMR* spectra were recorded on Bruker Avance III 400 MHz NMR spectrometer and were calibrated using residual undeuterated solvent as an internal reference.

*Mass spectrometry*. Electron ionization was 70 eV and the spectrometer was scanned from 1000 to 50 m/z at low resolution.

*Computations* were performed using ADF2014.10[173-174]. A triple-ζ STO basis set with one polarization function (TZP) was used in all calculations. Molecular geometries were calculated with the VWN functional with the Stoll correction implemented.[175] Relativistic effects were taken into account by using the scalar ZORA formalism.[176] Theoretical stretching frequencies were calculated analytically and the lack of imaginary frequencies showed that the geometry were true minima. Solvation effects were modeled through the

conductor-like screening model (COSMO).[177] Electronic absorption spectra were calculated using time-dependent DFT (TD-DFT) using the PBE functional.[178] Calculated singlet excitation states were red shifted by 5 nm in Figure 3.3 of the manuscript.

*$TiO_2$ sol-gel* was prepared following our previously published procedure.[133] Briefly, 7.3 mL (11 wt%) of tetraisopropyl orthotitanate was added dropwise (110 mL/hr) to an ice cooled, rapidly stirring (300 rpm) 125 mL Erlenmeyer flask containing a solution of 0.42 mL nitric acid in 60 mL deionized water. The slurry was stirred for 15 min after which the flask was covered with aluminum foil and heated up to 95 °C. The sample was held at this temperature until the volume was reduced, through evaporation, to 18 mL. The solution was placed in an acid digestion vessel (VWR, 25227-094) and heated in a box furnace (Thermo Scientific, BF51866A-1) at 200 °C at 10.5 h. Upon cooling to room temperature, the solution was transferred to a glass vial. To the solution, 1g (5.3 wt%) of carbowax copolymer (ground to powder with a mortar and pestle) and the mixture was stirred for another 48 h.

*Film Preparation.* FTO glass substrates were sonicated in ethanol and then HCl/Ethanol (15/85% mix) for 20 min. Nanocrystalline $TiO_2$ films ~2.4 μm thick, coating an area of 7 × 7 mm on top of FTO glass were prepared by doctor blading (1 layer of scotch tape) with the $TiO_2$ paste and subsequently sintering them at 500 °C for 30 min. The $TiO_2$-**2** film was prepared by soaking $TiO_2$ in a 0.50 mM solution of **2** in DMSO for 24 hours followed by rinsing with MeOH and drying under a stream of air.

*DSSC Fabrication.* The $TiO_2$ films ($TiO_2$ and $TiO_2$–**2**) on FTO glass (1.4 × 1.9 $cm^2$) served as the photoanode of the DSSCs. The cathode was prepared by first drilling a

small hole (d = 1.1 mm) into the corner of the 2.0 × 2.2 $cm^2$ glass slide. The drilled slides were thereafter sonicated with ethanol for 10 min. This was followed by deposition of platinum by drop casting 75 μL of a ~4 mM solution of $H_2PtCl_6$ in ethanol on FTO glass followed by heat treatment (400 °C) using a Leister hot air blower. DSSC sandwich cells were prepared using a home-built assembly apparatus.[133, 179] A 2 mm wide 1.2 × 1.2 $cm^2$ Surlyn thermoplastic (25 μm thick Meltonix 1170- 25 from Solaronix) was placed between the anode and the cathode and the entire ensemble was heated to ~150 °C for 7 s. The $Fe(bpy)_3^{3+/2+}$ electrolyte solution (0.1 M $Fe^{II}(bpy)3(BF_4)_2$, 0.01 M $Fe^{III}(bpy)_3(PF_6)_3$, 0.1 M 4-tert-butylpyridine) was introduced into the cell through a hole on the counter electrode using a Vac'n Fill Syringe (65209, Solaronix). The cell was then sealed by heating a meltonix film and a 4 × 4 $mm^2$ portion of a micro cover glass slide (18 × 18 $mm^2$ VWR).

### 3.6 References


1. Lamansky, S.; Djurovich, P.; Murphy, D.; Abdel-Razzaq, F.; Lee, H.-E.; Adachi, C.; Burrows, P. E.; Forrest, S. R.; Thompson, M. E., Highly Phosphorescent Bis-Cyclometalated Iridium Complexes: Synthesis, Photophysical Characterization, and Use in Organic Light Emitting Diodes. *J. Am. Chem. Soc.* **2001,** *123* (18), 4304-4312.

2. Mayo, E. I.; Kilså, K.; Tirrell, T.; Djurovich, P. I.; Tamayo, A.; Thompson, M. E.; Lewis, N. S.; Gray, H. B., Cyclometalated iridium(iii)-sensitized titanium dioxide solar cells. *Photochem. Photobiol. Sci.* **2006,** *5* (10), 871-873.

3. Ogunsolu, O. O.; Murphy, I. A.; Wang, J. C.; Das, A.; Hanson, K., Energy and Electron Transfer Cascade in Self-Assembled Bilayer Dye-Sensitized Solar Cells. *ACS Appl. Mater. Interfaces* **2016,** *8* (42), 28633-28640.

4. Légalité, F.; Escudero, D.; Pellegrin, Y.; Blart, E.; Jacquemin, D.; Fabrice, O., "Iridium effect" in cyclometalated iridium complexes for p-type dye sensitized solar cells. *Dyes Pigm.* **2019,** *171*, 107693-107702.

5. Blakemore, J. D.; Crabtree, R. H.; Brudvig, G. W., Molecular Catalysts for Water Oxidation. *Chem. Rev. (Washington, DC, U. S.)* **2015,** *115* (23), 12974-13005.

6. Salpage, S. R.; Paul, A.; Som, B.; Banerjee, T.; Hanson, K.; Smith, M. D.; Vannucci, A. K.; Shimizu, L. S., Structural, electrochemical and photophysical properties of an exocyclic di-ruthenium complex and its application as a photosensitizer. *Dalton Trans.* **2016,** *45* (23), 9601-9607.

7. Lo, K. K.-W.; Chan, J. S.-W.; Lui, L.-H.; Chung, C.-K., Novel Luminescent Cyclometalated Iridium(III) Diimine Complexes That Contain a Biotin Moiety. *Organometallics* **2004,** *23* (13), 3108-3116.

8. Ashford, D. L.; Gish, M. K.; Vannucci, A. K.; Brennaman, M. K.; Templeton, J. L.; Papanikolas, J. M.; Meyer, T. J., Molecular Chromophore–Catalyst Assemblies for Solar Fuel Applications. *Chem. Rev. (Washington, DC, U. S.)* **2015,** *115* (23), 13006-13049.

9. Mills, I. N.; Porras, J. A.; Bernhard, S., Judicious Design of Cationic, Cyclometalated Ir(III) Complexes for Photochemical Energy Conversion and Optoelectronics. *Acc. Chem. Res.* **2018,** *51* (2), 352-364.

10. McDaniel, N. D.; Coughlin, F. J.; Tinker, L. L.; Bernhard, S., Cyclometalated iridium(III) aquo complexes: Efficient and tunable catalysts for the homogeneous oxidation of water. *J. Am. Chem. Soc.* **2008,** *130* (1), 210-217.

11. Paul, A.; Smith, M. D.; Vannucci, A. K., Photoredox-Assisted Reductive Cross-Coupling: Mechanistic Insight into Catalytic Aryl–Alkyl Cross-Couplings. *J. Org. Chem.* **2017,** *82* (4), 1996-2003.

12. Slinker, J. D.; Gorodetsky, A. A.; Lowry, M. S.; Wang, J.; Parker, S.; Rohl, R.; Bernhard, S.; Malliaras, G. G., Efficient Yellow Electroluminescence from a Single Layer of a Cyclometalated Iridium Complex. *J. Am. Chem. Soc.* **2004,** *126* (9), 2763-2767.

13. De Angelis, F.; Fantacci, S.; Evans, N.; Klein, C.; Zakeeruddin, S. M.; Moser, J.-E.; Kalyanasundaram, K.; Bolink, H. J.; Grätzel, M.; Nazeeruddin, M. K., Controlling Phosphorescence Color and Quantum Yields in Cationic Iridium Complexes: A Combined Experimental and Theoretical Study. *Inorg. Chem.* **2007,** *46* (15), 5989-6001.

14. Nazeeruddin, M. K.; Wegh, R. T.; Zhou, Z.; Klein, C.; Wang, Q.; De Angelis, F.; Fantacci, S.; Grätzel, M., Efficient Green-Blue-Light-Emitting Cationic Iridium Complex for Light-Emitting Electrochemical Cells. *Inorg. Chem.* **2006,** *45* (23), 9245-9250.

15. Lowry, M. S.; Bernhard, S., Synthetically Tailored Excited States: Phosphorescent, Cyclometalated Iridium(III) Complexes and Their Applications. *Chem-Eru. J.* **2006,** *12* (31), 7970-7977.

16. Lowry, M. S.; Hudson, W. R.; Pascal, R. A.; Bernhard, S., Accelerated Luminophore Discovery through Combinatorial Synthesis. *J. Am. Chem. Soc.* **2004,** *126* (43), 14129-14135.

17. Paul, A.; Das, N.; Halpin, Y.; Vos, J. G.; Pryce, M. T., Carboxy derivatised Ir(iii) complexes: synthesis, electrochemistry, photophysical properties and photocatalytic hydrogen generation. *Dalton Trans.* **2015,** *44* (22), 10423-10430.

18. Baranoff, E.; Yum, J.-H.; Graetzel, M.; Nazeeruddin, M. K., Cyclometallated iridium complexes for conversion of light into electricity and electricity into light. *J. Organomet. Chem.* **2009,** *694* (17), 2661-2670.

19. King, K. A.; Watts, R. J., Dual emission from an ortho-metalated iridium(III) complex. *J. Am. Chem. Soc.* **1987,** *109* (5), 1589-1590.

20. Tsuboyama, A.; Iwawaki, H.; Furugori, M.; Mukaide, T.; Kamatani, J.; Igawa, S.; Moriyama, T.; Miura, S.; Takiguchi, T.; Okada, S.; Hoshino, M.; Ueno, K., Homoleptic Cyclometalated Iridium Complexes with Highly Efficient Red Phosphorescence and Application to Organic Light-Emitting Diode. *J. Am. Chem. Soc.* **2003,** *125* (42), 12971-12979.

21. Sajoto, T.; Djurovich, P. I.; Tamayo, A.; Yousufuddin, M.; Bau, R.; Thompson, M. E.; Holmes, R. J.; Forrest, S. R., Blue and Near-UV Phosphorescence from Iridium Complexes with Cyclometalated Pyrazolyl or N-Heterocyclic Carbene Ligands. *Inorg. Chem.* **2005,** *44* (22), 7992-8003.

22. Hanson, K.; Losego, M. D.; Kalanyan, B.; Parsons, G. N.; Meyer, T. J., Stabilizing Small Molecules on Metal Oxide Surfaces Using Atomic Layer Deposition. *Nano Lett.* **2013,** *13* (10), 4802-4809.

23. Materna, K. L.; Crabtree, R. H.; Brudvig, G. W., Anchoring groups for photocatalytic water oxidation on metal oxide surfaces. *Chem. Soc. Rev.* **2017,** *46* (20), 6099-6110.

24. Hanson, K.; Brennaman, M. K.; Luo, H. L.; Glasson, C. R. K.; Concepcion, J. J.; Song, W. J.; Meyer, T. J., Photostability of Phosphonate-Derivatized, Ru-II Polypyridyl Complexes on Metal Oxide Surfaces. *ACS Appl. Mater. Interfaces* **2012,** *4* (3), 1462-1469.

25. Gillaizeau-Gauthier, I.; Odobel, F.; Alebbi, M.; Argazzi, R.; Costa, E.; Bignozzi, C. A.; Qu, P.; Meyer, G. J., Phosphonate-based bipyridine dyes for stable photovoltaic devices. *Inorg. Chem.* **2001,** *40* (23), 6073-6079.

26. Colombo, M. G.; Guedel, H. U., Synthesis and high-resolution optical spectroscopy of bis[2-(2-thienyl)pyridinato-C3,N'](2,2'-bipyridine)iridium(III). *Inorg. Chem.* **1993,** *32* (14), 3081-3087.

27. Hanson, K.; Brennaman, M. K.; Ito, A.; Luo, H.; Song, W.; Parker, K. A.; Ghosh, R.; Norris, M. R.; Glasson, C. R. K.; Concepcion, J. J.; Lopez, R.; Meyer, T. J., Structure–Property Relationships in Phosphonate-Derivatized, Ru II Polypyridyl Dyes on Metal Oxide Surfaces in an Aqueous Environment. *J. Phys. Chem. C* **2012,** *116* (28), 14837-14847.

28. Shaw, M. H.; Twilton, J.; MacMillan, D. W. C., Photoredox Catalysis in Organic Chemistry. *J. Org. Chem.* **2016,** *81,* 6898-6926.

29. Vannucci, A. K.; Alibabaei, L.; Losego, M. D.; Concepcion, J. J.; Kalanyan, B.; Parsons, G. N.; Meyer, T. J., Crossing the divide between homogeneous and heterogeneous catalysis in water oxidation. *Proc. Natl. Acad. Sci.* **2013,** *110,* 20918-20922.

30. Hoertz, P. G.; Chen, Z.; Kent, C. A.; Meyer, T. J., Application of High Surface Area Tin-Doped Indium Oxide Nanoparticle Films as Transparent Conducting Electrodes. *Inorg. Chem.* **2010,** *49* (18), 8179-8181.

31. Song, W. J.; Vannucci, A. K.; Farnum, B. H.; Lapides, A. M.; Brennaman, M. K.; Kalanyan, B.; Alibabaei, L.; Concepcion, J. J.; Losego, M. D.; Parsons, G. N.; Meyer, T. J., Visible Light Driven Benzyl Alcohol Dehydrogenation in a Dye-Sensitized Photoelectrosynthesis Cell. *J. Am. Chem. Soc.* **2014,** *136* (27), 9773-9779.

32. Feldt, S. M.; Gibson, E. A.; Gabrielsson, E.; Sun, L.; Boschloo, G.; Hagfeldt, A., Design of Organic Dyes and Cobalt Polypyridine Redox Mediators for High-Efficiency Dye-Sensitized Solar Cells. *J. Am. Chem. Soc.* **2010,** *132* (46), 16714-16724.

33. Giribabu, L.; Bolligarla, R.; Panigrahi, M., Recent Advances of Cobalt(II/III) Redox Couples for Dye-Sensitized Solar Cell Applications. *Chem. Rec.* **2015,** *15* (4), 760-788.

34. Rodrigues, R. R.; Peddapuram, A.; Dorris, A. L.; Hammer, N. I.; Delcamp, J. H., Thienopyrroledione-Based Photosensitizers as Strong Photoinduced Oxidants: Oxidation

of Fe(bpy)32+ in a >1.3 V Dye-Sensitized Solar Cell. *ACS Appl. Energy Mater.* **2019,** *2* (8), 5547-5556.

35. Rodrigues, R. R.; Cheema, H.; Delcamp, J. H., A High-Voltage Molecular-Engineered Organic Sensitizer–Iron Redox Shuttle Pair: 1.4 V DSSC and 3.3 V SSM-DSSC Devices. *Angew. Chem. Int. Edit.* **2018,** *57* (19), 5472-5476.

36. Bock, C. R.; Connor, J. A.; Gutierrez, A. R.; Meyer, T. J.; Whitten, D. G.; Sullivan, B. P.; Nagle, J. K., Estimation of excited-state redox potentials by electron-transfer quenching. Application of electron-transfer theory to excited-state redox processes. *J. Am. Chem. Soc.* **1979,** *101* (17), 4815-4824.

37. Felton, G. A. N.; Mebi, C. A.; Petro, B. J.; Vannucci, A. K.; Evans, D. H.; Glass, R. S.; Lichtenberger, D. L., Review of electrochemical studies of complexes containing the Fe2S2 core characteristic of [FeFe]-hydrogenases including catalysis by these complexes of the reduction of acids to form dihydrogen. *J. Organomet. Chem.* **2009,** *694* (17), 2681-2699.

38. Hagfeldt, A.; Boschloo, G.; Sun, L.; Kloo, L.; Pettersson, H., Dye-sensitized solar cells. *Chem. Rev. (Washington, DC, U. S.)* **2010,** *110* (11), 6595-6663.

39. Carella, A.; Borbone, F.; Centore, R., Research Progress on Photosensitizers for DSSC. *Front. Chem.* **2018,** *6*, 481-481.

40. Nazeeruddin, M. K.; Baranoff, E.; Grätzel, M., Dye-sensitized solar cells: A brief overview. *Sol. Energy* **2011,** *85* (6), 1172-1178.

41. Ardo, S.; Meyer, G. J., Photodriven heterogeneous charge transfer with transition-metal compounds anchored to TiO2 semiconductor surfaces. *Chem. Soc. Rev.* **2009,** *38* (1), 115-164.

42. Zuo, Z.; Ahneman, D. T.; Chu, L.; Terrett, J. A.; Doyle, A. G.; MacMillan, D. W. C., Merging photoredox with nickel catalysis: Coupling of a-carboxyl sp3-carbons with aryl halides. *Science* **2014,** *345*, 437-440.

43. Bouzaid, J.; Schultz, M.; Lao, Z.; Bartley, J.; Bostrom, T.; McMurtrie, J., Supramolecular selection in molecular alloys. *Cryst. Growth Des.* **2012,** *12* (8), 3906-3916.

44. DeSimone, R. E.; Drago, R. S., Magnetic resonance studies of some low-spin d5 tris diimine complexes. *J. Am. Chem. Soc.* **1970,** *92* (8), 2343-2352.

45. Theoretical Chemistry, V. U. A., ADF, Amsterdam density functional program, http://www.scm.com.

46. te Velde, G.; Bickelhaupt, F. M.; Baerends, E. J.; Fonseca Guerra, C.; van Gisbergen, S. J. A.; Snijders, J. G.; Ziegler, T., Chemistry with ADF. *J. Comput. Chem.* **2001,** *22* (9), 931-967.

47. Stoll, H.; Pavlidou, C. M. E.; Preuß, H., On the calculation of correlation energies in the spin-density functional formalism. *Theor. Chim. Acta* **1978,** *49* (2), 143-149.

48. van Lenthe, E.; Ehlers, A. W.; Baerends, E., Geometry optimizations in the zero order regular approximation for relativistic effects. *J. Chem. Phys.* **1999,** *110*, 8943-8953.

49. Klamt, A., Conductor-like Screening Model for Real Solvents: A New Approach to the Quantitative Calculation of Solvation Phenomena. *J. Phys. Chem.* **1995,** *99*, 2224-2235.

50. Perdew, J. P.; Burke, K.; Ernzerhof, M., Generalized Gradient Approximation Made Simple. *Phys. Rev. Lett.* **1996,** *77* (18), 3865-3868.

51. Ogunsolu, O. O.; Wang, J. C.; Hanson, K., Inhibiting Interfacial Recombination Events in Dye-Sensitized Solar Cells using Self-Assembled Bilayers. *ACS Appl. Mater. Interfaces* **2015,** *7* (50), 27730-27734.

# CHAPTER 4

# CONCLUSIONS AND FUTURE WORK

Advancements in photocatalysis have opened a plethora of synthetic pathways utilizing both organic and inorganic based catalysts. These elegant systems achieve unique and targeted reactivity while maintaining mild catalytic conditions. This work presents a structural based tuning of organic photocatalyst design based upon an established photoactive backbone, such as Eosin Y, which allows for a baseline for electrochemical and photophysical characteristics upon which this work builds. Many historically used organic photocatalysts like acridinium and cyanoarenes, have recently been applied to systematic structure alteration producing a new multitude of complexes for the field.

A new series of Eosin Y based organic photocatalysts were developed. The photophysical and electrochemical properties were determined for each, as well as the catalytic performance of each. This study produced photocatalysts with higher stability and enhanced catalytic activity, compared to the parent, Eosin Y. Tunability of the series was further supported by the reduction potentials that ranged by 120 mV. Further application of this work lies in the ability to easily functionalize the xanthene backbone on Eosin Y, supported by our initial results.

The formation of charge transfer (CT) states, analogous to the metal to ligand charge transfer (MLCT) for transition metal photocatalysts, enable the significant excited state lifetimes seen for some organic photocatalysts.[15, 180] These CT states are caused by the presence of large aromatic donor and acceptor functional groups on organic photocatalysts. For this reason, the further functionalization of the xanthene backbone (Chapter 2) with aromatic groups, such as A, B, and C in Figure 4.1, should facilitate the synthesis of a donor/acceptor catalyst. Additionally the alteration of functional groups

such as D and E in Figure 4.1 would allow the inclusion of the resulting catalysts in dye sensitized solar cells (DSSCs).[13]

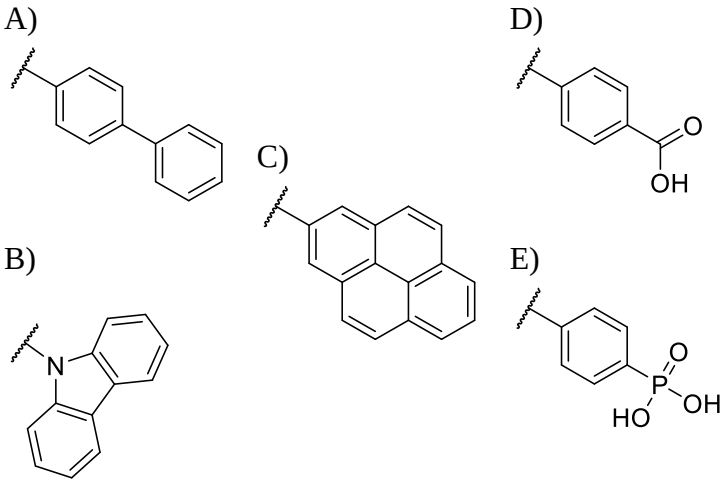


**Figure 4.1.** Proposed functional groups for future applications of Eosin Y based photocatalysts.

Solar energy conversion has become a major focal point of the renewable energy field and highly efficient organic DSSCs are a major focus to help accomplish this goal. The addition of binding groups to photoactive catalyst allow for their inclusion in DSSCs.[13] Carboxyl and phosphonic groups are ideal for binding of photocatalysts to appropriate supports, allowing for Eosin Y based compounds to be utilized in these devices.[129] The iridium phosphonic acid ([Ir(ppy)2(4,4'-bis(phosphonomethyl)-2,2'-bipyridine)]$PF_6$) catalyst reported in Chapter 3 was supported on both Sn(IV)-doped $In_2O_3$ and $TiO_2$ and maintained redox reversibility. These results show that the presence of surface binding groups did not inhibit the photophysical or electrochemical properties of the photocatalyst. Also, the poor efficiency of the DSSCs developed with the iridium phosphonate catalyst were attributed to the small spectral overlap between the photocatalyst and the solar spectrum. Eosin Y based photocatalysts absorb light well into

the solar spectrum and exhibit an order of magnitude higher molar absorptivity, than the transition metal-based complex, supporting that they may result in more efficient systems. This reasoning leads to the possibility that properly functionalized Eosin Y based photocatalysts would be prime candidates for organic DSSC devices.

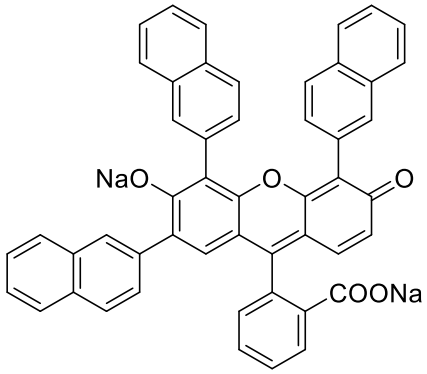


**Figure 4.2.** Structure of naphthyl derivative of Eosin Y based photocatalysts (E-naph$_3$).

The naphthyl derivative of the Eosin Y photocatalysts series shown in Figure 4.2 showed potential for application in electrode mounted photocatalysts. Differential pulse voltammetry (DPV) of E-naph$_3$ began showing abnormal results, prompting us to investigate deeper. DPV is a much slower electrochemical method, than CV. Sharp peaks in electrochemical scans are indicative of the attachment of the complex of interest to the electrode surface. Because the sharp peak only occurs with the naphthyl derivative and not the entire series, we hypothesized that the extended planar functional groups around the xanthene core are inserting between the sheets of graphene on the working surface of the glassy carbon electrode. This was assessed by allowing the electrode to soak in a solution of the photocatalyst overnight and running DPV scans again without polishing the electrode. The sharp peak shown in Figure 4.3 is initial confirmation of this

hypothesis. These results allude to the applications E-naph$_3$ and other similar photocatalysts in photoelectrochemical systems.

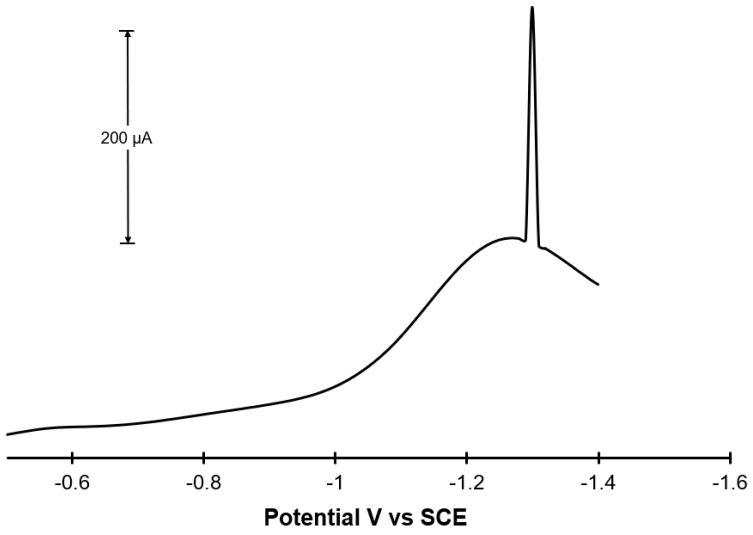


**Figure 4.3.** Reductive DPV of E-naph$_3$, in 1 mM solution of E-naph$_3$ with 100 mM TBAH in dry acetonitrile. Glassy carbon working electrode was soaked in E-naph$_3$ solution overnight before DPV was scanned.

## Reference

1. Lim, C.-H.; Ryan, M. D.; McCarthy, B. G.; Theriot, J. C.; Sartor, S. M.; Damrauer, N. H.; Musgrave, C. B.; Miyake, G. M., Intramolecular charge transfer and ion pairing in N, N-diaryl dihydrophenazine photoredox catalysts for efficient organocatalyzed atom transfer radical polymerization. *J. Am. Chem. Soc.* **2017,** *139* (1), 348-355.

2. McCarthy, B. G.; Pearson, R. M.; Lim, C.-H.; Sartor, S. M.; Damrauer, N. H.; Miyake, G. M., Structure–property relationships for tailoring phenoxazines as reducing photoredox catalysts. *J. Am. Chem. Soc.* **2018,** *140* (15), 5088-5101.

3. Hagfeldt, A.; Boschloo, G.; Sun, L.; Kloo, L.; Pettersson, H., Dye-sensitized solar cells. *Chem. Rev. (Washington, DC, U. S.)* **2010,** *110* (11), 6595-6663.

4. Hazebroucq, S.; Labat, F.; Lincot, D.; Adamo, C., Theoretical insights on the electronic properties of eosin Y, an organic dye for photovoltaic applications. *J. Phys. Chem. A* **2008,** *112* (31), 7264-7270.

# REFERENCES


Pitre, S. P.; McTiernan, C. D.; Scaiano, J. C., Library of cationic organic dyes for visible-light-driven photoredox transformations. *ACS omega* **2016,** *1* (1), 66-76.

Juris, A.; Balzani, V.; Barigelletti, F.; Campagna, S.; Belser, P. l.; von Zelewsky, A. v., Ru (II) polypyridine complexes: photophysics, photochemistry, eletrochemistry, and chemiluminescence. *Coord. Chem. Rev.* **1988,** *84*, 85-277.

Flamigni, L.; Barbieri, A.; Sabatini, C.; Ventura, B.; Barigelletti, F., Photochemistry and photophysics of coordination compounds: iridium. In *Photochemistry and Photophysics of Coordination Compounds II*, Springer: 2007; pp 143-203.

Ballardini, R.; Varani, G.; Indelli, M. T.; Scandola, F.; Balzani, V., Free energy correlation of rate constants for electron transfer quenching of excited transition metal complexes. *J. Am. Chem. Soc.* **1978,** *100* (23), 7219-7223.

Jun Xuan, W.-J. X., Visible Light Photoredox Catalysis. *Angew. Chem.* **2012,** *51*, 6828-6838.

Prier, C. K., Rankic, D. A., MacMillan, D. W. C., Visible Light Photoredox Catalysis with Transition Metal Complexes: Applications in Organic Synthesis. *Chem. Rev.* **2013,** *113*, 5322-5363.

Yoon, T. P., Ischay, M. A., Du, J., Visible light photocatalysis as a greener approach to photochemical synthesis. *Nature Chem.* **2010,** *2*, 527-532.

Zeitler, K., Photoredox catalysis with visible light. *Angew. Chem. Int. Edit.* **2009,** *48* (52), 9785-9789.

Tucker, J. W.; Stephenson, C. R., Shining light on photoredox catalysis: theory and synthetic applications. *J. Org. Chem.* **2012,** *77* (4), 1617-1622.

Dumur, F., Recent Advances on Visible Light Metal-Based Photocatalysts for Polymerization under Low Light Intensity. *Catalysts* **2019,** *9* (9), 736-776.

Nazeeruddin, M. K.; Baranoff, E.; Grätzel, M., Dye-sensitized solar cells: A brief overview. *Sol. Energy* **2011,** *85* (6), 1172-1178.

Grätzel, M., Dye-sensitized solar cells. *J. Photoch. Photobio. C* **2003,** *4* (2), 145-153.

Hagfeldt, A.; Boschloo, G.; Sun, L.; Kloo, L.; Pettersson, H., Dye-sensitized solar cells. *Chem. Rev. (Washington, DC, U. S.)* **2010,** *110* (11), 6595-6663.

Dasgupta, S.; Brunschwig, B. S.; Winkler, J. R.; Gray, H. B., Solar fuels editorial. *Chem. Soc. Rev.* **2013,** *42* (6), 2213-2214.

McCarthy, B. G.; Pearson, R. M.; Lim, C.-H.; Sartor, S. M.; Damrauer, N. H.; Miyake, G. M., Structure–property relationships for tailoring phenoxazines as reducing photoredox catalysts. *J. Am. Chem. Soc.* **2018,** *140* (15), 5088-5101.

Du, Y.; Pearson, R. M.; Lim, C. H.; Sartor, S. M.; Ryan, M. D.; Yang, H.; Damrauer, N. H.; Miyake, G. M., Strongly reducing, visible-light organic photoredox catalysts as sustainable alternatives to precious metals. *Chemistry–A European Journal* **2017,** *23* (46), 10962-10968.

McCusker, J. K., Femtosecond absorption spectroscopy of transition metal charge-transfer complexes. *Acc. Chem. Res.* **2003,** *36* (12), 876-887.

Yeh, A. T.; Shank, C. V.; McCusker, J. K., Ultrafast electron localization dynamics following photo-induced charge transfer. *Science* **2000,** *289* (5481), 935-938.

Zhang, Y.; Petersen, J. L.; Milsmann, C., A luminescent zirconium (IV) complex as a molecular photosensitizer for visible light photoredox catalysis. *J. Am. Chem. Soc.* **2016,** *138* (40), 13115-13118.

Azzaroni, O., Polymer Brushes Here, There, and Everywhere: Recent Advances in their Practical Applications and Emerging Opportunities in Multiple Research Fields. *J. Polym. Sci. A Polym. Chem.* **2012,** *50* (16), 3225-3258.

Hari, D. P., Konig, B., Synthetic applications of eosin Y in photoredox catalysis. *Chem. Commun.* **2014,** *50*, 6688-6699.

Nicewicz, D. A., Nguyen, T. M., Recent Applications of Organic Dyes as Photoredox Catalyst in Organic Synthesis. *ACS catal.* **2013,** (4), 355-360.

Majek, M., Filace, F., von Wangelin, A. J., On the mechanism of photocatalytic reactions with eosin Y. *Beilstein J. Org. Chem.* **2014,** *10*, 981-989.

Srivastava, V.; Singh, P. P., Eosin Y catalysed photoredox synthesis: a review. *RSC Advances* **2017,** *7* (50), 31377-31392.

Pitre, S. P.; McTiernan, C. D.; Ismaili, H.; Scaiano, J. C., Mechanistic insights and kinetic analysis for the oxidative hydroxylation of arylboronic acids by visible light photoredox catalysis: A metal-free alternative. *J. Am. Chem. Soc.* **2013,** *135* (36), 13286-13289.

Guo, S.; Zhang, H.; Huang, L.; Guo, Z.; Xiong, G.; Zhao, J., Porous material-immobilized iodo-Bodipy as an efficient photocatalyst for photoredox catalytic

organic reaction to prepare pyrrolo [2, 1-a] isoquinoline. *Chem. Commun. (Cambridge, U. K.)* **2013,** *49* (77), 8689-8691.

Huang, L.; Zhao, J.; Guo, S.; Zhang, C.; Ma, J., Bodipy derivatives as organic triplet photosensitizers for aerobic photoorganocatalytic oxidative coupling of amines and photooxidation of dihydroxylnaphthalenes. *J. Org. Chem.* **2013,** *78* (11), 5627-5637.

Heitz, D. R.; Rizwan, K.; Molander, G. A., Visible-Light-Mediated Alkenylation, Allylation, and Cyanation of Potassium Alkyltrifluoroborates with Organic Photoredox Catalysts. *J. Org. Chem.* **2016,** *81* (16), 7308-7313.

Neumann, M.; Füldner, S.; König, B.; Zeitler, K., Metal-free, cooperative asymmetric organophotoredox catalysis with visible light. *Angew. Chem. Int. Edit.* **2011,** *50* (4), 951-954.

Gassman, P. G.; Bottorff, K. J., Photoinduced lactonization. A useful but mechanistically complex single electron transfer process. *J. Am. Chem. Soc.* **1987,** *109* (24), 7547-7548.

Lewis, F. D.; Dykstra, R. E.; Gould, I. R.; Farid, S., Cage escape yields and direct observation of intermediates in photoinduced electron-transfer reactions of cis- and trans-stilbene. *J. Phys. Chem.* **1988,** *92* (25), 7042-7043.

Romero, N. A., Nicewicz, D. A., Organic Photoredox Catalysis. *Chem. Rev. (Washington, DC, U. S.)* **2016**, 92.

Speckmeier, E.; Fischer, T. G.; Zeitler, K., A toolbox approach to construct broadly applicable metal-free catalysts for photoredox chemistry: deliberate tuning of

redox potentials and importance of halogens in donor–acceptor cyanoarenes. *J. Am. Chem. Soc.* **2018,** *140* (45), 15353-15365.

Shang, T.-Y.; Lu, L.-H.; Cao, Z.; Liu, Y.; He, W.-M.; Yu, B., Recent advances of 1, 2, 3, 5-tetrakis (carbazol-9-yl)-4, 6-dicyanobenzene (4CzIPN) in photocatalytic transformations. *Chem. Commun. (Cambridge, U. K.)* **2019,** *55* (38), 5408-5419.

Song, Z.-Y.; Zhang, C.-L.; Ye, S., Visible light promoted coupling of alkynyl bromides and Hantzsch esters for the synthesis of internal alkynes. *Org. Biomol. Chem.* **2019,** *17* (1), 181-185.

Sherwood, T. C.; Xiao, H.-Y.; Bhaskar, R. G.; Simmons, E. M.; Zaretsky, S.; Rauch, M. P.; Knowles, R. R.; Dhar, T. M., Decarboxylative intramolecular arene alkylation using N-(acyloxy) phthalimides, an organic photocatalyst, and visible light. *J. Org. Chem.* **2019,** *84* (13), 8360-8379.

Patel, N. R.; Kelly, C. B.; Siegenfeld, A. P.; Molander, G. A., Mild, redox-neutral alkylation of imines enabled by an organic photocatalyst. *ACS catal.* **2017,** *7* (3), 1766-1770.

Lima, F.; Grunenberg, L.; Rahman, H. B.; Labes, R.; Sedelmeier, J.; Ley, S. V., Organic photocatalysis for the radical couplings of boronic acid derivatives in batch and flow. *Chem. Commun. (Cambridge, U. K.)* **2018,** *54* (44), 5606-5609.

Jiang, H.; Studer, A., Transition-Metal-Free Three-Component Radical 1, 2-Amidoalkynylation of Unactivated Alkenes. *Chemistry–A European Journal* **2019,** *25* (2), 516-520.

Huang, Z.; Gu, Y.; Liu, X.; Zhang, L.; Cheng, Z.; Zhu, X., Metal-Free Atom Transfer Radical Polymerization of Methyl Methacrylate with ppm Level of Organic Photocatalyst. *Macromol. Rapid Commun.* **2017,** *38* (10), 1600461.

Ju, T.; Fu, Q.; Ye, J. H.; Zhang, Z.; Liao, L. L.; Yan, S. S.; Tian, X. Y.; Luo, S. P.; Li, J.; Yu, D. G., Selective and Catalytic Hydrocarboxylation of Enamides and Imines with CO2 to Generate α, α-Disubstituted α-Amino Acids. *Angew. Chem. Int. Edit.* **2018,** *57* (42), 13897-13901.

Santandrea, J.; Minozzi, C.; Cruché, C.; Collins, S. K., Photochemical Dual-Catalytic Synthesis of Alkynyl Sulfides. *Angew. Chem. Int. Edit.* **2017,** *56* (40), 12255-12259.

Joshi-Pangu, A., Levesque, F., Roth, H. G., Oliver, S. F., Campeau, L., Nicewicz, D., DiRocco, D. A., Acridinium-Based Photocatalysts: A Sustainable Option in Photoredox Catalyst. *J. Org. Chem.* **2016,** *81*, 7244-7249.

Ohkubo, K.; Kobayashi, T.; Fukuzumi, S., Direct oxygenation of benzene to phenol using quinolinium ions as homogeneous photocatalysts. *Angew. Chem. Int. Edit.* **2011,** *50* (37), 8652-8655.

Margrey, K. A.; Nicewicz, D. A., A general approach to catalytic alkene anti-Markovnikov hydrofunctionalization reactions via acridinium photoredox catalysis. *Acc. Chem. Res.* **2016,** *49* (9), 1997-2006.

Romero, N. A.; Nicewicz, D. A., Mechanistic insight into the photoredox catalysis of anti-markovnikov alkene hydrofunctionalization reactions. *J. Am. Chem. Soc.* **2014,** *136* (49), 17024-17035.

Benniston, A. C.; Harriman, A.; Li, P.; Rostron, J. P.; van Ramesdonk, H. J.; Groeneveld, M. M.; Zhang, H.; Verhoeven, J. W., Charge shift and triplet state formation in the 9-mesityl-10-methylacridinium cation. *J. Am. Chem. Soc.* **2005,** *127* (46), 16054-16064.

Fukuzumi, S.; Kotani, H.; Ohkubo, K.; Ogo, S.; Tkachenko, N. V.; Lemmetyinen, H., Electron-transfer state of 9-mesityl-10-methylacridinium ion with a much longer lifetime and higher energy than that of the natural photosynthetic reaction center. *J. Am. Chem. Soc.* **2004,** *126* (6), 1600-1601.

White, A. R.; Wang, L.; Nicewicz, D. A., Synthesis and Characterization of Acridinium Dyes for Photoredox Catalysis. *Synlett* **2019,** *30* (07), 827-832.

Fagnoni, M.; Dondi, D.; Ravelli, D.; Albini, A., Photocatalysis for the Formation of the C− C Bond. *Chem. Rev. (Washington, DC, U. S.)* **2007,** *107* (6), 2725-2756.

Meyer, A. U.; Berger, A. L.; König, B., Metal-free C–H sulfonamidation of pyrroles by visible light photoredox catalysis. *Chem. Commun. (Cambridge, U. K.)* **2016,** *52* (72), 10918-10921.

Gesmundo, N. J.; Grandjean, J.-M. M.; Nicewicz, D. A., Amide and amine nucleophiles in polar radical crossover cycloadditions: synthesis of γ-lactams and pyrrolidines. *Org. Lett.* **2015,** *17* (5), 1316-1319.

Nguyen, T. M.; Nicewicz, D. A., Anti-Markovnikov hydroamination of alkenes catalyzed by an organic photoredox system. *J. Am. Chem. Soc.* **2013,** *135* (26), 9588-9591.

Fukuzumi, S.; Ohkubo, K.; Suenobu, T., Long-lived charge separation and applications in artificial photosynthesis. *Acc. Chem. Res.* **2014,** *47* (5), 1455-1464.

Hering, T.; Slanina, T.; Hancock, A.; Wille, U.; König, B., Visible light photooxidation of nitrate: the dawn of a nocturnal radical. *Chem. Commun. (Cambridge, U. K.)* **2015,** *51* (30), 6568-6571.

Romero, N. A.; Margrey, K. A.; Tay, N. E.; Nicewicz, D. A., Site-selective arene CH amination via photoredox catalysis. *Science* **2015,** *349* (6254), 1326-1330.

Matsui, J. K.; Molander, G. A., Organocatalyzed, Photoredox Heteroarylation of 2-Trifluoroboratochromanones via C–H Functionalization. *Org. Lett.* **2017,** *19* (4), 950-953.

Kotani, H.; Ohkubo, K.; Fukuzumi, S., Photocatalytic oxygenation of anthracenes and olefins with dioxygen via selective radical coupling using 9-mesityl-10-methylacridinium ion as an effective electron-transfer photocatalyst. *J. Am. Chem. Soc.* **2004,** *126* (49), 15999-16006.

Hering, T.; Meyer, A. U.; König, B., Photocatalytic anion oxidation and applications in organic synthesis. *J. Org. Chem.* **2016,** *81* (16), 6927-6936.

Perkowski, A. J.; Nicewicz, D. A., Direct catalytic anti-Markovnikov addition of carboxylic acids to alkenes. *J. Am. Chem. Soc.* **2013,** *135* (28), 10334-10337.

Das, M.; Vu, M. D.; Zhang, Q.; Liu, X.-W., Metal-free visible light photoredox enables generation of carbyne equivalents via phosphonium ylide C–H activation. *Chemical science* **2019,** *10* (6), 1687-1691.

Perkin, W. H., LXXIV.—On mauveine and allied colouring matters. *J. Chem. Soc.* **1879,** *35*, 717-732.

Laursen, J. B.; Nielsen, J., Phenazine natural products: biosynthesis, synthetic analogues, and biological activity. *Chem. Rev. (Washington, DC, U. S.)* **2004,** *104* (3), 1663-1686.

Venkataraman, K., *The chemistry of synthetic dyes*. Elsevier: 2012; Vol. 4.

Kirk, R. E.; Othmer, D. F.; Mann, C. A., Encyclopedia of Chemical Technology. Vol. II. *J. Phys. Chem.* **1949,** *53* (4), 591-591.

Dietrich, L. E.; Teal, T. K.; Price-Whelan, A.; Newman, D. K., Redox-active antibiotics control gene expression and community behavior in divergent bacteria. *Science* **2008,** *321* (5893), 1203-1206.

Theriot, J. C.; Lim, C.-H.; Yang, H.; Ryan, M. D.; Musgrave, C. B.; Miyake, G. M., Organocatalyzed atom transfer radical polymerization driven by visible light. *Science* **2016,** *352* (6289), 1082-1086.

Koyama, D.; Dale, H. J.; Orr-Ewing, A. J., Ultrafast observation of a photoredox reaction mechanism: photoinitiation in organocatalyzed atom-transfer radical polymerization. *J. Am. Chem. Soc.* **2018,** *140* (4), 1285-1293.

Cole, J. P.; Federico, C. R.; Lim, C.-H.; Miyake, G. M., Photoinduced organocatalyzed atom transfer radical polymerization using low ppm catalyst loading. *Macromolecules* **2019,** *52* (2), 747-754.

Podemska, K.; Podsiadły, R.; Szymczak, A. M.; Sokołowska, J., Diazobenzo [a] fluorene derivatives as visible photosensitizers for free radical polymerization. *Dyes Pigm.* **2012,** *94* (1), 113-119.

Podemska, K.; Podsiadly, R.; Orzel, A.; Sokołowska, J., The photochemical behavior of benzo [a] pyrido [2′, 1′: 2, 3] imidazo [4, 5-c] phenazine dyes. *Dyes Pigm.* **2013,** *99* (3), 666-672.

Kayser, R.; Young, R., The photoreduction of methylene blue by amines—I. A flash photolysis study of the reaction between triplet methylene blue and amines. *Photochem. Photobiol.* **1976,** *24* (5), 395-401.

Ohlow, M. J.; Moosmann, B., Phenothiazine: the seven lives of pharmacology's first lead structure. *Drug Discov. Today* **2011,** *16* (3-4), 119-131.

Weil, L.; Seibles, T. S.; Herskovits, T. T., Photooxidation of bovine insulin sensitized by methylene blue. *Arch. Biochem. Biophys.* **1965,** *111* (2), 308-320.

Timpe, H.-J.; Neuenfeld, S., Photoreduction of some dyes by styrene. *J. Chem. Soc., Faraday Trans.* **1992,** *88* (16), 2329-2336.

Ohno, T.; Lichtin, N. N., Electron transfer in the quenching of triplet methylene blue by complexes of iron (II). *J. Am. Chem. Soc.* **1980,** *102* (14), 4636-4643.

Steiner, U.; Winter, G.; Kramer, H. E., Investigation of physical triplet quenching by electron donors. *J. Phys. Chem.* **1977,** *81* (11), 1104-1110.

Fischer, H.; Kramer, H. E.; Maute, A., Blitzlichtuntersuchungen über die ausbleichreaktion von thionin mit allylthioharnstoff, II. *Z. Phys. Chem. (Muenchen, Ger.)* **1970,** *69* (3_4), 113-131.

Cocquet, G.; Ferroud, C.; Guy, A., A mild and efficient procedure for ring-opening reactions of piperidine and pyrrolidine derivatives by single electron transfer photooxidation. *Tetrahedron* **2000,** *56* (19), 2975-2984.

Pitre, S. P.; McTiernan, C. D.; Ismaili, H.; Scaiano, J. C., Metal-free photocatalytic radical trifluoromethylation utilizing methylene blue and visible light irradiation. *ACS catal.* **2014,** *4* (8), 2530-2535.

Jiang, H.; Mao, G.; Wu, H.; An, Q.; Zuo, M.; Guo, W.; Xu, C.; Sun, Z.; Chu, W., Synthesis of dibenzocycloketones by acyl radical cyclization from aromatic carboxylic acids using methylene blue as a photocatalyst. *Green Chem.* **2019,** *21* (19), 5368-5373.

Zhang, H.; Zhan, Z.; Lin, Y.; Shi, Y.; Li, G.; Wang, Q.; Deng, Y.; Hai, L.; Wu, Y., Visible light photoredox catalyzed thiophosphate synthesis using methylene blue as a promoter. *Org. Chem. Front.* **2018,** *5* (9), 1416-1422.

Alonso, F.; Beletskaya, I. P.; Yus, M., Metal-mediated reductive hydrodehalogenation of organic halides. *Chem. Rev. (Washington, DC, U. S.)* **2002,** *102* (11), 4009-4092.

Poelma, S. O.; Burnett, G. L.; Discekici, E. H.; Mattson, K. M.; Treat, N. J.; Luo, Y.; Hudson, Z. M.; Shankel, S. L.; Clark, P. G.; Kramer, J. W., Chemoselective radical dehalogenation and C–C bond formation on aryl halide substrates using organic photoredox catalysts. *J. Org. Chem.* **2016,** *81* (16), 7155-7160.

Stockmann, A.; Kurzawa, J.; Fritz, N.; Acar, N.; Schneider, S.; Daub, J.; Engl, R.; Clark, T., Conformational control of photoinduced charge separation within phenothiazine− pyrene dyads. *J. Phys. Chem. A* **2002,** *106* (34), 7958-7970.

Manav, N.; Verma, V.; Pandey, V.; Rather, H.; Vasita, R.; Gupta, I., Synthesis and studies of phenothiazine based AIE fluorogens. *Indian Journal of Chemistry, Section B* **2019,** *58B*, 238-246.

Treat, N. J.; Sprafke, H.; Kramer, J. W.; Clark, P. G.; Barton, B. E.; Read de Alaniz, J.; Fors, B. P.; Hawker, C. J., Metal-free atom transfer radical polymerization. *J. Am. Chem. Soc.* **2014,** *136* (45), 16096-16101.

Discekici, E. H.; Pester, C. W.; Treat, N. J.; Lawrence, J.; Mattson, K. M.; Narupai, B.; Toumayan, E. P.; Luo, Y.; McGrath, A. J.; Clark, P. G., Simple benchtop approach to polymer brush nanostructures using visible-light-mediated metal-free atom transfer radical polymerization. *ACS Macro Letters* **2016,** *5* (2), 258-262.

Pan, X.; Lamson, M.; Yan, J.; Matyjaszewski, K., Photoinduced metal-free atom transfer radical polymerization of acrylonitrile. *ACS Macro Letters* **2015,** *4* (2), 192-196.

Chen, M.; MacLeod, M. J.; Johnson, J. A., Visible-light-controlled living radical polymerization from a trithiocarbonate iniferter mediated by an organic photoredox catalyst. *ACS Macro Letters* **2015,** *4* (5), 566-569.

Yan, J.; Pan, X.; Schmitt, M.; Wang, Z.; Bockstaller, M. R.; Matyjaszewski, K., Enhancing initiation efficiency in metal-free surface-initiated atom transfer radical polymerization (SI-ATRP). *ACS Macro Letters* **2016,** *5* (6), 661-665.

Boyington, A. J.; Seath, C. P.; Zearfoss, A. M.; Xu, Z.; Jui, N. T., Catalytic Strategy for Regioselective Arylethylamine Synthesis. *J. Am. Chem. Soc.* **2019,** *141* (9), 4147-4153.

Discekici, E. H.; Treat, N. J.; Poelma, S. O.; Mattson, K. M.; Hudson, Z. M.; Luo, Y.; Hawker, C. J.; de Alaniz, J. R., A highly reducing metal-free photoredox catalyst: design and application in radical dehalogenations. *Chem. Commun. (Cambridge, U. K.)* **2015,** *51* (58), 11705-11708.

Ma, B.; Lu, F.; Yang, H.; Gu, X.; Li, Z.; Li, R.; Pei, H.; Luo, D.; Zhang, H.; Lei, A., Visible Light Mediated External Oxidant Free Selective C5 Bromination of 8-Aminoquinoline Amides under Ambient Conditions. *Asian J. Org. Chem.* **2019,** *8* (7), 1136-1140.

Smith, J. L., On the simultaneous staining of neutral fat and fatty acid by oxazine dyes. *J Pathol Bacteriol* **1908,** *12* (1), 4.

Lin, C.-W.; Shulok, J. R.; Kirley, S. D.; Cincotta, L.; Foley, J. W., Lysosomal localization and mechanism of uptake of Nile blue photosensitizers in tumor cells. *Cancer Res.* **1991,** *51* (10), 2710-2719.

Daehne, S.; Resch-Genger, U.; Wolfbeis, O. S., *Near-infrared dyes for high technology applications*. Springer Science & Business Media: 2012; Vol. 52.

Jose, J.; Burgess, K., Benzophenoxazine-based fluorescent dyes for labeling biomolecules. *Tetrahedron* **2006,** *62* (48), 11021-11037.

Greenspan, P.; Mayer, E. P.; Fowler, S. D., Nile red: a selective fluorescent stain for intracellular lipid droplets. *J. Cell Biol.* **1985,** *100* (3), 965-973.

Sartor, S. M.; Lattke, Y. M.; McCarthy, B. G.; Miyake, G. M.; Damrauer, N. H., Effects of Naphthyl Connectivity on the Photophysics of Compact Organic Charge-Transfer Photoredox Catalysts. *J. Phys. Chem. A* **2019,** *123* (22), 4727-4736.

Berger, A. L.; Donabauer, K.; König, B., Photocatalytic Barbier reaction–visible-light induced allylation and benzylation of aldehydes and ketones. *Chemical science* **2018,** *9* (36), 7230-7235.

Ramsey, B. L.; Pearson, R. M.; Beck, L. R.; Miyake, G. M., Photoinduced organocatalyzed atom transfer radical polymerization using continuous flow. *Macromolecules* **2017,** *50* (7), 2668-2674.

McCarthy, B.; Miyake, G. M., Organocatalyzed atom transfer radical polymerization catalyzed by core modified N-aryl phenoxazines performed under air. *ACS macro letters* **2018,** *7* (8), 1016-1021.

Lee, D. S.; Kim, C. S.; Iqbal, N.; Park, G. S.; Son, K.-s.; Cho, E. J., Organophotocatalytic Arene Functionalization: C–C and C–B Bond Formation. *Org. Lett.* **2019**.

Shi, L.; Xia, W., Photoredox functionalization of C–H bonds adjacent to a nitrogen atom. *Chem. Soc. Rev.* **2012,** *41* (23), 7687-7697.

Pan, Y.; Kee, C. W.; Chen, L.; Tan, C.-H., Dehydrogenative coupling reactions catalysed by Rose Bengal using visible light irradiation. *Green Chem.* **2011,** *13* (10), 2682-2685.

Yajima, T.; Ikegami, M., Metal-Free Visible-Light Radical Iodoperfluoroalkylation of Terminal Alkenes and Alkynes. *Eur. J. Org. Chem.* **2017,** *2017* (15), 2126-2129.

Choi, A.; Miller, S. C., Silicon Substitution in Oxazine Dyes Yields Near-Infrared Azasiline Fluorophores That Absorb and Emit beyond 700 nm. *Org. Lett.* **2018,** *20* (15), 4482-4485.

Ghosh, I.; Ghosh, T.; Bardagi, J. I.; König, B., Reduction of aryl halides by consecutive visible light-induced electron transfer processes. *Science* **2014,** *346* (6210), 725-728.

Ghosh, I.; Marzo, L.; Das, A.; Shaikh, R.; König, B., Visible light mediated photoredox catalytic arylation reactions. *Acc. Chem. Res.* **2016,** *49* (8), 1566-1577.

Li, Z.; Zhang, W.; Zhao, Q.; Gu, H.; Li, Y.; Zhang, G.; Zhang, F.; Fan, X., Eosin Y covalently anchored on reduced graphene oxide as an efficient and recyclable photocatalyst for the aerobic oxidation of α-aryl halogen derivatives. *ACS Sustain. Chem. Eng.* **2015,** *3* (3), 468-474.

Rohokale, R. S.; Koenig, B.; Dhavale, D. D., Synthesis of 2, 4, 6-trisubstituted pyridines by oxidative Eosin Y photoredox catalysis. *J. Org. Chem.* **2016,** *81* (16), 7121-7126.

Yan, D. M.; Chen, J. R.; Xiao, W. J., New Roles for Photoexcited Eosin Y in Photochemical Reactions. *Angew. Chem. Int. Edit.* **2019,** *58* (2), 378-380.

Hering, T.; Hari, D. P.; König, B., Visible-light-mediated α-arylation of enol acetates using aryl diazonium salts. *J. Org. Chem.* **2012,** *77* (22), 10347-10352.

Edmondson, S.; Danishefsky, S. J.; Sepp-Lorenzino, L.; Rosen, N., Total synthesis of spirotryprostatin A, leading to the discovery of some biologically promising analogues. *J.*

Goehring, R. R.; Sachdeva, Y. P.; Pisipati, J. S.; Sleevi, M. C.; Wolfe, J. F., Photoinduced cyclizations of mono-and dianions of N-acyl-o-chloroanilines and N-acyl-o-chlorobenzylamines as general methods for the synthesis of oxindoles and 1, 4-dihydro-3 (2H)-isoquinolinones. *J. Am. Chem. Soc.* **1985,** *107* (2), 435-443.

Shaw, M. H., Twilton, J., MacMillan, D. W. C., Photoredox Catalysis in Organic Chemistry. *J. Org. Chem.* **2016**.

Narayanam, J. M.; Stephenson, C. R., Visible light photoredox catalysis: applications in organic synthesis. *Chem. Soc. Rev.* **2011,** *40* (1), 102-113.

Meyer, A. U.; Slanina, T. s.; Yao, C.-J.; König, B., Metal-free perfluoroarylation by visible light photoredox catalysis. *ACS catal.* **2015,** *6* (1), 369-375.

Ravelli, D.; Fagnoni, M., Dyes as visible light photoredox organocatalysts. *ChemCatChem* **2012,** *4* (2), 169-171.

Marin, M. L.; Santos-Juanes, L.; Arques, A.; Amat, A. M.; Miranda, M. A., Organic photocatalysts for the oxidation of pollutants and model compounds. *Chem. Rev. (Washington, DC, U. S.)* **2011,** *112* (3), 1710-1750.

Fukuzumi, S.; Ohkubo, K., Selective photocatalytic reactions with organic photocatalysts. *Chemical Science* **2013,** *4* (2), 561-574.

Jiang, Z.; Sun, H.; Wang, T.; Wang, B.; Wei, W.; Li, H.; Yuan, S.; An, T.; Zhao, H.; Yu, J., Nature-based catalyst for visible-light-driven photocatalytic CO 2 reduction. *Energy & Environmental Science* **2018,** *11* (9), 2382-2389.

Fukuzumi, S.; Ohkubo, K., Organic synthetic transformations using organic dyes as photoredox catalysts. *Org. Biomol. Chem.* **2014,** *12* (32), 6059-6071.

Meyer, A. U.; Strakova, K.; Slanina, T.; Koenig, B., Eosin Y (EY) photoredox-catalyzed sulfonylation of alkenes: scope and mechanism. *Chemistry–A European Journal* **2016,** *22* (25), 8694-8699.

Yu, X.; Yang, Z.; Qiu, B.; Guo, S.; Yang, P.; Yu, B.; Zhang, H.; Zhao, Y.; Yang, X.; Han, B., Eosin Y-Functionalized Conjugated Organic Polymers for Visible-Light-Driven CO2 Reduction with H2O to CO with High Efficiency. *Angew. Chem. Int. Edit.* **2019,** *58* (2), 632-636.

Abe, R.; Hara, K.; Sayama, K.; Domen, K.; Arakawa, H., Steady hydrogen evolution from water on Eosin Y-fixed TiO2 photocatalyst using a silane-coupling reagent under visible light irradiation. *Journal of Photochemistry and Photobiology A: Chemistry* **2000,** *137* (1), 63-69.

Manivannan, G.; Mailhot, G.; Bolte, M.; Lessard, R., Xanthene dye sensitized dichromated poly (vinyl alcohol) recording materials: holographic characterization and ESR spectroscopic study. *Pure and Applied Optics: Journal of the European Optical Society Part A* **1994,** *3* (5), 845.

Hazebroucq, S.; Labat, F.; Lincot, D.; Adamo, C., Theoretical insights on the electronic properties of eosin Y, an organic dye for photovoltaic applications. *J. Phys. Chem. A* **2008,** *112* (31), 7264-7270.

Hopkinson, M. N., Sahoo, B., Jun-Long Li, Glorius, F., Dual Catalysis Sees the Light: Combining Photoredox with Organo-, Acid, and Transition-Metal Catalysis. *Chem. Eur. J.* **2014,** *20*, 3874-3886.

Lamansky, S.; Djurovich, P.; Murphy, D.; Abdel-Razzaq, F.; Lee, H.-E.; Adachi, C.; Burrows, P. E.; Forrest, S. R.; Thompson, M. E., Highly Phosphorescent Bis-Cyclometalated Iridium Complexes: Synthesis, Photophysical Characterization, and Use in Organic Light Emitting Diodes. *J. Am. Chem. Soc.* **2001,** *123* (18), 4304-4312.

Mayo, E. I.; Kilså, K.; Tirrell, T.; Djurovich, P. I.; Tamayo, A.; Thompson, M. E.; Lewis, N. S.; Gray, H. B., Cyclometalated iridium(iii)-sensitized titanium dioxide solar cells. *Photochem. Photobiol. Sci.* **2006,** *5* (10), 871-873.

Ogunsolu, O. O.; Murphy, I. A.; Wang, J. C.; Das, A.; Hanson, K., Energy and Electron Transfer Cascade in Self-Assembled Bilayer Dye-Sensitized Solar Cells. *ACS Appl. Mater. Interfaces* **2016,** *8* (42), 28633-28640.

Légalité, F.; Escudero, D.; Pellegrin, Y.; Blart, E.; Jacquemin, D.; Fabrice, O., "Iridium effect" in cyclometalated iridium complexes for p-type dye sensitized solar cells. *Dyes Pigm.* **2019,** *171*, 107693.

Blakemore, J. D.; Crabtree, R. H.; Brudvig, G. W., Molecular Catalysts for Water Oxidation. *Chem. Rev. (Washington, DC, U. S.)* **2015,** *115* (23), 12974-13005.

Salpage, S. R.; Paul, A.; Som, B.; Banerjee, T.; Hanson, K.; Smith, M. D.; Vannucci, A. K.; Shimizu, L. S., Structural, electrochemical and photophysical properties of an exocyclic di-ruthenium complex and its application as a photosensitizer. *Dalton Trans.* **2016,** *45* (23), 9601-9607.

Lo, K. K.-W.; Chan, J. S.-W.; Lui, L.-H.; Chung, C.-K., Novel Luminescent Cyclometalated Iridium(III) Diimine Complexes That Contain a Biotin Moiety. *Organometallics* **2004,** *23* (13), 3108-3116.

Ashford, D. L.; Gish, M. K.; Vannucci, A. K.; Brennaman, M. K.; Templeton, J. L.; Papanikolas, J. M.; Meyer, T. J., Molecular Chromophore–Catalyst Assemblies for Solar Fuel Applications. *Chem. Rev. (Washington, DC, U. S.)* **2015,** *115* (23), 13006-13049.

Mills, I. N.; Porras, J. A.; Bernhard, S., Judicious Design of Cationic, Cyclometalated Ir(III) Complexes for Photochemical Energy Conversion and Optoelectronics. *Acc. Chem. Res.* **2018,** *51* (2), 352-364.

McDaniel, N. D.; Coughlin, F. J.; Tinker, L. L.; Bernhard, S., Cyclometalated iridium(III) aquo complexes: Efficient and tunable catalysts for the homogeneous oxidation of water. *J. Am. Chem. Soc.* **2008,** *130* (1), 210-217.

Paul, A.; Smith, M. D.; Vannucci, A. K., Photoredox-Assisted Reductive Cross-Coupling: Mechanistic Insight into Catalytic Aryl–Alkyl Cross-Couplings. *J. Org. Chem.* **2017,** *82* (4), 1996-2003.

Slinker, J. D.; Gorodetsky, A. A.; Lowry, M. S.; Wang, J.; Parker, S.; Rohl, R.; Bernhard, S.; Malliaras, G. G., Efficient Yellow Electroluminescence from a Single Layer of a Cyclometalated Iridium Complex. *J. Am. Chem. Soc.* **2004,** *126* (9), 2763-2767.

De Angelis, F.; Fantacci, S.; Evans, N.; Klein, C.; Zakeeruddin, S. M.; Moser, J.-E.; Kalyanasundaram, K.; Bolink, H. J.; Grätzel, M.; Nazeeruddin, M. K., Controlling Phosphorescence Color and Quantum Yields in Cationic Iridium Complexes: A Combined Experimental and Theoretical Study. *Inorg. Chem.* **2007,** *46* (15), 5989-6001.

Nazeeruddin, M. K.; Wegh, R. T.; Zhou, Z.; Klein, C.; Wang, Q.; De Angelis, F.; Fantacci, S.; Grätzel, M., Efficient Green-Blue-Light-Emitting Cationic Iridium Complex for Light-Emitting Electrochemical Cells. *Inorg. Chem.* **2006,** *45* (23), 9245-9250.

Lowry, M. S.; Bernhard, S., Synthetically Tailored Excited States: Phosphorescent, Cyclometalated Iridium(III) Complexes and Their Applications. *Chemistry – A European Journal* **2006,** *12* (31), 7970-7977.

Lowry, M. S.; Hudson, W. R.; Pascal, R. A.; Bernhard, S., Accelerated Luminophore Discovery through Combinatorial Synthesis. *J. Am. Chem. Soc.* **2004,** *126* (43), 14129-14135.

Paul, A.; Das, N.; Halpin, Y.; Vos, J. G.; Pryce, M. T., Carboxy derivatised Ir(iii) complexes: synthesis, electrochemistry, photophysical properties and photocatalytic hydrogen generation. *Dalton Trans.* **2015,** *44* (22), 10423-10430.

Baranoff, E.; Yum, J.-H.; Graetzel, M.; Nazeeruddin, M. K., Cyclometallated iridium complexes for conversion of light into electricity and electricity into light. *J. Organomet. Chem.* **2009,** *694* (17), 2661-2670.

King, K. A.; Watts, R. J., Dual emission from an ortho-metalated iridium(III) complex. *J. Am. Chem. Soc.* **1987,** *109* (5), 1589-1590.

Tsuboyama, A.; Iwawaki, H.; Furugori, M.; Mukaide, T.; Kamatani, J.; Igawa, S.; Moriyama, T.; Miura, S.; Takiguchi, T.; Okada, S.; Hoshino, M.; Ueno, K., Homoleptic Cyclometalated Iridium Complexes with Highly Efficient Red Phosphorescence and Application to Organic Light-Emitting Diode. *J. Am. Chem. Soc.* **2003,** *125* (42), 12971-12979.

Sajoto, T.; Djurovich, P. I.; Tamayo, A.; Yousufuddin, M.; Bau, R.; Thompson, M. E.; Holmes, R. J.; Forrest, S. R., Blue and Near-UV Phosphorescence from Iridium Complexes with Cyclometalated Pyrazolyl or N-Heterocyclic Carbene Ligands. *Inorg. Chem.* **2005,** *44* (22), 7992-8003.

Hanson, K.; Losego, M. D.; Kalanyan, B.; Parsons, G. N.; Meyer, T. J., Stabilizing Small Molecules on Metal Oxide Surfaces Using Atomic Layer Deposition. *Nano Lett.* **2013,** *13* (10), 4802-4809.

Materna, K. L.; Crabtree, R. H.; Brudvig, G. W., Anchoring groups for photocatalytic water oxidation on metal oxide surfaces. *Chem. Soc. Rev.* **2017,** *46* (20), 6099-6110.

Hanson, K.; Brennaman, M. K.; Luo, H. L.; Glasson, C. R. K.; Concepcion, J. J.; Song, W. J.; Meyer, T. J., Photostability of Phosphonate-Derivatized, Ru-II Polypyridyl Complexes on Metal Oxide Surfaces. *ACS Appl. Mater. Interfaces* **2012,** *4* (3), 1462-1469.

Gillaizeau-Gauthier, I.; Odobel, F.; Alebbi, M.; Argazzi, R.; Costa, E.; Bignozzi, C. A.; Qu, P.; Meyer, G. J., Phosphonate-based bipyridine dyes for stable photovoltaic devices. *Inorg. Chem.* **2001,** *40* (23), 6073-6079.

Colombo, M. G.; Guedel, H. U., Synthesis and high-resolution optical spectroscopy of bis[2-(2-thienyl)pyridinato-C3,N'](2,2'-bipyridine)iridium(III). *Inorg. Chem.* **1993,** *32* (14), 3081-3087.

Hanson, K.; Brennaman, M. K.; Ito, A.; Luo, H.; Song, W.; Parker, K. A.; Ghosh, R.; Norris, M. R.; Glasson, C. R. K.; Concepcion, J. J.; Lopez, R.; Meyer, T. J., Structure–Property Relationships in Phosphonate-Derivatized, RuII Polypyridyl Dyes on Metal Oxide Surfaces in an Aqueous Environment. *J. Phys. Chem. C* **2012,** *116* (28), 14837-14847.

Shaw, M. H.; Twilton, J.; MacMillan, D. W. C., Photoredox Catalysis in Organic Chemistry. *J. Org. Chem.* **2016,** *81*, 6898-6926.

Vannucci, A. K.; Alibabaei, L.; Losego, M. D.; Concepcion, J. J.; Kalanyan, B.; Parsons, G. N.; Meyer, T. J., Crossing the divide between homogeneous and heterogeneous catalysis in water oxidation. *Proc. Natl. Acad. Sci.* **2013,** *110*, 20918-20922.

Hoertz, P. G.; Chen, Z.; Kent, C. A.; Meyer, T. J., Application of High Surface Area Tin-Doped Indium Oxide Nanoparticle Films as Transparent Conducting Electrodes. *Inorg. Chem.* **2010,** *49* (18), 8179-8181.

Song, W. J.; Vannucci, A. K.; Farnum, B. H.; Lapides, A. M.; Brennaman, M. K.; Kalanyan, B.; Alibabaei, L.; Concepcion, J. J.; Losego, M. D.; Parsons, G. N.; Meyer, T. J., Visible Light Driven Benzyl Alcohol Dehydrogenation in a Dye-Sensitized Photoelectrosynthesis Cell. *J. Am. Chem. Soc.* **2014,** *136* (27), 9773-9779.

Feldt, S. M.; Gibson, E. A.; Gabrielsson, E.; Sun, L.; Boschloo, G.; Hagfeldt, A., Design of Organic Dyes and Cobalt Polypyridine Redox Mediators for High-Efficiency Dye-Sensitized Solar Cells. *J. Am. Chem. Soc.* **2010,** *132* (46), 16714-16724.

Giribabu, L.; Bolligarla, R.; Panigrahi, M., Recent Advances of Cobalt(II/III) Redox Couples for Dye-Sensitized Solar Cell Applications. *The Chemical Record* **2015,** *15* (4), 760-788.

Rodrigues, R. R.; Peddapuram, A.; Dorris, A. L.; Hammer, N. I.; Delcamp, J. H., Thienopyrroledione-Based Photosensitizers as Strong Photoinduced Oxidants: Oxidation of Fe(bpy)32+ in a >1.3 V Dye-Sensitized Solar Cell. *ACS Appl. Energy Mater.* **2019,** *2* (8), 5547-5556.

Rodrigues, R. R.; Cheema, H.; Delcamp, J. H., A High-Voltage Molecular-Engineered Organic Sensitizer–Iron Redox Shuttle Pair: 1.4 V DSSC and 3.3 V SSM-DSSC Devices. *Angew. Chem. Int. Edit.* **2018,** *57* (19), 5472-5476.

Bock, C. R.; Connor, J. A.; Gutierrez, A. R.; Meyer, T. J.; Whitten, D. G.; Sullivan, B. P.; Nagle, J. K., Estimation of excited-state redox potentials by electron-transfer

quenching. Application of electron-transfer theory to excited-state redox processes. *J. Am. Chem. Soc.* **1979,** *101* (17), 4815-4824.

Felton, G. A. N.; Mebi, C. A.; Petro, B. J.; Vannucci, A. K.; Evans, D. H.; Glass, R. S.; Lichtenberger, D. L., Review of electrochemical studies of complexes containing the Fe2S2 core characteristic of [FeFe]-hydrogenases including catalysis by these complexes of the reduction of acids to form dihydrogen. *J. Organomet. Chem.* **2009,** *694* (17), 2681-2699.

Carella, A.; Borbone, F.; Centore, R., Research Progress on Photosensitizers for DSSC. *Front. Chem.* **2018,** *6*, 481-481.

Ardo, S.; Meyer, G. J., Photodriven heterogeneous charge transfer with transition-metal compounds anchored to TiO2 semiconductor surfaces. *Chem. Soc. Rev.* **2009,** *38* (1), 115-164.

Zuo, Z.; Ahneman, D. T.; Chu, L.; Terrett, J. A.; Doyle, A. G.; MacMillan, D. W. C., Merging photoredox with nickel catalysis: Coupling of a-carboxyl sp3-carbons with aryl halides. *Science* **2014,** *345*, 437-440.

Bouzaid, J.; Schultz, M.; Lao, Z.; Bartley, J.; Bostrom, T.; McMurtrie, J., Supramolecular selection in molecular alloys. *Cryst. Growth Des.* **2012,** *12* (8), 3906-3916.

DeSimone, R. E.; Drago, R. S., Magnetic resonance studies of some low-spin d5 tris diimine complexes. *J. Am. Chem. Soc.* **1970,** *92* (8), 2343-2352.

Theoretical Chemistry, V. U. A., ADF, Amsterdam density functional program, http://www.scm.com.

te Velde, G.; Bickelhaupt, F. M.; Baerends, E. J.; Fonseca Guerra, C.; van Gisbergen, S. J. A.; Snijders, J. G.; Ziegler, T., Chemistry with ADF. *J. Comput. Chem.* **2001,** *22* (9), 931-967.

Stoll, H.; Pavlidou, C. M. E.; Preuß, H., On the calculation of correlation energies in the spin-density functional formalism. *Theor. Chim. Acta* **1978,** *49* (2), 143-149.

van Lenthe, E.; Ehlers, A. W.; Baerends, E., *J. Chem. Phys.* **1999,** *110*, 8943-8953.

Klamt, A., *J. Phys. Chem.* **1995,** *99*, 2224-2235.

Perdew, J. P.; Burke, K.; Ernzerhof, M., Generalized Gradient Approximation Made Simple. *Phys. Rev. Lett.* **1996,** *77* (18), 3865-3868.

Ogunsolu, O. O.; Wang, J. C.; Hanson, K., Inhibiting Interfacial Recombination Events in Dye-Sensitized Solar Cells using Self-Assembled Bilayers. *ACS Appl. Mater. Interfaces* **2015,** *7* (50), 27730-27734.

Lim, C.-H.; Ryan, M. D.; McCarthy, B. G.; Theriot, J. C.; Sartor, S. M.; Damrauer, N. H.; Musgrave, C. B.; Miyake, G. M., Intramolecular charge transfer and ion pairing in N, N-diaryl dihydrophenazine photoredox catalysts for efficient organocatalyzed atom transfer radical polymerization. *J. Am. Chem. Soc.* **2017,** *139* (1), 348-355.

APEX3 Version 2016.5-0 and SAINT+ Version 8.38A. Bruker AXS, I., Madison, Wisconsin, USA, 2016.

Krause, L.; Herbst-Irmer, R.; Sheldrick, G. M.; Stalke, D., Comparison of silver and molybdenum microfocus X-ray sources for single-crystal structure determination. J. Appl. Crystallogr. 2015, 48 (1), 3-10.

Sheldrick, G., SHELXT - Integrated space-group and crystal-structure determination. Acta Crystallogr., Sect. A: Found. Crystallogr. 2015, 71 (1), 3-8.

Sheldrick, G., Crystal structure refinement with SHELXL. Acta Crystallogr., Sect. C: Cryst. Struct. Commun. 2015, 71 (1), 3-8.

Dolomanov, O. V.; Bourhis, L. J.; Gildea, R. J.; Howard, J. A. K.; Puschmann, H., OLEX2: a complete structure solution, refinement and analysis program. J. Appl. Crystallogr. 2009, 42 (2), 339-341.

# APPENDIX A

# EXPERIMENTAL DETAILS AND CHARACTERIZATION INFORMATION FOR CHAPTER 2

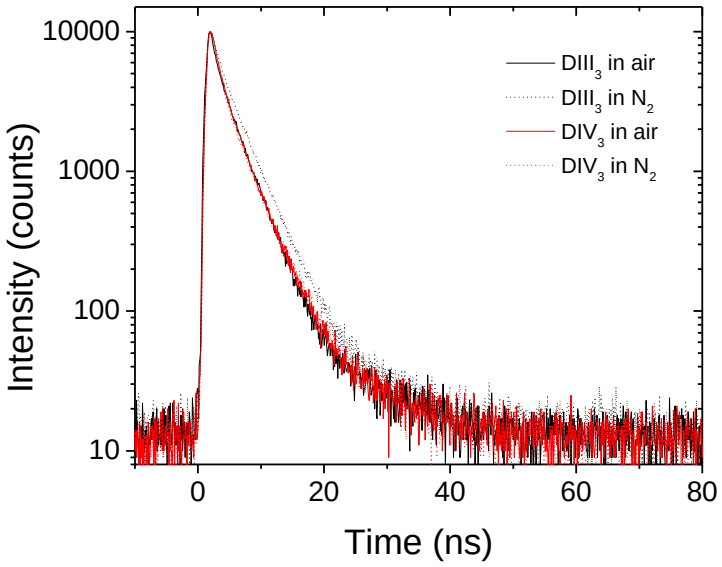


**Figure A.1.** Emission decays at 585 nm of E-naph$_3$ (DIII$_3$) and E-tertbutylph$_3$ (DIV$_3$) in MeCN in air and $N_2$ excited at 445 nm with a 495 nm long pass filter.

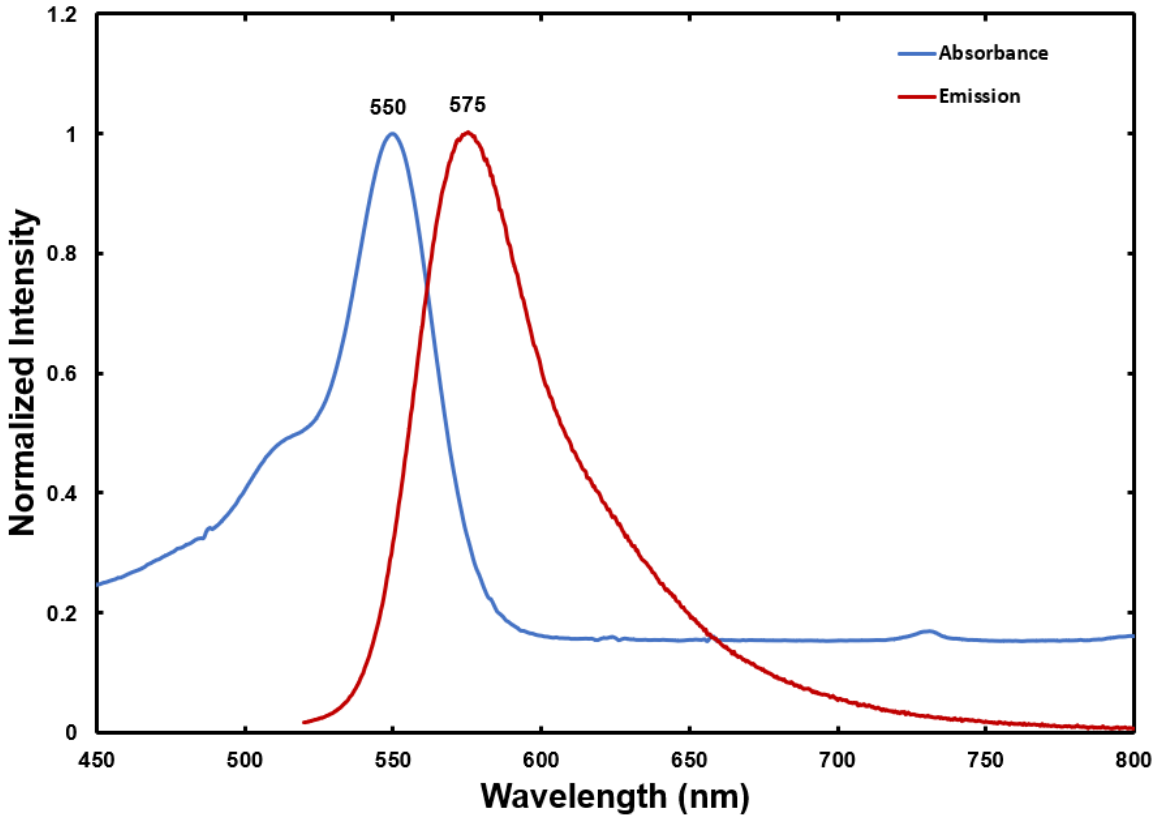


**Figure A.2.** Overlay of normalized absorption and emission spectra of E-ph$_3$. Spectra obtained in anhydrous acetonitrile and excitation at 490nm.

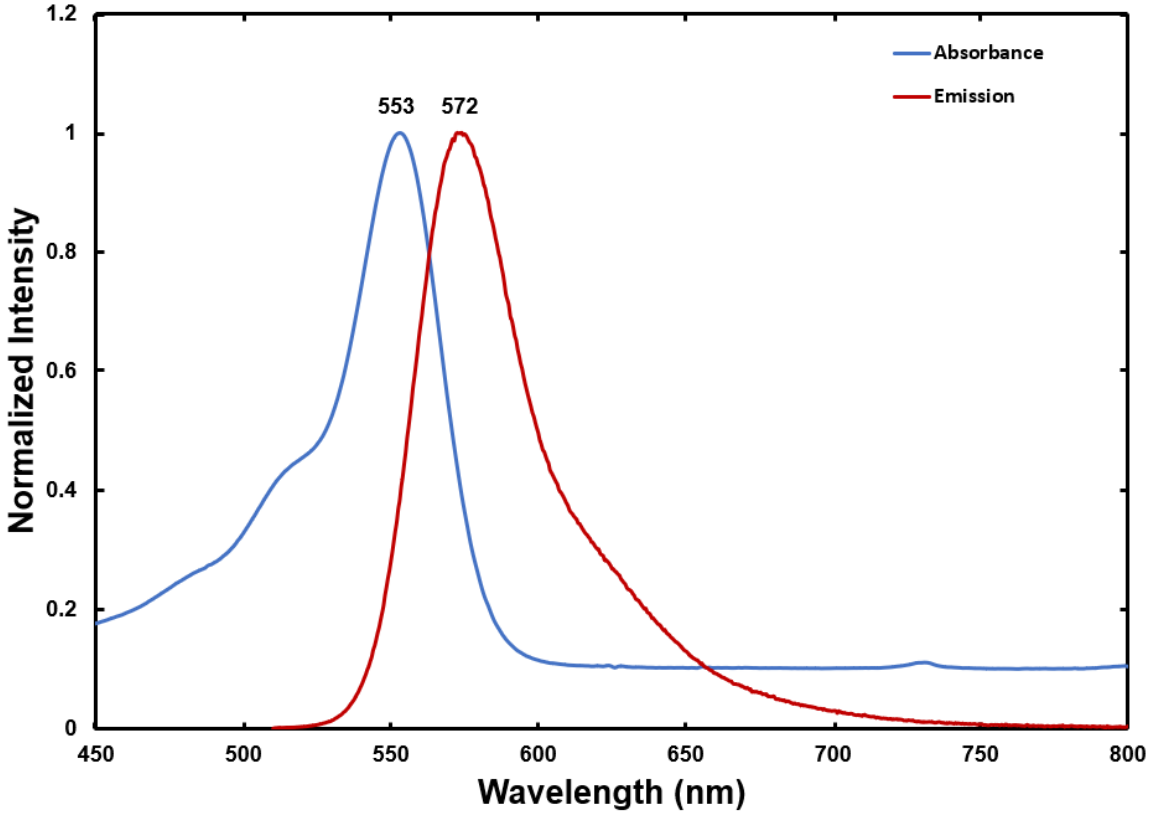


**Figure A.3.** Overlay of normalized absorption and emission spectra of E-trifluoromethylph$_3$. Spectra obtained in anhydrous acetonitrile and excitation at 490nm.

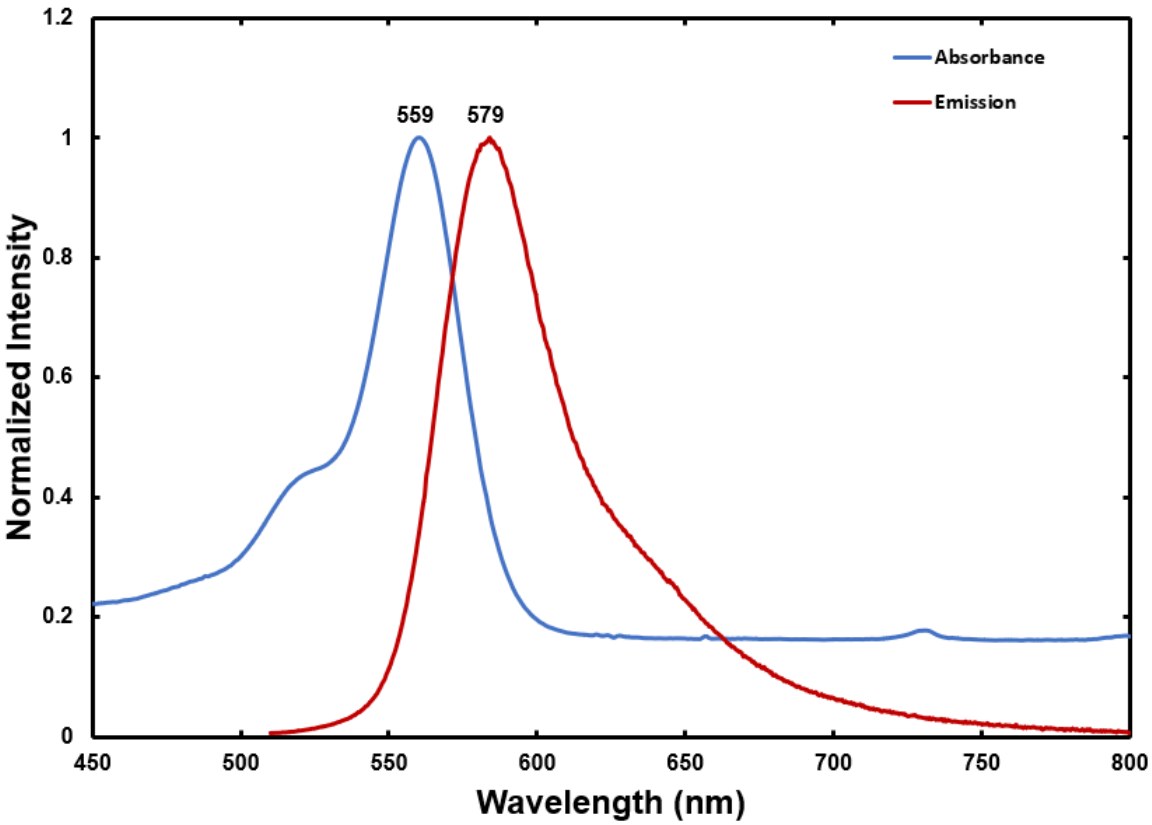


**Figure A.4.** Overlay of normalized absorption and emission spectra of E-tertbutylph$_3$. Spectra obtained in anhydrous acetonitrile and excitation at 490nm.

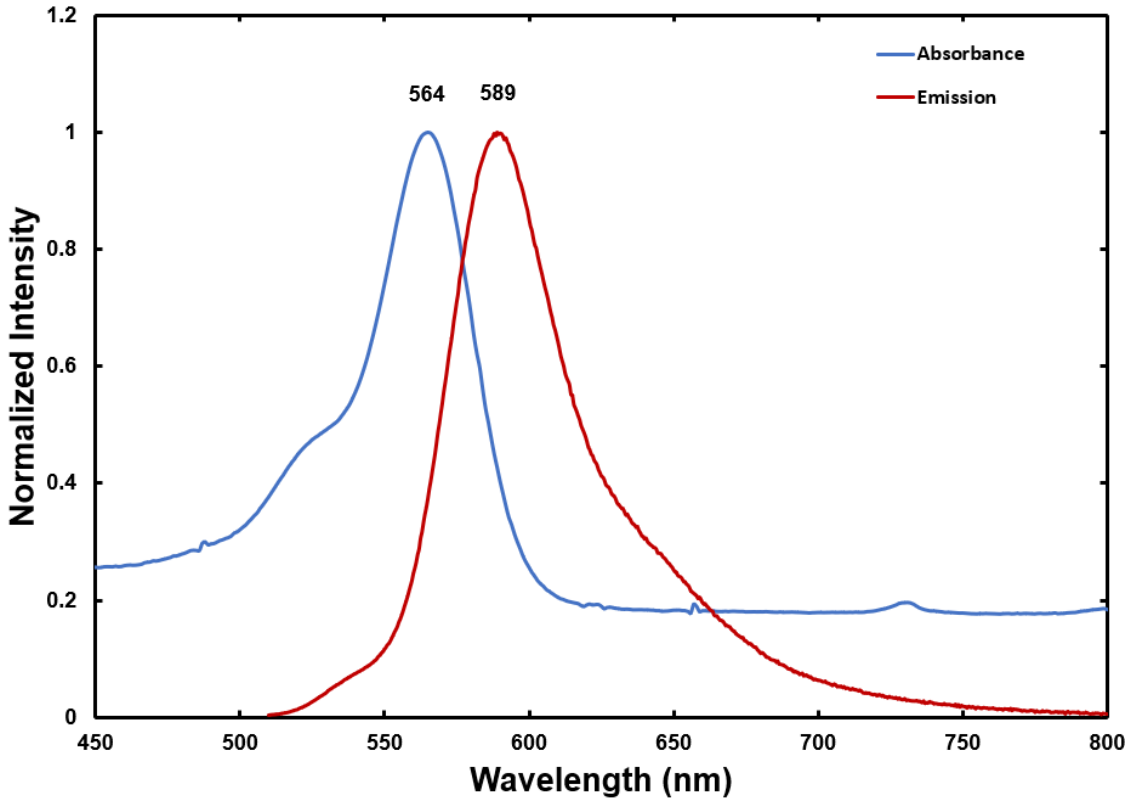


**Figure A.5.** Overlay of normalized absorption and emission spectra of E-naph$_3$. Spectra obtained in anhydrous acetonitrile and excitation at 490nm.

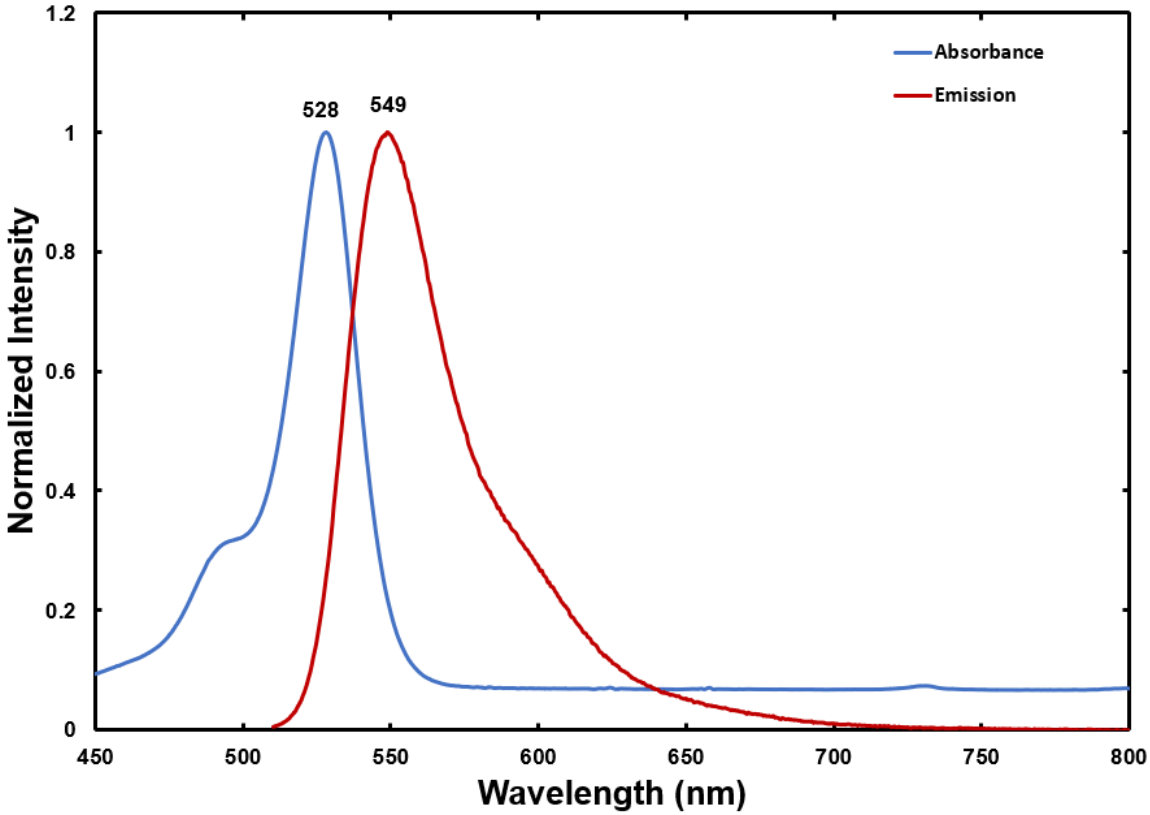


**Figure A.6.** Overlay of normalized absorption and emission spectra of Eosin Y. Spectra obtained in anhydrous acetonitrile and excitation at 490nm.

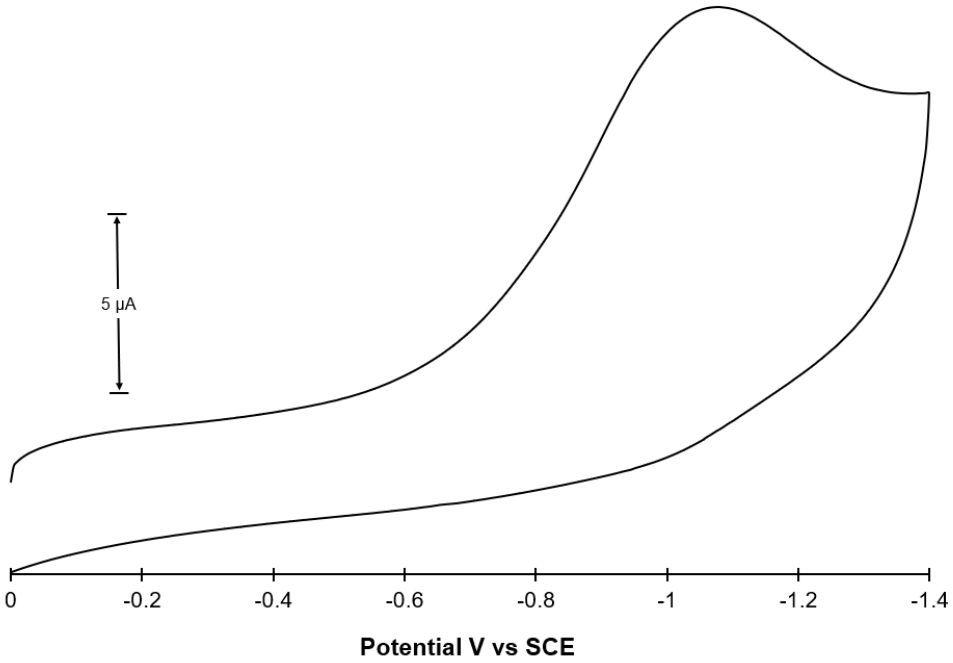


**Figure A.7.** Reductive cyclic voltammogram at 100 mV/s of 0.05 mM Eosin Y in anhydrous acetonitrile with 100 mM tetrabutylammonium hexafluorophosphate.

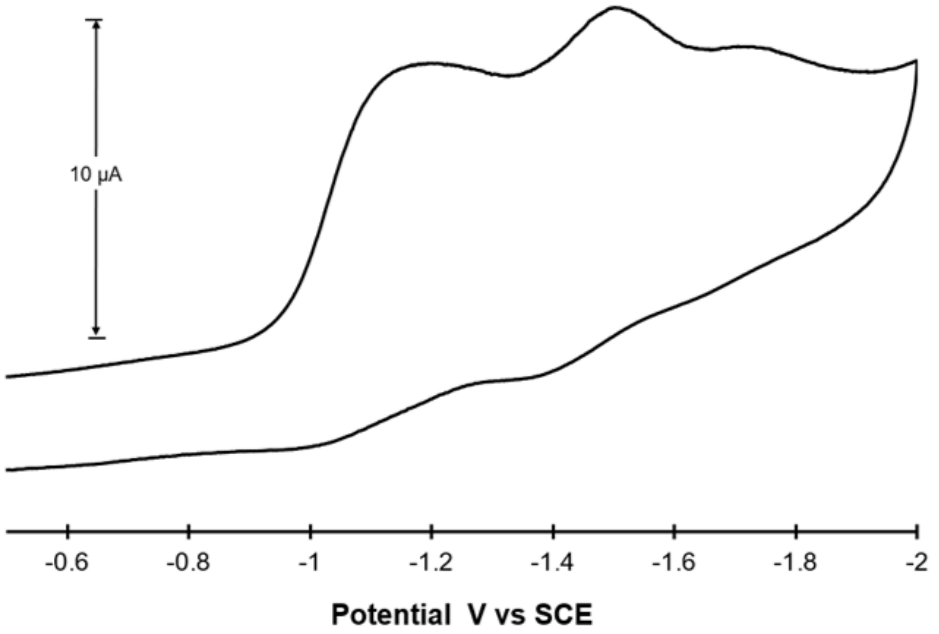


**Figure A.8.** Reductive cyclic voltammogram at 100 mV/s of 0.05 mM E-$ph_3$ in anhydrous acetonitrile with 100 mM tetrabutylammonium hexafluorophosphate

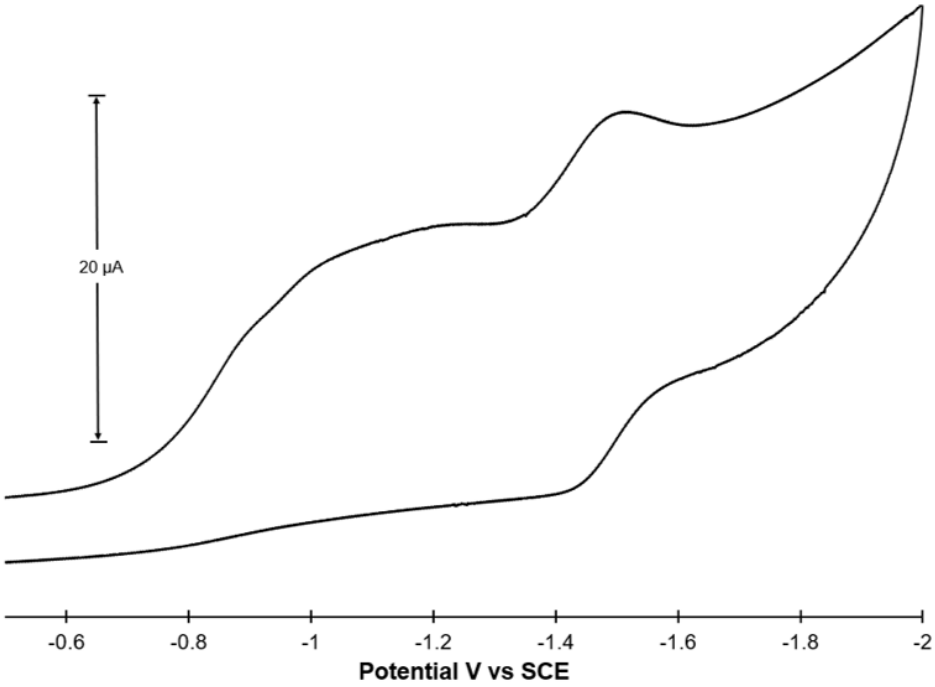


**Figure A.9.** Reductive cyclic voltammogram at 100 mV/s of 0.05 mM E-trifluoromethylph$_3$ in anhydrous acetonitrile with 100 mM tetrabutylammonium hexafluorophosphate

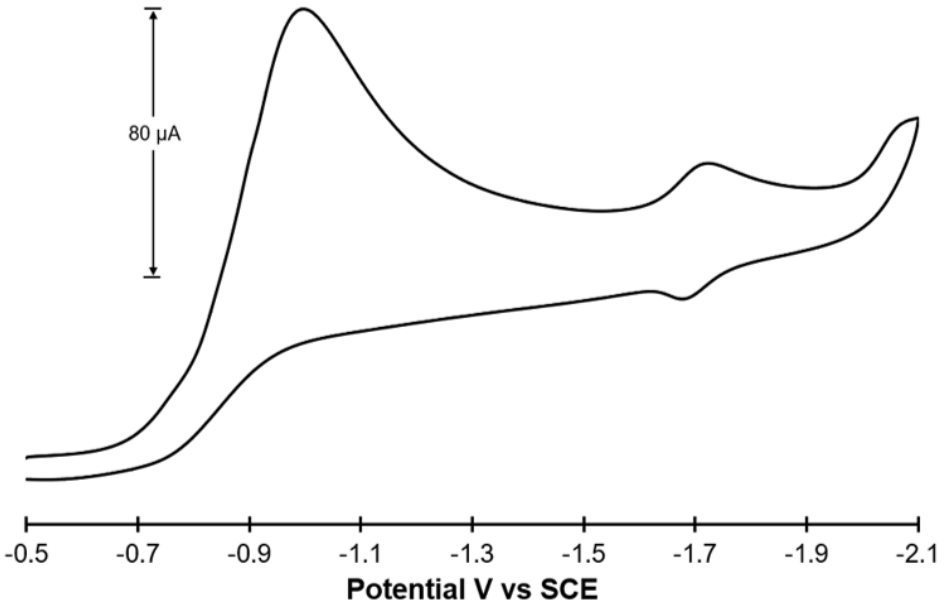


**Figure A.10.** Reductive cyclic voltammogram at 100 mV/s of 0.05 mM E-tertbutylph$_3$ in anhydrous acetonitrile with 100 mM tetrabutylammonium hexafluorophosphate

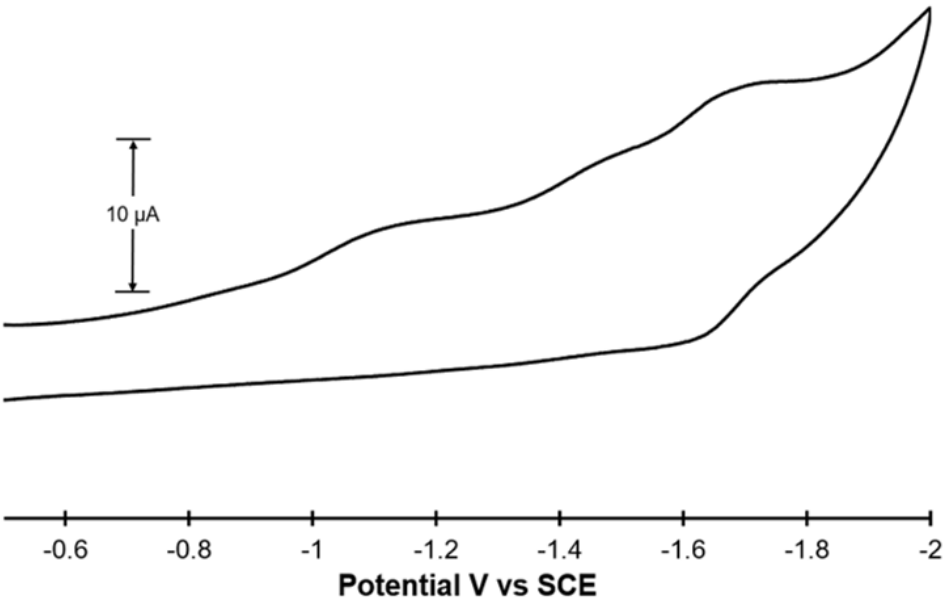


**Figure A.11.** Reductive cyclic voltammogram at 100 mV/s of 0.05 mM E-$naph_3$ in anhydrous acetonitrile with 100 mM tetrabutylammonium hexafluorophosphate

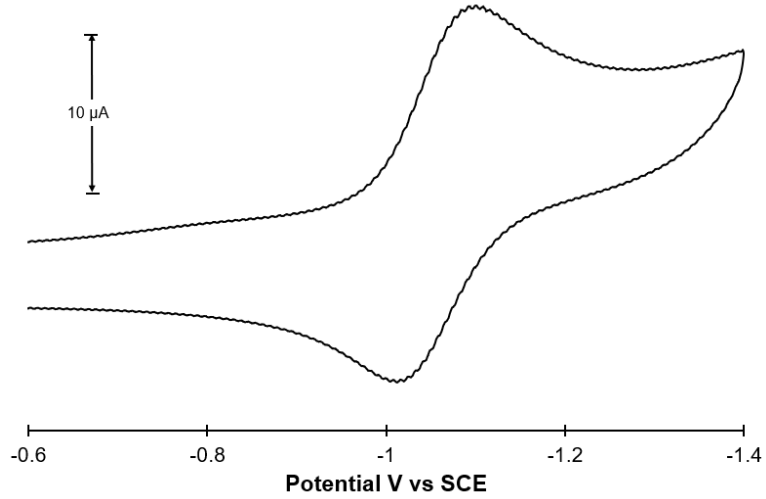


**Figure A.12** Reductive cyclic voltammogram at 100 mV/s of 1.0 mM Eosin Y in 1:1 acetonitrile/$H_2O$ with 100 mM tetrabutylammonium hexafluorophosphate.

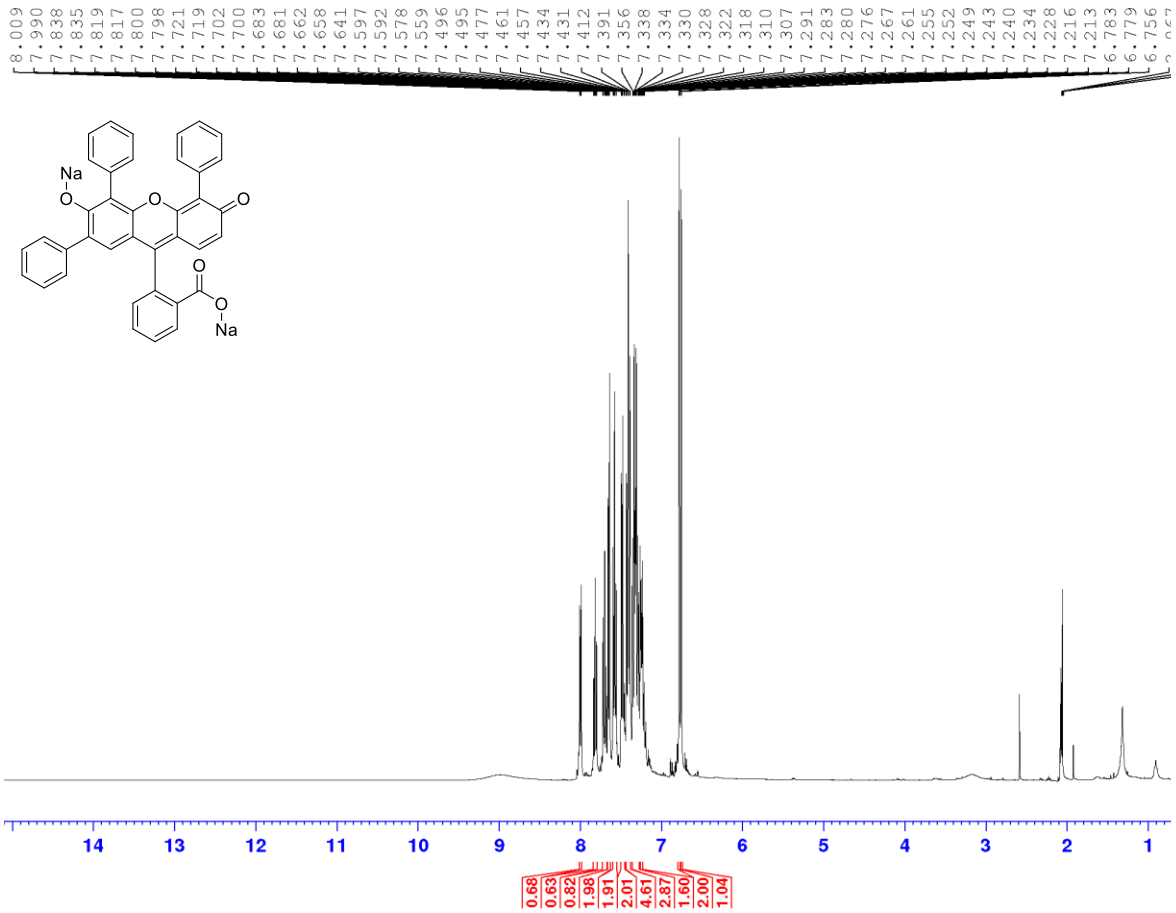


**Figure A.13.** $^{1}H$ NMR (400 MHz, $(CD_3)_2CO$) of E-$ph_3$

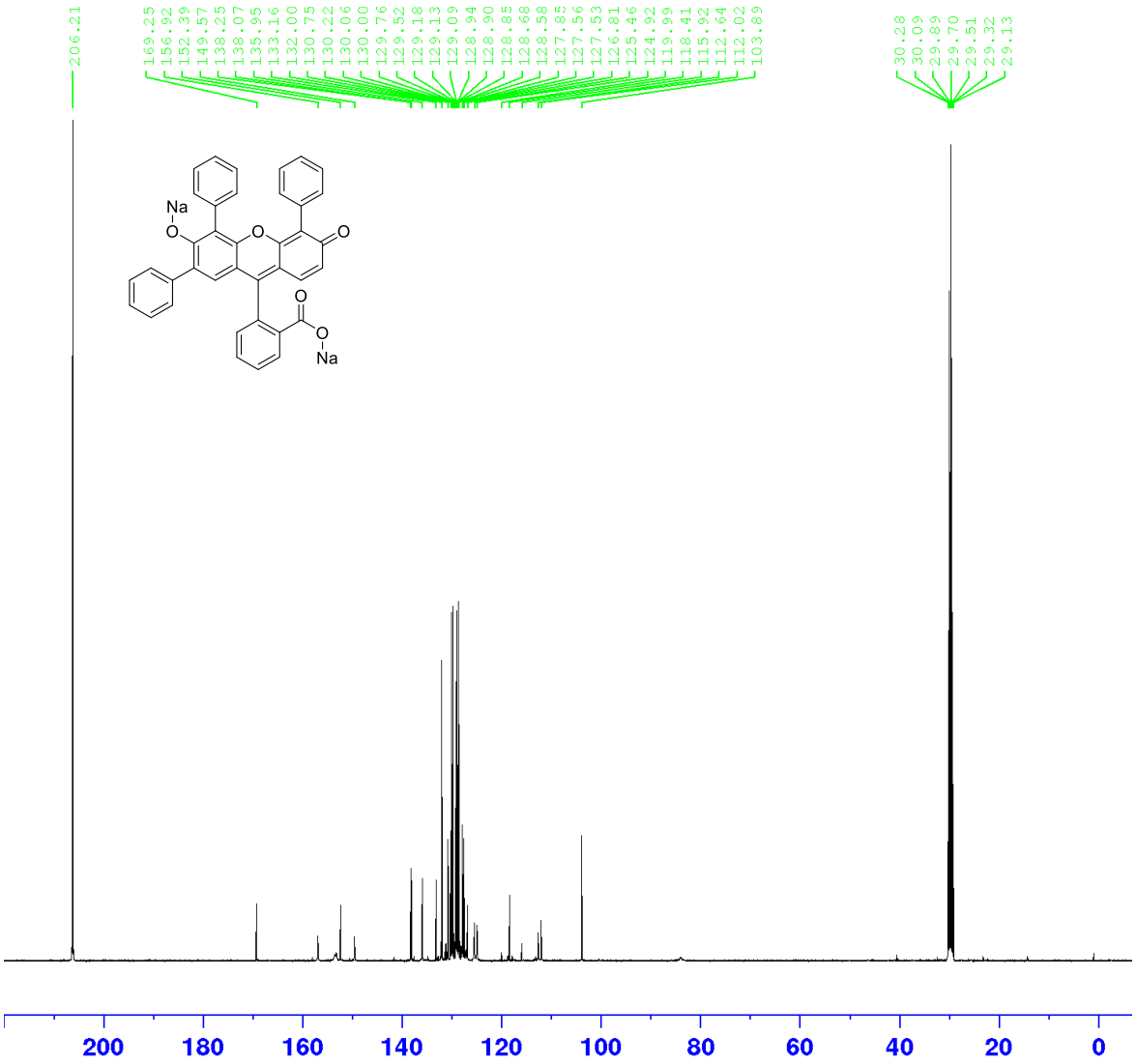


**Figure A.14.** $^{13}C$ NMR (400 MHz, $(CD_3)_2CO$) of E-ph$_3$

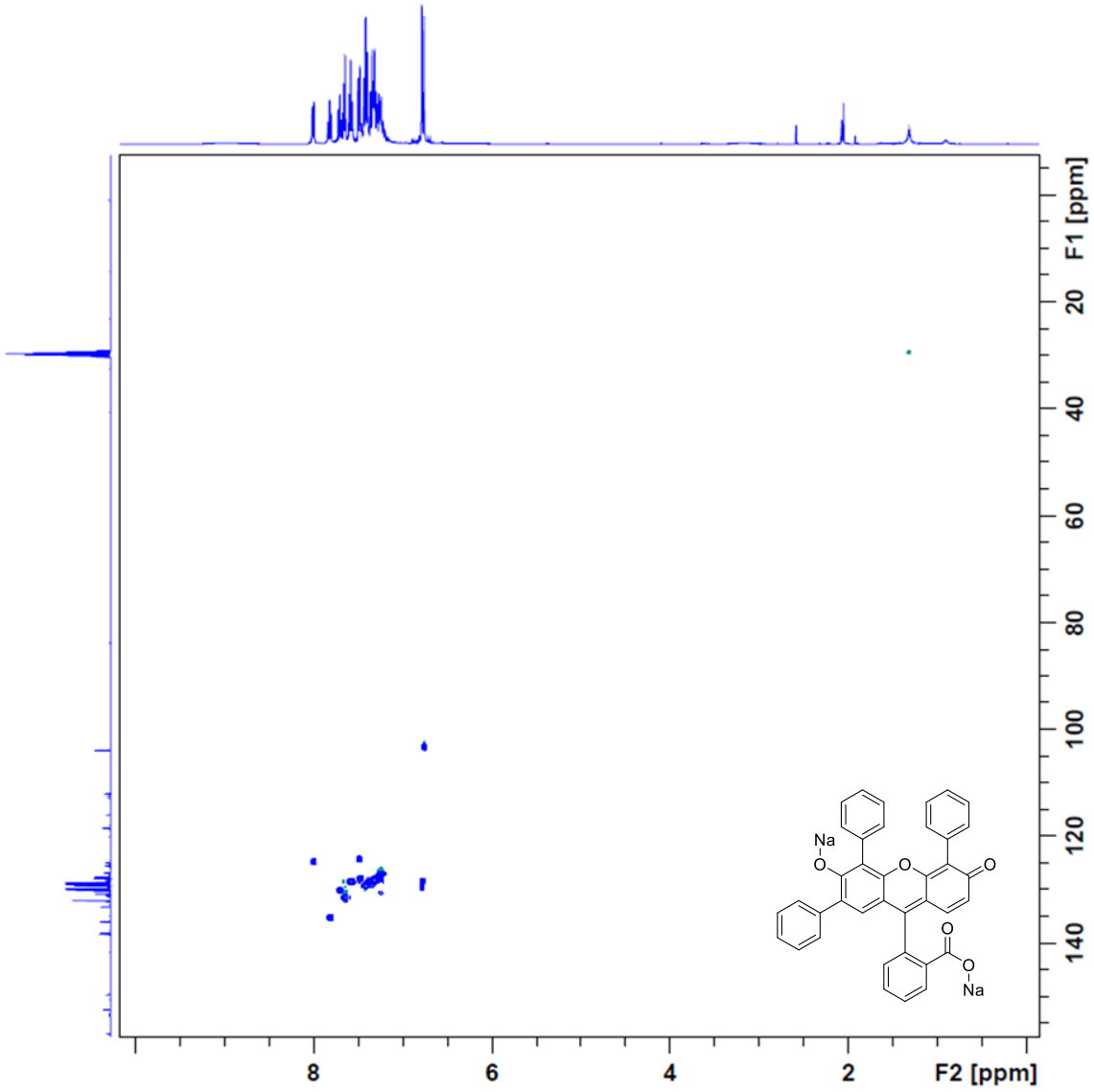


**Figure A.15.** 2D NMR (400 MHz, $(CD_3)_2CO$) of E-ph$_3$

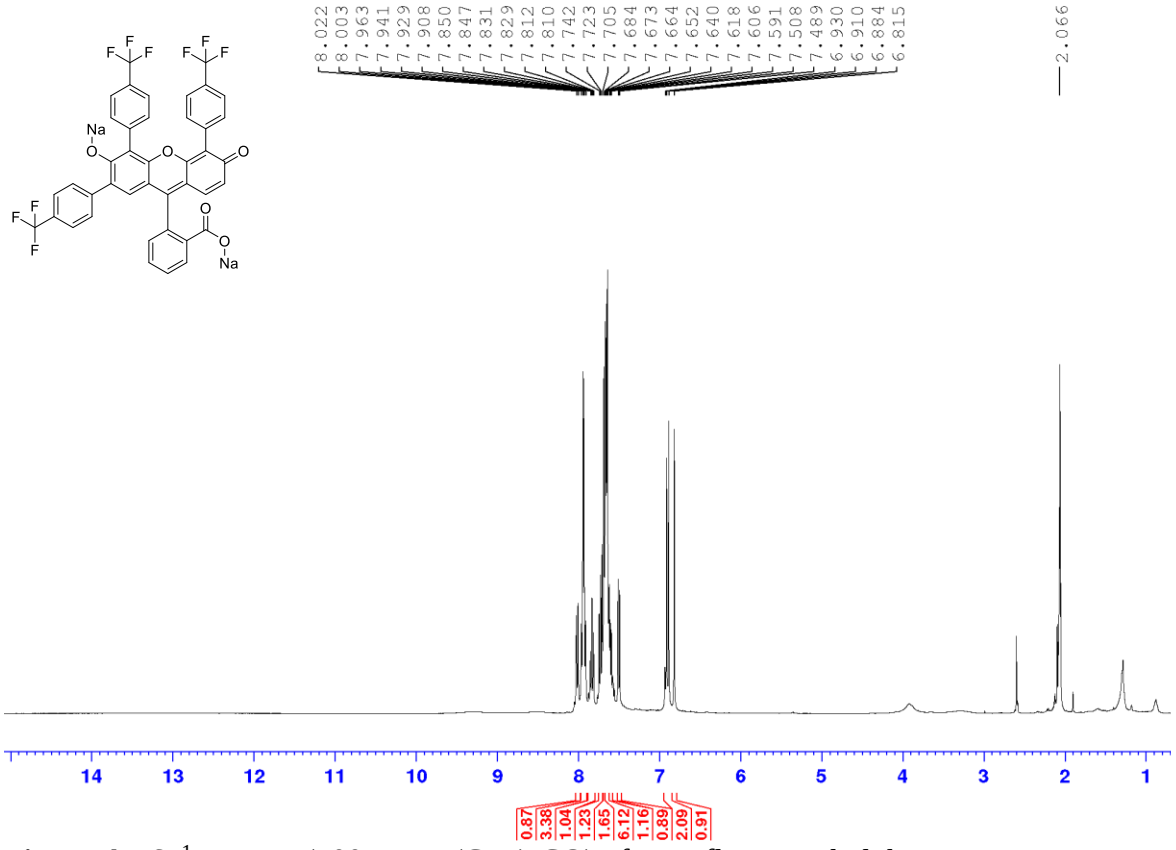


**Figure A.16.** $^{1}$H NMR (400 MHz, $(CD_3)_2CO$) of E- trifluoromethylph$_3$

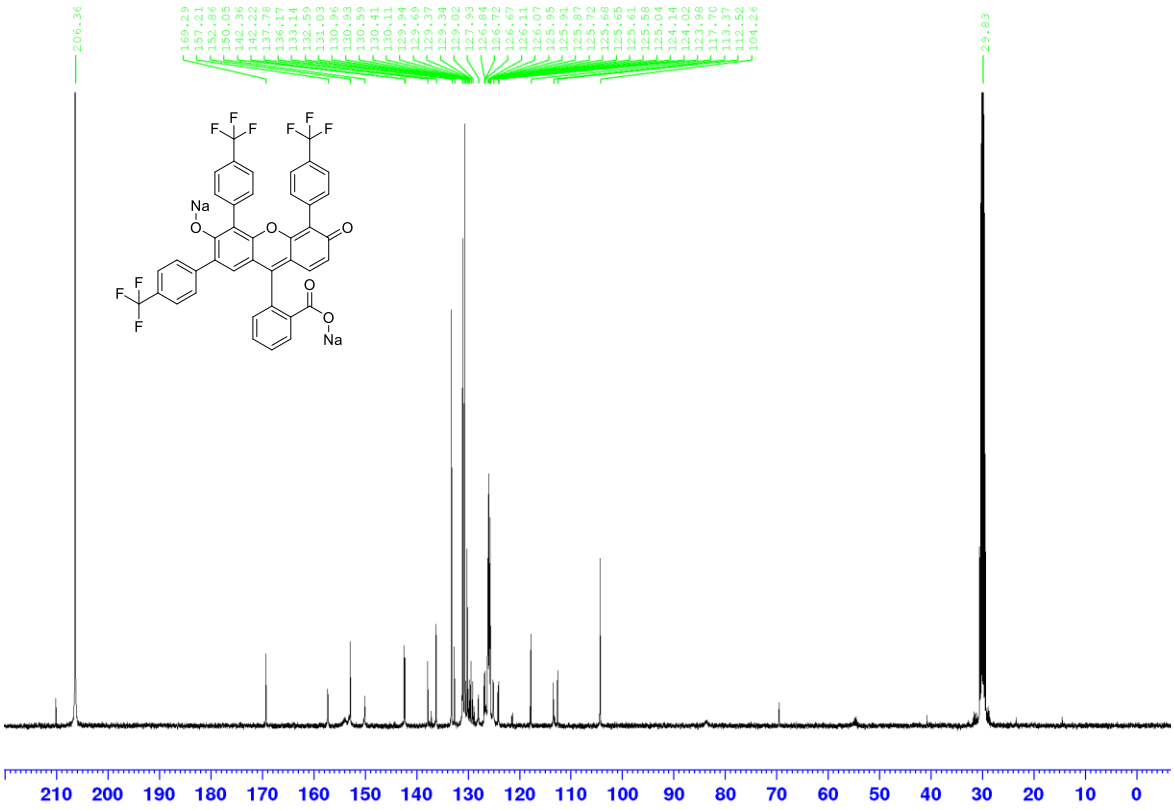


**Figure A.17.** $^{13}C$ NMR (400 MHz, $(CD_3)_2CO$) of E- trifluoromethylph$_3$

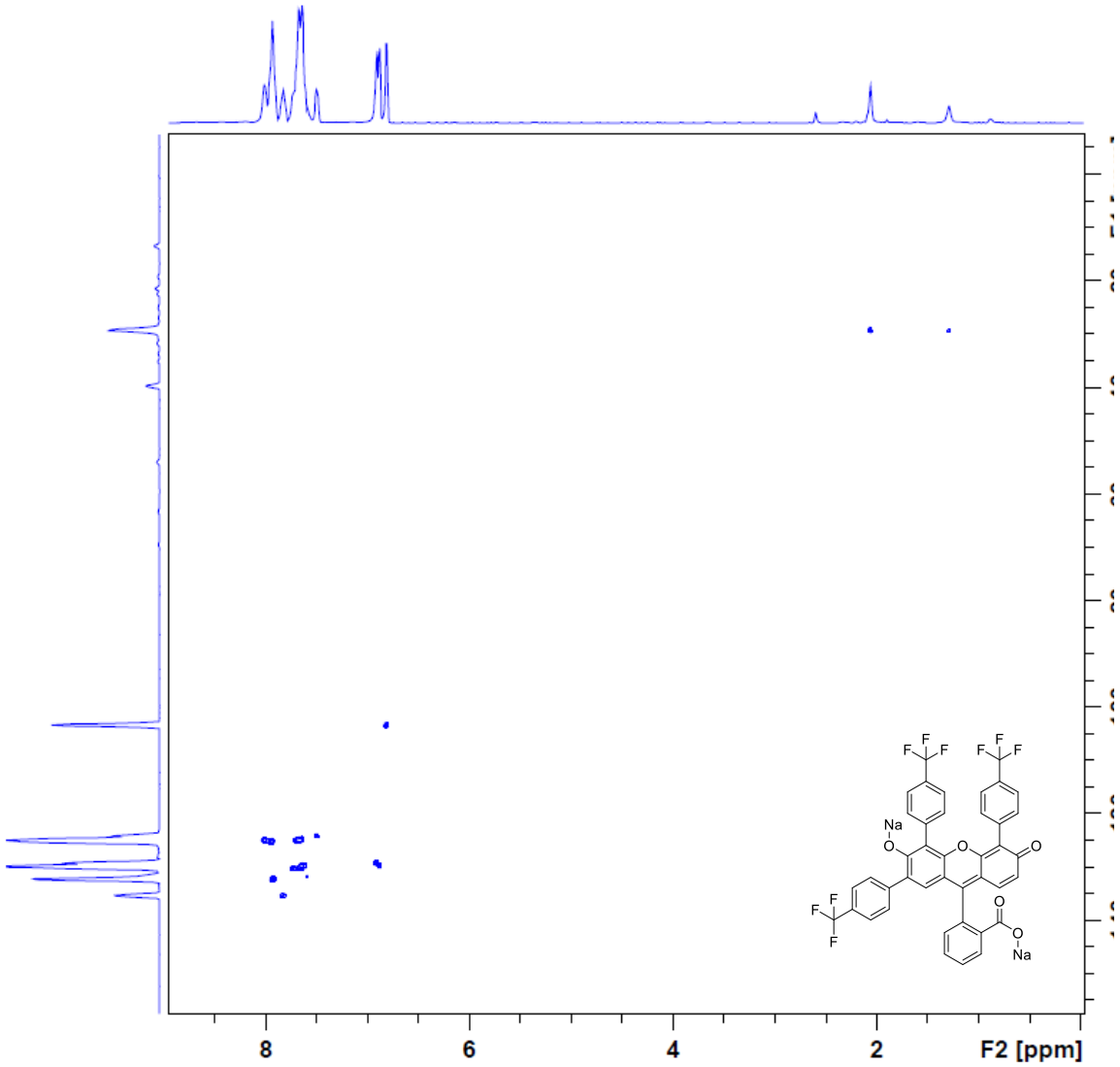


**Figure A.18.** 2D NMR (400 MHz, $(CD_3)_2CO$) of E-trifluoromethylph$_3$

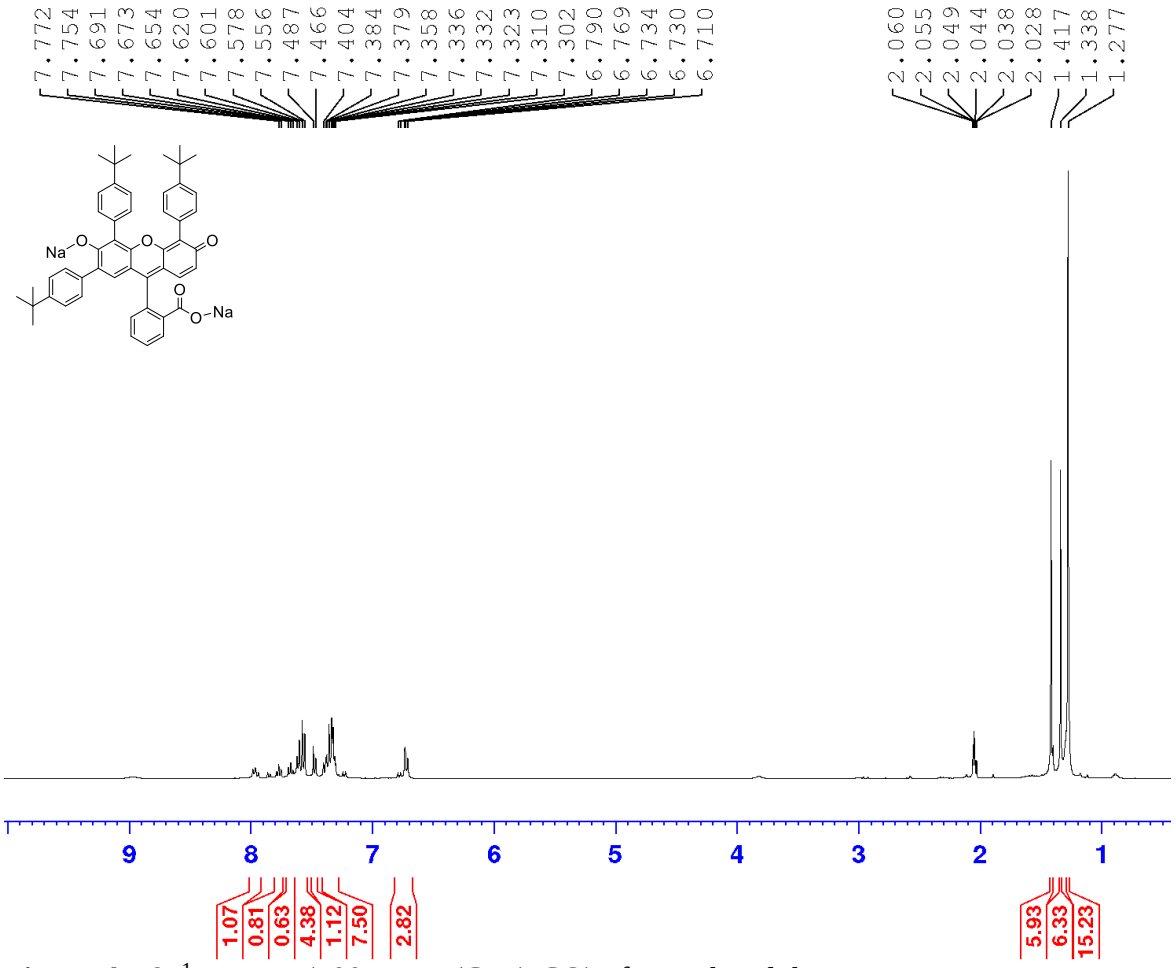


**Figure A.19.** $^{1}$H NMR (400 MHz, $(CD_3)_2CO$) of E-tertbutylph$_3$

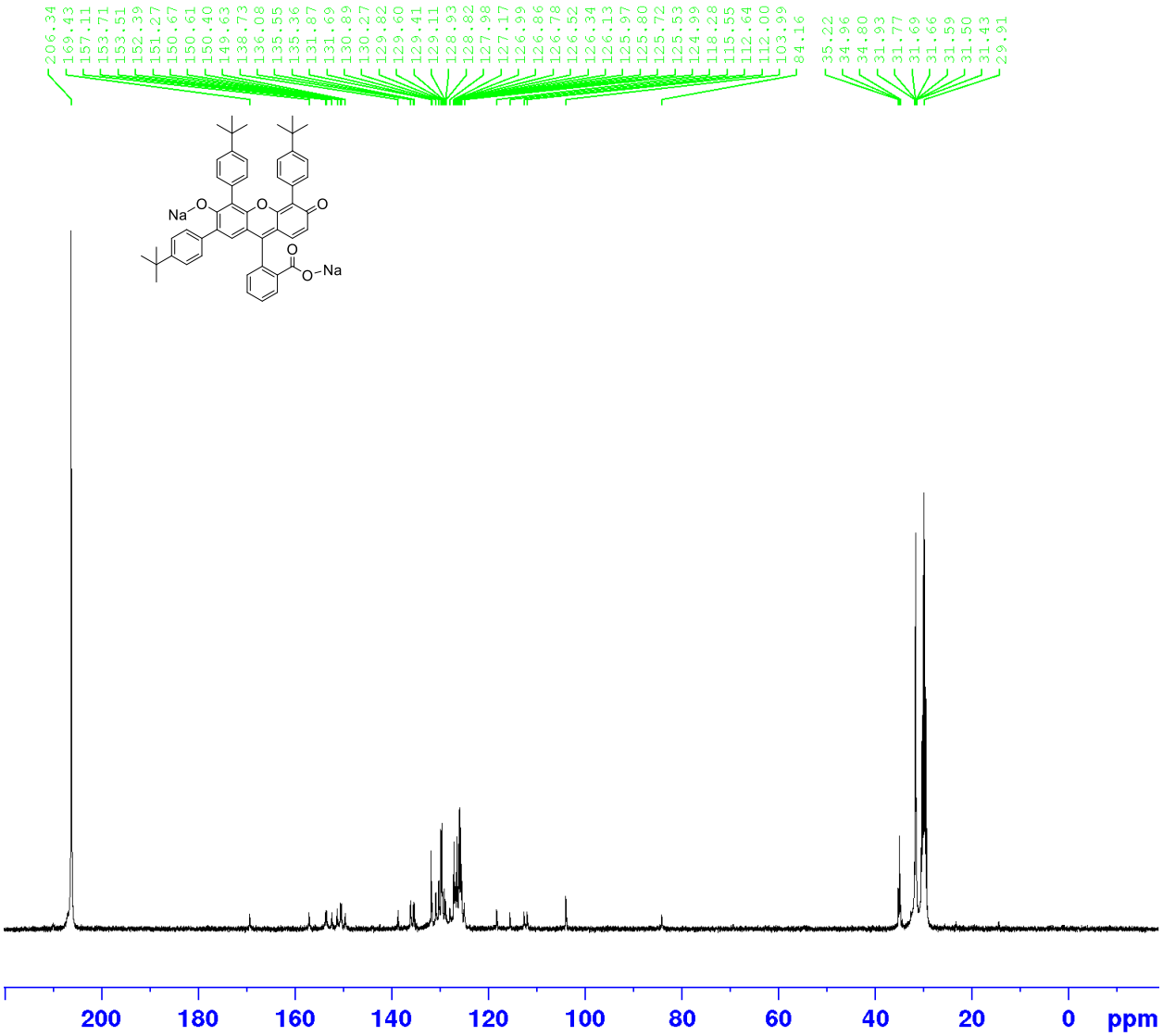


**Figure A.20.** $^{13}C$ NMR (400 MHz, $(CD_3)_2CO$) of E-tertbutylph$_3$

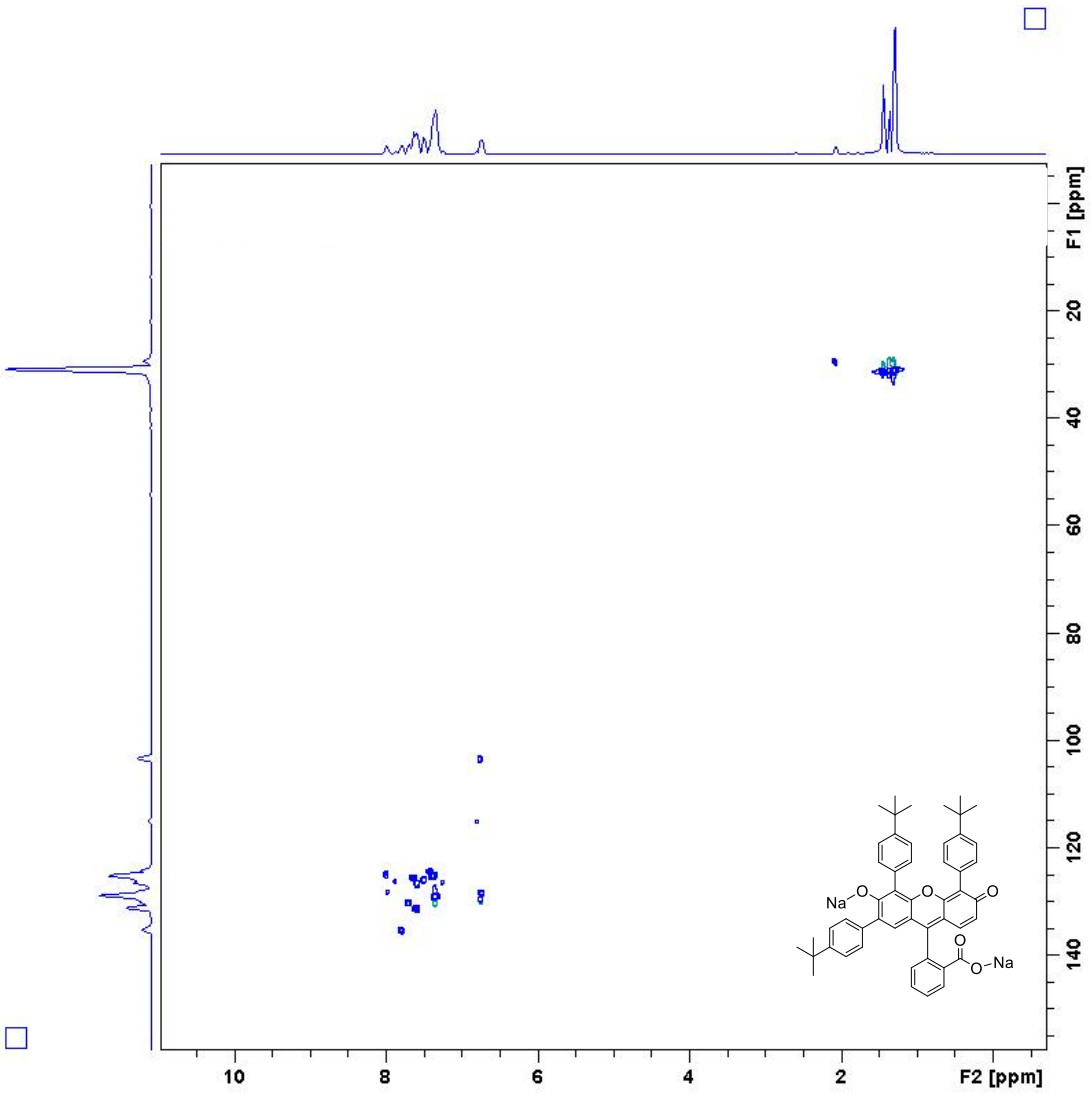


**Figure A.21.** 2D NMR (400 MHz, $(CD_3)_2CO$) of E-tertbutylph$_3$

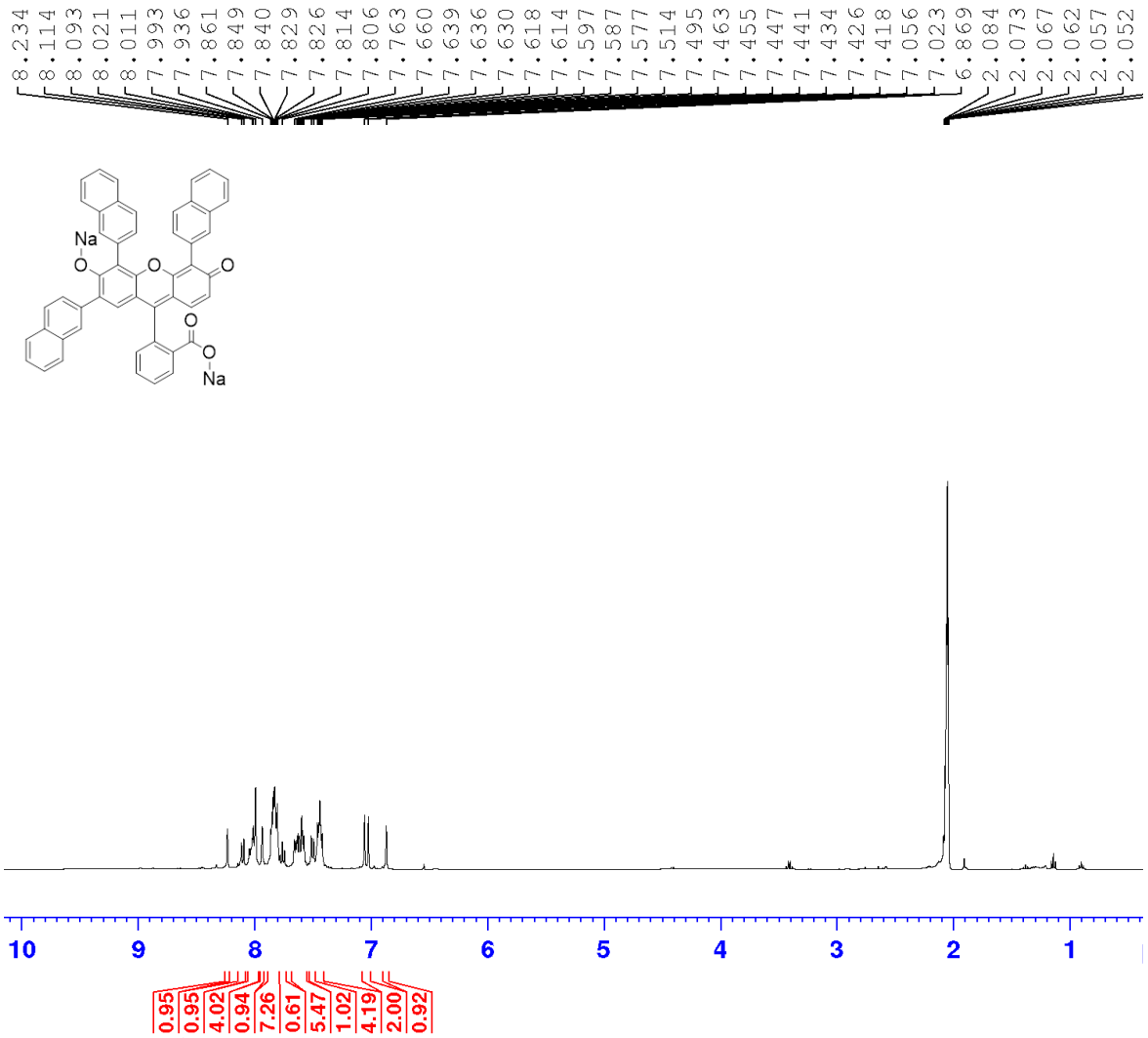


**Figure A.22.** $^{1}$H NMR (400 MHz, $(CD_3)_2CO$) of E-naph$_3$

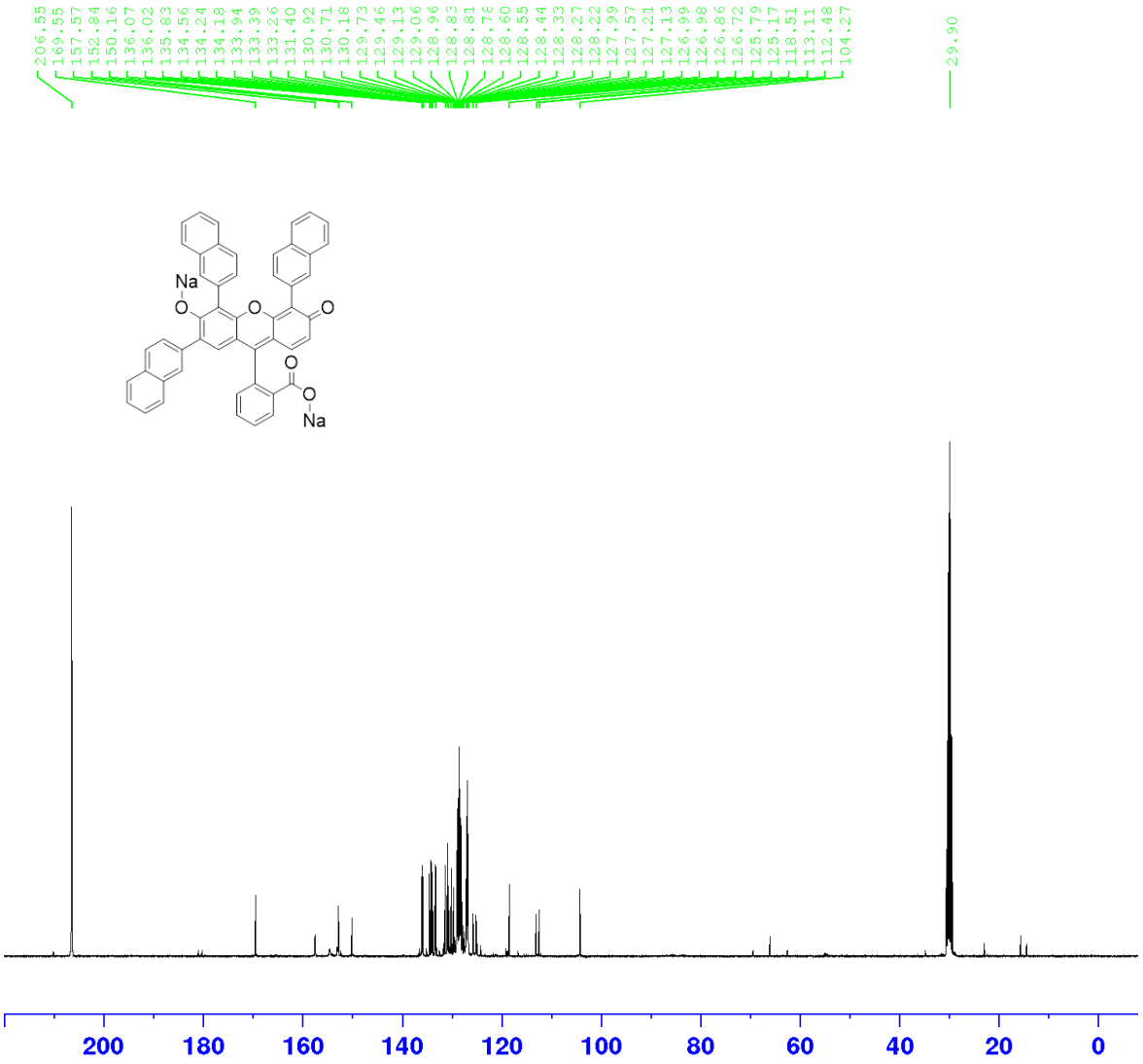


**Figure A.23.** $^{13}C$ NMR (400 MHz, $(CD_3)_2CO$) of E-naph$_3$

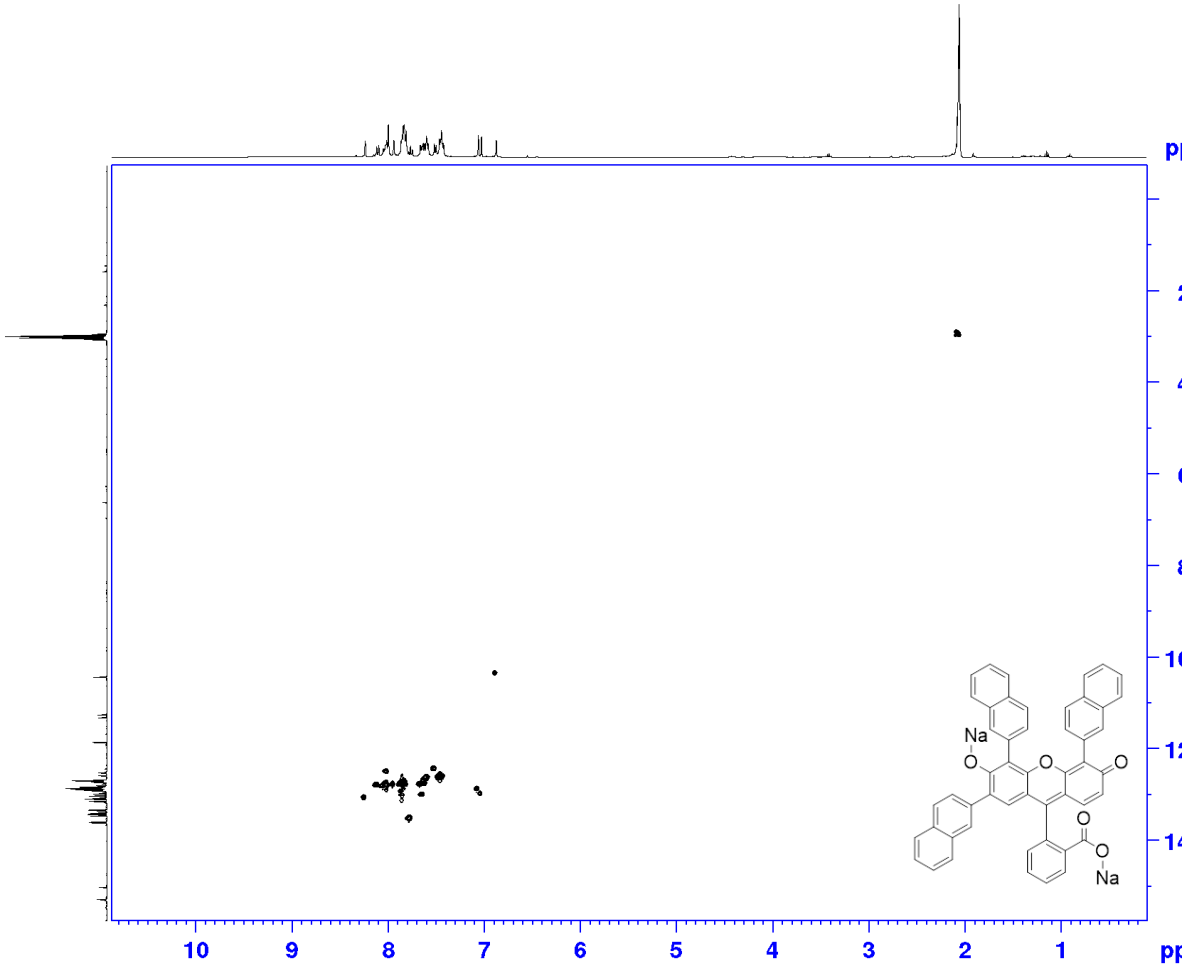


**Figure A.24.** 2D NMR (400 MHz, $(CD_3)_2CO$) of E-naph$_3$

# APPENDIX B

# EXPERIMENTAL DETAILS AND CHARACTERIZATION INFORMATION FOR CHAPTER 2

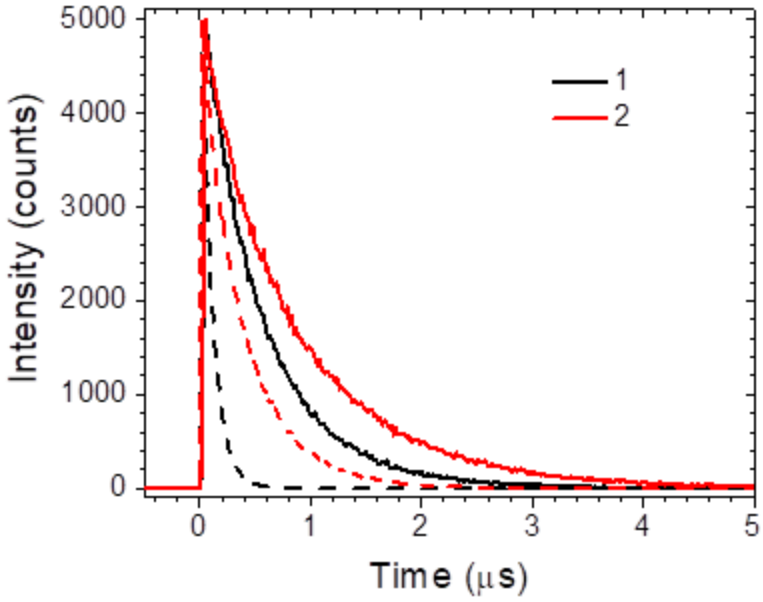


**Figure B.1.** Time resolved emission decay traces for **1** (black) in acetonitrile and **2** (red) in DMF at room temperature ($\lambda_{ex}$ = 405 nm). The solid lines are in $N_2$ deaerated solutions and the dashed lines are in air saturated solutions.

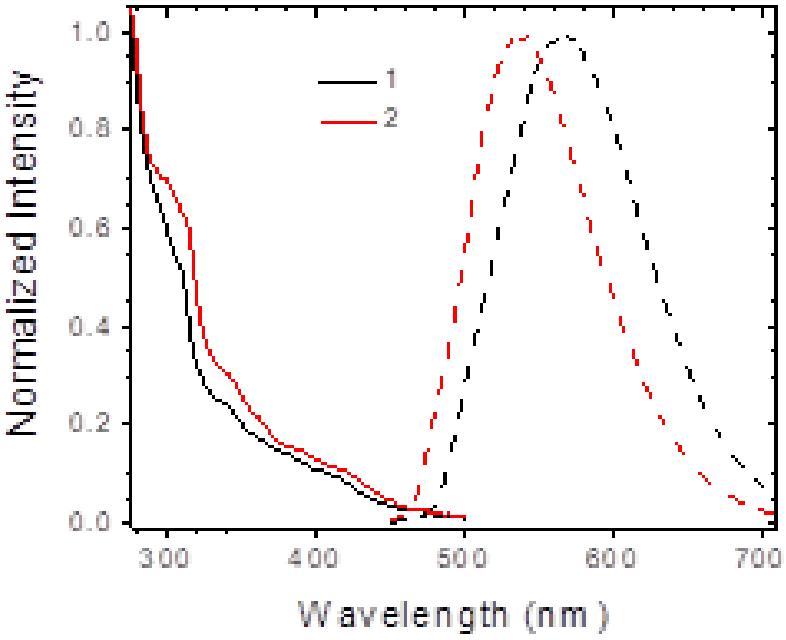


**Figure B.2**. Absorption (solid line) and emission (dashed line) spectra of **1** and **2** in $N_2$ deaerated acetonitrile and DMF respectively, at room temperature ($\lambda_{ex}$ = 355 nm).

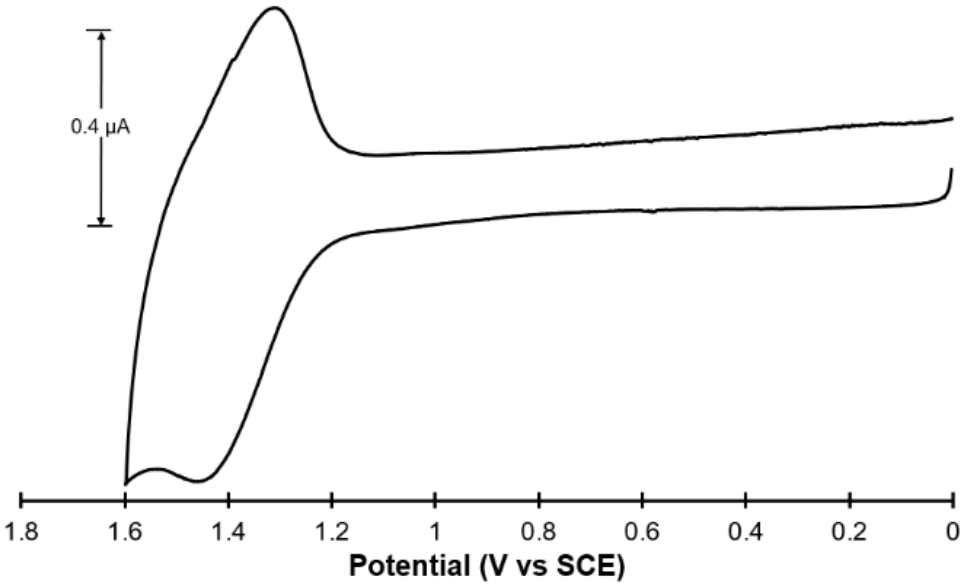


**Figure B.3**. Cyclic voltammogram of a nanoITO electrode derivatized with **2**. DMF solution with 0.1 M $NBu_4PF_6$ supporting electrolyte (Pt counter electrode; scan rate = 20 $mVs^{-1}$).

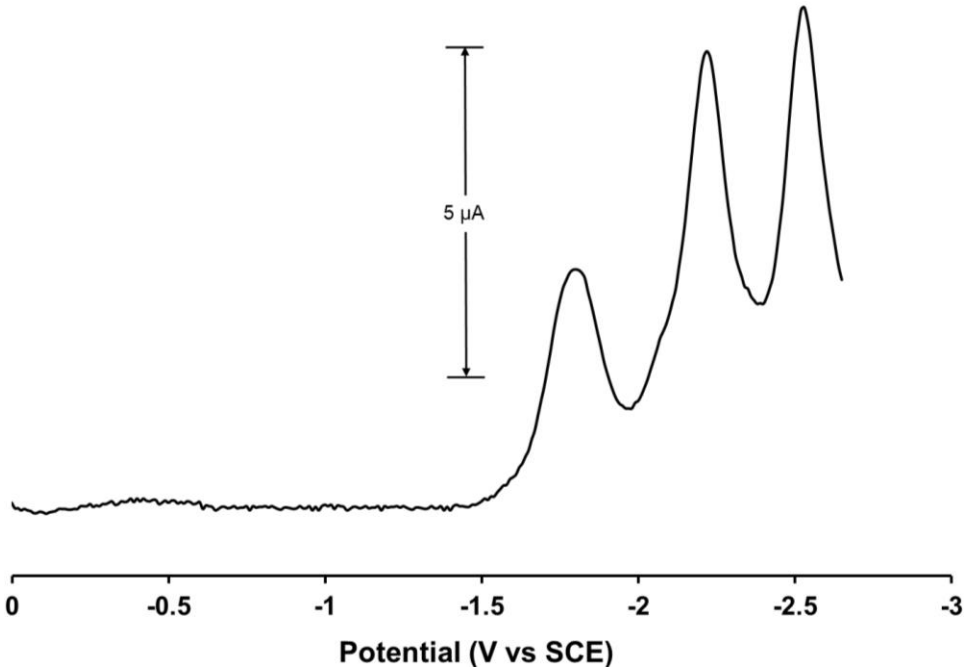


**Figure B.4**. DPV of 0.20 mM **2** in DMF with 0.1 M $NBu_4PF_6$ supporting electrolyte. Glassy carbon working electrode; Pt counter electrode. DPV parameters: pulse amplitude = 10 mV; pulse width = 100 ms, pulse period = 1000 ms; step increment = 1.5 mV; sample period = 3 ms.

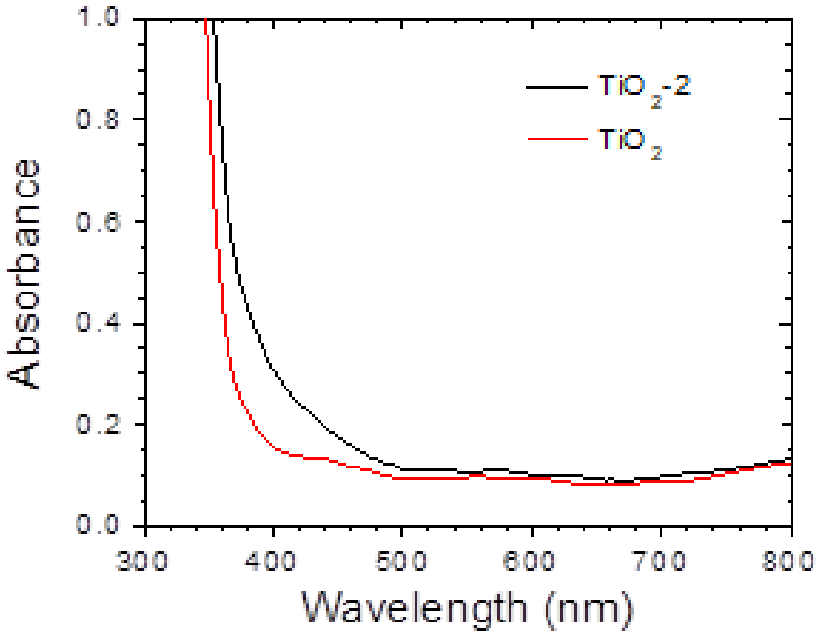


**Figure B.5.** UV-vis absorption spectra for $TiO_2$ (red) and $TiO_2$-**2** (black).

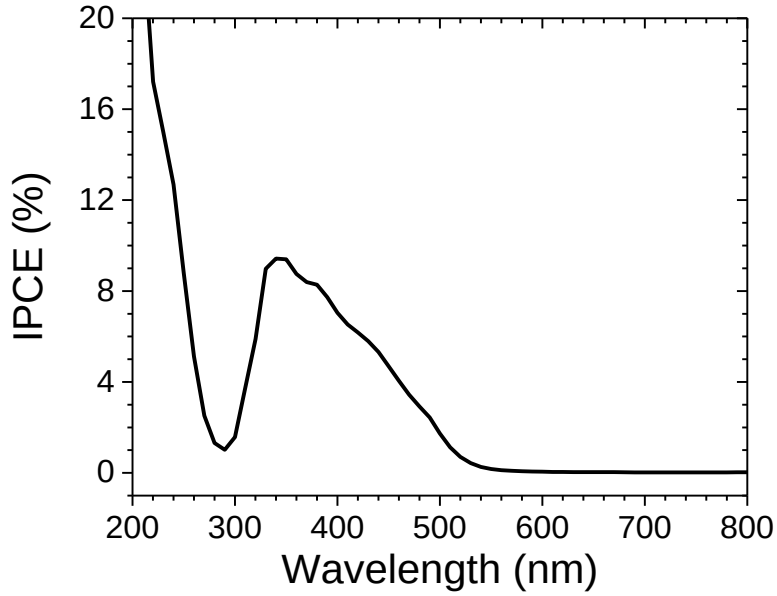


**Figure B.6.** Incident photon-to-current efficiency spectra for a DSSC with a photoanode composed of $TiO_2$-**2** with $Fe(bpy)^{2+/3+}$ redox mediator under AM1.5 solar irradiation.

**Table B.1.** Quantum yield and excited state lifetime for **1** in MeCN and **2** in DMF in atmosphere and after $N_2$ deaeration.

| | Φ | | τ (ns) | |
|---|---|---|---|---|
| | N2 | Air | $N_2$ | Air |
| **1** | 0.39 | 0.026 | 570 | 98 |
| **2** | 0.146 | 0.095 | 890 | 410 |

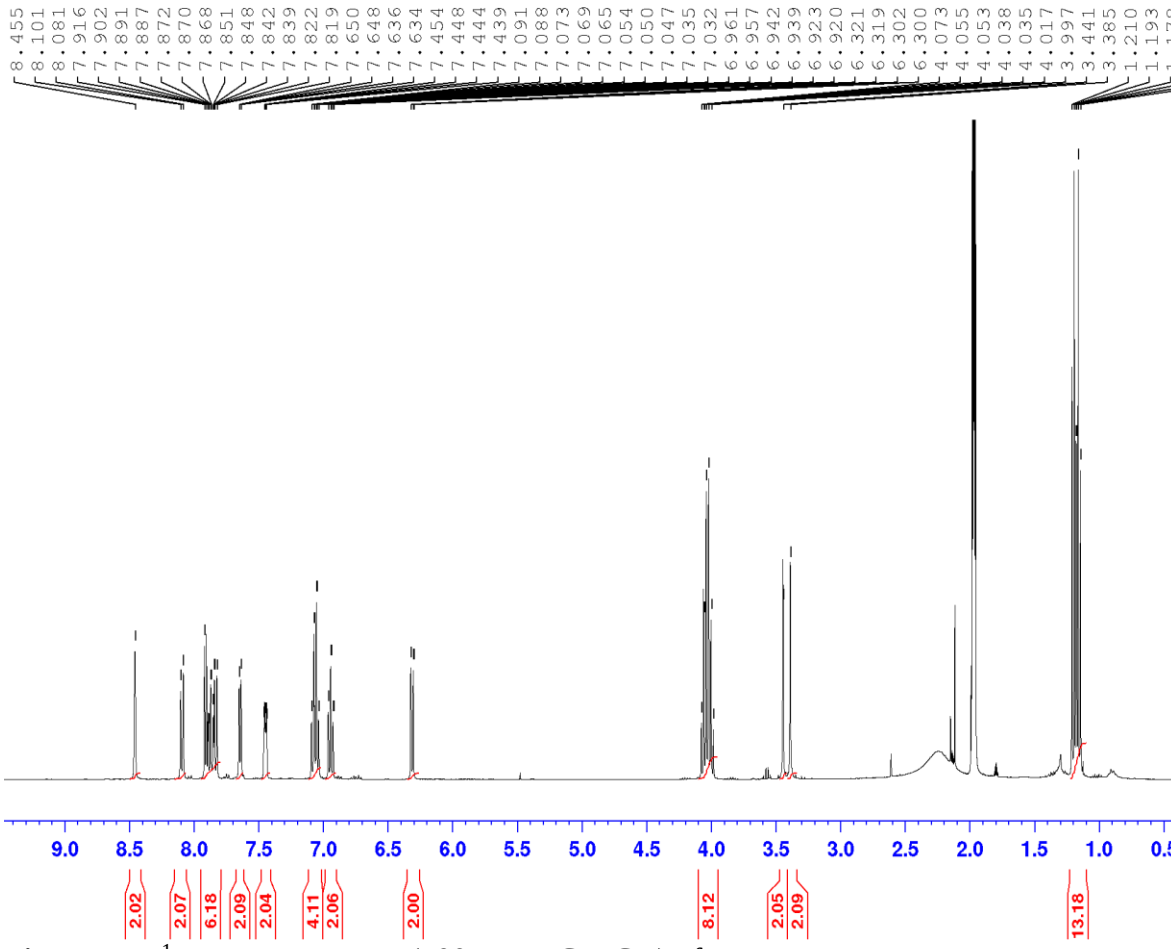


**Figure B.7.** $^{1}$H NMR spectrum (400 MHz, $CD_3CN$) of **1**

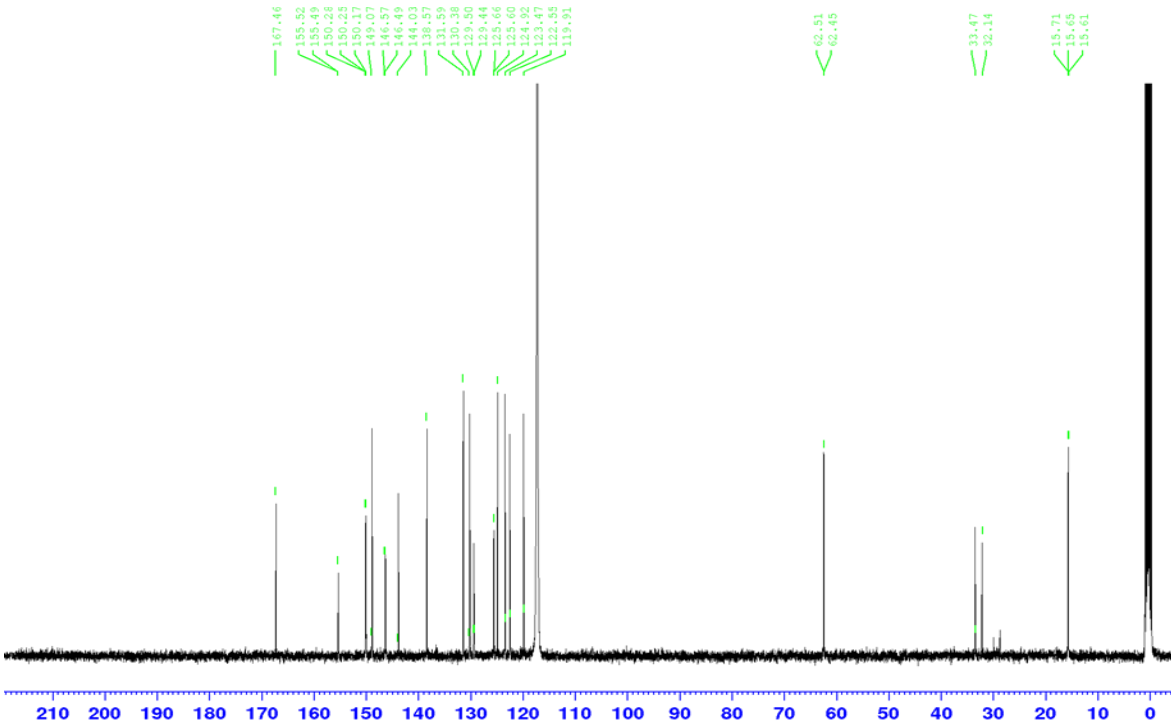


**Figure B.8.** $^{13}C$ NMR spectrum (100 MHz, $CD_3CN$) of **1**

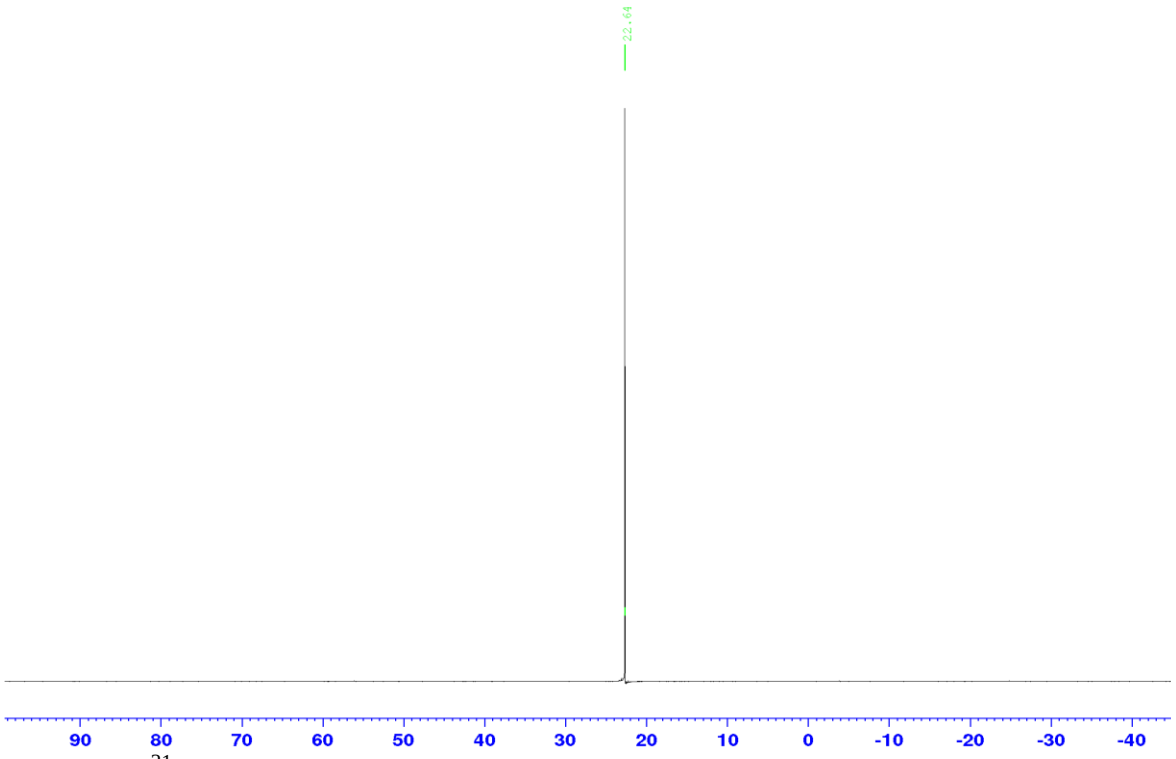


**Figure B.9.** $^{31}$P NMR spectrum (121.5 MHz, $CD_3CN$) of **1**

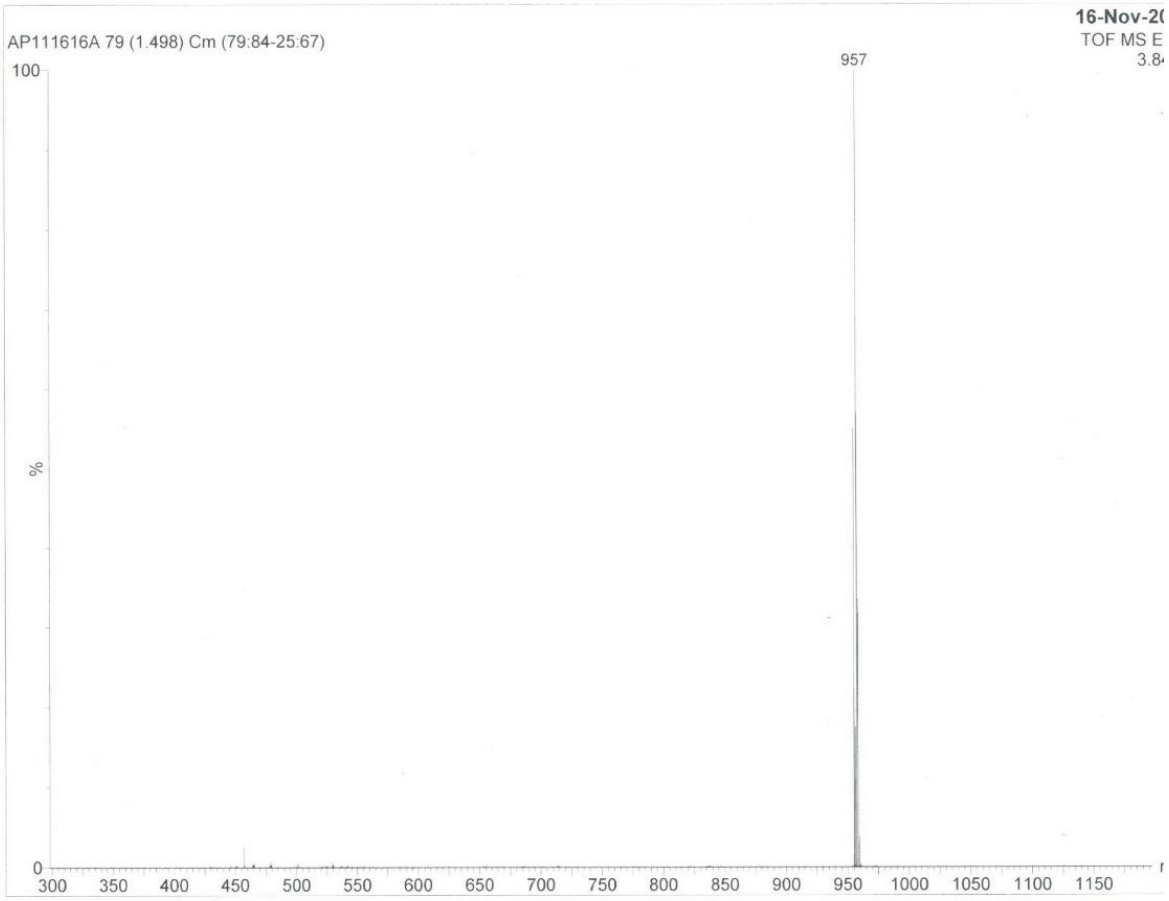


**Figure B.10.** ESI mass spectrum of **1**

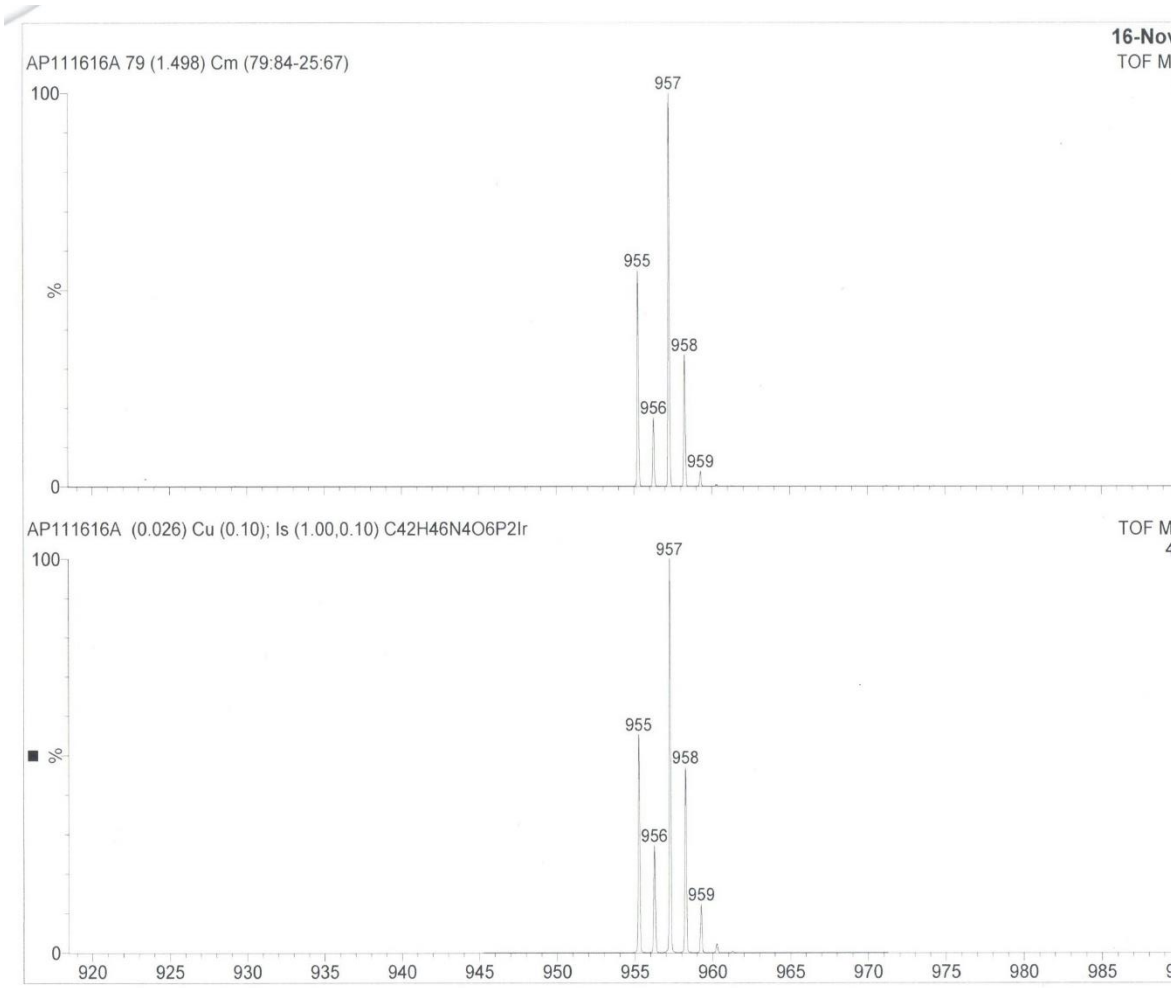


**Figure B.11.** ESI mass spectrum fragmentation of **1**

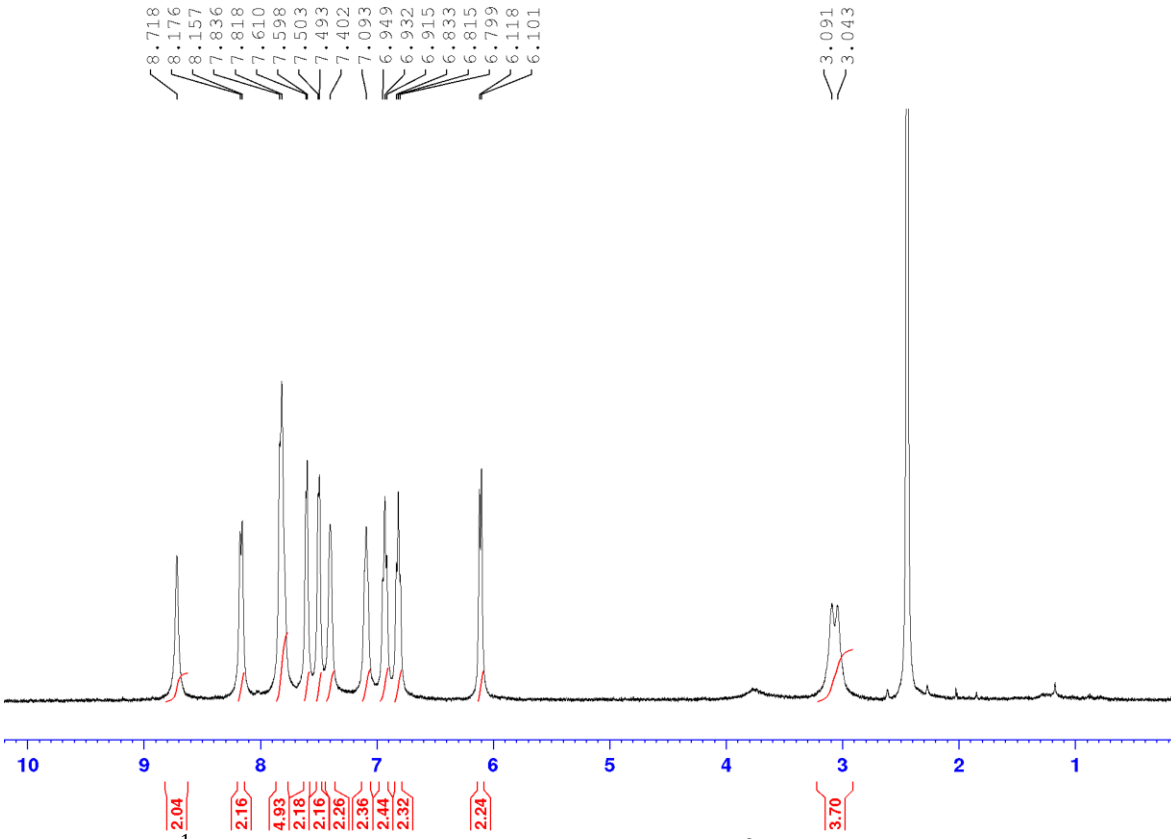


**Figure B.12.** $^{1}$H NMR spectrum (400 MHz, $d_6$-DMSO) of **2**

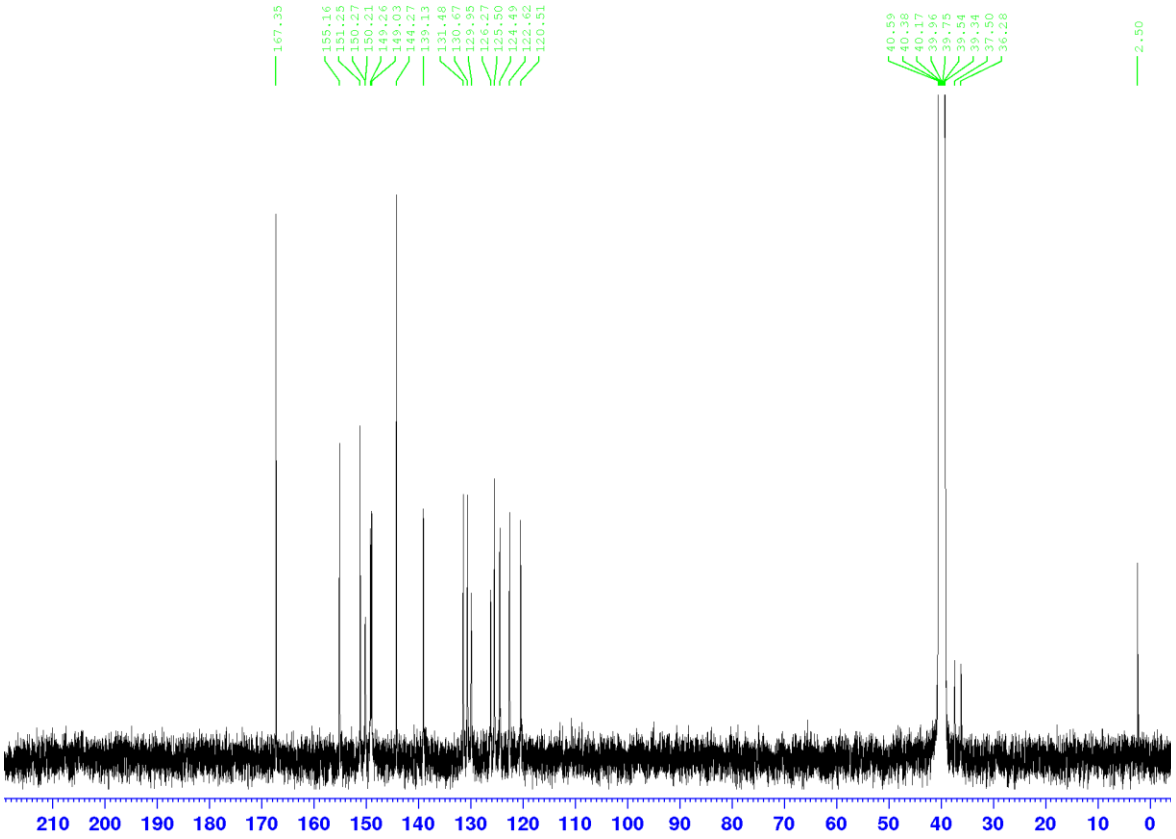


**Figure B.13.** $^{13}C$ NMR spectrum (100 MHz, $d_6$-DMSO) of **2**

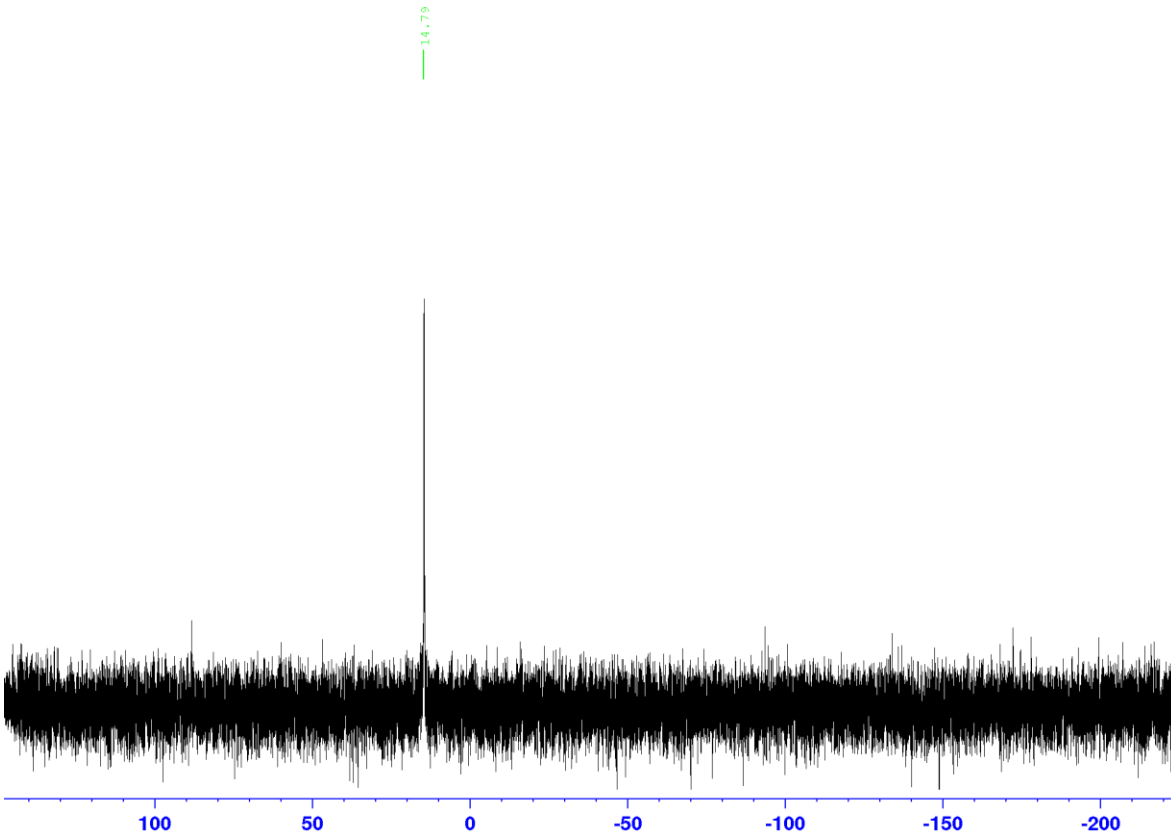


**Figure B.14.** $^{31}$P NMR spectrum of (121.5 MHz, $d_6$-DMSO) **2**

**B.2 X-Ray Structure Determination, $[Ir(C_{11}H_8N)_2(C_{20}H_{30}N_2O_6P_2)](PF_6)$ ( 1 )**

X-ray intensity data from a yellow plate were collected at 100(2) K using a Bruker D8 QUEST diffractometer equipped with a PHOTON-100 CMOS area detector and an Incoatec microfocus source (Mo Kα radiation, λ = 0.71073 Å). The raw area detector data frames were reduced and corrected for absorption effects using the Bruker APEX3, SAINT+ and SADABS programs.[181-182] Final unit cell parameters were determined by least-squares refinement of 9755 reflections taken from the data set. The structure was solved with SHELXT.[183-184] Subsequent difference Fourier calculations and full-matrix least-squares refinement against $F^2$ were performed with SHELXL-2016[183] using OLEX2.[185]

The compound crystallizes in the monoclinic system. The pattern of systematic absences in the intensity data was consistent with the space groups *C*2/*c* and *Cc*, the former of which was confirmed by structure solution. The asymmetric unit in *C*2/*c* consists of one $[Ir(C_{11}H_8N)_2(C_{20}H_{30}N_2O_6P_2)]$ cation and half each of two independent hexafluorophosphate anions. One $PF_6^-$ anion (P3) is located on a crystallographic two-fold axis of rotation and the other (P4) is located on a crystallographic inversion center. One ethoxy group (atoms O3, C14, C15) attached to phosphorus P1 is disordered over two positions with occupancies A/B = 0.730(7)/0.270(7). One $-CH_2P(O)(OCH_2CH_3)_2$ grouping (associated with phosphorus atom P2) is badly disordered and was modeled using three different group conformations A/B/C. The geometries of all three disorder components were restrained to be similar to that of the ordered group associated with phosphorus P1 by means of SHELX SAME instructions. Nearly superimposed atoms were refined with equal displacement parameters, and an enhanced rigid-bond restraint (SHELX RIGU) was applied to the $U_{ij}$ parameters for these atoms to maintain physically reasonable displacement ellipsoids. Eventually all non-hydrogen atoms were refined with anisotropic displacement parameters. Hydrogen atoms bonded to carbon were placed in geometrically idealized positions and included as riding atoms with *d*(C-H) = 0.95 Å and *U*iso(H) = 1.2*U*eq(C) for aromatic hydrogen atoms, *d*(C-H) = 0.99 Å and *U*iso(H) = 1.2*U*eq(C) for methylene hydrogen atoms and *d*(C-H) = 0.98 Å and *U*iso(H) = 1.5*U*eq(C) for methyl hydrogens. The methyl hydrogens were allowed to rotate as a rigid group to the orientation of maximum observed electron density. The largest residual electron density peak in the final difference map is 1.42 $e^-/Å^3$, located 0.79 Å from Ir1.

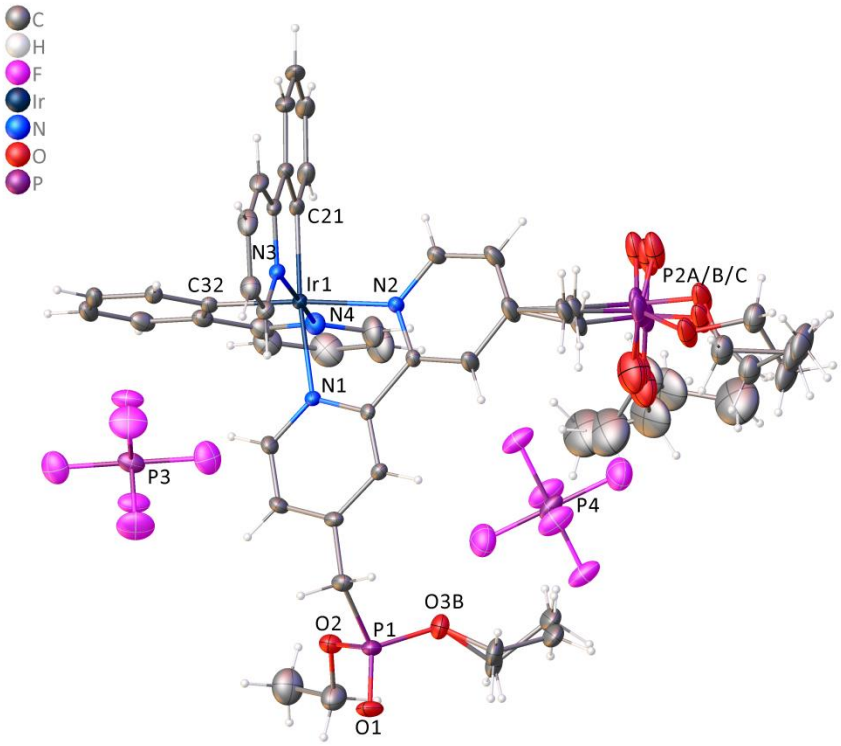


**Figure B.15.** Asymmetric unit of the crystal. Displacement ellipsoids drawn at the 40% probability level. Disorder in both -$CH_2PO_3Et_2$ groups. Entire group of phosphorus P2 disordered over three conformations A/B/C. Both $PF_6^-$ anions are on symmetry elements and only half of each is present per Ir cation.

**Table B.2.** Crystal data and structure refinement for **1**.

| | |
|---|---|
| Identification code | AVI_PS2P |
| Empirical formula | $C_{42}H_{46}F_6IrN_4O_6P_3$ |
| Formula weight | 1101.94 |
| Temperature/K | 100(2) |
| Crystal system | monoclinic |
| Space group | C2/c |
| a/Å | 23.1647(9) |
| b/Å | 10.7494(4) |
| c/Å | 35.4089(13) |
| α/° | 90 |
| β/° | 98.3820(10) |
| γ/° | 90 |
| Volume/Å$^3$ | 8722.9(6) |
| Z | 8 |
| $\rho_{calc}$g/cm$^3$ | 1.678 |
| μ/mm$^{-1}$ | 3.249 |
| F(000) | 4400.0 |
| Crystal size/mm$^3$ | 0.4 × 0.26 × 0.18 |
| Radiation | MoKα (λ = 0.71073) |
| 2Θ range for data collection/° | 4.274 to 60.252 |
| Index ranges | $-32 \leq h \leq 32$, $-15 \leq k \leq 15$, $-49 \leq l \leq 49$ |
| Reflections collected | 188483 |
| Independent reflections | 12826 [$R_{int}$ = 0.0530, $R_{sigma}$ = 0.0267] |
| Data/restraints/parameters | 12826/286/634 |
| Goodness-of-fit on F$^2$ | 1.065 |

| | |
|---|---|
| Final R indexes [I>=2σ (I)] | $R_1$ = 0.0299, $wR_2$ = 0.0570 |
| Final R indexes [all data] | $R_1$ = 0.0426, $wR_2$ = 0.0604 |
| Largest diff. peak/hole / e Å$^{-3}$ | 1.43/-1.13 |

**Table B.3.** Fractional Atomic Coordinates ($\times 10^4$) and Equivalent Isotropic Displacement Parameters ($Å^2 \times 10^3$) for **1**. $U_{eq}$ is defined as 1/3 of the trace of the orthogonalized $U_{IJ}$ tensor.

| Atom | *x* | *y* | *z* | U(eq) |
|---|---|---|---|---|
| Ir1 | 6253.0(2) | 4814.9(2) | 6668.1(2) | 17.32(3) |
| N1 | 5451.1(9) | 3876(2) | 6475.8(6) | 18.9(4) |
| N2 | 6356.6(9) | 4178(2) | 6110.7(6) | 20.0(4) |
| N3 | 6677.7(9) | 3225(2) | 6871.2(6) | 19.8(4) |
| N4 | 5883.4(11) | 6502(2) | 6517.1(7) | 27.3(5) |
| C1 | 4988.2(12) | 3816(3) | 6664.3(8) | 27.8(6) |
| C2 | 4507.5(12) | 3093(3) | 6540.7(8) | 31.7(7) |
| C3 | 4487.5(11) | 2380(3) | 6212.7(8) | 26.1(6) |
| C4 | 4957.0(11) | 2471(3) | 6010.6(7) | 23.3(5) |
| C5 | 5430.9(11) | 3219(2) | 6146.7(7) | 19.3(5) |
| C6 | 5951.4(11) | 3361(3) | 5951.5(7) | 20.9(5) |
| C7 | 6025.9(13) | 2703(3) | 5625.6(8) | 31.9(7) |
| C8 | 6523.8(15) | 2891(3) | 5454.7(9) | 40.8(8) |
| C9 | 6916.1(14) | 3790(3) | 5608.8(9) | 38.6(8) |
| C10 | 6826.4(12) | 4400(3) | 5936.8(8) | 28.1(6) |
| C21 | 7064.5(12) | 5498(3) | 6803.0(7) | 25.0(6) |
| C22 | 7255.9(15) | 6724(3) | 6772.3(8) | 34.3(7) |
| C23 | 7841.4(16) | 7023(4) | 6863.5(9) | 44.2(9) |
| C24 | 8250.7(15) | 6130(4) | 6986.2(9) | 46.7(10) |
| C25 | 8077.6(13) | 4911(4) | 7023.4(8) | 37.5(8) |
| C26 | 7488.5(12) | 4595(3) | 6935.6(7) | 27.2(6) |
| C27 | 7266.9(11) | 3336(3) | 6976.0(7) | 23.9(6) |
| C28 | 7592.0(12) | 2300(3) | 7116.3(8) | 31.7(7) |
| C29 | 7326.6(14) | 1177(3) | 7148.5(8) | 34.9(7) |

| | | | | |
|---|---|---|---|---|
| C30 | 6726.8(14) | 1081(3) | 7043.6(8) | 30.8(6) |
| C31 | 6420.0(12) | 2119(3) | 6907.2(7) | 23.7(5) |
| C32 | 6096.1(11) | 5398(2) | 7182.9(7) | 21.4(5) |
| C33 | 6215.9(12) | 4789(3) | 7534.5(7) | 26.1(6) |
| C34 | 6088.8(13) | 5340(3) | 7868.5(8) | 32.8(7) |
| C35 | 5837.5(14) | 6498(3) | 7861.2(9) | 38.4(8) |
| C36 | 5714.5(13) | 7133(3) | 7519.9(9) | 34.1(7) |
| C37 | 5844.0(12) | 6589(3) | 7181.9(8) | 26.8(6) |
| C38 | 5728.6(13) | 7193(3) | 6808.9(9) | 30.5(6) |
| C39 | 5487.5(16) | 8373(3) | 6736.7(11) | 42.7(8) |
| C40 | 5407.6(19) | 8835(4) | 6369.7(13) | 55.7(11) |
| C41 | 5565.8(19) | 8126(4) | 6077.0(12) | 57.1(11) |
| C42 | 5801.4(16) | 6965(3) | 6158.3(10) | 42.2(8) |
| C11 | 3988.3(12) | 1501(3) | 6091.6(9) | 32.1(7) |
| P1 | 3336.9(3) | 2122.1(8) | 5817.9(2) | 30.70(17) |
| O1 | 2857.1(9) | 1221(2) | 5761.3(7) | 41.7(6) |
| O2 | 3221.2(9) | 3339(2) | 6042.2(6) | 34.9(5) |
| C12 | 2661.3(16) | 3961(4) | 5938.4(11) | 50.3(9) |
| C13 | 2619(2) | 5010(4) | 6204.4(13) | 63.6(12) |
| O3A | 3534.5(10) | 2615(2) | 5439.0(6) | 41.2(6) |
| C14A | 3417(2) | 1856(6) | 5096.4(12) | 52.5(15) |
| C15A | 3528(4) | 2649(10) | 4761.6(17) | 58(2) |
| O3B | 3534.5(10) | 2615(2) | 5439.0(6) | 41.2(6) |
| C14B | 3208(5) | 2824(18) | 5068(2) | 52.5(15) |
| C15B | 3639(11) | 3040(40) | 4793(5) | 58(2) |
| C16A | 6660(9) | 2211(8) | 5098(2) | 37.3(15) |
| P2A | 6627(3) | 3323(5) | 4715.4(13) | 50.0(7) |
| O4A | 7015(6) | 4402(11) | 4777(3) | 54.1(13) |

| | | | | |
|---|---|---|---|---|
| O5A | 6805(4) | 2585(8) | 4359(2) | 51.2(12) |
| C17A | 6438(5) | 1528(9) | 4187(3) | 44.6(14) |
| C18A | 6449(7) | 1691(16) | 3756(3) | 64(2) |
| O6A | 5949(5) | 3646(16) | 4616(5) | 73.8(18) |
| C19A | 5704(9) | 4706(17) | 4396(5) | 96(3) |
| C20A | 5688(8) | 4255(18) | 3978(4) | 120(4) |
| C16B | 6498(9) | 2363(12) | 5051(2) | 37.3(15) |
| P2B | 6516(4) | 3383(8) | 4646(2) | 50.0(7) |
| O4B | 6970(10) | 4310(20) | 4699(5) | 54.1(13) |
| O5B | 6637(5) | 2375(15) | 4339(3) | 51.2(12) |
| C17B | 6209(6) | 2163(14) | 3987(4) | 44.6(14) |
| C18B | 6572(11) | 1450(30) | 3730(5) | 64(2) |
| O6B | 5826(6) | 3630(20) | 4563(8) | 73.8(18) |
| C19B | 5444(12) | 4670(20) | 4457(7) | 96(3) |
| C20B | 5190(20) | 5150(40) | 4807(8) | 120(4) |
| C16C | 6648(9) | 1939(8) | 5155(2) | 37.3(15) |
| P2C | 6626.2(17) | 2712(3) | 4702.4(9) | 50.0(7) |
| O4C | 7114(3) | 3560(7) | 4683.0(19) | 54.1(13) |
| O5C | 6569(3) | 1596(7) | 4413.7(18) | 51.2(12) |
| C17C | 6741(4) | 1703(9) | 4037(2) | 44.6(14) |
| C18C | 6211(6) | 2105(14) | 3765(3) | 64(2) |
| O6C | 5978(5) | 3299(15) | 4654(5) | 73.8(18) |
| C19C | 5822(8) | 4576(17) | 4558(6) | 96(3) |
| C20C | 5237(11) | 4920(20) | 4680(7) | 120(4) |
| P3 | 5000 | 1153.9(10) | 7500 | 30.5(2) |
| F31 | 5100.7(10) | 1138.1(19) | 7061.1(6) | 51.2(5) |
| F32 | 4517.8(7) | 2201.1(17) | 7410.1(6) | 39.6(4) |
| F33 | 4518.5(10) | 94.4(19) | 7407.5(8) | 60.4(6) |

| | | | | |
|---|---|---|---|---|
| P4 | 5000 | 0 | 5000 | 32.8(3) |
| F41 | 5601.6(9) | -4.1(17) | 5286.5(6) | 46.3(5) |
| F42 | 4650.7(11) | -91(2) | 5355.5(6) | 58.3(6) |
| F43 | 5026.3(10) | -1481.2(18) | 4980.0(6) | 51.7(6) |

**Table B.4.** Anisotropic Displacement Parameters ($Å^2 \times 10^3$) for **1**. The Anisotropic displacement factor exponent takes the form: $-2\pi^2[h^2a^{*2}U_{11}+2hka^*b^*U_{12}+\ldots]$.

| Atom | $U_{11}$ | $U_{22}$ | $U_{33}$ | $U_{23}$ | $U_{13}$ | $U_{12}$ |
|---|---|---|---|---|---|---|
| Ir1 | 15.49(5) | 22.27(5) | 14.01(4) | -0.77(4) | 1.50(3) | -2.69(4) |
| N1 | 13.6(10) | 27.2(11) | 15.5(10) | -0.3(8) | 1.0(8) | 0.0(8) |
| N2 | 17.2(10) | 26.2(12) | 17(1) | -0.2(8) | 3.6(8) | -4.5(8) |
| N3 | 15.4(10) | 28.1(12) | 15.6(10) | -0.5(8) | 1.0(8) | 0.1(8) |
| N4 | 29.6(13) | 26.1(12) | 26.2(12) | 4.5(10) | 4.4(10) | 1.8(10) |
| C1 | 19.8(13) | 43.9(17) | 20.9(13) | -5.5(12) | 6.7(11) | -0.3(12) |
| C2 | 16.8(13) | 53.1(19) | 26.9(15) | -4.5(13) | 8.6(11) | -5.8(12) |
| C3 | 15.3(12) | 39.8(16) | 22.5(13) | 2.3(11) | 0.6(10) | -5.0(11) |
| C4 | 20.5(13) | 32.3(14) | 16.6(12) | -1.4(10) | 0.6(10) | -6.9(11) |
| C5 | 16.9(12) | 27.7(13) | 13.2(11) | 2.1(9) | 1.5(9) | -1.1(10) |
| C6 | 20.2(13) | 28.0(13) | 15.2(12) | -1.2(10) | 4.7(10) | -5.2(10) |
| C7 | 31.9(16) | 41.4(17) | 24.7(14) | -12.3(12) | 12.3(12) | -16.2(13) |
| C8 | 44.0(19) | 53(2) | 30.6(16) | -14.5(15) | 22.3(15) | -18.0(16) |
| C9 | 33.6(17) | 53(2) | 34.3(17) | -9.3(15) | 20.5(14) | -16.5(15) |
| C10 | 22.8(14) | 37.9(16) | 25.0(14) | -4.1(12) | 7.6(11) | -10.8(12) |
| C21 | 24.1(13) | 36.1(15) | 15.0(12) | -5(1) | 3.9(10) | -12.2(11) |
| C22 | 42.0(18) | 41.3(18) | 19.9(14) | -1.3(12) | 5.2(12) | -18.9(14) |
| C23 | 46(2) | 64(2) | 23.2(15) | -1.8(15) | 5.3(14) | -38.2(18) |
| C24 | 29.5(17) | 86(3) | 24.4(16) | -6.3(17) | 3.6(13) | -34.2(18) |
| C25 | 19.5(13) | 69(2) | 23.5(14) | -3.7(14) | 1.8(11) | -11.4(14) |
| C26 | 18.9(13) | 46.3(18) | 16.3(12) | -5.2(11) | 2.5(10) | -8.9(12) |
| C27 | 16.5(12) | 41.4(16) | 13.8(12) | -3.2(11) | 2.5(9) | 0.6(11) |
| C28 | 18.5(14) | 53(2) | 22.5(14) | -2.5(13) | 0.1(11) | 9.2(13) |
| C29 | 36.7(17) | 43.0(18) | 25.2(15) | 4.5(13) | 5.2(13) | 17.7(14) |
| C30 | 34.5(16) | 31.5(15) | 26.5(15) | 3.1(12) | 4.8(12) | 3.4(12) |

| | | | | | | |
|---|---|---|---|---|---|---|
| C31 | 20.7(13) | 29.7(14) | 20.0(13) | 0.7(10) | 1(1) | -0.8(10) |
| C32 | 19.1(12) | 26.1(14) | 19.4(12) | -4.2(10) | 4.1(9) | -8.7(10) |
| C33 | 24.3(13) | 34.0(14) | 20.2(12) | -2.1(11) | 4.1(10) | -10.6(12) |
| C34 | 31.1(15) | 48.4(19) | 19.6(13) | -4.4(12) | 6.8(11) | -17.3(14) |
| C35 | 30.4(16) | 59(2) | 28.3(16) | -17.2(15) | 13.0(13) | -16.4(15) |
| C36 | 25.5(15) | 35.7(17) | 42.9(18) | -14.7(14) | 11.7(13) | -5.4(12) |
| C37 | 20.6(13) | 31.1(15) | 29.6(15) | -5.7(12) | 5.9(11) | -5.7(11) |
| C38 | 28.9(15) | 25.5(14) | 38.0(17) | -3.0(12) | 8.2(13) | -1.7(11) |
| C39 | 46(2) | 30.9(17) | 52(2) | -1.4(15) | 10.5(17) | 7.1(14) |
| C40 | 63(3) | 34.1(19) | 71(3) | 16.2(19) | 14(2) | 17.7(18) |
| C41 | 73(3) | 50(2) | 50(2) | 25.9(19) | 13(2) | 17(2) |
| C42 | 55(2) | 41.4(19) | 31.8(17) | 11.8(14) | 11.5(15) | 10.1(16) |
| C11 | 21.3(14) | 47.2(18) | 27.7(15) | 1.1(13) | 2.8(11) | -11.1(13) |
| P1 | 17.0(3) | 50.2(5) | 24.7(4) | -4.6(3) | 2.4(3) | -8.8(3) |
| O1 | 19.2(11) | 59.7(15) | 45.4(14) | -12.5(12) | 2.1(9) | -13(1) |
| O2 | 23.8(11) | 48.2(13) | 33.1(12) | -3.8(10) | 5.5(9) | -6.6(9) |
| C12 | 38(2) | 72(3) | 40(2) | -6.8(18) | 3.2(16) | 9.2(18) |
| C13 | 78(3) | 53(3) | 61(3) | -3(2) | 13(2) | 13(2) |
| O3A | 39.7(13) | 62.4(16) | 20.9(11) | 0.1(10) | 2.7(9) | -5.0(11) |
| C14A | 47(3) | 92(4) | 18.0(19) | -10(2) | 3.9(19) | -4(3) |
| C15A | 34(4) | 114(9) | 24(2) | 5(3) | -3(2) | -10(3) |
| O3B | 39.7(13) | 62.4(16) | 20.9(11) | 0.1(10) | 2.7(9) | -5.0(11) |
| C14B | 47(3) | 92(4) | 18.0(19) | -10(2) | 3.9(19) | -4(3) |
| C15B | 34(4) | 114(9) | 24(2) | 5(3) | -3(2) | -10(3) |
| C16A | 40(4) | 50(4) | 27(2) | -12(2) | 21(3) | -12(4) |
| P2A | 71.5(15) | 58.5(14) | 25.5(10) | -18.9(14) | 24.9(10) | -16.0(16) |
| O4A | 89(3) | 44(2) | 37(3) | -9(2) | 35(3) | -17(2) |
| O5A | 67(3) | 59(3) | 33.7(18) | -23(2) | 27(2) | -34(2) |

| | | | | | | |
|---|---|---|---|---|---|---|
| C17A | 56(4) | 48(3) | 31(3) | -7(3) | 8(2) | -3(3) |
| C18A | 84(8) | 76(8) | 30(3) | -22(3) | 3(4) | 23(4) |
| O6A | 100(3) | 71(5) | 54(4) | 24(4) | 24(3) | 16(3) |
| C19A | 110(8) | 79(5) | 100(8) | 61(6) | 20(8) | 1(5) |
| C20A | 123(8) | 122(10) | 109(8) | 42(8) | 1(7) | 41(7) |
| C16B | 40(4) | 50(4) | 27(2) | -12(2) | 21(3) | -12(4) |
| P2B | 71.5(15) | 58.5(14) | 25.5(10) | -18.9(14) | 24.9(10) | -16.0(16) |
| O4B | 89(3) | 44(2) | 37(3) | -9(2) | 35(3) | -17(2) |
| O5B | 67(3) | 59(3) | 33.7(18) | -23(2) | 27(2) | -34(2) |
| C17B | 56(4) | 48(3) | 31(3) | -7(3) | 8(2) | -3(3) |
| C18B | 84(8) | 76(8) | 30(3) | -22(3) | 3(4) | 23(4) |
| O6B | 100(3) | 71(5) | 54(4) | 24(4) | 24(3) | 16(3) |
| C19B | 110(8) | 79(5) | 100(8) | 61(6) | 20(8) | 1(5) |
| C20B | 123(8) | 122(10) | 109(8) | 42(8) | 1(7) | 41(7) |
| C16C | 40(4) | 50(4) | 27(2) | -12(2) | 21(3) | -12(4) |
| P2C | 71.5(15) | 58.5(14) | 25.5(10) | -18.9(14) | 24.9(10) | -16.0(16) |
| O4C | 89(3) | 44(2) | 37(3) | -9(2) | 35(3) | -17(2) |
| O5C | 67(3) | 59(3) | 33.7(18) | -23(2) | 27(2) | -34(2) |
| C17C | 56(4) | 48(3) | 31(3) | -7(3) | 8(2) | -3(3) |
| C18C | 84(8) | 76(8) | 30(3) | -22(3) | 3(4) | 23(4) |
| O6C | 100(3) | 71(5) | 54(4) | 24(4) | 24(3) | 16(3) |
| C19C | 110(8) | 79(5) | 100(8) | 61(6) | 20(8) | 1(5) |
| C20C | 123(8) | 122(10) | 109(8) | 42(8) | 1(7) | 41(7) |
| P3 | 25.5(5) | 19.7(5) | 47.4(7) | 0 | 9.0(5) | 0 |
| F31 | 67.0(15) | 39.6(11) | 50.0(13) | -6.9(9) | 18.9(11) | 4.5(10) |
| F32 | 22.6(9) | 32.7(10) | 62.5(13) | -4.7(9) | 3.0(8) | 3.6(7) |
| F33 | 58.4(14) | 34.2(11) | 87.4(18) | -4.7(11) | 6.6(13) | -22.2(10) |
| P4 | 42.4(6) | 24.2(6) | 26.9(5) | -1.8(4) | -11.1(5) | -4.2(4) |

| | | | | | | |
|---|---|---|---|---|---|---|
| F41 | 48.6(12) | 36.0(11) | 45.8(11) | -0.9(8) | -21.6(9) | -4.9(9) |
| F42 | 64.3(15) | 68.4(16) | 42.1(12) | 8.7(11) | 7.4(11) | 5.5(12) |
| F43 | 61.2(14) | 24.4(10) | 60.4(13) | -3.6(9) | -21.7(11) | -3.4(9) |

**Table B.5.** Bond Lengths for **1**.

| Atom | Atom | Length/Å | Atom | Atom | Length/Å |
|---|---|---|---|---|---|
| Ir1 | N1 | 2.136(2) | C41 | C42 | 1.376(5) |
| Ir1 | N2 | 2.135(2) | C11 | P1 | 1.799(3) |
| Ir1 | N3 | 2.050(2) | P1 | O1 | 1.466(2) |
| Ir1 | N4 | 2.043(2) | P1 | O2 | 1.573(2) |
| Ir1 | C21 | 2.010(3) | P1 | O3A | 1.571(2) |
| Ir1 | C32 | 2.010(3) | O2 | C12 | 1.458(4) |
| N1 | C1 | 1.345(3) | C12 | C13 | 1.482(5) |
| N1 | C5 | 1.357(3) | O3A | C14A | 1.454(5) |
| N2 | C6 | 1.348(3) | C14A | C15A | 1.513(8) |
| N2 | C10 | 1.348(3) | O3B | C14B | 1.436(8) |
| N3 | C27 | 1.366(3) | C14B | C15B | 1.510(11) |
| N3 | C31 | 1.345(3) | C16A | P2A | 1.800(6) |
| N4 | C38 | 1.363(4) | P2A | O4A | 1.464(7) |
| N4 | C42 | 1.352(4) | P2A | O5A | 1.596(6) |
| C1 | C2 | 1.376(4) | P2A | O6A | 1.597(9) |
| C2 | C3 | 1.387(4) | O5A | C17A | 1.494(9) |
| C3 | C4 | 1.390(4) | C17A | C18A | 1.540(10) |
| C3 | C11 | 1.506(4) | O6A | C19A | 1.449(10) |
| C4 | C5 | 1.389(4) | C19A | C20A | 1.552(15) |
| C5 | C6 | 1.482(3) | C16B | P2B | 1.809(7) |
| C6 | C7 | 1.386(4) | P2B | O4B | 1.441(9) |
| C7 | C8 | 1.393(4) | P2B | O5B | 1.589(9) |
| C8 | C9 | 1.383(4) | P2B | O6B | 1.605(10) |
| C8 | C16A | 1.531(7) | O5B | C17B | 1.492(11) |
| C8 | C16B | 1.530(8) | C17B | C18B | 1.535(12) |
| C8 | C16C | 1.531(7) | O6B | C19B | 1.441(12) |

| | | | | | |
|---|---|---|---|---|---|
| C9 | C10 | 1.376(4) | C19B | C20B | 1.533(15) |
| C21 | C22 | 1.399(4) | C16C | P2C | 1.799(7) |
| C21 | C26 | 1.412(4) | P2C | O4C | 1.462(7) |
| C22 | C23 | 1.386(4) | P2C | O5C | 1.569(6) |
| C23 | C24 | 1.374(6) | P2C | O6C | 1.615(8) |
| C24 | C25 | 1.383(5) | O5C | C17C | 1.450(8) |
| C25 | C26 | 1.397(4) | C17C | C18C | 1.510(10) |
| C26 | C27 | 1.461(4) | O6C | C19C | 1.447(11) |
| C27 | C28 | 1.395(4) | C19C | C20C | 1.524(14) |
| C28 | C29 | 1.367(5) | P3 | $F31^{1}$ | 1.605(2) |
| C29 | C30 | 1.389(4) | P3 | F31 | 1.605(2) |
| C30 | C31 | 1.372(4) | P3 | $F32^{1}$ | 1.5851(19) |
| C32 | C33 | 1.398(4) | P3 | F32 | 1.5851(19) |
| C32 | C37 | 1.406(4) | P3 | $F33^{1}$ | 1.594(2) |
| C33 | C34 | 1.392(4) | P3 | F33 | 1.594(2) |
| C34 | C35 | 1.373(5) | P4 | $F41^{2}$ | 1.5995(18) |
| C35 | C36 | 1.381(5) | P4 | F41 | 1.5996(18) |
| C36 | C37 | 1.404(4) | P4 | F42 | 1.596(2) |
| C37 | C38 | 1.461(4) | P4 | $F42^{2}$ | 1.596(2) |
| C38 | C39 | 1.394(4) | P4 | $F43^{2}$ | 1.595(2) |
| C39 | C40 | 1.378(5) | P4 | F43 | 1.595(2) |
| C40 | C41 | 1.378(6) | | | |

$^{1}$1-X,+Y,3/2-Z; $^{2}$1-X,-Y,1-Z

**Table B.6.** Bond Angles for **1**.

| Atom | Atom | Atom | Angle/° | Atom | Atom | Atom | Angle/° |
|---|---|---|---|---|---|---|---|
| N2 | Ir1 | N1 | 76.32(8) | C40 | C39 | C38 | 119.7(3) |
| N3 | Ir1 | N1 | 93.92(8) | C39 | C40 | C41 | 119.7(3) |
| N3 | Ir1 | N2 | 86.80(8) | C42 | C41 | C40 | 119.0(4) |
| N4 | Ir1 | N1 | 91.39(9) | N4 | C42 | C41 | 121.8(3) |
| N4 | Ir1 | N2 | 98.16(9) | C3 | C11 | P1 | 118.0(2) |
| N4 | Ir1 | N3 | 173.47(9) | O1 | P1 | C11 | 112.84(15) |
| C21 | Ir1 | N1 | 171.13(10) | O1 | P1 | O2 | 115.88(13) |
| C21 | Ir1 | N2 | 96.29(9) | O1 | P1 | O3A | 114.56(14) |
| C21 | Ir1 | N3 | 80.62(11) | O2 | P1 | C11 | 103.16(14) |
| C21 | Ir1 | N4 | 94.56(11) | O3A | P1 | C11 | 105.04(13) |
| C21 | Ir1 | C32 | 87.53(10) | O3A | P1 | O2 | 104.08(13) |
| C32 | Ir1 | N1 | 99.95(9) | C12 | O2 | P1 | 117.7(2) |
| C32 | Ir1 | N2 | 176.07(9) | O2 | C12 | C13 | 109.1(3) |
| C32 | Ir1 | N3 | 94.76(10) | C14A | O3A | P1 | 118.7(3) |
| C32 | Ir1 | N4 | 80.57(10) | O3A | C14A | C15A | 107.7(5) |
| C1 | N1 | Ir1 | 125.71(18) | O3B | C14B | C15B | 107.7(13) |
| C1 | N1 | C5 | 118.1(2) | C8 | C16A | P2A | 108.2(5) |
| C5 | N1 | Ir1 | 116.04(16) | O4A | P2A | C16A | 117.1(8) |
| C6 | N2 | Ir1 | 115.49(16) | O4A | P2A | O5A | 106.8(5) |
| C10 | N2 | Ir1 | 124.94(18) | O4A | P2A | O6A | 115.0(9) |
| C10 | N2 | C6 | 118.9(2) | O5A | P2A | C16A | 106.1(5) |
| C27 | N3 | Ir1 | 115.57(18) | O5A | P2A | O6A | 107.0(8) |
| C31 | N3 | Ir1 | 125.00(18) | O6A | P2A | C16A | 104.0(8) |
| C31 | N3 | C27 | 119.4(2) | C17A | O5A | P2A | 120.2(6) |
| C38 | N4 | Ir1 | 115.61(19) | O5A | C17A | C18A | 103.1(8) |
| C42 | N4 | Ir1 | 124.7(2) | C19A | O6A | P2A | 125.8(12) |

| | | | | | | | |
|---|---|---|---|---|---|---|---|
| C42 | N4 | C38 | 119.7(3) | O6A | C19A | C20A | 102.7(13) |
| N1 | C1 | C2 | 122.4(3) | C8 | C16B | P2B | 120.8(8) |
| C1 | C2 | C3 | 120.3(3) | O4B | P2B | C16B | 114.6(10) |
| C2 | C3 | C4 | 117.3(3) | O4B | P2B | O5B | 111.2(9) |
| C2 | C3 | C11 | 121.0(2) | O4B | P2B | O6B | 126.7(13) |
| C4 | C3 | C11 | 121.6(3) | O5B | P2B | C16B | 99.0(7) |
| C5 | C4 | C3 | 120.0(2) | O5B | P2B | O6B | 105.0(11) |
| N1 | C5 | C4 | 121.7(2) | O6B | P2B | C16B | 96.3(9) |
| N1 | C5 | C6 | 114.7(2) | C17B | O5B | P2B | 120.9(11) |
| C4 | C5 | C6 | 123.6(2) | O5B | C17B | C18B | 102.5(10) |
| N2 | C6 | C5 | 115.9(2) | C19B | O6B | P2B | 137.3(19) |
| N2 | C6 | C7 | 121.2(2) | O6B | C19B | C20B | 110.0(17) |
| C7 | C6 | C5 | 123.0(2) | C8 | C16C | P2C | 109.0(5) |
| C6 | C7 | C8 | 119.9(3) | O4C | P2C | C16C | 114.1(7) |
| C7 | C8 | C16A | 124.9(8) | O4C | P2C | O5C | 116.0(4) |
| C7 | C8 | C16B | 115.5(8) | O4C | P2C | O6C | 117.7(7) |
| C7 | C8 | C16C | 117.0(7) | O5C | P2C | C16C | 102.5(4) |
| C9 | C8 | C7 | 117.9(3) | O5C | P2C | O6C | 103.9(8) |
| C9 | C8 | C16A | 117.2(8) | O6C | P2C | C16C | 100.4(7) |
| C9 | C8 | C16B | 124.1(7) | C17C | O5C | P2C | 122.0(6) |
| C9 | C8 | C16C | 124.2(8) | O5C | C17C | C18C | 107.6(8) |
| C10 | C9 | C8 | 119.7(3) | C19C | O6C | P2C | 126.3(11) |
| N2 | C10 | C9 | 122.2(3) | O6C | C19C | C20C | 111.4(11) |
| C22 | C21 | Ir1 | 128.4(2) | F31 | P3 | $F31^{1}$ | 178.79(17) |
| C22 | C21 | C26 | 117.4(3) | F32 | P3 | F31 | 90.61(11) |
| C26 | C21 | Ir1 | 114.1(2) | F32 | P3 | $F31^{1}$ | 90.25(11) |
| C23 | C22 | C21 | 120.7(3) | $F32^{1}$ | P3 | $F31^{1}$ | 90.62(11) |

| | | | | | | | |
|---|---|---|---|---|---|---|---|
| C24 | C23 | C22 | 121.2(3) | $F32^{1}$ | P3 | F31 | 90.24(11) |
| C23 | C24 | C25 | 119.7(3) | $F32^{1}$ | P3 | F32 | 89.51(14) |
| C24 | C25 | C26 | 119.8(3) | $F32^{1}$ | P3 | F33 | 179.51(14) |
| C21 | C26 | C27 | 115.6(2) | F32 | P3 | F33 | 90.84(11) |
| C25 | C26 | C21 | 121.1(3) | F32 | P3 | $F33^{1}$ | 179.51(14) |
| C25 | C26 | C27 | 123.3(3) | $F32^{1}$ | P3 | $F33^{1}$ | 90.84(11) |
| N3 | C27 | C26 | 113.9(2) | $F33^{1}$ | P3 | $F31^{1}$ | 89.40(13) |
| N3 | C27 | C28 | 119.5(3) | F33 | P3 | F31 | 89.40(13) |
| C28 | C27 | C26 | 126.5(3) | $F33^{1}$ | P3 | F31 | 89.73(13) |
| C29 | C28 | C27 | 120.6(3) | F33 | P3 | $F31^{1}$ | 89.74(13) |
| C28 | C29 | C30 | 119.2(3) | $F33^{1}$ | P3 | F33 | 88.82(19) |
| C31 | C30 | C29 | 118.7(3) | $F41^{2}$ | P4 | F41 | 180.00(13) |
| N3 | C31 | C30 | 122.5(3) | $F42^{2}$ | P4 | F41 | 90.31(12) |
| C33 | C32 | Ir1 | 128.5(2) | $F42^{2}$ | P4 | $F41^{2}$ | 89.69(12) |
| C33 | C32 | C37 | 117.2(2) | F42 | P4 | F41 | 89.70(12) |
| C37 | C32 | Ir1 | 114.3(2) | F42 | P4 | $F41^{2}$ | 90.30(12) |
| C34 | C33 | C32 | 121.2(3) | F42 | P4 | $F42^{2}$ | 180.0 |
| C35 | C34 | C33 | 120.8(3) | F43 | P4 | F41 | 89.43(10) |
| C34 | C35 | C36 | 119.8(3) | $F43^{2}$ | P4 | F41 | 90.57(10) |
| C35 | C36 | C37 | 119.8(3) | F43 | P4 | $F41^{2}$ | 90.57(10) |
| C32 | C37 | C38 | 115.4(2) | $F43^{2}$ | P4 | $F41^{2}$ | 89.43(10) |
| C36 | C37 | C32 | 121.2(3) | $F43^{2}$ | P4 | F42 | 89.93(12) |
| C36 | C37 | C38 | 123.5(3) | F43 | P4 | $F42^{2}$ | 89.93(12) |
| N4 | C38 | C37 | 114.1(3) | F43 | P4 | F42 | 90.06(12) |
| N4 | C38 | C39 | 120.0(3) | $F43^{2}$ | P4 | $F42^{2}$ | 90.07(12) |

| | | | | | | | |
|---|---|---|---|---|---|---|---|
| C39 | C38 | C37 | 125.9(3) | | $F43^2$ | P4 | F43 | 180.0 |

$^1$1-X,+Y,3/2-Z; $^2$1-X,-Y,1-Z

**Table B.7.** Hydrogen Atom Coordinates ($Å \times 10^4$) and Isotropic Displacement Parameters ($Å^2 \times 10^3$) for **1**.

| Atom | *x* | *y* | *z* | U(eq) |
|---|---|---|---|---|
| H1 | 4993.31 | 4289.64 | 6891.22 | 33 |
| H2 | 4187.6 | 3082.36 | 6680.81 | 38 |
| H4 | 4953.82 | 2022.02 | 5779.31 | 28 |
| H7 | 5737.82 | 2123.59 | 5518.81 | 38 |
| H9 | 7245.85 | 3985.17 | 5488.77 | 46 |
| H10 | 7104.84 | 4998.33 | 6044.19 | 34 |
| H22 | 6981.37 | 7357.37 | 6687.99 | 41 |
| H23 | 7962.17 | 7860.95 | 6840.91 | 53 |
| H24 | 8650.92 | 6350.01 | 7045.12 | 56 |
| H25 | 8358.57 | 4289.64 | 7108.48 | 45 |
| H28 | 8001.5 | 2375.55 | 7190.18 | 38 |
| H29 | 7549.7 | 470.82 | 7241.45 | 42 |
| H30 | 6532.67 | 312.17 | 7065.83 | 37 |
| H31 | 6009.68 | 2053.45 | 6835.51 | 28 |
| H33 | 6387.13 | 3984.48 | 7545.61 | 31 |
| H34 | 6176.89 | 4909.63 | 8104.16 | 39 |
| H35 | 5748.51 | 6862.01 | 8090.32 | 46 |
| H36 | 5542.72 | 7936.95 | 7513.93 | 41 |
| H39 | 5378.77 | 8856.24 | 6939.59 | 51 |
| H40 | 5244.01 | 9638.26 | 6318.65 | 67 |
| H41 | 5512.84 | 8434.69 | 5822.9 | 69 |
| H42 | 5909.64 | 6475.02 | 5956.59 | 51 |
| H11A | 3877.74 | 1115.98 | 6324.83 | 39 |
| H11B | 4133.91 | 825.42 | 5940.4 | 39 |
| H12A | 2339.21 | 3365.42 | 5952.73 | 60 |

| | | | | |
|---|---|---|---|---|
| H12B | 2627.7 | 4275.32 | 5673.28 | 60 |
| H13A | 2651.99 | 4693.1 | 6466.17 | 95 |
| H13B | 2242.36 | 5428.5 | 6137.05 | 95 |
| H13C | 2935.36 | 5602.75 | 6185.99 | 95 |
| H14A | 3006.27 | 1567.65 | 5059.9 | 63 |
| H14B | 3674.73 | 1117.63 | 5118.95 | 63 |
| H15A | 3261.77 | 3362.28 | 4736.96 | 87 |
| H15B | 3462.87 | 2152.2 | 4527.28 | 87 |
| H15C | 3932.35 | 2946.97 | 4803.84 | 87 |
| H14C | 2950.75 | 3557.37 | 5073.05 | 63 |
| H14D | 2961.64 | 2090.95 | 4986.73 | 63 |
| H15D | 3838.63 | 3837.06 | 4852.57 | 87 |
| H15E | 3430.99 | 3064.98 | 4531.35 | 87 |
| H15F | 3925.8 | 2367.07 | 4816.9 | 87 |
| H16A | 6371.29 | 1539.72 | 5027.71 | 45 |
| H16B | 7053.07 | 1833.39 | 5147.79 | 45 |
| H17A | 6035.31 | 1587.02 | 4247.54 | 54 |
| H17B | 6607.64 | 717.61 | 4277.79 | 54 |
| H18A | 6472.67 | 2578.27 | 3696.22 | 96 |
| H18B | 6091.69 | 1340.25 | 3612.83 | 96 |
| H18C | 6788.91 | 1258.39 | 3683.7 | 96 |
| H19A | 5955.1 | 5450.31 | 4447.91 | 115 |
| H19B | 5307.63 | 4901.74 | 4451.51 | 115 |
| H20A | 6084.77 | 4251.6 | 3912.63 | 180 |
| H20B | 5442.84 | 4817.66 | 3805.39 | 180 |
| H20C | 5526.2 | 3412.2 | 3952.29 | 180 |
| H16C | 6136.31 | 1864.29 | 4998.14 | 45 |
| H16D | 6828.59 | 1775.58 | 5056.51 | 45 |

| | | | | |
|---|---|---|---|---|
| H17C | 6065.04 | 2960.53 | 3868.84 | 54 |
| H17D | 5872.16 | 1663.88 | 4043.22 | 54 |
| H18D | 6841.52 | 884.67 | 3886.52 | 96 |
| H18E | 6795.15 | 2036.36 | 3597.27 | 96 |
| H18F | 6312.06 | 961.74 | 3542.27 | 96 |
| H19C | 5123.17 | 4411.91 | 4256.95 | 115 |
| H19D | 5663.73 | 5347.82 | 4352.77 | 115 |
| H20D | 4828.4 | 4696.79 | 4829.05 | 180 |
| H20E | 5106.56 | 6038.01 | 4777.66 | 180 |
| H20F | 5472.43 | 5008.54 | 5037.31 | 180 |
| H16E | 6351.67 | 1268.94 | 5134.1 | 45 |
| H16F | 7036.74 | 1559.99 | 5231.67 | 45 |
| H17E | 6885.63 | 892.89 | 3956.51 | 54 |
| H17F | 7057.24 | 2324.99 | 4040.38 | 54 |
| H18G | 5896.44 | 1499.83 | 3771.78 | 96 |
| H18H | 6310.09 | 2152.55 | 3505.73 | 96 |
| H18I | 6082.53 | 2924.59 | 3841.29 | 96 |
| H19E | 5800.3 | 4696.21 | 4279.49 | 115 |
| H19F | 6128.66 | 5135.62 | 4687.17 | 115 |
| H20G | 4927.38 | 4416.96 | 4534.82 | 180 |
| H20H | 5157.62 | 5802.33 | 4628.76 | 180 |
| H20I | 5250.54 | 4754.41 | 4952.97 | 180 |

**Table B.8.** Atomic Occupancy for **1**.

| Atom | *Occupancy* | Atom | *Occupancy* | Atom | *Occupancy* |
|---|---|---|---|---|---|
| O3A | 0.730(7) | C14A | 0.730(7) | H14A | 0.730(7) |
| H14B | 0.730(7) | C15A | 0.730(7) | H15A | 0.730(7) |
| H15B | 0.730(7) | H15C | 0.730(7) | O3B | 0.270(7) |
| C14B | 0.270(7) | H14C | 0.270(7) | H14D | 0.270(7) |
| C15B | 0.270(7) | H15D | 0.270(7) | H15E | 0.270(7) |
| H15F | 0.270(7) | C16A | 0.379(3) | H16A | 0.379(3) |
| H16B | 0.379(3) | P2A | 0.379(3) | O4A | 0.379(3) |
| O5A | 0.379(3) | C17A | 0.379(3) | H17A | 0.379(3) |
| H17B | 0.379(3) | C18A | 0.379(3) | H18A | 0.379(3) |
| H18B | 0.379(3) | H18C | 0.379(3) | O6A | 0.379(3) |
| C19A | 0.379(3) | H19A | 0.379(3) | H19B | 0.379(3) |
| C20A | 0.379(3) | H20A | 0.379(3) | H20B | 0.379(3) |
| H20C | 0.379(3) | C16B | 0.245(3) | H16C | 0.245(3) |
| H16D | 0.245(3) | P2B | 0.245(3) | O4B | 0.245(3) |
| O5B | 0.245(3) | C17B | 0.245(3) | H17C | 0.245(3) |
| H17D | 0.245(3) | C18B | 0.245(3) | H18D | 0.245(3) |
| H18E | 0.245(3) | H18F | 0.245(3) | O6B | 0.245(3) |
| C19B | 0.245(3) | H19C | 0.245(3) | H19D | 0.245(3) |
| C20B | 0.245(3) | H20D | 0.245(3) | H20E | 0.245(3) |
| H20F | 0.245(3) | C16C | 0.3760(19) | H16E | 0.3760(19) |
| H16F | 0.3760(19) | P2C | 0.3760(19) | O4C | 0.3760(19) |
| O5C | 0.3760(19) | C17C | 0.3760(19) | H17E | 0.3760(19) |
| H17F | 0.3760(19) | C18C | 0.3760(19) | H18G | 0.3760(19) |
| H18H | 0.3760(19) | H18I | 0.3760(19) | O6C | 0.3760(19) |
| C19C | 0.3760(19) | H19E | 0.3760(19) | H19F | 0.3760(19) |
| C20C | 0.3760(19) | H20G | 0.3760(19) | H20H | 0.3760(19) |
| H20I | 0.3760(19) | | | | |

**Crystal Data** for $C_{42}H_{46}F_6IrN_4O_6P_3$ ($M$ =1101.94 g/mol): monoclinic, space group C2/c (no. 15), $a$ = 23.1647(9) Å, $b$ = 10.7494(4) Å, $c$ = 35.4089(13) Å, $\beta$ = 98.3820(10)°, $V$ = 8722.9(6) Å$^3$, $Z$ = 8, $T$ = 100(2) K, μ(MoKα) = 3.249 mm$^{-1}$, $Dcalc$ = 1.678 g/cm$^3$, 188483 reflections measured (4.274° ≤ 2Θ ≤ 60.252°), 12826 unique ($R_{int}$ = 0.0530, $R_{sigma}$ = 0.0267) which were used in all calculations. The final $R_1$ was 0.0299 (I > 2σ(I)) and $wR_2$ was 0.0604 (all data).

**Computed Structure 2**

| | | | |
|---|---|---|---|
| 1.Ir | -4.121444 | -1.690625 | -2.081082 |
| 2.C | -1.570381 | -1.943202 | -3.519170 |
| 3.C | -1.227629 | -1.670037 | -1.205657 |
| 4.C | -0.185843 | -2.019278 | -3.709916 |
| 5.C | 0.147785 | -1.743176 | -1.353239 |
| 6.H | -1.707718 | -1.529855 | -0.222686 |
| 7.C | 0.678736 | -1.921795 | -2.631456 |
| 8.H | 0.202793 | -2.159076 | -4.730737 |
| 9.H | 0.791462 | -1.657949 | -0.464585 |
| 10.H | 1.768459 | -1.984588 | -2.783573 |
| 11.C | -2.571318 | -2.037358 | -4.572427 |
| 12.C | -2.249474 | -2.204905 | -5.928150 |
| 13.C | -3.916228 | -1.938120 | -4.139560 |
| 14.C | -3.264270 | -2.276326 | -6.874723 |
| 15.H | -1.197809 | -2.280163 | -6.255140 |
| 16.C | -4.915955 | -2.014407 | -5.116841 |
| 17.C | -4.598537 | -2.181523 | -6.467066 |
| 18.H | -3.018120 | -2.407028 | -7.940557 |
| 19.H | -5.980924 | -1.938868 | -4.826068 |
| 20.H | -5.404259 | -2.239874 | -7.218781 |
| 21.C | -6.964347 | -0.733308 | -2.222868 |
| 22.C | -6.671966 | -3.028827 | -1.899559 |
| 23.C | -8.338588 | -0.869885 | -2.232938 |
| 24.H | -6.480627 | 0.249089 | -2.339111 |
| 25.C | -8.054184 | -3.216924 | -1.895026 |
| 26.C | -8.915743 | -2.140107 | -2.071965 |
| 27.H | -8.983466 | 0.021275 | -2.323143 |
| 28.H | -8.462878 | -4.231063 | -1.754975 |
| 29.C | -5.689799 | -4.090044 | -1.745487 |
| 30.C | -5.996297 | -5.436094 | -1.544817 |
| 31.C | -4.984012 | -6.380726 | -1.418152 |
| 32.H | -7.051553 | -5.749172 | -1.486403 |
| 33.C | -3.405599 | -4.579178 | -1.684356 |
| 34.C | -3.658677 | -5.922056 | -1.486977 |
| 35.H | -2.377886 | -4.187943 | -1.741329 |
| 36.H | -2.822219 | -6.627057 | -1.343032 |

| | | | |
|---|---|---|---|
| 37.C | -3.928761 | 1.026612 | -0.976129 |
| 38.C | -3.952990 | 1.058442 | -3.330449 |
| 39.C | -3.837114 | 2.423362 | -0.963677 |
| 40.C | -3.864918 | 2.440642 | -3.359551 |
| 41.H | -4.000449 | 0.451761 | -4.250227 |
| 42.C | -3.805752 | 3.136506 | -2.151238 |
| 43.H | -3.791138 | 2.944240 | 0.005422 |
| 44.H | -3.840452 | 2.960302 | -4.329422 |
| 45.H | -3.734208 | 4.236214 | -2.138964 |
| 46.C | -3.973717 | 0.175744 | 0.204496 |
| 47.C | -3.916910 | 0.674078 | 1.515233 |
| 48.C | -4.070953 | -1.213699 | -0.053787 |
| 49.C | -3.957800 | -0.205334 | 2.590314 |
| 50.H | -3.838337 | 1.758595 | 1.705476 |
| 51.C | -4.113973 | -2.074033 | 1.050021 |
| 52.C | -4.058738 | -1.580174 | 2.355821 |
| 53.H | -3.911197 | 0.179514 | 3.621571 |
| 54.H | -4.188667 | -3.167426 | 0.897699 |
| 55.H | -4.093793 | -2.278014 | 3.209861 |
| 56.C | -5.282436 | -7.831114 | -1.209491 |
| 57.C | -10.400728 | -2.318037 | -2.089382 |
| 58.H | -4.860166 | -8.446091 | -2.035995 |
| 59.H | -6.373224 | -8.033075 | -1.164323 |
| 60.H | -10.697272 | -3.372213 | -1.905653 |
| 61.H | -10.825709 | -2.016384 | -3.073385 |
| 62.N | -6.131180 | -1.785384 | -2.068094 |
| 63.N | -4.392636 | -3.665959 | -1.814073 |
| 64.N | -3.990186 | 0.361485 | -2.174578 |
| 65.N | -2.072632 | -1.772822 | -2.253844 |
| 66.P | -11.231327 | -1.255145 | -0.874768 |
| 67.P | -4.502211 | -8.474917 | 0.297679 |
| 68.O | -4.968864 | -10.016039 | 0.353266 |
| 69.O | -5.410410 | -7.749975 | 1.408535 |
| 70.O | -10.774114 | -1.975996 | 0.487065 |
| 71.O | -12.786537 | -1.643472 | -1.030946 |
| 72.O | -10.947002 | 0.197300 | -0.996397 |
| 73.O | -3.033257 | -8.277961 | 0.386230 |
| 74.H | -13.310096 | -0.838291 | -1.262163 |
| 75.H | -10.901692 | -1.388350 | 1.271027 |
| 76.H | -5.021221 | -7.833187 | 2.312804 |
| 77.H | -4.175447 | -10.604447 | 0.332255 |

**Computed TD-DFT transitions**

| E/eV | f | mu (x,y,z) | | |
|---|---|---|---|---|
| 2.5653 | 0.65330E-02 | -0.23240 | -0.22135 | 0.30727E-01 |
| 2.6842 | 0.56741E-02 | 0.10580 | -0.17918 | -0.20733 |
| 2.7107 | 0.12083E-02 | -0.42312E-01 | 0.11709 | -0.51915E-01 |
| 2.7186 | 0.29882E-02 | 0.17255 | -0.96787E-01 | 0.75663E-01 |
| 2.7913 | 0.16463E-01 | 0.38763 | -0.22670 | 0.19771 |
| 2.8088 | 0.31164E-01 | -0.42868 | -0.50913 | 0.99463E-01 |
| 2.8522 | 0.68156E-03 | -0.70663E-01 | -0.67735E-01 | 0.13133E-01 |
| 2.8700 | 0.19332E-01 | -0.32313 | 0.30695 | -0.27625 |
| 2.9092 | 0.16058E-01 | 0.33575 | 0.32849 | -0.68312E-01 |
| 2.9793 | 0.15259E-02 | -0.74838E-01 | 0.10367 | -0.67510E-01 |
| 3.1011 | 0.96407E-01 | -0.55354 | 0.94085 | -0.27809 |
| 3.1027 | 0.69019E-01 | 0.87769 | 0.37048 | -0.19395E-01 |
| 3.1619 | 0.36529E-01 | 0.54878 | 0.41164 | -0.30736E-01 |
| 3.1781 | 0.67274E-02 | 0.16785 | -0.24068 | 0.17273E-01 |
| 3.1982 | 0.41014E-01 | 0.40784 | 0.57711 | -0.15507 |
| 3.2096 | 0.41319E-01 | -0.51337 | 0.38533 | -0.33680 |
| 3.2744 | 0.28797E-02 | -0.14909 | -0.11639 | 0.11141E-01 |
| 3.3181 | 0.98544E-01 | -0.36278 | 0.49150 | 0.91600 |

**B.2 References**


1. APEX3 Version 2016.5-0 and SAINT+ Version 8.38A. Bruker AXS, I., Madison, Wisconsin, USA, 2016.

2. Krause, L.; Herbst-Irmer, R.; Sheldrick, G. M.; Stalke, D., Comparison of silver and molybdenum microfocus X-ray sources for single-crystal structure determination. *J. Appl. Crystallogr.* **2015,** *48* (1), 3-10.

3. Sheldrick, G., SHELXT - Integrated space-group and crystal-structure determination. *Acta Crystallogr., Sect. A: Found. Crystallogr.* **2015,** *71* (1), 3-8.

4. Sheldrick, G., Crystal structure refinement with SHELXL. *Acta Crystallogr., Sect. C: Cryst. Struct. Commun.* **2015,** *71* (1), 3-8.

5. Dolomanov, O. V.; Bourhis, L. J.; Gildea, R. J.; Howard, J. A. K.; Puschmann, H., OLEX2: a complete structure solution, refinement and analysis program. *J. Appl. Crystallogr*. **2009,** *42* (2), 339-341.

# APPENDIX C

# PERMISSION TO REPRINT

**Permission to reprint chapter 3.**

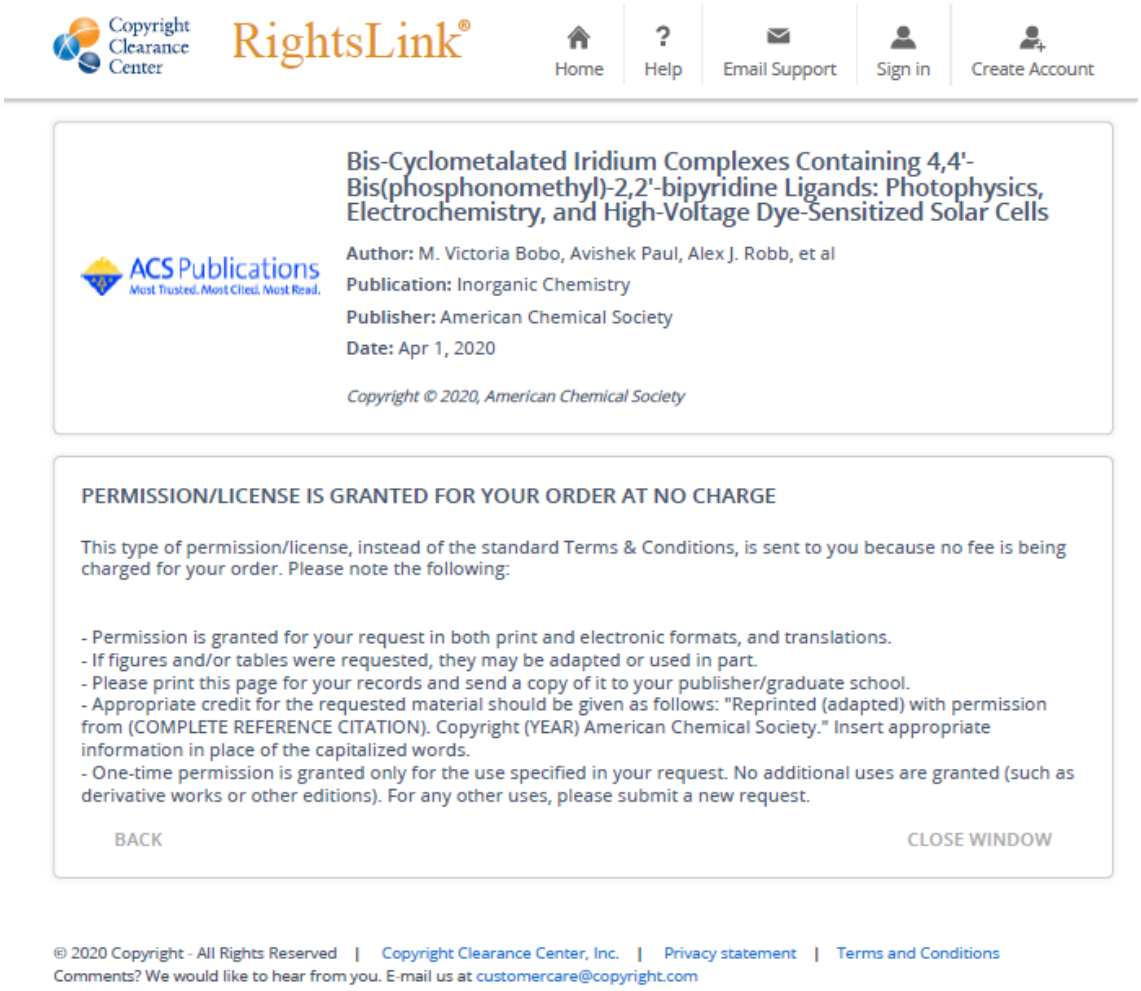

Copyright Clearance Center RightsLink®

Home | Help | Email Support | Sign in | Create Account

Bis-Cyclometalated Iridium Complexes Containing 4,4'-Bis(phosphonomethyl)-2,2'-bipyridine Ligands: Photophysics, Electrochemistry, and High-Voltage Dye-Sensitized Solar Cells

ACS Publications
Most Trusted. Most Cited. Most Read.

**Author:** M. Victoria Bobo, Avishek Paul, Alex J. Robb, et al
**Publication:** Inorganic Chemistry
**Publisher:** American Chemical Society
**Date:** Apr 1, 2020

*Copyright © 2020, American Chemical Society*

PERMISSION/LICENSE IS GRANTED FOR YOUR ORDER AT NO CHARGE

This type of permission/license, instead of the standard Terms & Conditions, is sent to you because no fee is being charged for your order. Please note the following:

- Permission is granted for your request in both print and electronic formats, and translations.
- If figures and/or tables were requested, they may be adapted or used in part.
- Please print this page for your records and send a copy of it to your publisher/graduate school.
- Appropriate credit for the requested material should be given as follows: "Reprinted (adapted) with permission from (COMPLETE REFERENCE CITATION). Copyright (YEAR) American Chemical Society." Insert appropriate information in place of the capitalized words.
- One-time permission is granted only for the use specified in your request. No additional uses are granted (such as derivative works or other editions). For any other uses, please submit a new request.

BACK CLOSE WINDOW

© 2020 Copyright - All Rights Reserved | Copyright Clearance Center, Inc. | Privacy statement | Terms and Conditions
Comments? We would like to hear from you. E-mail us at customercare@copyright.com